Thermal Decomposition of Solids and Melts

New Thermochemical Approach to the Mechanism, Kinetics and Methodology

Boris V. L'vov

Thermal Decomposition of Solids and Melts

Hot Topics in Thermal Analysis and Calorimetry

Volume 7

Series Editor:
Judit Simon, *Budapest University of Technology and Economics, Hungary*

The titles published in this series are listed at the end of this volume.

Thermal Decomposition of Solids and Melts

New Thermochemical Approach to the Mechanism, Kinetics and Methodology

by

Boris V. L'vov

St. Petersburg State Polytechnic University
St. Petersburg, Russian Federation

Springer

Boris V. L'vov
St. Petersburg State Polytechnic University
St. Petersburg
Russian Federation

Series Editor:
Judit Simon
Budapest University of Technology and Economics
Hungary

To Anna, my Wife with love

Contents

Preface

The appearance of this English edition of my book, first published in Russian in mid-2006, is related to the help and support of two prominent scientists: Professor Michael Brown (Rhodes University Grahamstown, South Africa) and Dr. Judit Simon (Budapest University of Technology and Economics, Hungary).

The story is as follows. In the winter of 2006, in the process of exchange of views by email with Michael on some problems of decomposition kinetics, I asked him about the possibility of publishing my book in English. He suggested that I should contact Judit, the Series Editor of "Hot Topics in Thermal Analysis and Calorimetry". My application was kindly accepted, considered, and approved. As a result, Judit strongly recommended this book to Springer for publication, and Michael kindly agreed to help me with linguistic improvements of my hurriedly translated book. In the process of editing, he made some critical comments and questions, which stimulated me to improve and clarify the text, but we did have to agree to put our differences of scientific opinions aside so as not to delay the process. Without this invaluable help, this book would not be as "readable" as I hope it is now. The author uses this opportunity to express his sincere thanks to Michael and Judit for their significant help and support.

Although only about a year has gone after the preparation of the original edition of the book (in Russian), this English version of the manuscript has undergone considerable revision. These changes refer to Sections 2.2, 2.4, 2.5, 8.2, 16.4, and Chapter 13. A new Section 15.6, Tables 13.1 and 13.2, and Figures 5.2 and 16.1 are added and many tables and figures have been improved. All these changes were made to clarify the explanation of the basic concepts of the new thermochemical approach to thermal decomposition, including mechanisms, kinetics, and methodology, and to make it suitable as a textbook for students.

The author gratefully acknowledges the kind permission to use some figures from other sources of publication: figures reprinted from *Spectrochimica Acta Part B*, *Spectrochimica Acta Review*, *Progress in Analytical Atomic Spectroscopy*, and *Thermochimica Acta* with kind permission from Elsevier Science, Amsterdam, the Netherlands; figures reprinted from the Proceedings

of the Royal Society with kind permission from the Royal Society of London, UK; figures reprinted from *Journal of the American Ceramic Society* with kind permission of Blackwell Publishing, Oxford, UK and figures reprinted from *Analytical Chemistry* with kind permission from the American Chemical Society, Washington DC, USA.

The exact references are given in the figure captions.

St. Petersburg, February 2007   Boris V. L'vov

Foreword

It has been an interesting task helping Professor Boris L'vov with the production of an English version of his book. Although we have, unfortunately, never met in person, we have had many contacts by email. He kindly presented me with a copy of the Russian edition of his book soon after publication and I was immediately frustrated by not being able to read it. Professor L'vov's work is both original and controversial, and spread over an impressive number of primary publications. This literature had been condensed by the chief author into a book of manageable size, but still needed to be made accessible to the English-speaking world. One of my motives in offering to assist with the English edition was to "force" myself to pay close attention to his complex ideas and suggestions. I think I have come out of the process with a greater appreciation of some aspects, but still have to undergo a full "conversion experience"! Time just did not allow lengthy exchanges between us and these will, perhaps, have to be postponed for future debates in the literature. My hope is that this translation will bring Professor L'vov's work to the attention of a wider audience and that this will promote constructive discussion of the assumptions made.

Grahamstown, February 2007 Michael E. Brown

Preface (Original Russian Edition)

Solid-state reactions and, particularly, processes involved in the thermal decompositions of solid substances are a subject of intense interest for a very broad class of specialists: researchers, engineers, and technologists engaged in metallurgy, chemical industry, and materials sciences, including those specializing in the area of novel technologies (chemical vapour deposition, self-propagating high-temperature synthesis, mechanochemistry, and nanotechnologies). Nevertheless, very few monographs, reference handbooks, and especially textbooks on this and related issues have been published. This may be attributable to some stagnation in the field of theoretical description of these processes, which became evident as far back as the 1970s–1980s.

The present monograph suggests a new approach to the reaction mechanisms, kinetics, and methodology of measurements, which is based on a thermochemical analysis of such processes. This approach draws on studies of the author performed during the last 25 years with the use of electrothermal atomic absorption spectrometry (AAS) and mass spectrometry (MS) and, recently, of the methods of thermal analysis (TA) as well. The concepts developed are capable of accounting for the main features of reactions, including the mechanisms governing individual stages of a process, as well as of providing quantitative interpretation of many problems and unusual observations (for instance, the Topley–Smith effect) that have accumulated in this field. This approach has essentially laid a cornerstone for development of a self-consistent and rigorous theory of thermal decomposition of solids and melts.

The new methods of measurement and calculation proposed have radically improved the precision and accuracy of determining the thermochemical parameters and, in this way, expanded considerably the potential use of TA in kinetics studies. The methods have been employed to obtain, for the first time, reliable kinetic characteristics and to uncover the mechanism of decomposition of several tens of substances belonging to different classes of inorganic compounds (crystalline hydrates, oxides, hydroxides, nitrides, azides, nitrates, sulfates, carbonates, and oxalates). The results obtained in these studies have been published in the literature in various journals spanning the period from 1981 to 2006). This book draws the work together to make it more accessible for researchers confronted with these issues.

The exposition is divided into three main parts. The first part elucidates the basic physicochemical concepts (mechanism, kinetics, and methodology), which, in the second part, are used for the interpretation of the effects and phenomena making up the basis of research in the kinetics of solid-state reactions. Definition and substantiation of the basic physicochemical concepts is necessary because readers unacquainted with other publications of the author might find these points fairly unusual. The third part of the monograph contains a brief description of thermogravimetric (TG) experiments and the basic experimental and thermochemical data used by the author in the second part of the book. These data may turn out to be useful as subsidiary material in the practical activities of a reader confronted by corresponding problems. Also, as calculation methods become more sophisticated and the values of thermodynamic functions more accurate, these data may find use in refining the conclusions obtained. The Appendix to the book lists some additional tabulated data and physical constants used in the corresponding calculations.

The terminology used has undergone the usual changes or refinements with time and experience. The terms "mechanism of dissociative vaporization", "physical approach", and "specific enthalpy", introduced in previous communications by the author, have been replaced in this book by "mechanism of congruent dissociative vaporization", "thermochemical approach", and "molar enthalpy". The notation of some physical quantities has likewise undergone changes.

The author sincerely hopes that the material in this book will arouse the interest of the readers and stimulate revision of many ideas that have become established in this area. It is likely that some of the ideas expressed here will raise objections and initiate heated discussions. In the final count, this could only favour progress in the field. Any constructive critical comments of the readers will be accepted gratefully by the author and taken into account in our subsequent studies.

The author feels deeply indebted to his students and colleagues who have taken active part in studies of thermal decomposition problems with electrothermal AAS, quadrupole MS, thermal analysis, and computational modelling. Their names feature in the list of authors of the corresponding publications. Particular thanks are due to Dr. Valery L. Ugolkov (Institute of Silicate Chemistry, St. Petersburg), whose active participation in our research during the recent 5 years has made it possible to complete the series of thermochemical studies that provided solid support for the ideas of the author and a justifiable purpose for the writing of this book; my colleague, Dr. Leonid K. Polzik, who has read carefully through the manuscript and suggested valuable corrections and comments; and, finally, but not least importantly, Dr. Andrew K. Galwey (Belfast), whose long-standing moral support has been invaluable in helping the author to maintain self-control and optimism in the hardest times of collision of his ideas with the generally accepted concepts.

St. Petersburg, February 2006   Boris V. L'vov

Abbreviations

A, B, C	Reaction products
A	Absorbance
A	Pre-exponential ("frequency") factor in the Arrhenius equation
A, B, C, D, E	Parameters used in calculations of temperature distribution in powders
a, b, c	Stoichiometric coefficients related to products A, B, C
C_v	Molar heat capacity (at constant volume)
c_1	Coefficient $c_1 \equiv \log(P_{eq}/P_\infty)$
c_2	Coefficient $c_2 \equiv \ln[-\Delta_c H_T^\circ/(RT)]$
c_{eq}	Equilibrium concentration
D	Diffusion coefficient
D_0	Diffusion coefficient under standard conditions (0°C, 1 bar)
d	Diameter
E	Base of decimal logarithms
E	E parameter ("activation energy") in the Arrhenius equation
e	Base of natural logarithms
f	Stoichiometry coefficient ($f = a^a b^b c^c$)
H_T°	Standard value of enthalpy at temperature T
J	Absolute rate of vaporization
J_c	Absolute rate of vaporization for crystal
J_p	Absolute rate of vaporization for powder
K_P	Equilibrium constant
k	Rate constant
M	Metal (unspecified)
M	Molar mass
$\overline{M}$	Geometric average of molar masses for several products
m	Mass
N_A	Avogadro constant
n	Number of layers
n_e	Effective number of layers
n_t	Total number of layers

P	Pressure
P_a	Air pressure
P_eq	Equilibrium pressure
P_eqp	Equilibrium pressure of primary product of vaporization
$\overline{P}$	Generalized value of pressure for several gas products
P_w	Pressure of water vapour
P_∞	Saturation vapour pressure
R	Reactant
R	Gas constant
r	Correlation coefficient
r	Radius
S	Oversaturation
S_T°	Standard value of entropy at temperature T
s	Standard deviation
s_r	Relative standard deviation
s_0	Initial surface area
s_m	Surface area at the instant of measurement
s_eff	Cross-section of effusion orifice
T	Thermodynamic temperature
T_app	Temperature for appearance of atomic absorption signal
T_f	Furnace temperature
T_in	Initial decomposition temperature
T_s	Temperature of the sample
T_sub	Temperature of sublimation
T_θ	Isokinetic temperature
t	Time
$\bar{u}$	Average velocity of molecules
W_C	Clausing factor considering the orifice shape in the effusion cell
α	Decomposition degree
α_m	Decomposition degree at the instant of measurement
α_v	Coefficient of vaporization
β	Coefficient considering the vaporization congruence (at $\nu = 2$)
γ	Surface tension
γ	Conversion factor from bar to Pascal
Δ	Finite change
δ	Coefficient considering the vaporization congruence (at $\nu > 2$)
ε	Emittance
λ	Length of free path
ν	Stoichiometric number
ρ	Density
σ	Stefan–Boltzmann constant
τ	Coefficient considering the condensation energy transfer to reactant

States of aggregation

(s)	Solid
(l)	Liquid
(g)	Gas or vapour

Subscripts to change values of thermodynamic functions

c	Condensation
d	Desorption
f	Formation
r	Reaction
s	Sublimation
v	Vaporization

Superscripts to symbols of vapour pressure and vaporization rate

e	Equimolar (mode)
i	Isobaric (mode)
ext	External (pressure of gaseous product, in excess)

Crystal systems

I	Cubic
II	Tetragonal
III	Hexagonal
IIIa	Trigonal
IV	Rhombic
V	Monoclinic
VI	Triclinic

Acronyms

AAS	Atomic absorption spectrometry
BET	Brunauer–Emmett–Teller (equation)
CDV	Congruent dissociative vaporization
MS	Mass spectrometry
TA	Thermal analysis
TG	Thermogravimetry
T–S	Topley–Smith (effect)

Part I

Thermal Decomposition: Basic Concepts

Chapter 1
Historical Overview

Thermal decomposition of solids and melts is a process of basic significance involved in many natural phenomena and industrial technologies. Karst phenomenon and volcanic activity, rock weathering, dehydration of rock-salt deposits, which are actually manifestations of the evolution of the Earth and of the Universe as a whole, have been subjects of curiosity of mankind from the time immemorial. The history of our civilization is intimately connected with development of a variety of technologies based on heat treatment of natural materials with the purpose of obtaining new objects of practical importance. Among them are both the oldest earthenware and building crafts and pyrometallurgy, and many modern technologies closely associated with industrial chemistry, production of catalysts, ceramics and optoelectronic materials. Table 1.1 presents examples illustrating the use of thermal decomposition in science and technology.

There is nothing strange therefore that research in this area started and proceeded concurrently with progress in chemical kinetics as a whole. The 1880s stand out as the years in which the famous "Etudes de dynamique

Table 1.1 Applications of thermal decomposition studies

Field of Science or Technology	Example of Possible Use
Physical chemistry of heterogeneous reactions	Development of the fundamentals of kinetics. Processes of burning of powders, rocket fuels
Chemistry of solids	Influence of crystal structure on the composition of the primary products of decomposition
Thermal analysis	Rise of the accuracy, precision, and efficiency of measurements
TG after Knudsen–Langmuir	Interpretation of vaporization coefficients
Electrothermal AAS	Studying of the atomization mechanism
Chemical manufacture	Production of technological materials (lime, soda, alumina)
Pyrometallurgy	Production of metals (iron, cobalt, copper)
Manufacture of catalysts	Oxides and mixed catalysts
Building manufacture	Manufacturing of cement, concrete
Manufacture of ceramics	Refractory ceramics, a brick
Potter's manufacture	Faience and porcelain
Pharmaceutical manufacture	Safe life of medicines
Production of explosives	Terms and conditions of safe storage
Polymers	Recycling (processing) of products
Geology and mineralogy	Formation and evolution of breeds (karsts)
Cosmochemistry	Evolution of the Solar System and the Universe
Chemical vapour deposition (CVD)	Development of technologies for the production of materials for optoelectronics (GaN)

Fig. 1.1 Jacob van't Hoff (1852–1911). The Dutch chemist. One of the founders of physical chemistry, chemical kinetics, and stereochemistry. The first Nobel Prize Laureate in chemistry (1901)

Fig. 1.2 Svante Arrhenius (1859–1927). The Swedish physical chemist. The founder of the theory of electrolytic dissociation. The Nobel Prize Laureate in chemistry (1903)

chimique" by van't Hoff (Fig. 1.1) and the paper by Arrhenius (Fig. 1.2) with an interpretation of the exponential dependence of the rate of inversion of a water solution of sugar cane on temperature appeared [1, 2]. At about the same time Lehmann published a monograph [3] on solid-state reactions, where he reviewed studies of earlier researchers dealing with weathering, vaporization, and thermal dissociation of many substances, including the oxides of silver, mercury, copper, and iridium; the carbonates of ammonium and some metals; the sulphates of calcium, strontium, barium, and lead; and crystalline hydrates of a number of inorganic salts.

Lehmann drew attention to some features in solid-state reactions, including the curious observations described in 1834 by Faraday, which are now considered as pioneering experimental studies of the structural sensitivity of the dehydration rate of crystalline hydrates. Crystals of easily eroding sodium salts (carbonates, phosphates, and sulphates), stored by Faraday for a few years, did not exhibit any visible deterioration. A fresh scratch on the crystal surface (birth of mechanochemistry) initiated, however, the onset of intense dehydration with a gradual expansion of the erosion zone until it covered the crystal's entire surface.

The 120 years that have elapsed after the beginning of systematic studies in the area of thermal decomposition of solids have witnessed an accumulation of an immense amount of experimental and theoretical material on the mechanisms and kinetics of this process. Three different approaches to the investigation of this problem have become established by now. The most popular approach is based on the concept of Arrhenius that chemical reactions involve only some of the molecules, the so-called "active" particles, their

Fig. 1.3 Henrich Hertz (1857–1894). The German physicist. The discoverer of electromagnetic waves and the creator of the theory of electromagnetic radiation. The unit of frequency (Hz) is named after him

Fig. 1.4 Irving Langmuir (1881–1957). The American physicist and physical chemist. His studies were devoted to high-temperature reactions and the chemistry of surface phenomena. The Nobel Prize Laureate in chemistry (1932)

actual fraction being determined by the energy barrier of the reaction and the temperature. The second approach makes use of the concepts of Hertz (Fig. 1.3), Knudsen and Langmuir (Fig. 1.4) on the vaporization of solids and differences in the kinetics of their decomposition in vacuum under equilibrium (in Knudsen's effusion cells) and non-equilibrium (as it is believed to be) vaporization from a free surface (by Langmuir). The third approach, which has branched off the second approach fairly recently, rests upon the assumed equilibrium mechanism of congruent dissociative vaporization (CDV) as a primary stage in the thermal decomposition of any (solid or melted) substance with subsequent condensation of decomposition products with low volatility. Table 1.2 presents, necessarily briefly, the chronology of the most important events that have contributed to evolution of the above approaches [1–58].

A careful analysis of these data leads one to the following conclusions. First of all there is a parallelism in the establishment of the first two approaches. Both appeared roughly at the same time in the 1880s. The paper by Hertz [31] that stimulated the later studies of Knudsen [32] and Langmuir [33] was published in 1882, 2 years before that of van't Hoff [1] and 7 years earlier than that by Arrhenius [2]. Subsequent accumulation of knowledge and the appearance of new ideas for both approaches also occurred concurrently and became practically completed by the 1960s. The further course of events in this field, as seen from the table, turned out to be limited to accumulation of experimental data and their analysis and generalization only.

While the two approaches pursue essentially the same goals, which reduce to revealing the mechanism and developing the kinetic theory of the process, they evolved and still continue to evolve almost independently of one another.

Table 1.2 Chronology of the most important events in the development of various kinetic approaches

Years	The approach After Arrhenius	The Approach After Knudsen–Langmuir	Thermochemical Approach
1880s	Thermodynamic deduction of exponential dependence of the reaction rate on temperature [1]. Interpretation of exponential dependence of reaction rate on temperature by Arrhenius [2]. The first monograph on thermal decomposition [3]	Calculation of vapour condensation rate instead of vaporization rate in equilibrium conditions and verification of theory on an example of mercury evaporation [31]	
1900s	Quantitative research of thermal decomposition Ag_2O [4]	Derivation of the equation for an effusion of vapour in a vacuum and introduction of concept of vaporization coefficient [32]	
1910s	Thermodynamic substantiation of thermal decomposition on the surface of solid phase [5]. The concept of topochemical reactions [6] is introduced	Derivation of the equation for the evaporation rate from a free surface and its practical application for low-volatility metals [33, 34]	
1920s	Application of the Arrhenius equation to heterogeneous reactions [7, 8]. Polanyi–Wigner equation [9]		
1930s	The Topley–Smith effect [10]. The Zawadzki–Bretsznajder rule [11]. Herzfeld equation [12]	The mechanism of multistage evaporation [35] is proposed	
1940s	The equations of the formal kinetics: after Avrami [13], Mampel [14], Prout–Tompkins [15], Erofeev [16]		
1950s	Development of methods of non-isothermal kinetics: Erdey–Paulik–Paulik [17]. Theoretical and experimental generalization of studies: Garner [18]. Development of solid reactivity conception: Boldyrev [19]	Development of effusion MS [36]. An improvement of an effusion cell model [37]. Development of the mechanism of multistage evaporation [38]	

(continued)

Table 1.2 (continued)

1960s	Collection, analysis, and extension of studies: Young [20]. Appearance of the commercial equipment for TA. Foundation of *Journal of Thermal Analysis*. Analysis and extension of studies: Delmon [21]	Vapour pressure of metals (review): Nesmeyanov [39]. Measurement of coefficients of evaporation [40–43]. Vapour pressure of refractory compounds (review): Fesenko–Bolgar [44]	Langmuir diffusion equation is used for calculation of the rate of Al_2O_3 dissociative vaporization [50]
1970s	Foundation of *Thermochimica Acta* journal. Collection, analysis and extension of studies: Barret [22]; Prodan–Pavlyuchenko–Prodan [23]	Vapour pressure above oxides (reviews): Semenov–Nikolaev–Frantseva [45]; Kazenas–Chizhikov [46]	
1980s	Collection, analysis, and extension of studies: Brown–Dollimore–Galwey [24]; Prodan [25]		The method of absolute rate of decomposition has appeared [51]. Substantiation of the equimolar and isobaric modes of evaporation [52]. First MS study of evaporation of Pb [53] and Ni [54] nitrates
1990s	Collection, analysis, and extension of studies: Prodan [26]; Manelis et al. [27]; Boldyrev [28]; Galwey–Brown [29]; Boldyreva–Boldyrev [30]	Vapour pressure above oxides (reviews): Semenov–Stolyarova [47]; Kazenas–Tsvetkov [48]	The CDV mechanism is proposed [55]. Interpretation of coefficients of vaporization [56]. Modelling of the Topley–Smith effect [57]
2000s		Vapour pressure above oxides (review): Kazenas [49]	Application of the third-law method for determination of the reaction enthalpy [58]

Except for the monographs [24] and [29], where the methods of Knudsen–Langmuir are discussed on less than one page out of 340 and on about 10 pages out of 600, respectively, the other monographs of this list [18–30] ignore completely their existence. Monographs [44–49], in their turn, do not make any references to studies performed using the Arrhenius approach.

The thermochemical approach was an outgrowth of the studies started in the 1960s [50–52] of the kinetics and mechanism of atomization of substances

by flame and electrothermal atomic absorption spectrometry (AAS). In the 1980s, they were complemented by studies of electrothermal vaporization using vacuum quadrupole mass spectrometry (QMS) [53, 54]. These series of studies laid a foundation for development of a thermochemical approach to interpretation of the process of thermal decomposition based, as already mentioned, on the mechanism of CDV of substances with subsequent condensation of low-volatility products of decomposition [55]. A characteristic of this direction is the broad use of experimental data accumulated earlier in the other two approaches.

Regrettably, despite the progress reached in elaboration of a self-consistent theory of thermal decomposition and in quantitative interpretation of many unusual effects [56–58], the thermochemical approach has not received support and further development by other researchers. One should possibly ascribe this attitude to the fatigue and apathy that have built up in the recent decades as a result of futile attempts at coming closer to the final goal by traditional methods. The state of stagnation is admitted even by leading specialists in the field [59]. It became manifest, in particular, in the decay or reorientation of interests of the universally recognized scientific schools established in the middle of the last century by Professor Garner (University of Bristol), Profs. Brewer and Searcy (University of California, Berkeley), Profs. Pavlyuchenko and Prodan (Institute of General and Inorganic Chemistry, Minsk), and Prof. Boldyrev in the 1980s (Institute of Solid State Chemistry, Novosibirsk), in reduction of the volume of publications on solid-state reactions in the periodic press and at meetings and, as a consequence, in closing in 1990 of a specialized Journal "Reactivity of Solids" and in the refusal of leading physicochemical journals to publish papers reporting on studies in this field.

This book is aimed at reviving interest in the investigation of the mechanisms and kinetics of thermal decomposition based on new concepts and a new methodology and generalization and quantitative interpretation of many of the most significant results obtained during the more than a 100-year period of history of these studies.

References

1. Van't Hoff JH (1884) Etudes de dynamique chemique. Frederik Müller et Co, Amsterdam
2. Arrhenius S (1889) Z Phys Chem 4:226–248
3. Lehmann O (1889) Molekularphysik. Verlag von Wilhelm Engelmann, Leipzig
4. Lewis GN (1905) Z Phys Chem 52:310–326
5. Langmuir I (1916) J Am Chem Soc 38:2221–2295
6. Kohlschütter V (1919) Z Anorg Allg Chem 105:1–25
7. Hinshelwood CN, Bowen EJ (1921) Proc Roy Soc A99:203–212
8. Bružs B (1926) J Phys Chem 30:680–693
9. Polanyi M, Wigner E (1928) Z Phys Chem A139:439

10. Topley B, Smith ML (1931) Nature 128:302
11. Zawadzki J, Bretsznajder S (1935) Z Elektrochem 41:215–223
12. Herzfeld KF (1935) J Chem Phys 3:319–323
13. Avrami MJ (1940) J Chem Phys 8:212–224
14. Mampel LH (1940) Z Phys Chem A187:43–57
15. Prout EG, Tompkins FC (1944) Trans Farad Soc 40:488–493
16. Erofeev BV (1946) Dokl Akad Nauk SSSR 52:515–519 (in Russian)
17. Erdey L, Paulik F, Paulik J (1955) Nature 174:885
18. Garner WE (1955) (ed) Chemistry of the solid state. Butterworths, London
19. Boldyrev VV (1958) Methods for investigation of the kinetics of thermal decomposition of solids. Tomsk University Press, Tomsk (in Russian)
20. Young DA (1966) Decomposition of solids. Pergamon, Oxford
21. Delmon B (1969) Introduction a la cinétique hétérogène. Technip, Paris
22. Barret P (1975) (ed) Reaction kinetics in heterogeneous chemical systems. Elsevier, Amsterdam
23. Prodan EA, Pavlyuchenko MM, Prodan SA (1976) Regularities of topochemical reactions. Nauka Tekhnika, Minsk (in Russian)
24. Brown ME, Dollimore D, Galwey AK (1980) Reactions in the solid state. Elsevier, London
25. Prodan EA (1986) Inorganic topochemistry. Nauka Tekhnika, Minsk (in Russian)
26. Prodan EA (1990) Topochemistry of crystals. Nauka Tekhnika, Minsk (in Russian)
27. Manelis GB, Nazin GM, Rubtsov YuI, Strunin VA (1996) Thermal decomposition and combustion of explosives and powders. Nauka, Moscow (in Russian)
28. Boldyrev VV (1997) Reactivity of solids (on the example of thermal decomposition reactions). Siberian Branch Russian Academy of Sciences, Novosibirsk (in Russian)
29. Galwey AK, Brown ME (1999) Thermal decomposition of ionic solids. Elsevier, Amsterdam
30. Boldyreva EV, Boldyrev VV (1999) Reactivity of molecular solids. Wiley, Chichester
31. Hertz H (1882) Ann Phys Chem 17:177–200
32. Knudsen M (1909) Ann Physik 29:179–193
33. Langmuir I (1913) Phys Rev 2:329–342
34. Langmuir I, Mackay GMJ (1914) Phys Rev 4:377–386
35. Volmer M (1939) Kinetik der Phasenbildung. Steinkopff, Leipzig
36. Chupka WA, Inghram MG (1953) J Chem Phys 21:371–372
37. Motzfeldt K (1955) J Phys Chem 59:139–147
38. Hirth JP, Pound GM (1957) J Chem Phys 26:1216–1224
39. Nesmeyanov AN (1961) Vapour pressure of chemical elements. Akad Nauk SSSR, Moscow (in Russian)
40. Hirth JP, Pound GM (1963) Condensation and evaporation. Nucleation and growth kinetics. Pergamon, Oxford
41. Rutner E, Goldfinger P, Hirth JP (1964) (eds) Condensation and evaporation of solids. Gordon & Breach Science, New York
42. Somorjai GA, Lester JE (1967) Evaporation mechanism of solids. In: Reiss H (ed) Progress in solid state chemistry. Pergamon, Oxford, pp 1–52
43. Searcy AW (1968) The kinetics of evaporation and condensation reactions. In: Searcy AW, Ragone D, Colombo U (eds) Chemical and mechanical behavior of inorganic materials. Wiley, New York, pp 107–133
44. Fesenko VV, Bolgar AS (1966) Evaporation of refractory compounds. Metallurgiya, Moscow (in Russian)
45. Semenov GA, Nikolaev EN, Frantseva KE (1976) Application of mass spectrometry in inorganic chemistry. Khimiya, Leningrad (in Russian)
46. Kazenas YeK, Chizhikov DM (1976) Vapour pressure and composition under oxides of chemical elements. Nauka, Moscow (in Russian)

47. Semenov GA, Stolyarova VA (1990) Mass spectrometric study of vaporization of oxide systems. Nauka, Leningrad (in Russian)
48. Kazenas YeK, Tsvetkov YuV (1997) Vaporization of oxides. Nauka, Moscow (in Russian)
49. Kazenas YeK (2004) Vaporization thermodynamics of double oxides. Nauka, Moscow (in Russian)
50. L'vov BV (1966) Atomic absorption spectral analysis. Nauka, Moscow (in Russian)
51. L'vov BV, Ryabchuk GN (1981) Zh Analit Khim 36:2085–2096 (in Russian)
52. L'vov BV, Fernandez HGA (1984) Zh Analit Khim 39:221–231 (in Russian)
53. Sturgeon RE, Mitchell DF, Berman SS (1983) Anal Chem 55:1059–1064
54. Dressler MS, Holcombe JA (1987) Spectrochim Acta B 42:981–994
55. L'vov BV (1990) Zh Analit Khim 45:2144–2153 (in Russian)
56. L'vov BV, Novichikhin AV (1997) Thermochim Acta 290:239–251
57. L'vov BV, Novichikhin AV, Dyakov AO (1998) Thermochim Acta 15:145–157
58. L'vov BV (2004) Thermochim Acta 424:183–199
59. Galwey AK, Brown ME (2000) J Therm Anal Cal 60:863–877

Chapter 2
Decomposition Mechanism

2.1 Preliminary Remarks

It appears reasonable to define the concept "decomposition mechanism", to be discussed below, before we cross over to its consideration. (As René Descartes said: "Define the meaning of the words, and you will free mankind of half of its misconceptions.") One may find in the literature different approaches to interpretation of this concept. This should be largely assigned to the methods employed by researchers to unravel it, and the goals pursued in its subsequent application.

Besides the universally accepted kinetic description of a process based on a proper analysis of the shape of vaporization curves (see Sect. 2.4), the Arrhenius approach has been widely used to probe the mechanism of decomposition at the level of elementary processes in solids, which are associated with rearrangement of the crystal lattice. These studies rest on two fundamental branches of the physical chemistry of solids, namely, the theory of disorder and the theory of transport, whose foundations had been laid in the 1920s–1930s by the outstanding Russian physicist, Frenkel, and the well-known German physical chemists, Wagner and Schottky.

The relation between disorder and the reactivity of crystals became a subject of research in a number of laboratories in the 1950–1960s. In Russia, these studies have been headed, starting from the 1950s, by Boldyrev [1, 2], who believes that it is the displacements of protons, ions, and electrons in the lattice that give rise to the rupture or formation of chemical bonds and, eventually, to decomposition of the reactant. The presence of defects influences strongly the rate-limiting stage of the reaction. Therefore, the main methods of investigation are based essentially on studying the effect of lattice disorder, introduced by doping, or mechanical treatment, or irradiation of the reactant, on its electrophysical properties (electrical conductivity, thermopower, and transport numbers) and the decomposition rate. This approach has received wide recognition in the classification of decomposition reactions. Analysis of the ionic and molecular changes occurring during the course of decomposition appears to have an extremely attractive potential. Its application to estimation of the kinetic parameters of a reaction is, however, curtailed by a lack of knowledge of the energetics of the individual stages in a reaction. Another stumbling block is the large diversity of schemes employed in interpretation of the decomposition mechanisms of different substances.

The above can be readily exemplified by a description of the mechanisms of the rate-limiting stages in the decompositions of some compounds [2]: "The reaction of thermal decomposition of potassium permanganate is a typical

redox reaction, with electron transfer playing a significant role. Decomposition of silver oxalate is a reaction in which transport of silver ions, particularly of interstitials, over the lattice plays a crucial role, especially in the initial stage. In the case of the aluminum hydride, the process is the same, but the hydride ion transfers over the anion lattice. In ammonium perchlorate, transport is mediated by proton transfer from the cation to the anion sublattice and its subsequent motion over the anion sublattice until capture by a proton trap, followed by regeneration of the acceptor center." It remains unclear how one could use these schemes to control a reaction and predict the behaviour of a reactant when the conditions of its storage or decomposition change (atmospheric environment, temperature, sample morphology, aggregate state, etc.). The ways leading to this goal are too obscure indeed, a point recognized by the author of the monograph himself [2].

Interpretation of the decomposition mechanism along the lines of the Knudsen–Langmuir approach is based on the difference between the real vaporization rate of a reactant from a free surface (after Langmuir) and that of the same reactant in practically equilibrium conditions from effusion cells (after Knudsen). The ratio of these rates is called the vaporization coefficient, α_v. Its value turns out in many cases to be smaller (quite frequently, by several orders of magnitude) than unity. As pointed out by Somorjai and Lester [3]: "All the information on the evaporation mechanism is hidden into a 'correction factor' which is applied to adjust the deviation of the evaporation rate far from the maximum evaporation rate in equilibrium."

Over the 90 years that have elapsed since the introduction of the vaporization coefficient into calculation of the gas effusion rate by Knudsen [4], interpretation of the quantity α_v and, hence, of vaporization mechanisms has been the subject of numerous studies. The difference of α_v from unity is usually assigned to the multistage nature of the vaporization process, specific features of the surface relief, or impurities and lattice defects of the reactant. Sometimes one adds among the reasons "difficulty of decomposition", by which one understands the difference of the molecular form of primary gaseous products from the structure they usually assume in condensed phase. In the case of incongruent vaporization, one adds effusion or diffusion limitations encountered by gaseous products as they escape through the layer of the solid product. On the occasions where attempts at revealing any physical or chemical reasons for the difference of α_v from unity fail, one assigns the decomposition mechanism to non-equilibrium processes without, however, offering a sound explanation of the nature of these non-equilibrium conditions [3]. No attempts to theoretically estimate the vaporization coefficients or find their interpretation on a common physical or chemical basis have been made before the appearance of the thermochemical approach.

We believe that the major motivations for unraveling the mechanism of decomposition consists in its subsequent use for interpretation and prediction of the kinetics under different conditions of interest to the researcher, i.e., in the possibility of theoretical estimation of the thermochemical characteristics

of a process, in particular, of the heat (enthalpy) of reaction. If one accepts this approach, there will be no need to consider details of a reaction at the ionic-molecular level (at any rate, with our present fairly superficial knowledge of the mechanism as a whole). One should only determine the actual path of the process (as represented by one or several consecutive reactions) and know the composition, aggregate state, and stoichiometry of the reactants and products. The general mechanism of CDV being considered below allows to produce such thermochemical analysis.

2.2 Basics of the Congruent Dissociative Vaporization (CDV) Mechanism

Foundation Thermal decomposition of a solid reactant, R, is usually described by two types of reaction: by congruent dissociative vaporization of a reactant R into gaseous products A(g) and B(g), i.e., according to the scheme:

$$R(s/l) \leftrightarrow A(g) + B(g) \qquad (2.1)$$

or by incongruent dissociative vaporization involving formation of a solid product A(s) and a gaseous product B(g) by the scheme:

$$R(s/l) \leftrightarrow A(s) + B(g) \qquad (2.2)$$
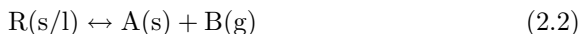
The existence of these two fundamentally different schemes of decomposition is recognized (e.g., [5–7]) and is usually accepted without evoking any objections or doubt. However, in contrast to the first scheme, the second scheme appears, on closer examination, rather questionable. The point is that the forming solid product differs significantly from the solid reactant, not only in crystal structure, but also in its morphology. This manifests itself in the formation of conglomerates of separated nanoparticles of product that are practically "transparent" for an exhaust flow of gaseous products. Of even greater importance is the formation, in some rare cases, of two solid products in the form of two different phases. This occurs, for example, in the decomposition of talc ($3MgO \cdot 4SiO_2 \cdot H_2O$), when enstatite ($MgSiO_3$) and the amorphous form of SiO_2 are produced simultaneously (see Sect. 2.6). *It is difficult to imagine such a transformation of a solid reactant into solid product(s), with the different from initial spatial distribution, without any intermediate stage related to a change of its aggregate state.*

It appears much more probable to assume that solid products form as a result of collisions and condensation of low-volatility particles (atoms and molecules) that became free in the gaseous phase through decomposition by a *common* mechanism of CDV, i.e., by the scheme

$$R(s/l) \leftrightarrow A(g) + B(g) \rightarrow A(s) + B(g) \qquad (2.3)$$
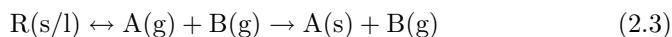
This scheme may be condensed to the form

$$R(s/l) \leftrightarrow A(g)_{\downarrow} + B(g) \qquad (2.4)$$

This reasoning leads to the main assumption (I) that *the decomposition of all compounds most likely proceeds by CDV* and, in the case of formation of low-volatility products, includes an additional stage of condensation of these products. The reader may find this reasoning not convincing enough. Therefore, other arguments, both direct and indirect, will be presented below for the validity of this assumption.

Other Basic Assumptions In addition to this main assumption (I), which forms the foundation for the CDV mechanism, there are two other, more obvious assumptions, namely, (II) that *primary products of decomposition may differ from their equilibrium forms,* and (III) that *the energy released in condensation of a low-volatility product in the reaction interface decreases partially the total enthalpy of the decomposition reaction* (including the condensation stage) compared to that of the primary stage of dissociative vaporization.

Consider now the essence and validity of these assumptions. The decompositions of oxides of some metals (CuO, HgO, PtO$_2$, and ZnO) at comparatively low temperatures ($<1,000$ K) were shown long ago [8] to proceed with liberation of oxygen in the form of free atoms. There are other similar examples [6] that support assumption II. The appearance of low-volatility products in the gaseous phase in congruent vaporization (in other than their equilibrium aggregate state) is a part of this assumption.

The situation with assumption III, first formulated in [9], is more complex. Although the idea of the energy released in the reaction interface in condensation of a low-volatility product contributing partially to the enthalpy of decomposition appears plausible enough, the mechanism by which this energy is transferred to a reactant and its magnitude still remain a subject of research. This problem will be discussed in considerable detail later.

2.3   Direct Observation of the Primary Decomposition Products

In the 1980s interest in the mechanism of atomization of substances in electrothermal AAS stimulated investigation of this process by mass spectrometry (MS) techniques [10–19]. Investigation of the thermal decompositions of salts of some metals revealed *the presence of low-volatility decomposition products in the gaseous phase*, an observation that provided, as already mentioned, a stimulus to studying the mechanism of CDV. The experimental conditions and the results accumulated in these observations are summarized in Table 2.1.

The experiments were carried out in vacuum and in a nitrogen environment. In vacuum, a miniature graphite heater in the form of a flat platform with the sample deposited on top was placed in the spectrometer chamber evacuated to

Table 2.1 Mass spectrometry studies of thermal decomposition of metal nitrates

Reactant	Medium	Sample Mass[a] (μg)	Heating Rate (K s^{-1})	Metal Containing Species		T_{app} (K)	Ref.
				Major	Minor		
AgNO$_3$	Vacuum	10	1	Ag	AgNO$_3$	580	[18]
Cd(NO$_3$)$_2$	Vacuum	0.26	300	CdNO$_3$	Cd	550	[15]
Cd(NO$_3$)$_2$	Vacuum	10	1	CdNO$_3$	CdO, Cd	570	[18]
Co(NO$_3$)$_2 \cdot$ 6H$_2$O	Vacuum	0.5	500	CoO		400	[13]
Cr(NO$_3$)$_3$	Vacuum	0.15	780	CrO	Cr$_2$O$_3$, Cr	400	[17]
Cu(NO$_3$)$_2 \cdot$ 3H$_2$O	Vacuum	1	200	CuO	Cu	340	[14]
Cu(NO$_3$)$_2 \cdot$ 3H$_2$O	Vacuum	10	1	Cu(NO$_3$)$_2$	CuNO$_3$, CuO, Cu	350	[19]
Ni(NO$_3$)$_2 \cdot$ 6H$_2$O	Vacuum	0.5	500	NiO	Ni(NO$_3$)$_2$	625	[12]
Pb(NO$_3$)$_2$	Vacuum	0.15	1,000	PbO	Pb	550	[10]
Pb(NO$_3$)$_2$	Vacuum	0.4	600	PbO	Pb	550	[11]
Pb(NO$_3$)$_2$	Vacuum	10	1	PbNO$_3$	PbO, Pb	530	[18]
Mg(NO$_3$)$_2 \cdot$ 6H$_2$O	1 atm N$_2$	0.05	2,000	Mg(OH)$_2$	MgO	400	[16]
Ca(NO$_3$)$_2 \cdot$ 4H$_2$O	1 atm N$_2$	0.05	2,000	Ca(OH)$_2$		610	[16]
Sr(NO$_3$)$_2 \cdot$ 4H$_2$O	1 atm N$_2$	0.05	2,000	Sr(OH)$_2$		400	[16]

[a] Reduced to metal
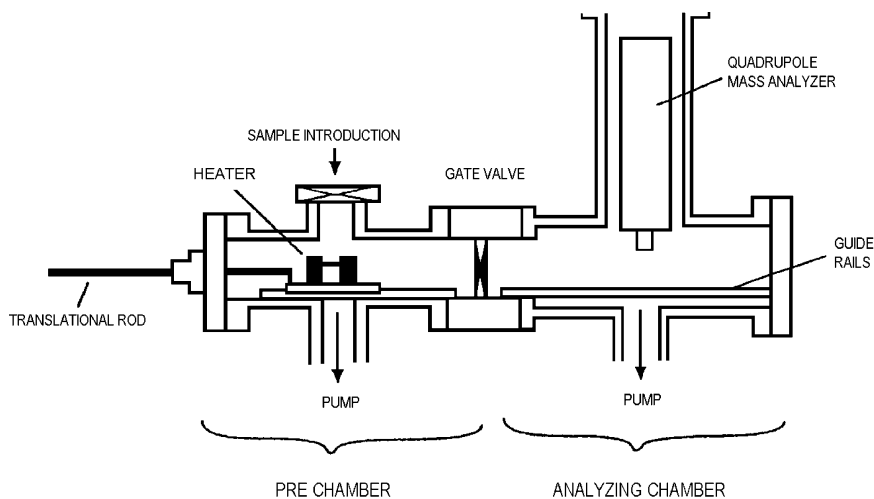
Fig. 2.1 Mass spectrometer vacuum system. The atomizer and furnace support are shown in the loading position. Movement of a furnace along a rail is produced by means of a guide pin. (Reproduced from [11], with permission.)

5×10^{-3} Pa (Fig. 2.1). In the second method, the nitrogen flow that had passed through the heated graphite tube containing the sample was directed into a quadrupole mass spectrometer through a system of two cones provided with small orifices (Fig. 2.2). An essential feature of these experiments was that particles vaporizing from the surface of a decomposing reactant propagated
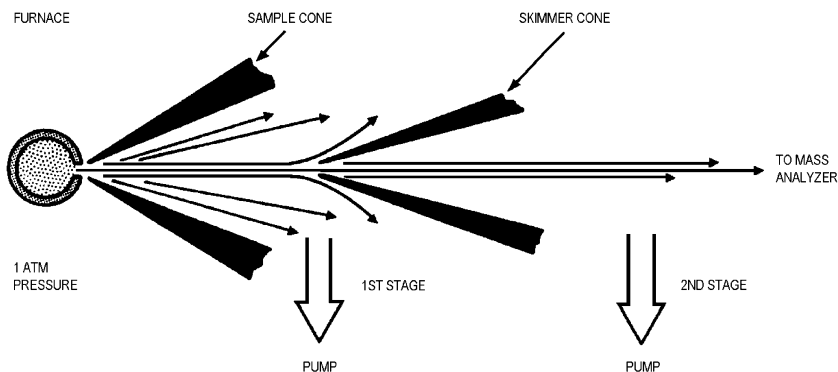
Fig. 2.2 Schematic representation of the nested-pair of cones used for sampling and molecular-beam formation. Species entering the sampling cone are entrained in a free-jet expansion into the vacuum stage (5×10^{-3} Pa). Only those species having moments directed along the cone axis enter the skimmer cone. (Reproduced from [16], with permission.)

in straight paths to the ionizer, without collisions with the surfaces at which a "non-equilibrium" particle could transfer to the equilibrium state, be it condensation or association. Some of the construction details of the quadrupole mass spectrometer make it particularly suitable for observing such processes.

As seen from Table 2.1, the low-volatility products (salt molecules, oxides, and metal atoms) appeared in the gaseous phase at temperatures (T_{app}) ranging from 340 to 625 K, which correspond to the beginning of thermal decomposition of the salts or their hydrates. The differences in composition of the products observed by different authors should be assigned to differences in the techniques employed and the actual measurement conditions.

Significantly, in the cases where the samples were heated to their complete evaporation, two peaks were observed (a low-temperature and a high-temperature one). The first of them corresponds to thermal decomposition of the salts, and the second, to that of the oxides (CdO, Cr_2O_3, CuO, NiO, and PbO).

For illustration, Figs. 2.3 and 2.4 present decomposition recordings of $Ni(NO_3)_2$ and $Pb(NO_3)_2$ samples. The areas of both (the low- and high-temperature) peaks turn out to be approximately equal. This implies that the decomposition of these salts (the first peak) proceeds in a congruent way, with half of the metal or oxide vapours, as this should be expected from geometric considerations, condensing on the flat heater surface. In case of sample evaporation in the form of metal-nitrate molecules only, it would be impossible to explain the formation of the second peak. Although all studies of atomization by MS of which we are aware were performed with nitrate salts only (these compounds are most frequently used in electrothermal AAS), it appears reasonable to suggest that CDV may be a primary stage in the decomposition of other compounds as well.
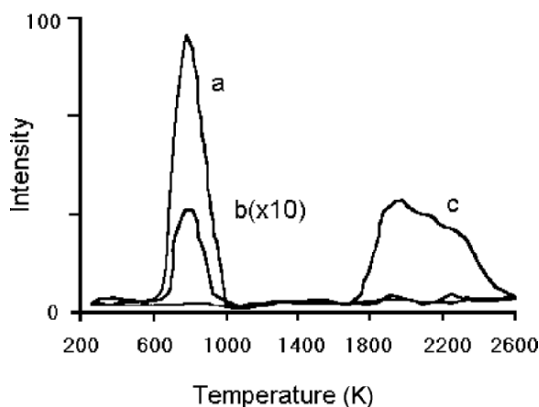
Fig. 2.3 Mass intensity signals of Ni species for the thermal decomposition of a nickel nitrate sample containing 0.5 μg Ni: (a) NiO^+, (b) $Ni(NO_3)_2^+$, and (c) Ni^+. The experimental conditions are indicated in Table 2.1. (Reprinted from [12], with permission.)
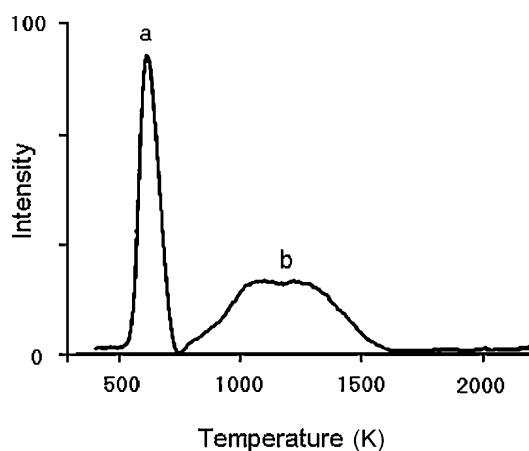
Fig. 2.4 Mass intensity signals of Pb species for the thermal decomposition of a lead nitrate sample containing 0.4 μg Pb: (a) PbO^+ and (b) Pb^+. The experimental conditions are indicated in Table 2.1. (Reprinted from [11], with permission.)

A specific feature of the anhydrous nitrates of many metals (Ag, Ba, Ca, Cd, K, Li, Na, Rb, Tl, etc.), and of some crystalline hydrates, is that they melt before the onset of decomposition. Unlike a solid compound, the surface of a melt is free of a layer of the final solid product of decomposition, which would limit the entry of molecules of a low-volatility product from the reaction zone into the vacuum medium. This permits one to "see", as illustrated in Figs. 2.3

and 2.4, the flow of the corresponding product. In the case of decomposition of many high-melting compounds, for instance, of the carbonates or phosphates, this possibility is not realized because of the vapour condensation in the solid product shell.

2.4   Induction and Acceleratory Periods and the Localization Effect

Shapes of Kinetic Curves Among the most characteristic features of the isothermal decomposition reactions of a variety of solid substances are the stages of induction (slow decomposition) and acceleration in the kinetic curves $\alpha = f(t)$, as well as localization of the decomposition process in certain areas of the reactant surface. The first two features are illustrated by Fig. 2.5. Section A is not associated in any way with decomposition. It could be due, for instance, to escape of adsorbed water. Section B marks the end of the induction period, which usually culminates in the formation of stable germ nuclei. Section C reflects an acceleratory period corresponding to the growth of nuclei. This process may be accompanied by further nucleation, up to the maximum reaction rate at point D, after which the nuclei begin to overlap. The process of decomposition reaches the steady-state regime corresponding to the constant value of the absolute rate of decomposition (reduced to the unit of the efficient surface area of reactant). However, because the reactant surface begins to decrease, the total rate of decomposition starts to decrease as well. This
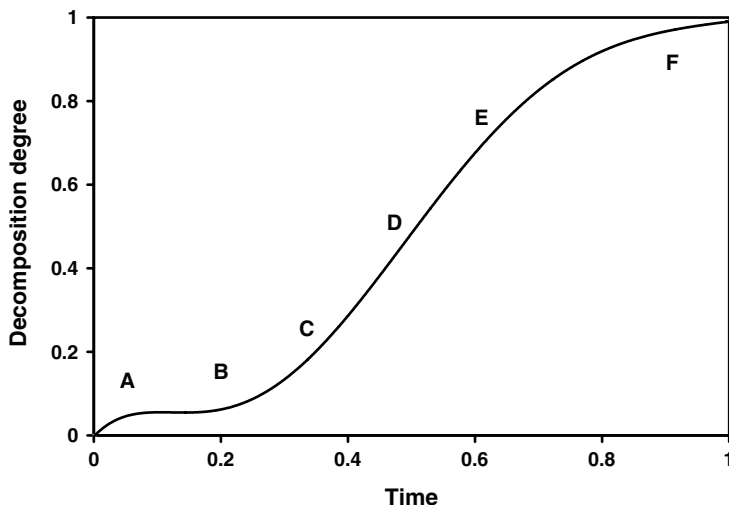
Fig. 2.5 The general view of the kinetic curve $\alpha = f(t)$ typical for the thermal decomposition of substances with formation of solid products
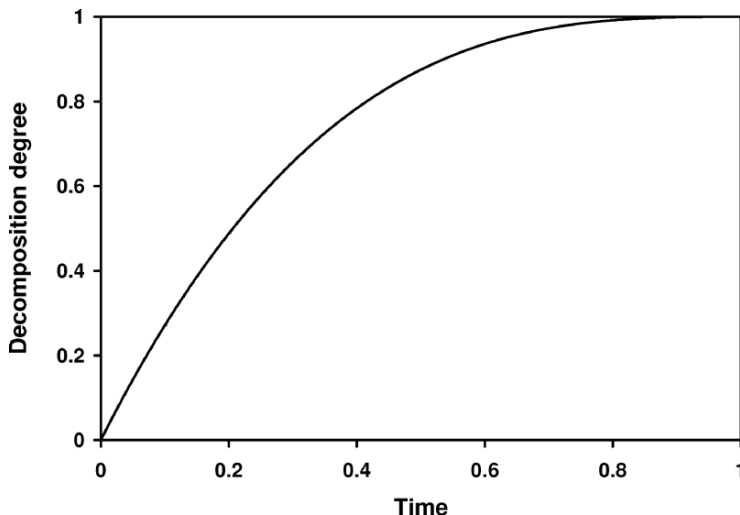
Fig. 2.6 Kinetic curve $\alpha = f(t)$, the shape of which (in an ideal case) is defined only by the decrease of the surface area according to the model of a "contracting sphere"

accounts for the onset of the deceleratory period E lasting until the completion of reaction F. One or several sections of the curve preceding D point may be negligible in extent or be absent altogether (Fig. 2.6).

Attempts at a mathematical simulation of the shape of these different sections in the kinetics curves and a physical interpretation of the appearance (or absence) of the induction and acceleration periods have been dealt with in numerous papers summed up in excellent reviews and monographs (e.g., [5, 6, 20–25]). A variety of models based on fairly arbitrary assumptions and describing formation of nuclei and their growth have been proposed. These assumptions are not, however, substantiated by physical and/or thermodynamic laws and real mechanisms which could account for the formation and accelerated growth of the nuclei.

Formation and Growth of Nuclei Nuclei form at specific points of the reactant crystal lattice. These points are located in regions with disordered structure, for instance, where dislocations emerge onto the surface, at vacancies, at interstitial-ion or impurity clusters. At these points of the lattice the molecules of the original substance may not be as fully coordinated as on an ideal (defect-free) surface and this makes them more susceptible to decomposition.

However, a further development of the process, in particular, the transformation of a thermodynamically unstable, germ nucleus into a stable growth nucleus in the framework of this "disordered structure" concept remains unclear. Jacobs, one of the founders of formal kinetics, admits [23] that "we have no knowledge of how the first few hundred atoms are added to a nucleus". The driving force behind the subsequent growth of nuclei, which occurs at a

rate higher than that of their formation, remains unclear as well. The approach developed in the present monograph, which is based on the CDV mechanism, presents a simple and straightforward explanation for both of these features. The formation and initial growth of germ nuclei are suggested to be driven by condensation on the reactant surface of oversaturated vapour of the low-volatility product, while the accelerated evolution of the growth nuclei is the result of contributions to the enthalpy of nuclei growth due to vapour condensation and the accompanying liberation of heat in the product/reactant interface (basic assumption III).

Vapour Oversaturation One of the essential conditions for the CDV mechanism for reactions ending in the formation of solid products is the *presence of oversaturated vapours* of these products above the reactant surface. This becomes obvious when we compare the equilibrium vapour pressure P_{eq} for the product species at the primary stage of the CDV reaction (disregarding the condensation stage) with the saturated vapour pressure $P_{\infty}(A)$ for the solid product A. Table 2.2 illustrates this reasoning with the corresponding data calculated for some well-known decomposition reactions. This relation is apparently valid for the decomposition of *any compound* decomposed up to the solid product.

Contrary to the prevalent opinion, *the equilibrium pressure of low-volatility products at the primary stage of the CDV reactions for all compounds is actually much higher than the saturated pressure of these products.* For example, the P_{eq} values of the MgO, BaO, and CO_2 species for the decomposition of $MgCO_3$ and $BaCO_3$ at 900 K are equal to about 10^{-12} bar, which value is only 3–4 orders of magnitude less than the pressure typical for the observable onset of decomposition. At the same time, the saturated pressures for solid MgO and BaO at 900 K are only 6×10^{-28} and 6×10^{-17} bar, respectively.

For the PbC_2O_4 decomposition, the equilibrium pressures of products (PbO, CO, and O_2) in the primary stage of the CDV reaction are close to 10^{-10} bar. The 3,000-fold rise of P_{eq} value as compared with that for $Ag_2C_2O_4$ is related to the difference in the ratios (in moles) of gaseous products (CO, CO_2,

Table 2.2 Vapour oversaturation of the low-volatility products (P_{eq}/P_{∞}) in the process of CDV

Primary Stage of Decomposition	T (K)	P_{eq} (bar)	$P_{\infty}(A)^a$ (bar)	P_{eq}/P_{∞}
$Ag_2O \leftrightarrow 2Ag(g) + 1/2O_2$	500	3E–19	6E–24	5E+04
$Ag_2C_2O_4 \leftrightarrow 2Ag(g) + CO_2 + CO + 1/2O_2$	400	3E–14	4E–31	8E+16
$PbC_2O_4 \leftrightarrow PbO(g) + 2CO + 1/2O_2$	550	8E–11	3E–19	3E+08
$Zn(OH)_2 \leftrightarrow ZnO(g) + H_2O$	400	4E–25	1E–50	4E+25
$Cd(OH)_2 \leftrightarrow CdO(g) + H_2O$	400	3E–18	8E–36	4E+17
$Li_2SO_4 \cdot H_2O \leftrightarrow Li_2SO_4(g) + H_2O$	350	7E–25	2E–48	4E+23
$CaCO_3 \leftrightarrow CaO(g) + CO_2$	900	7E–17	7E–31	1E+14
$MgCO_3 \leftrightarrow MgO(g) + CO_2$	900	9E–13	6E–28	2E+15
$BaCO_3 \leftrightarrow BaO(g) + CO_2$	900	3E–12	6E–17	5E+04

^{a}A: a low-volatility product

and O_2) to low-volatility products (Ag or PbO) for these reactions (1.25 for $Ag_2C_2O_4$ and 2.5 for PbC_2O_4). "Dilution" of the vapour of the low-volatility product with stable gaseous species, in line with the corresponding thermochemical calculations, should increase the equilibrium pressure of this product. In this context, the low P_{eq} value in the Ag_2O decomposition (3×10^{-19} bar) and comparatively low value of oversaturation (5×10^4) are related to the low ratio of O_2 to Ag species (dilution factor), which is only 0.25.

When the equilibrium vapour pressure of the low-volatility products is low, the concentration of atoms or molecules is sometimes as low as a few particles per $1\,cm^3$ (four atoms of Ag in the Ag_2O decomposition) or lower. Nevertheless, being in oversaturated concentration, they should condense on the reactant surface with the possible formation of germ nuclei. The value of the equilibrium pressure of products can be used to interpret some features of this process. For example, from comparison of P_{eq} values in Table 2.2 it may be proposed that the formation of germ nuclei of Ag, in the process of Ag_2O decomposition, is more difficult and takes more time (the longer induction period) than that for $Ag_2C_2O_4$ decomposition (all other factors being equal).

Depending on the actual reactant and temperature, the magnitude of the oversaturation (P_{eq}/P_∞) varies within a very broad range. As we shall see later (Sect. 8.1), the value of P_{eq}/P_∞ accounts for the dominant contribution of the condensation energy to the enthalpy of nucleus growth.

Acceleration Nucleus growth into the reactant is conducted by the reaction localized at the product/reactant interface. Unlike the enthalpy of the decomposition reaction occurring at the free surface in the induction period (in the absence of nuclei), that of the reaction at the interface decreases because of a partial contribution of the energy released in the product condensation in this zone. This gives rise to an increase in the rate of reactant decomposition and the onset of the acceleratory period in the kinetics curve. The acceleration depends on the difference between the above enthalpies, i.e., on the condensation energy contributed to the heat of the pure vaporization process.

Reaction Localization The difference between the rates of decomposition from a free surface and at the product/reactant interface accounts also for the reaction being localized near the growth nuclei. The higher rate of decomposition at the reaction interface between two solid phases brings about an increase in particle concentration (vapour pressure) of the low-volatility product around the nucleus. This favours formation on the surface of new germ nuclei adjoining the original nucleus.

Absence of Induction and Acceleration Stages There are two types of decomposition reactions for which the stages of induction and acceleration cannot exist in principle. The first type includes those decompositions which do not produce low-volatility products, and, hence, in which the reaction interface between two solid phases is absent. The second type includes the decompositions of

Table 2.3 Interpretation of some features of decomposition kinetics

Problem	Offered Physical Explanation
Appearance of induction periods and nuclei formation stages	Condensation of oversaturated vapour of the low-volatility product on the reactant surface
Origin of the acceleratory stage of decomposition	Decrease of the enthalpy of nuclei growth in comparison with their formation enthalpy, due to the enthalpy of condensation
Localization of reaction	Additional vapour oversaturation near to growing nuclei
The absence of an induction period and/or an acceleratory stage for some reactions	Absence of low-volatility products of decomposition, melting of reagent prior to the beginning of decomposition

melts, in which such reaction zones cannot form because of the melting of the reactant. Our studies (Part III) of the decompositions of some oxides (HgO, CdO, and ZnO) and nitrides (Mg_3N_2, AlN, GaN, InN, and Si_3N_4), which decompose completely to gaseous products, as well as an analysis of literature data, support this conclusion. The kinetics curves of MgH_2, HgO, HgC_2O_4, NH_4IO_3, and NH_4NO_3 were found [5, 6] to satisfy the equation of a contracting sphere. Silver azide, which melts at 523 K [5], and melts of the silver and cadmium nitrates with melting temperatures of 483 and 633 K, respectively, (see Sect. 8.3) decompose in the same way.

Kinetics curves may often lack, or have barely discernible, induction and acceleration stages, even in the presence of low-volatility products. This can sometimes be achieved by accelerating the slowest stage of the decomposition by creating artificial nuclei of the solid phase by mixing and grinding preliminarily the powders of the reactant and the product (e.g., Ag_2O and Ag [26]). A still more efficient way is to coat Ag_2O particles with a silver film by deposition from metal vapour [26]. With crystalline hydrates, one can reach the same goal by degrading mechanically the surface (for instance, by treating the surface of a single-crystal of $Li_2SO_4 \cdot H_2O$ with an abrasive [27]).

The thermochemical approach thus offers the possibility of interpreting all of the above features, which for many years have been remaining blanks in the decomposition kinetics of solids. For clarity, the main points discussed in this section are summarized in Table 2.3. The phenomena associated with nucleation from oversaturated vapour are examined in Sects. 2.5 and 2.6, and with the effect of oversaturation on the enthalpy of the decomposition process in Sect. 8.1.

2.5 Shape and Position of the Nucleus

One of the simplest and most convincing arguments for or against the CDV mechanism being developed here should be the position of the germ nucleus on the reactant surface. According to the prevailing concept: "The germ nucleus

may be defined as a small particle of the product phase *embedded* (our italics) in reactant. ... The transformation yielding a germ nucleus is usually identified with a change in crystal structure. ... The product effectively occupies the volume formerly filled with reactant" [28] so that, as it was stated earlier [6], "the nucleation process involves conversion of a small volume of reactant into a stable particle of product".

An obvious consequence of the CDV mechanism and of nucleation through condensation of oversaturated vapour of a low-volatility product is that germ nuclei form *on the surface* rather than inside the reactant. Hence, to substantiate the validity of a mechanism, one has to analyse the results accumulated in the literature on studies of nucleation by optical and scanning electron microscopy. Universally recognized in this area are studies carried out by Garner with followers in the 1930s–1960s and Galwey with colleagues in the 1970s–1990s, which are summarized partially in monographs [5] and [6, 25], respectively.

Garner et al. [5] obtained many excellent optical microscopic images of the nuclei forming in the course of decomposition of crystalline hydrates of various salts. (Remarkably, the nuclei frequently resemble in shape crystals crystallizing out of *oversaturated solution*. This could be support for formation of germ nuclei through condensation of oversaturated vapour). For alums [29, 30], the nuclei appear as rounded-off hemispheres with a slight pit at the centre and uneven edges (see Fig. 2.7). The most important observation is,
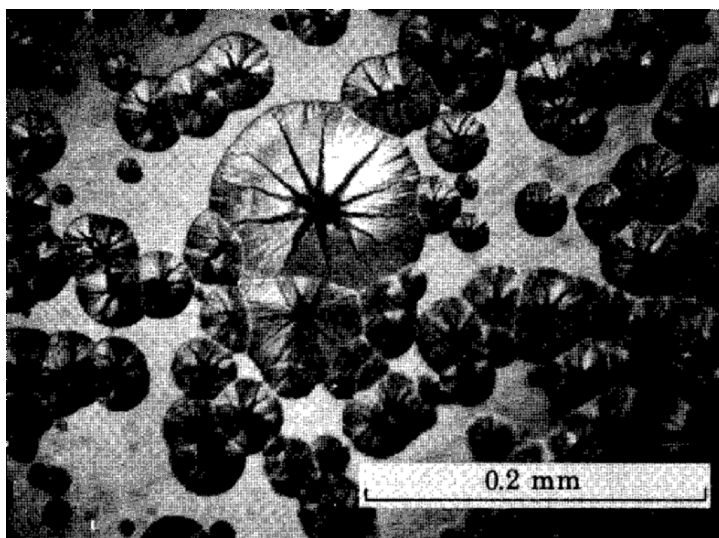
Fig. 2.7 A photomicrograph of typical nuclei formed on a surface of an alum crystal $KCr(SO_4)_2 \cdot 12H_2O$. (Reprinted from [30], with permission)

Nucleus

Azide crystal
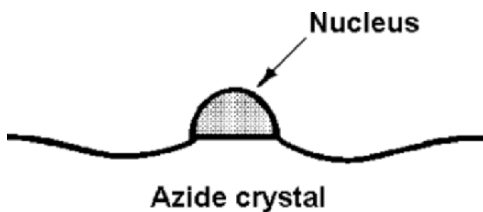
Fig. 2.8 A view of a nucleus on a surface of barium azide. (Reproduced from [31], with permission.)

however, that "the nuclei are always formed on the surface, never within the solid phase" [29].

Studies of the barium azide decomposition led Mott [31] to the same conclusion "that nuclei are probably formed only at surfaces and that they grow outwards". As a result of material loss, a pit forms on the surface around the nucleus, as shown in the figure from a study by Mott (Fig. 2.8). Formation of a small pit in the upper part of the nucleus is most probably associated with the dynamics of transport and condensation of decomposition products on a hemispherical surface. Galwey et al. [30], in full agreement with the above observations [29, 30] and in conflict with the definition of the nucleus given in [6, 28], point out (for the alum decomposition) that "the first stage is the appearance on the crystal surface of a small mound (*ca.* 5 μm diameter) with central pitting". Later Galwey et al. [32] have shown that randomly distributed product particles of 0.2–1.0 μm, with rounded corners and sometimes equidimensional, were observed on the original surface of single crystals of $Li_2SO_4 \cdot H_2O$.

The nuclei formed in the decomposition of some substances, for example, of potassium permanganate, are spherical, 1–2 μm in diameter [33]. Each nucleus sits in a small pit on the crystal surface and represents a complex aggregate of smaller, ring-shaped crystals (Fig. 2.9).

That these nuclei were formed by condensation, is corroborated by the knotty spherical formations, practically identical in shape, that appear in condensation of carbon vapour on the cooler parts of graphite tubes used in electrothermal AAS [34]. Another feature accompanying the nucleation in the decomposition of $KMnO_4$ consists in the formation of a thin layer of the product (0.1–0.2 μm thick) coating uniformly the whole surface of the crystal. At the slightest touch it breaks up and flakes off. It grows, most probably, under intensive condensation of gaseous products during the reactor cooling (at the end of the treatment period at 500 K). The "unmodified" (perhaps, amorphous) character of this film is accounted for, as will be shown below (Sect. 2.6), by the high vapour oversaturation at the moment of condensation. Combination of all the above observations leaves no place for doubt that *the germ nuclei form on the surface rather than inside the reactant body.*
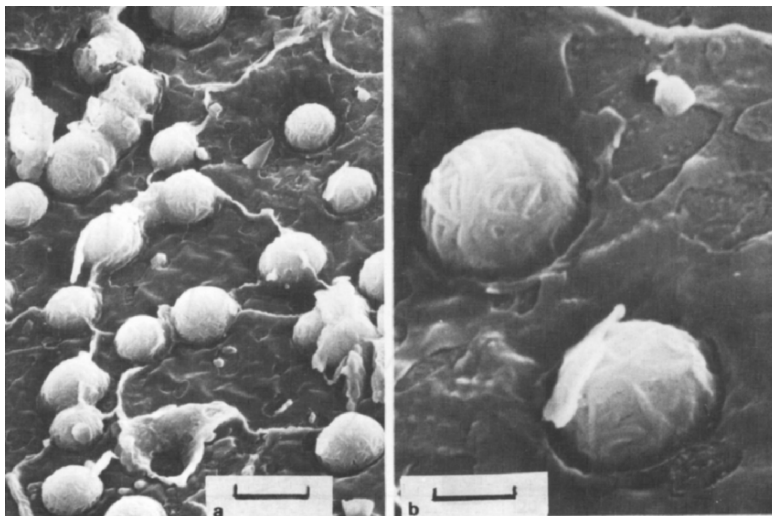
Fig. 2.9 An electron micrograph of a surface of partially decomposed $KMnO_4$ ($\alpha = 0.05$) at $500\,K$ (after removal of the superficial film of product). The scale bar is (a) $3\,\mu m$ and (b) $1\,\mu m$. (Reprinted from [33], with permission)

2.6 Structure and Composition of the Solid Product

Product Structure A feature frequently observed in the decomposition of crystalline hydrates, which has not yet been given a convincing interpretation in the framework of universally accepted ideas, is the formation of solid products in either an amorphous or a crystalline state, depending on the actual water vapour pressure in the reactor. This phenomenon was observed by Kohlschütter and Nitschmann in 1931 [35] and has been the subject of numerous publications, including the study of Volmer and Seydel [36], who used it as a basis for explaining the Topley–Smith (T–S) effect, and a series of articles by Frost et al. [37–39]. Dehydration of many crystalline hydrates in vacuum entails formation of an X-ray amorphous (finely dispersed) residue and, in the presence of water vapour, formation of a crystalline product. The highest H_2O pressure at which an amorphous product can still form varies for different hydrates from a few tenths to a few Torr (Table 2.4). As the decomposition temperature increases, the boundary of formation of the crystalline product shifts towards higher H_2O pressures.

Most of the researchers [36–39] attribute this effect to accelerated recrystallization of the dehydrated amorphous product initiated by the presence of water vapour, although the mechanism responsible for this influence is far from being obvious.

It appears much simpler to explain the differences in formation of the X-ray amorphous and crystalline products as due to a change of the real temperature

Table 2.4 Maximum pressure of H_2O vapour that corresponds
to the formation of amorphous product [38]

Hydrate	Temperature (°C)	Pressure (Torr)
$MnC_2O_4 \cdot 2H_2O$	60	0.2
$CuSO_4 \cdot 5H_2O$	40	0.25
$MnSO_4 \cdot 4H_2O$	50	1.2
$ZnSO_4 \cdot 7H_2O$	40	1.5
$NiSO_4 \cdot 6H_2O$	60	2.0
$MgSO_4 \cdot 7H_2O$	40	4.5
$MgSO_4 \cdot 7H_2O$	50	8.0
$MgSO_4 \cdot 7H_2O$	60	12.5

of the crystalline hydrate at the instant of decomposition and the accompanying differences in vapour oversaturation. Although the reactor temperature is maintained constant in experiments on dehydration in the presence of water vapour, the temperatures of the hydrate decomposing in vacuum and in the presence of water vapour may differ by ten or more degrees because of the intense self-cooling of the hydrate (see Sects. 6.4 and 7.2).

We assume that the differences in formation of the condensates with different structures (or, to be exact, of crystallites differing in size) are determined by the degree of oversaturation of the vapour of the condensing substance, which can be defined as the ratio of the real pressure of a substance, P, to that of the saturated pressure, $P_\infty(T)$, for this substance:

$$S \equiv P/P_\infty(T) \tag{2.5}$$

In connection with this assumption, one can refer to the Gibbs–Thomson equation:

$$\ln S = \frac{2M\gamma}{RT\rho r} \tag{2.6}$$

which is valid for drops of a liquid with a molar mass, M, surface tension, γ, and density, ρ, in equilibrium with oversaturated vapour. The magnitude of oversaturation can be identified with a certain critical radius, r, of the primary condensation nuclei. This equation shows that the critical radius of particles decreases with increasing oversaturation, but does not predict the final size of particles of the solid product forming under the conditions of dissociative vaporization and condensation of a product, which are rather far from those of equilibrium between oversaturated vapour and liquid drops. It suggests, however, that the dependence of particles size on vapour oversaturation is a feature common to these processes.

The effect of this factor on the size of particles formed in the process of chemical vapour condensation has been reliably established. For instance, in the decomposition of iron pentacarbonil $Fe(CO)_5$ in Ar atmosphere, the average size of the iron particles doubles (from 12 to 25 nm) with increasing decomposition temperature from 400 to $1,100\,°C$ [40]. The saturation pressure

of iron vapour increases in this temperature interval by about 14 orders of magnitude.

The above-listed features of the formation of X-ray amorphous and crystalline products are observed in the decompositions of many other compounds. Haul and Schöning [41] applied an X-ray method (line-width technique) to study the structure of the decomposition products of dolomite as a function of temperature. The experiments were carried out both in vacuum and in a CO_2 environment. In vacuum, decomposition proceeded to the CaO and MgO oxides, and in a CO_2 environment, to $CaCO_3$ and MgO. This difference is reasonable. It originates from the calcium carbonate being more stable than the magnesium carbonate (the enthalpies of formation of $CaCO_3$ and $MgCO_3$ at 800 K are $-1,154$ and $-1,045$ kJ mol^{-1}, respectively). The size of the crystallites formed in vacuum [41] increased monotonically from 6 nm for MgO and 13 nm for CaO to 120–140 nm with the temperature increasing within the range 700–1,000° C. (Oversaturation decreases in these conditions from 10^{16} to 10^8 for MgO, and from 10^{19} to 10^{11} for CaO.)

Searcy and colleagues [42–44] observed that the decompositions of magnesium hydroxide, and magnesium and barium carbonates obeyed the same relations. The MgO residue obtained after decomposition of $Mg(OH)_2$ and $Mg(CO_3)_2$ (at 540 and 675 K, respectively) was a high-porosity X-ray amorphous product which partially retained (as in epitaxial deposition) the structure of the primary materials. The size of the MgO cubic particles measured by transmission electron microscopy was found to be, accordingly, 2 and 3 nm [42]. In contrast to MgO, the barium oxide obtained in the decomposition of $BaCO_3$ exhibited a clearly pronounced NaCl crystal structure [44]. These differences in structure are compared in Table 2.5 with the oversaturation magnitudes for MgO and BaO vapours for the decompositions of $Mg(OH)_2$, $MgCO_3$, and $BaCO_3$. The table also contains similar data obtained for $CaCO_3$ and talc $(3MgO \cdot 4SiO_2 \cdot H_2O)$.

As seen from the table, oversaturation turns out to be significantly lower for the $BaCO_3$ decomposition than in all other cases. This accounts for the formation of crystalline BaO rather than amorphous products under these conditions. The above differences in MgO crystallite size, a factor of 1.5 between $MgCO_3$ and $Mg(OH)_2$, and of 2.0 between $CaMg(CO_3)_2$ [41] and $MgCO_3$ [42], fit the difference in the magnitude of oversaturation.

Table 2.5 Crystal structure of the product and vapour oversaturation in the process of decomposition of some carbonates and hydroxides

Reactant	Product	Structure	T(K)	$\log S$	Ref.
$BaCO_3$	BaO	Crystal	1,080	4.6	[44]
$3MgO \cdot 4SiO_2 \cdot H_2O$	SiO_2	Amorphous	1,200	8.2	[45]
$CaCO_3$	CaO	Amorphous	800	27.0	[43]
$MgCO_3$	MgO	Amorphous	675	31.7	[42]
$Mg(OH)_2$	MgO	Amorphous	540	43.9	[42]

Product Composition From the CDV standpoint, the formation of solid products in the decomposition of talc is of particular interest. This reaction was shown to produce two solid products, enstatite ($MgSiO_3$) and an amorphous form of SiO_2 [45–48]. Following the CDV approach, these products may be considered as resulting from primary congruent vaporization of talc with subsequent condensation of MgO and SiO_2 vapours [49]:

$$3MgO \cdot 4SiO_2 \cdot H_2O(s) \leftrightarrow 3MgO(g) + 4SiO_2(g) + H_2O \rightarrow$$

$$\rightarrow 3MgSiO_3(s) + SiO_2(s) + H_2O \tag{2.7}$$
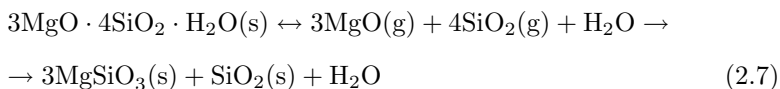
The enthalpy of formation of enstatite ($-1,548.9\,\text{kJ mol}^{-1}$) is less than the total enthalpy of formation of the MgO and SiO_2 oxides ($-1,512.2\,\text{kJ mol}^{-1}$). Therefore, formation of a more stable product in condensation of vapours appears reasonable. There is nothing unexpected either in condensation of the excess SiO_2 molecules (above the MgO molecules present) in the form of an X-ray amorphous residue, considering the fairly high oversaturation of SiO_2 vapour (see Table 2.5).

Thus, the CDV mechanism offers a possibility of interpreting, within a common physical framework, the results obtained for widely diverse decomposition reactions, which proceed under widely differing conditions.

2.7 Thermal Stability of Complex Gaseous Molecules

This discussion would be incomplete if we did not consider one of the arguments against extending the CDV mechanism to thermal decomposition of any compound. This is the allegedly low probability of the existence in the gaseous phase of complex molecules, in particular, of those metal salts produced in the thermal decomposition of crystalline hydrates. The thermal stability of these compounds is believed to be so low as to make the presence of their vapours at the decomposition temperatures hardly probable. This belief is, however, dispelled by MS observations accumulated in the recent three decades [50–57].

In his recently published monograph, "Vaporization Thermodynamics of Double Oxides", Kazenas [57] presents a wealth of collected, systematized, and generalized material on the vapour pressure and composition of metal borates, aluminates, carbonates, silicates, nitrates, sulphates, phosphates, chromates, and other double oxides. This material is based on studies by Kazenas and his group and the results reported in the literature. In a foreword to this book, Kazenas [57] claims: "Observation of new types of molecules completely disproved the view on the high-temperature vapour as a medium which is poor in molecular forms. It has been established, in particular, that the molecular composition of the vapour phase for many chemical compounds is more complex and diverse than it was assumed earlier." By the use of effusion MS,

many molecules were revealed and thermodynamically described at about
1,000–1,500 K. Among them are, for example, molecules of alkaline metals:
MBO_2, M_2CO_3, M_2SiO_3, MNO_3, MPO_3, $M(PO_3)_3$, M_2SO_4, MOH, M_2CrO_4,
M_2MoO_4, M_2WO_4, and $MReO_4$. It should be noted that effusion MS does not
allow one to study the vapour composition at low temperatures typical of the
decomposition of hydrates. However, in principle, the stability of molecules at
lower temperatures should only increase.

MS with free-surface vaporization (after Langmuir) is undoubtedly the most
efficient way for direct study of the composition of the gaseous phase, par-
ticularly, in the decomposition of melts, in the absence of a layer of solid
phase interfering with the escape of vapours of low-volatility products from
the reactant surface. As an illustration, we present in Fig. 2.10 a quadrupole
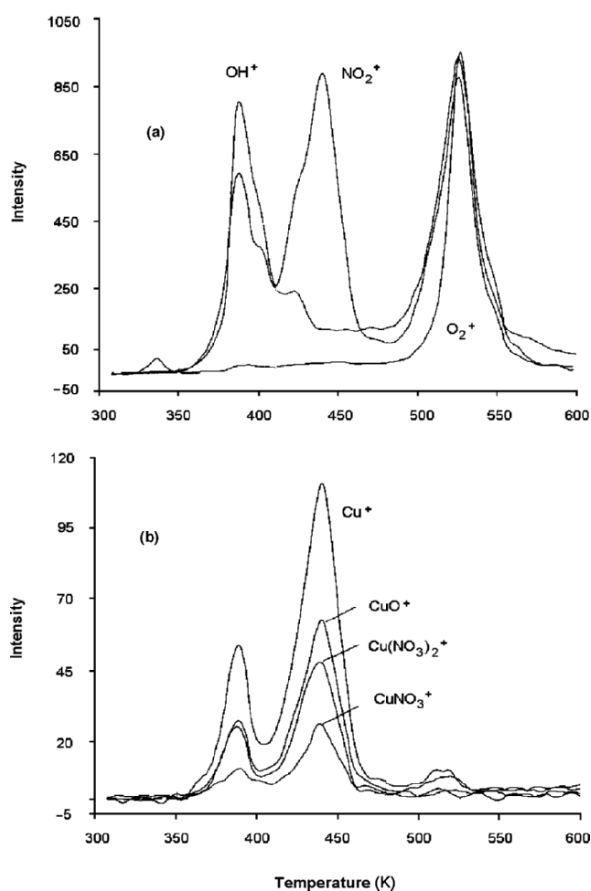

Fig. 2.10 Mass intensity signals for the decomposition of 12 µg of $Cu(NO_3)_2 \cdot 3H_2O$ heated
at $1\,K\,s^{-1}$ on a graphite platform: (a) volatile and (b) non-volatile species. (Reproduced
from [19], with permission.)

MS recording of the vapour composition obtained in the process of dehydration of $Cu(NO_3)_2 \cdot 3H_2O$ [19].

It is easy to see that two-stage decomposition of the hydrate with a melting point of $387\,K$ is accompanied by the appearance of $Cu(NO_3)_2$ molecules, as well as of their fragmentation products ($CuNO_3$, CuO, and Cu). It is a pity that this variant of MS is applied for these purposes on much fewer occasions than it certainly should.[a]

2.8 Conclusions

The above arguments in support of the CDV mechanism are based partially on experimental observations, and partially, on theoretical considerations. Among the most reliable experimental observations are the direct mass-spectrometry detection of gaseous low-volatility products over decomposing compounds (Sect. 2.3), and optical and electron microscopic investigation of the shape and position of nuclei on the reactant surface (Sect. 2.5). The most convincing theoretical arguments include the interpretation of the shape of kinetics curves $\alpha = f(t)$ and, particularly, substantiation of the mechanism of nucleation initiated by the appearance above the reactant surface of oversaturated vapour of a low-volatility product (Sect. 2.4). To our knowledge, this phenomenon was first revealed and discussed in this work.

The effect of the degree of vapour oversaturation on the particle size of the product and its solid structure certainly deserves further study. While the correlation revealed fits the present theory, the material accumulated does not appear sufficient to warrant a reliable quantitative analysis.

References

1. Boldyrev VV (1963) Impact of crystal defects on the rate of thermal decomposition of solids. Tomsk University Press, Tomsk (in Russian)
2. Boldyrev VV (1997) Reactivity of solids (on the example of thermal decomposition reactions). Siberian Branch Russian Academy of Science, Novosibirsk (in Russian)
3. Somorjai GA, Lester JE (1967) Evaporation mechanism of solids. In: Reiss H (ed) Progress in solid state chemistry. Pergamon, Oxford, pp 1–52
4. Knudsen M (1915) Ann. Phys (Leipzig) 47:697–700
5. Garner WE (1955) (ed) Chemistry of the solid state. Butterworths, London
6. Galwey AK, Dollimore D, Brown ME (1980) Reactions in the solid state. Elsevier, Amsterdam
7. Prodan EA, Pavlyuchenko MM, Prodan SA (1976) Regularities of topochemical reactions. Nauka Tekhnika, Minsk (in Russian)
8. Harano Y (1961) Nippon Kagaku Zasshi 82:152–155

---

[a]The coupled STA409 CD-QMS 403/5 thermal analyzer (Netzsch) is suitable for these studies providing a vacuum in the sample compartment is $<10^{-4}$ bar.

9. L'vov BV (1991) Evaporation, thermal dissociation, carbothermal reduction and thermal decomposition of substances. A general approach to the theoretical calculation of kinetics. Invited lecture at the XXVII CSI, Bergen, Norway. Book of Abstracts, A-5.2
10. Sturgeon RE, Mitchell DF, Berman SS (1983) Anal Chem 55:1059–1064
11. Bass DA, Holcombe JA (1987) Anal Chem 59:974–980
12. Dressler MS, Holcombe JA (1987) Spectrochim Acta B 42:981–994
13. Ham NS, McAllister T (1988) Spectrochim Acta B 43:789–797
14. Wang P, Majidi V, Holcombe JA (1989) Anal Chem 61:2652–2658
15. Hassell DC, Majidi V, Holcombe JA (1991) J Anal At Spectrom 6:105–108
16. Prell LJ, Styris DL, Redfield DA (1991) J Anal At Spectrom 5:25–32
17. Fonseca RW, Wolfe KI, Holcombe JA (1994) Spectrochim Acta B 49:411–429
18. L'vov BV, Novichikhin AV (1995) Spectrochim Acta B 50:1427–1448
19. L'vov BV, Novichikhin AV (1995) Spectrochim Acta B 50:1459–1468
20. Prodan EA, Pavlyuchenko MM (1965) (eds) Heterogeneous chemical reactions. Nauka Tekhnika, Minsk (in Russian)
21. Young DA (1966) Decomposition of solids. Pergamon, Oxford
22. Delmon B (1969) Introduction a la cinétique hétérogène. Technip, Paris
23. Jacobs PWM (1997) J Phys Chem 101:10086–10093
24. Barret P (1975) (ed) Reaction kinetics in heterogeneous chemical systems. Elsevier, Amsterdam
25. Galwey AK, Brown ME (1999) Thermal decomposition of ionic solids. Elsevier, Amsterdam
26. Dubinin MM, Kadlec O, Ponec B (1967) Kinet Katal 8:292–298 (in Russian)
27. Modestov AN, Poplaukhin PV, Lyakhov NZ (2001) J Therm Anal Cal 65:121–130
28. Galwey AK, Laverty GM (1990) Solid State Ionics 38:155–162
29. Cooper JA, Garner WE (1936) Trans Faraday Soc 32:1739–1744
30. Galwey AK, Spinicci R, Guarini GGT (1981) Proc Roy Soc A378:477–505
31. Mott NF (1939) Proc Roy Soc A172:325–335
32. Galwey AK, Koga N, Tanaka H (1990) J Chem Soc Faraday Trans 86:531–537
33. Brown ME, Galwey AK, Mohamed MA, Tanaka H (1994) Thermochim Acta 235: 255–270
34. Welz B, Schlemmer G, Ortner HM, Wegscheider W (1989) Prog Anal Spectrosc 12: 111–245
35. Kohlschütter V, Nitschmann H (1931) Z Phys Chem Bodenstein Festband 494–509
36. Volmer M, Seydel G (1937) Z Phys Chem A179:153–171
37. Frost GB, Moon KA, Tompkins EH (1951) Can J Chem 29:605–632
38. Frost GB, Campbell RA (1953) Can J Chem 31:107–119
39. Quinn HW, Missen RW, Frost GB (1955) Can J Chem 33:286–297
40. Choi CJ, Tolochko O, Kim BK (2002) Mat Lett 56: 289–294
41. Haul RAW, Schöning FRL (1952) Z Anorg Allg Chem 269:120–134
42. Kim MG, Dahmen U, Searcy AW (1987) J Am Ceram Soc 70:146–154
43. Ewing J, Beruto D, Searcy AW (1979) J Am Ceram Soc 62:580–584
44. Basu TK, Searcy AW (1976) J Chem Soc Faraday Trans I 72:1889–1895
45. Elwell RH, Bunting EN, Geller RF (1935) J Res Nat Bur Stand 15:551–556
46. Daw JD, Nicholson PS, Embury JD (1972) J Am Ceram Soc 55:149–151
47. Ward JR (1975) Thermochim Acta 13:7–14
48. MacKenzie KJD, Meinhold RH (1994) Thermochim Acta 244:195–203
49. L'vov BV, Ugolkov VL (2004) Thermochim Acta 413:7–15
50. Semenov GA, Nikolaev EN, Frantseva KE (1976) Application of mass spectrometry in inorganic chemistry. Khimiya, Leningrad (in Russian)
51. Kazenas YeK, Chizhikov DM (1976) Vapour pressure and composition under oxides of chemical elements. Nauka, Moscow (in Russian)
52. Gingerich KA (1980) Curr Top Mat Sci 6:345–462

53. Sidorov LN, Korobov MB, Zhuravleva LV (1985) Mass spectrometry thermodynamic investigations. Moscow University Press, Moscow (in Russian)
54. Semenov GA, Stolyarova VA (1990) Mass spectrometry study of vaporization of oxide systems. Nauka, Leningrad (in Russian)
55. Hilpert K (1990) Structure and Bonding 73: 99–198
56. Kazenas YeK, Tsvetkov YuV (1997) Vaporization of oxides. Nauka, Moscow (in Russian)
57. Kazenas YeK (2004) Vaporization thermodynamics of double oxides. Nauka, Moscow (in Russian)

Chapter 3
Decomposition Kinetics

3.1 Preliminary Remarks

By the kinetic description of decomposition reactions of solids one usually understands analysis of isothermal $\alpha - t$ curves which characterize the evolution of the degree of decomposition of the reactant (or of the product yield) α with time t. Such an analysis reduces essentially to choosing the equation that fits best the real kinetic curves. The set of equations derived from different models describing the mechanisms of separate stages (induction, acceleration, and deceleration), or of their combination, is well known and provides a basis for what is presently called formal kinetics [1–8]. The information obtained in this way on the contribution of these stages to the observed kinetics is used to develop mechanisms and schemes for the evolution of the decomposition process with time. This approach is not capable, however, of yielding any data on the thermochemical characteristics of a reaction (including the composition and stoichiometry of the products, the enthalpy and the entropy of the process) and on how the decomposition rate is affected by experimental conditions, such as the temperature and the presence of gaseous products in the reaction system.

Two approaches can be employed to take into account the effect of temperature on the decomposition rate. One of them (dominating in solid-state kinetics) is based on the Arrhenius idea that only "active" particles are involved in a reaction, whose fraction depends exponentially on the temperature and the height of the energy barrier in the reaction course, and the other (advanced by Hertz and further developed by Langmuir), on the dependence of the maximum vaporization rate of a substance from a free surface on its equilibrium vapour pressure. Both approaches fit equally well the exponential dependence of the decomposition rate on temperature, which was substantiated thermodynamically by van't Hoff (see below). Both these approaches are considered in more detail below.

3.2 The Arrhenius Equation

Van't Hoff's Contribution A close examination of the history of the appearance and subsequent development of the Arrhenius equation [9], which forms the basis for chemical kinetics, suggests that its formulation was initiated to a large extent by the fundamental treatise of van't Hoff [10] published in 1884. Van't Hoff showed that the equilibrium constant, K, of a reaction is related to temperature, T, and heat of the reaction, ΔH_T, through the relationship that is known as the van't Hoff equation

$$\frac{d \ln K}{dT} = \frac{\Delta H_T}{RT^2} \tag{3.1}$$

From here, it follows, as pointed out by van't Hoff, that because the equilibrium constant K is the ratio of the rate constants k_1 and k_{-1} in the direct and reverse directions, these constants should obey a similar equation, i.e.,

$$\frac{d \ln k}{dT} = \frac{E}{RT^2} \tag{3.2}$$

where E is a quantity that possibly depends on temperature. It thus follows that

$$k = A \exp(-E/RT) \tag{3.3}$$

Van't Hoff was thus the first to formulate and substantiate thermodynamically the exponential dependence of the reaction rate on temperature and Eqs. (3.2) and (3.3) could, justifiably, have been called the van't Hoff equations.

Arrhenius's Contribution In 1889, in the process of studying the rate of hydrolysis (inversion) of sugar cane by mineral acids, Arrhenius discovered that the effect of temperature on the rate was too high to be accounted for by a variation of translational energy of molecules or by the viscosity of the medium [11]. This observation led him to the conclusion that there are inactive (normal) and active molecules directly involved in a reaction and that these are in a sort of equilibrium. This equilibrium shifts with temperature in accordance with the exponential dependence predicted earlier by van't Hoff. This interpretation was presumably prompted by a paper of the Austrian physicist Pfaundler [12] published in 1867 and now practically forgotten, which discussed the effect of temperature on the exponential Maxwellian distribution of molecule velocities. One should not overlook, in this connection, the possible role of personal acquaintance and contacts with Boltzmann during the stay of Arrhenius at Boltzmann's laboratory (University of Gratz) in April 1887. Be it as it may, the exponential dependence of the reaction rate on temperature supported with this simple and convincing interpretation was assigned to Arrhenius and Eq. 3.3 was named the Arrhenius equation.

Validating the Arrhenius Equation This equation did not receive immediate recognition. In 1899, Bodenstein [13] published a series of papers bearing a common title "Gasreaktionen in der chemischen Kinetik". In a comprehensive study of the decomposition and formation reactions of HI, H_2S, H_2Se, and H_2O conducted at different temperatures, he showed convincingly that they obeyed the van't Hoff–Arrhenius theory.

As for the solid-state reactions, the Arrhenius concept on "active" particles was first used apparently only in 1921 in a paper by Hinshelwood and Bowen [14] entitled "The influence of physical conditions on the velocity of decomposition of certain crystalline solids". In 1926, a paper by Bružs [15] dealing with decomposition of the carbonates appeared, in which the Arrhenius equation was presented in its universally accepted form. Note that this equation was transferred from homogeneous to heterogeneous kinetics without any sound

theoretical substantiation. As a result, the interpretation of the parameter A as the frequency of molecular collisions along the course of reaction, which is accepted in the kinetics of homogeneous reactions, turned out to be devoid of any physical meaning.

Subsequent attempts at theoretical validation of the Arrhenius equation as applied to solid-state decompositions did not meet with much success. This relates both to the Polanyi–Wigner equation [16] and its later modifications based on the theory of the transition state (or the theory of absolute reaction rate) developed by Eyring [17], and Evans and Polanyi [18]. Application of these equations does not yield any significant results, except possibly rather rough theoretical estimates of the pre-exponential factor [6, 8]. Nevertheless, the Arrhenius equation, taken in its classical form, still remains the most widespread approach in estimating the effect of temperature on the rate of solid-state reactions through determination of the parameter E, the activation energy or the energy barrier in the reaction course. Its magnitude is assumed to be equal to, or above, the molar enthalpy of a reaction. Under some conditions, however, parameter E turns out to be smaller than the molar enthalpy [8]. Such reactions refer to multistage processes under the assumption (somewhat more than questionable, in our opinion) that their resultant rate is dominated by stages that do not depend on the molar enthalpy.

3.3   The Hertz–Langmuir Equation and Langmuir Diffusion Equations

Vaporization in Vacuum   In 1882, Heinrich Hertz, at the age of 25, published a paper [19] dealing with a study of the vaporization rate of mercury in vacuum and a comparison of the experimental data obtained with theory. Hertz apparently recognized the difficulties encountered in a direct theoretical calculation of the vaporization rate (the experience accumulated over more than a century of research in this area is in agreement with this appraisal). Therefore he decided, instead, to calculate the maximum rate of the reverse process, i.e., the condensation of vapour. A theoretical analysis and comparison with the experiments conducted by Hertz led to two fundamental conclusions. First, every substance has a maximum rate of evaporation which is dependent only upon the surface temperature and the properties of the substance; and, second, the maximum rate of evaporation cannot exceed the number of molecules from the vapour phase that are incident upon the surface of the condensate when equilibrium conditions are established.

The investigations of Hertz were given a new impetus only a few decades later in the studies of Knudsen [20] and Langmuir [21]. The interest of Knudsen in vaporization was prompted by his studies of thermal conductivity and rarefied gas flow, as well as by the possibility of development of the effusion

method for the determination of equilibrium vapour pressures. Langmuir addressed the vaporization problem by studying the volatility of tungsten in vacuum and its interaction with oxygen. In their work, both scientists referred to the fundamental paper of Hertz [19].

The condensation rate can be calculated readily from the kinetic theory of gases (see, e.g., [22]). Following the reasoning of Hertz, Knudsen, and Langmuir, it is determined by the number of molecules in the gas phase, which collide per unit time with the condensate surface (of unit area):

$$J_{\text{molecule}} = c_{\text{eq}}\bar{u}/4 \tag{3.4}$$

where c_{eq} is the equilibrium concentration of molecules per unit volume, and $\bar{u}$ is the average velocity of molecules of molar mass M defined as

$$\bar{u} = [8RT/(\pi M)]^{1/2} \tag{3.5}$$

Here R is the gas constant and T is the absolute temperature.

The equilibrium concentration of molecules can be replaced by the equilibrium pressure using the Clapeyron–Mendeleev equation

$$c_{\text{eq}} = \frac{N_{\text{A}} P_{\text{eq}}}{RT} \tag{3.6}$$

where N_{A} is the Avogadro constant. Substituting Eqs. 3.5 and 3.6 in Eq. 3.4

$$J_{\text{molecule}} = \frac{N_{\text{A}} P_{\text{eq}}}{(2\pi MRT)^{1/2}} \tag{3.7}$$

This relation, derived by Langmuir [21] in the form presented here, is properly called the Hertz–Langmuir equation.

Vaporization in a Foreign Gas In addition to the case of vaporization in vacuum, Langmuir derived two other equations for the rate of vaporization in a foreign gas [23]. In a foreign gas environment, the vaporization rate is limited by the diffusion of molecules from the near-surface layer. The thickness of this layer is approximately equal to the mean free-path length, and the molecules in the layer are in their equilibrium concentration. These assumptions are validated by methods of statistical mechanics. Invoking the Fick's first law for one-dimensional diffusion and the Clapeyron–Mendeleev equation, the molecular flux is

$$J_{\text{molecule}} = \frac{c_{\text{eq}} D}{z} = \frac{N_{\text{A}} D P_{\text{eq}}}{zRT} \tag{3.8}$$

Here D is the diffusion coefficient, and z is the distance from the vaporization surface to the sink where the concentration of the product molecules becomes zero. This relation was subsequently called the one-dimensional diffusion equation of Langmuir [23]. For vaporization of a single spherical particle of radius r, Eq. 3.8 can be recast in the form [23]

$$J_{\text{molecule}} = \frac{N_{\text{A}} D P_{\text{eq}}}{rRT} \tag{3.9}$$

Equations 3.7–3.9 will be referred to in this text as the Langmuir vaporization equations.

Advantages of the Langmuir Vaporization Equations A comprehensive analysis of these equations lead us to the following conclusions.

- There are no fundamental reasons that could prevent the application of these vaporization equations to cases of thermal decomposition (dissociative vaporization) of a substance, except for the requirement that the rate J must be measured under a steady-state decomposition mode, corresponding to the deceleratory period in the $\alpha - t$ kinetic curve.
- All the quantities and parameters entering the vaporization equations have a simple physical meaning and can be quantitatively characterized.
- The vaporization equations satisfy the exponential dependence of the decomposition rate on temperature, substantiated thermodynamically by van't Hoff, provided that the exponential temperature dependence of the equilibrium pressure of decomposition products is taken into account.
- The vaporization equations permit determination of absolute values of the equilibrium partial pressures of decomposition products, P_{eq}, which are directly related to the thermodynamic characteristics (enthalpy and entropy) of the reaction, or calculation of absolute values of the decomposition rates through the available thermodynamic characteristics of the reaction.
- The vaporization equations are applicable to measurements both in vacuum and in the presence of foreign gases (provided that these gases are inert to both the reactant and the decomposition products).
- In some cases, the vaporization equations may require modification to account for the formation of more than one gaseous product in the course of decomposition.

Equilibrium Concept in Vaporization Kinetics Prior to further discussion of the vaporization equations, it is appropriate to comment on the application of the concepts of equilibrium and of the equilibrium pressure to kinetics. The existence of real equilibrium during the course of decomposition, as well as of decomposition under equilibrium conditions (particularly in a high vacuum), is out of the question. Both concepts are employed rather as categories applied to conceivable situations, in which the direct and the reverse processes (i.e., the vaporization and the condensation) are in a state of equilibrium, thus validating the estimation of the vaporization rate through the rate of the reverse process. For this reason, in describing the decomposition rate the term *equivalent* pressure is sometimes used.

Unlike true thermodynamic equilibrium, in which the multistage character of a process does not have any importance, in kinetics the resultant rate of a multistage reaction mechanism depends on the rates of all the constituent stages and is limited by that of the slowest stage. The CDV mechanism

assumes that the decomposition process consists of two stages, which include, in the general case, dissociative vaporization of the reactant into primary gaseous products, which may differ from their equilibrium forms, with subsequent formation of final (equilibrium) products in recombination or condensation of non-equilibrium primary components. Theoretical calculation of the rate of the primary (slowest) stage of the process assumes an imaginary analysis of the equilibrium existing between the reactant and the primary products of dissociative vaporization. This concept of equilibrium differs from its universally accepted counterpart and requires the introduction of a different term, *equilibrium of the primary stage.*

The term "equilibrium pressure" likewise seems somewhat out of place in kinetics. This quantity appears when the flow rate of products escaping from the reactant surface is estimated from the condensation rate of these products on the reactant surface under the conditions of imaginary equilibrium between these processes. Considered in the frame of the CDV mechanism, the condensation rate is governed by the equilibrium pressure of the primary products. Therefore, the equilibrium pressure (P_{eq}), a term of a general nature customarily identified with equilibrium of final decomposition products, should in this case (i.e., of vaporization from a free surface) be replaced with *equilibrium pressure of primary products* and denoted by P_{eqp}.

3.4 Modification of the Hertz–Langmuir Equation as Applied to Decomposition Reactions

Consider first the form of the Hertz–Langmuir equation for the particular case of decomposition of reactant R in vacuum into gaseous products A and B in the reaction

$$R(s) \leftrightarrow aA(g) + bB(g) \tag{3.10}$$
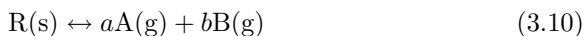
To apply Eq. 3.8 to reaction (3.10), we have first to recall the condition of congruent vaporization

$$\frac{J_A}{a} = \frac{J_B}{b} \tag{3.11}$$

where J_A and J_B are expressed in mol m^{-2} s^{-1}, or, in view of Eq. 3.7

$$\frac{P_A}{a(2\pi M_A RT)^{1/2}} = \frac{P_B}{b(2\pi M_B RT)^{1/2}} \tag{3.12}$$

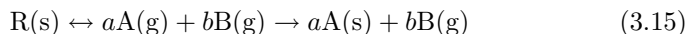The total flux of gaseous products J_Σ (in units of kg m^{-2} s^{-1}) in reaction (3.10) can be written as

$$J_\Sigma = M_A J_A + M_B J_B = \frac{M_A P_A}{(2\pi M_A RT)^{1/2}} + \frac{M_B P_B}{(2\pi M_B RT)^{1/2}} \tag{3.13}$$

Replacing P_B with P_A (or vice versa) with the use of Eq. 3.12, we arrive at

$$J_\Sigma = \frac{\gamma M_R P_A}{a(2\pi M_A RT)^{1/2}} = \frac{\gamma M_R P_B}{b(2\pi M_B RT)^{1/2}} \qquad (3.14)$$

where M_R is the molar mass of reactant. The coefficient $\gamma = 10^5 \, \text{Pa bar}^{-1}$ translates P values from bar, the unit, in which one conducts thermodynamic calculations involving equilibrium pressures, into Pascal.

Consider now the case of decomposition of reactant R in vacuum into a low-volatility product A and a gaseous product B in the reaction

$$R(s) \leftrightarrow aA(g) + bB(g) \rightarrow aA(s) + bB(g) \qquad (3.15)$$

Just as in the case of simple vaporization, the flux of gaseous product J_B (in units of kg m^{-2} s^{-1}) out of the reaction zone is

$$J_B = \frac{\gamma M_B P_B}{(2\pi M_B RT)^{1/2}} \qquad (3.16)$$

Here, as in Eq. 3.14, the quantity P_B is expressed in bar. Under steady-state decomposition conditions, the low-volatility product condenses totally in the reactant/product reaction zone.

3.5 Equilibrium Pressure of Products in the Equimolar and Isobaric Modes

The next step in the calculation of absolute decomposition rates with Eqs. 3.14 and 3.16 consists in determining the equilibrium pressures of the products, P_A and P_B, through the reaction equilibrium constant and the corresponding thermodynamic functions (the entropy and the enthalpy). The mode, equimolar or isobaric, in which the reactant is decomposing, should also be taken into account.

Equimolar and Isobaric Modes These key concepts were introduced into the kinetics of decomposition reactions more than 20 years ago [24]. *Equimolar* is the mode in which the actual pressure of the primary gaseous product in the reactor (P^{ext}) is lower than its equilibrium value (P_{eqp}), i.e., $P^{ext} < P_{eqp}$. This assumes not only the initial absence of the product in the reactor, but also that the product cannot accumulate during the course of decomposition. In the *isobaric* mode, the actual pressure of a gaseous product in the reactor exceeds by far its equilibrium value, i.e., $P^{ext} \gg P_{eqp}$, and, significantly, remains constant during the course of measurement ($P^{ext} = \text{const}$).

Both vaporization modes may occur during the same experiment and this reveals itself as a discontinuity in the Arrhenius plot because of the different
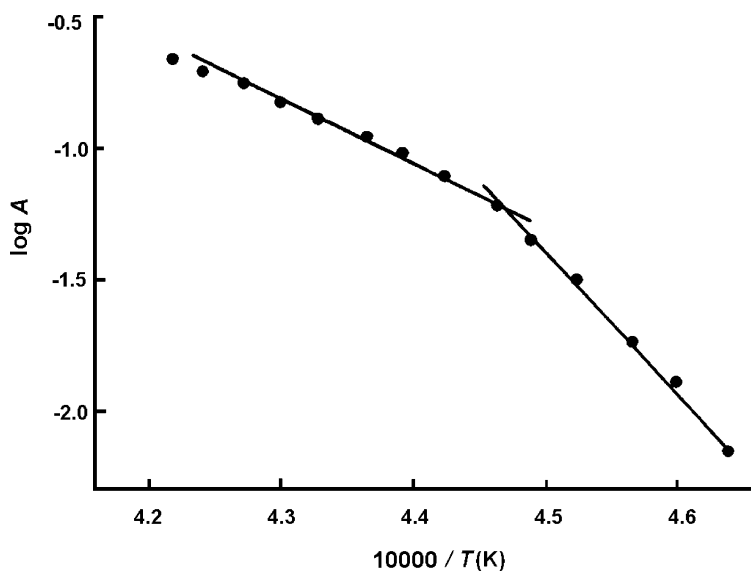
Fig. 3.1 Arrhenius plot for the atomization of $5\,\mathrm{ng}$ of Al_2O_3 in a flow of argon with content of about $0.01\%O_2$ at a heating rate of $1{,}000\,\mathrm{K\,s^{-1}}$. The E parameters for the low- and high-temperature parts of the plot are 980 and $480\,\mathrm{kJ\,mol^{-1}}$, respectively. (Reproduced from [27], with permission)

values of the molar enthalpy or E parameter for these modes (see Sect. 3.7). Such features in the shape of Arrhenius plots appear, in particular, in electrothermal AAS when studying atomization of metal oxides in an argon environment with an addition of oxygen [24, 25]. They were first observed by Sturgeon and Chakrabarti [26, 27] during atomization of the oxides of Al, Co, Cu, Ni, V, and Pb. Figure 3.1 displays an Arrhenius plot for Al_2O_3 drawn in the $\log A - 1/T$ coordinates, where A is the absorbance, which may, as a first approximation, be considered proportional to the vaporization rate [27].

Most of the researchers in AAS, starting with [26, 27], attributed these discontinuities in plots to changes in the vaporization mechanism and/or in the chemical form of the reactant, for instance, to a transition from oxide dissociation at low temperatures to sublimation of free metal in the high-temperature domain. Interpretation of the mechanism was attempted by identifying the only measured parameter E with thermal effects of a variety of conceivable processes (or of individual steps of the whole process). In 1981, a method was proposed [25] to determine absolute vaporization rates. It included measurement of both Arrhenius parameters (see Sect. 3.6).

On this basis, the existence of two different modes of dissociative vaporization (equimolar and isobaric) has been revealed [24]. This made it possible to abandon the arbitrariness in interpretation of the discontinuities [24].
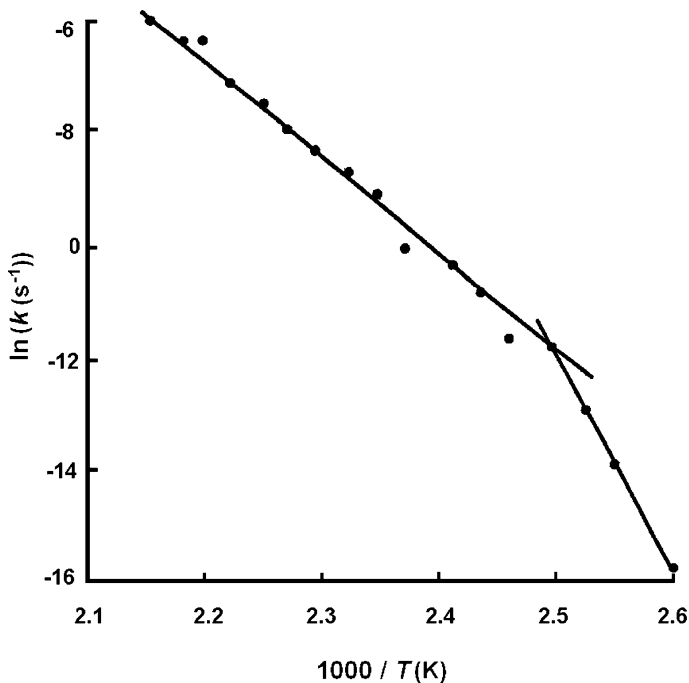
Fig. 3.2 Arrhenius plot for the dehydration of $CaC_2O_4 \cdot H_2O$ under an air atmosphere at a heating rate of $10\,K\,min^{-1}$. The E parameters for the low- and high-temperature parts of the plot are 281 and $147\,kJ\,mol^{-1}$, respectively. (Reproduced from [28], with permission)

(Nevertheless, in the quarter of a century that followed, no one except the present author made use of these concepts.)

Similar discontinuities in Arrhenius plots are observed in thermal analysis (TA) as well, in particular, in the dehydration of crystalline hydrates performed in humid air. For illustration, Fig. 3.2 reproduces an Arrhenius plot for the dehydration of calcium oxalate monohydrate in an air flow, carried out under non-isothermal conditions by Dollimore et al. [28]. The equilibrium pressure of water vapour P_{eqp} measured at temperatures of up to $400\,K$ and comparatively moderate decomposition rates turns out to be lower than its partial pressure in air P^{ext}, which implies that the decomposition occurs in the isobaric mode. Above $400\,K$, the equilibrium pressure of H_2O becomes higher than P^{ext}, with the process becoming equimolar. The slope of the plot decreases to one half of its former value in full agreement with theory (see Sect. 3.7).

Equilibrium Pressure of the Products The equilibrium quantity P_{eqp} is defined by the relation

$$\Delta_r H_T^\circ = T(\Delta_r S_T^\circ - R \ln K_P) \tag{3.17}$$

where $\Delta_r H_T^\circ$ and $\Delta_r S_T^\circ$ are, respectively, the enthalpy and the entropy of the decomposition reaction, and K_P is the equilibrium constant defined as

$$K_P = P_A^a \times P_B^b \tag{3.18}$$

As follows from the condition of congruent vaporization (3.14)

$$\frac{P_B}{P_A} = \frac{b}{a}\left(\frac{M_B}{M_A}\right)^{1/2} \equiv \beta \tag{3.19}$$

Replacing P_A with P_B in Eq. 3.18 and recalling Eq. 3.17, the relationship for the equimolar mode is

$$P_B^e = (\beta^a K_P)^{1/\nu} = \beta^{a/\nu} \exp\frac{\Delta_r S_T^\circ}{\nu R} \exp\left(-\frac{\Delta_r H_T^\circ}{\nu RT}\right) \tag{3.20}$$

and for the isobaric mode

$$P_B^i = \beta P_A^i = \beta\frac{K_P^{1/a}}{(P_B^{ext})^{b/a}} = \frac{\beta}{(P_B^{ext})^{b/a}} \exp\frac{\Delta_r S_T^\circ}{aR} \exp\left(-\frac{\Delta_r H_T^\circ}{aRT}\right) \tag{3.21}$$

Here P_B^{ext} means the excess (external) pressure of the gaseous product B in the reactor, the superscripts e and i denote the mode employed (equimolar or isobaric), and

$$\nu = a + b \tag{3.22}$$

Equations 3.20 and 3.21 occupy a key place in this derivation. They describe the effect of the excess pressure of a gaseous product on the equilibrium pressure of this product and its dependence on the temperature and reaction stoichiometry.

3.6 Absolute Rates of Decomposition

Decomposition in Vacuum Substitution of the quantities P_B^e and P_B^i into Eqs. 3.14 and 3.16 yields the final expressions for calculation of the absolute rates of decomposition. Thus, for the decomposition of reactant R into volatile gaseous products A and B in accordance with reaction (3.10):

$$J_\Sigma^e = \frac{\gamma M_R}{b(2\pi M_B RT)^{1/2}}\beta^{a/\nu} \exp\frac{\Delta_r S_T^\circ}{\nu R} \exp\left(-\frac{\Delta_r H_T^\circ}{\nu RT}\right) \tag{3.23}$$

for the equimolar mode, and

$$J_\Sigma^i = \frac{\gamma M_R}{(2\pi M_B RT)^{1/2}}\frac{\beta}{(P_B^{ext})^{b/a}} \exp\frac{\Delta_r S_T^\circ}{aR} \exp\left(-\frac{\Delta_r H_T^\circ}{aRT}\right) \tag{3.24}$$

for the isobaric mode. Similarly, when reactant R decomposes into a low-volatility product A and a gaseous product B by reaction (3.15):

$$J_{\mathrm{B}}^{\mathrm{e}} = \frac{\gamma M_{\mathrm{B}}}{(2\pi M_{\mathrm{B}} RT)^{1/2}} \beta^{a/\nu} \exp\frac{\Delta_{\mathrm{r}} S_T^{\circ}}{\nu R} \exp\left(-\frac{\Delta_{\mathrm{r}} H_T^{\circ}}{\nu RT}\right) \qquad (3.25)$$

for the equimolar mode, and

$$J_{\mathrm{B}}^{\mathrm{i}} = \frac{\gamma M_{\mathrm{B}}}{(2\pi M_{\mathrm{B}} RT)^{1/2}} \frac{\beta}{\left(P_{\mathrm{B}}^{\mathrm{ext}}\right)^{b/a}} \exp\frac{\Delta_{\mathrm{r}} S_T^{\circ}}{aR} \exp\left(-\frac{\Delta_{\mathrm{r}} H_T^{\circ}}{aRT}\right) \qquad (3.26)$$

for the isobaric mode.

Decomposition in a Foreign Gas Similarly, equations can be derived for the calculation of absolute decomposition rates in an atmosphere of foreign gases. Disregarding the differences in the diffusion coefficients of different gaseous products (A and B), one arrives eventually at the following final relations. For one-dimensional diffusion of both gaseous products from a plane surface:

$$J_{\Sigma}^{\mathrm{e}} = \frac{\gamma M_{\mathrm{R}} D}{zRT} \beta^{a/\nu} \exp\frac{\Delta_{\mathrm{r}} S_T^{\circ}}{\nu R} \exp\left(-\frac{\Delta_{\mathrm{r}} H_T^{\circ}}{\nu RT}\right) \qquad (3.27)$$

for the equimolar decomposition mode, and

$$J_{\Sigma}^{\mathrm{i}} = \frac{\gamma M_{\mathrm{R}} D}{zRT} \frac{\beta}{\left(P_{\mathrm{B}}^{\mathrm{ext}}\right)^{b/a}} \exp\frac{\Delta_{\mathrm{r}} S_T^{\circ}}{aR} \exp\left(-\frac{\Delta_{\mathrm{r}} H_T^{\circ}}{aRT}\right) \qquad (3.28)$$

for the isobaric mode. If only one gaseous product, B, escapes by one-dimensional diffusion from a plane surface:

$$J_{\mathrm{B}}^{\mathrm{e}} = \frac{\gamma M_{\mathrm{B}} D_{\mathrm{B}}}{zRT} \beta^{a/\nu} \exp\frac{\Delta_{\mathrm{r}} S_T^{\circ}}{\nu R} \exp\left(-\frac{\Delta_{\mathrm{r}} H_T^{\circ}}{\nu RT}\right) \qquad (3.29)$$

for the equimolar decomposition mode, and

$$J_{\mathrm{B}}^{\mathrm{i}} = \frac{\gamma M_{\mathrm{B}} D_{\mathrm{B}}}{zRT} \frac{\beta}{\left(P_{\mathrm{B}}^{\mathrm{ext}}\right)^{b/a}} \exp\frac{\Delta_{\mathrm{r}} S_T^{\circ}}{aR} \exp\left(-\frac{\Delta_{\mathrm{r}} H_T^{\circ}}{aRT}\right) \qquad (3.30)$$

for the isobaric mode. For a single spherical particle decomposing in a foreign gas, the expressions will be the same as Eqs. 3.27–3.30, but with z replaced with r.

3.7 Interpretation of *A* and *E* Parameters Through the Langmuir Vaporization Equations

Relation Between the Quantities *k* and *J* To compare the Arrhenius equation with the Langmuir vaporization equations, consider first how the rate constant k is related to the absolute decomposition rate J. For the steady-state

decomposition of a spherical particle, which corresponds to the contracting sphere model [5, 8],

$$\frac{d\alpha}{dt} = 3(1 - \alpha)^{2/3}k \qquad (3.31)$$

Equation 3.31 was proposed by Roginsky and Schultz [29] to describe the kinetics of a reaction at the stage where its rate slows down as a result of the decreasing crystal surface area. Using the relations connecting the mass (m), radius (r), and density (ρ) of a spherical particle, $\alpha \equiv 1 - m/m_0$; $m = (4/3)\pi r^3 \rho$ and $J = -(dm/dt)(4\pi r^2)^{-1}$, Eq. 3.31 can be transformed as shown in [30] to:

$$J = \rho r_0 k \qquad (3.32)$$

where m_0 and r_0 are the particle mass and radius at the initial instant of decomposition $(t = 0)$.

There is an essential difference between the decomposition rates expressed by the quantities J and k. Unlike J, which does not depend on the particle size, k is inversely proportional to the initial dimensions of the particle. For $\rho r_0 = 1$ (e.g., for $\rho = 2,000\,\text{kg m}^{-3}$ and $r_0 = 0.5\,\text{mm} = 5 \times 10^{-4}\,\text{m}$), the rates J and k are numerically equal. The difference between these rates increases proportionately with increasing size and density of the particles. Equation 3.32 permits conversion from relative values of the rate constants k expressed in per second to the absolute rates J in units of kg m^{-2} s^{-1}. This opens up an attractive possibility for the interpretation of data obtained by traditional measurement of the $\alpha - t$ kinetic curves in terms of the Langmuir vaporization equations.

Interpretation of A and E Parameters Let us turn now to interpretation of the parameters entering the van't Hoff thermodynamic relation (3.3), namely, of the A pre-exponential factor and the E parameter (the exponent). A comparison of Eq. 3.3 with the set of Eqs. (3.23)–(3.30) reveals that the exponential factor, $\exp[-E/(RT)]$, in Eq. 3.3 assumes two different forms in Eqs. 3.23–3.30, so that

$$E^e = \frac{\Delta_r H_T^\circ}{\nu} = \frac{\Delta_r H_T^\circ}{a + b} \qquad (3.33)$$

for the equimolar decomposition mode and

$$E^i = \frac{\Delta_r H_T^\circ}{\nu - b} = \frac{\Delta_r H_T^\circ}{a} \qquad (3.34)$$

for the isobaric mode. In both modes, parameter E corresponds to the *molar enthalpy*, i.e., to the reaction enthalpy per mole of primary decomposition products, with the exclusion of the product present in an excess amount. The difference between the physical meaning of parameter E used in the common (Arrhenius) and thermochemical approaches is illustrated schematically in Fig. 3.3.

Fig. 3.3 The physical meaning of the E parameter taken from the van't Hoff fundamental equation within the framework of the Arrhenius and thermochemical approaches
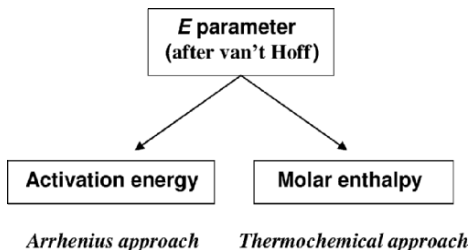
A consideration of Eqs. 3.33 and 3.34 suggests an extremely important conclusion, namely, that

$$\frac{E^i}{E^e} = \frac{\nu}{\nu - b} = \frac{a + b}{a} \tag{3.35}$$

A comparison of this result with experiment is given in Sects. 5.3-5.5.

The number of variables governing the A parameter is considerably larger. Two factors can be distinguished. The first (A_1) is (conventionally) connected with the transport of gaseous products, and the second (A_2), with the reaction entropy. These factors are listed in Table 3.1 (vacuum) and Table 3.2 (inert gas) according to the actual model and decomposition mode involved.

Experimental Verification To demonstrate the validity of these relations, the expected value of the A parameter for the decomposition of $CaCO_3$ in vacuum in the equimolar mode at 800 K (performed in the framework of an interlaboratory experiment [31]) was estimated. The following values of the quantities involved were used: $M_{CO2} = 0.044\,kg\,mol^{-1}$, $M_{CaO} = 0.056\,kg\,mol^{-1}$, $\Delta_r S^{\circ}_{800}/\nu = 159.1\,J\,mol^{-1}\,K^{-1}$, $r_0 = 7.5 \times 10^{-6}$ m and $\rho = 2,930\,kg\,m^{-3}$. Accordingly $A = A_1\,A_2 = (4.6 \times 10^3)(2.0 \times 10^8) \cong 10^{12}\,s^{-1}$. This value compares well with the vibrational frequency of the crystal lattice (at the interface) which can be theoretically estimated using the equation of Polanyi–Wigner [6] to be $\sim 10^{13}\,s^{-1}$. At the same time, the figure thus found exceeds by an order of magnitude the value $A \cong 10^{11}\,s^{-1}$ obtained by averaging the results obtained in the interlaboratory experiment [31]. The disagreement between the calculation and experiment could be expected because of the systematic underestimation of the experimental data (A and E) inherent in the Arrhenius plot method (see Sects. 4.2 and 6.3 below).

In the same manner, the value of A for the $CaCO_3$ decomposition in nitrogen carried out in the equimolar mode at 1,000 K was estimated. Factor A_1 contains additional parameters such as the diffusion coefficient of CO_2 in nitrogen at 1,000 K, $D_{CO2} = 1.43 \times 10^{-4}\,m^2\,s^{-1}$ [32], and parameter z, whose magnitude may be accepted as equal to the height of the crucible containing the sample ($\sim$5 mm). For 1,000 K, $\Delta_r S^{\circ}_{1000}/\nu = 155.6\,J\,mol^{-1}\,K^{-1}$ and so $A = A_1\,A_2 = (7.1 \times 10^{-1})(1.4 \times 10^8) \cong 10^8\,s^{-1}$. The mean

Table 3.1 Factors of the Arrhenius A parameter for congruent dissociative vaporization in a vacuum

Factor	$R(s/l) \leftrightarrow aA(g) + bB(g)$		$R(s/l) \leftrightarrow aA(g)_\downarrow + bB(g)$	
	e-mode	i-mode	e-mode	i-mode
A_1	$\dfrac{\gamma \beta^{a/\nu} M_R}{b\rho r_0 (2\pi M_B RT)^{1/2}}$	$\dfrac{\gamma \beta M_R}{b\rho r_0 (2\pi M_B RT)^{1/2}} \dfrac{1}{(P_B^{ext})^{b/a}}$	$\dfrac{\gamma \beta^{a/\nu} M_B}{\rho r_0 (2\pi M_B RT)^{1/2}}$	$\dfrac{\gamma \beta M_B}{\rho r_0 (2\pi M_B RT)^{1/2}} \dfrac{1}{(P_B^{ext})^{b/a}}$
A_2	$\exp[\Delta_r S_T^\circ/(\nu R)]$	$\exp[\Delta_r S_T^\circ/(aR)]$	$\exp[\Delta_r S_T^\circ/(\nu R)]$	$\exp[\Delta_r S_T^\circ/(aR)]$

Table 3.2 Factors of the Arrhenius A parameter for congruent dissociative vaporization in an atmosphere of foreign (inert) gas

Factor	$R(s/l) \leftrightarrow aA(g) + bB(g)$		$R(s/l) \leftrightarrow aA(g)_\downarrow + bB(g)$	
	e-mode	i-mode	e-mode	i-mode
A_1	$\dfrac{\gamma \beta^{a/\nu} M_R D}{\rho r_0 zRT}$	$\dfrac{\gamma \beta M_R D}{\rho r_0 zRT} \dfrac{1}{(P_B^{ext})^{b/a}}$	$\dfrac{\gamma \beta^{a/\nu} M_B D_B}{\rho r_0 zRT}$	$\dfrac{\gamma \beta M_B D_B}{\rho r_0 zRT} \dfrac{1}{(P_B^{ext})^{b/a}}$
A_2	$\exp[\Delta_r S_T^\circ/(\nu R)]$	$\exp[\Delta_r S_T^\circ/(aR)]$	$\exp[\Delta_r S_T^\circ/(\nu R)]$	$\exp[\Delta_r S_T^\circ/(aR)]$

value of A averaged from 11 independent measurements in the interlaboratory experiment [31] was $3 \times 10^6 \, \text{s}^{-1}$, which is smaller than the theoretical value by more than an order of magnitude for the same reason as explained above.

The equations presented in Tables 3.1 and 3.2 permit the estimation of both the absolute values of parameters A and their ratio for the isobaric and equimolar modes of decomposition. This ratio has the same form irrespective of the actual decomposition conditions (vacuum or foreign gas environment):

$$\frac{A^{\mathrm{i}}}{A^{\mathrm{e}}} = \frac{\beta^{b/\nu}}{(P_{\mathrm{B}}^{\mathrm{ext}})^{b/a}} \exp \frac{b \Delta S_T^{\circ}}{a \nu R} \qquad (3.36)$$

For illustration, the ratio $A^{\mathrm{i}}/A^{\mathrm{e}}$ for reactions with different stoichiometry, i.e., different b/a ratios, can be estimated. The mean value of the molar entropy $\Delta S_T^{\circ}/\nu$ is $160 \, \text{J} \, \text{mol}^{-1} \, \text{K}^{-1}$ (see Table 3.2) and assuming $P_{\mathrm{B}}^{\mathrm{ext}} = 1$ bar and $\beta \cong 1$, the $A^{\mathrm{i}}/A^{\mathrm{e}}$ ratios are $1.5 \times 10^4, 2.3 \times 10^8$, and 5.2×10^{16} for $b/a = 0.5$, 1, and 2, respectively. As $P_{\mathrm{B}}^{\mathrm{ext}}$ is decreased to 10^{-5} bar, the values of $A^{\mathrm{i}}/A^{\mathrm{e}}$ increase to 4.7×10^6, 2.3×10^{13}, and 5.2×10^{26}. This is accompanied by a low-temperature shift of the Arrhenius plots which retain, however, their slope. The largest $A^{\mathrm{i}}/A^{\mathrm{e}}$ ratios are reported [6] to be observed in dehydration of salts with a large content of water molecules. This fits the theory. For instance, when the dodecahydrate $NiNa_3P_3O_{10} \cdot 12H_2O$ decomposes to the dihydrate $NiNa_3P_3O_{10} \cdot 2H_2O$ (i.e., for $b/a = 10$) in vacuum and in the presence of 18 mbar H_2O, the $A^{\mathrm{i}}/A^{\mathrm{e}}$ ratio, in accordance with Eq. 3.36, should be 10^{101}. Pavlyuchenko et al. [33] found a value of 10^{66} for the $A^{\mathrm{i}}/A^{\mathrm{e}}$ ratio. Allowing for the huge error involved in measuring the slope of an Arrhenius plot (see Sect. 4.6) for the isobaric mode based on three closely lying experimental points at 60°C, 62°C, and 65°C, this disagreement between the theory and experiment may be considered quite reasonable.

3.8   Conclusions

The Langmuir vaporization equations thus open up broader possibilities for description of decomposition processes than the Arrhenius approach. First, the key physical quantity entering all vaporization equations is the equilibrium pressure of products, which is directly related to the thermodynamic parameters of the process. As a result, the A and E parameters of the Arrhenius equation receive a straightforward physical interpretation.

Second, these equations take into account, besides temperature, a variety of factors affecting the decomposition kinetics, such as the composition, stoichiometry, and thermochemical characteristics of the reaction, the pressure of the excess gaseous products and of the foreign (inert) gas in the reactor, and even, physical properties of the reactant (the size of particles, molar mass, and density).

Third, these equations permit the calculation of the absolute rates of a process, a possibility that had been believed unrealizable before their first application in 1981 to the kinetics of solid decomposition [25]. The interest in theories of the transition state and of the activated complex was primarily stimulated by the possibility of calculating absolute reaction rates, although the attempts to use them in studies of heterogeneous processes met with only limited success [1, 2]. In contrast, the first comparison of theoretical with experimental values of the A parameters performed within the framework of Langmuir vaporization equations was much more successful [25].

An analysis of the vaporization equations has yielded important conclusions, which have permitted a quantitative interpretation of such phenomena as the T–S and compensation effects (see Part II). Among these conclusions is also invariability of the E^i parameter of the Arrhenius equation for any excess pressure of a gaseous product, as well as the dependence of the E^i/E^e ratio on the stoichiometry of the decomposition products.

During the period 1940–1960, some researchers (in particular, Penner [34]) made attempts at deriving the vacuum vaporization equation from the van't Hoff–Arrhenius equation using the formalism of statistical mechanics [35]. The final expressions, however, all turned out to be similar to, or identical with, the Hertz–Langmuir equation. Contrasting the van't Hoff–Arrhenius relation with the Langmuir vaporization equation thus does not seem to be useful and *the van't Hoff–Arrhenius equation applied to the vaporization process may be considered as a starting step on the way to the Langmuir equations.*

References

1. Prodan EA, Pavlyuchenko MM (1965) (eds) Heterogeneous chemical reactions. Nauka Tekhnika, Minsk (in Russian)
2. Young DA (1966) Decomposition of solids. Pergamon, Oxford
3. Delmon B. (1969) Introduction a la cinétique hétérogène. Technip, Paris
4. Barret P (1975) (ed) Reaction kinetics in heterogeneous chemical systems. Elsevier, Amsterdam
5. Prodan EA, Pavlyuchenko MM, Prodan SA (1976) Regularities of topochemical reactions. Nauka Tekhnika, Minsk (in Russian)
6. Brown ME, Dollimore D, Galwey AK (1980) Reactions in the solid state. Elsevier, London
7. Prodan EA (1986) Inorganic topochemistry. Nauka Tekhnika, Minsk (in Russian)
8. Galwey AK, Brown ME (1999) Thermal decomposition of ionic solids. Elsevier, Amsterdam
9. Laidler JK (1984) J Chem Educ 61:494–498
10. Van't Hoff JH (1884) Etudes de dynamique chemique. Frederik Müller et Co, Amsterdam
11. Arrhenius S (1889) Z Phys Chem 4:226–248
12. Pfaundler L (1867) Ann Phys Chem 131:55
13. Bodenstein M (1899) Z Phys Chem 29:147–158, 295–314, 315–333, 429–448, 665–699
14. Hinshelwood CN, Bowen EJ (1921) Proc Roy Soc A99:203–212

15. Bružs B (1926) J Phys Chem 30:680–693
16. Polanyi M, Wigner E (1928) Z Phys Chem A139:439
17. Eyring H (1935) J Chem Phys 3:107–115
18. Evans MG, Polanyi M (1935) Trans Faraday Soc 31:875–894
19. Hertz H (1882) Ann Phys Chem 17:177–200
20. Knudsen M (1909) Ann Phys (Leipzig) 29:179–183
21. Langmuir I (1913) Phys Rev 2:329–342
22. Matveev AN (1987) Molecular physics. Vysshaya Shkola, Moscow (in Russian)
23. Langmuir I (1918) Phys Rev 12:368–370
24. L'vov BV, Fernandez HGA (1984) Zh Analit Khim 39:221–231 (in Russian)
25. L'vov BV, Ryabchuk GN (1981) Zh Analit Khim 36:2085–2096 (in Russian)
26. Sturgeon RE, Chakrabarti CL, Langford CH (1976) Anal Chem 48:1792–1807
27. Sturgeon RE, Chakrabarti CL (1978) Prog Anal At Spectrosc 1:5–199
28. Dollimore D, Evans TA, Lee JF, Wilburn FW (1992) Thermochim Acta 198:249–257
29. Roginsky S, Schultz E (1928) Z Phys Chem A138:21–41; Ukr Khim Zh 3:177–207 (in Russian)
30. L'vov BV (1997) Thermochim Acta 303:161–170
31. Brown ME, Maciejewski M, Vyazovkin S, et al. (2000) Thermochim Acta 355:125–143
32. Kikoin IK (1976) (ed) Tables of physical constants. Atomizdat, Moscow (in Russian)
33. Pavlyuchenko MM, Pysyak YaS, Zonov YaG, Prodan EA (1970) Vesti AN BSSR No 1:29–37 (in Russian)
34. Penner SS (1948) J Phys Chem 52:367, 949, 1262
35. Dettorre JF, Knorr TG, Hall EH (1966) Evaporation processes. In: Powell CF, Oxley JH, Blocher JM (eds) Vapour deposition. Wiley, New York, pp 62–101

Chapter 4
Methodology

4.1 Preliminary Remarks

Books and reviews dealing with the kinetics of solid-state reactions (e.g., [1–3]) usually pay little attention to the analysis and comparison of the metrological characteristics of the methods employed in TA measurements although a correct choice of the method to be used in measurement and calculation of the quantity of interest determines the reliability of the results obtained. This chapter addresses these points.

The parameters A and E (or ΔS and ΔH) are determined respectively with the use of an Arrhenius plot or the second-law (Knudsen–Langmuir) method. The third-law method, which has received wide recognition in equilibrium thermochemical studies [4], has not been used in kinetics investigations at all. The first publication on this subject appeared only in 2002 [5]. Studies of L'vov and his colleagues still remain the only attempts in this area (see review [6]).

4.2 The Arrhenius Plot Method

To determine the A and E parameters by the Arrhenius plot method, one usually invokes the Arrhenius equation in logarithmic form

$$\ln k = \ln A - E/RT \tag{4.1}$$

neglecting the temperature dependence of the A parameter, and plots the logarithm of the rate constant $(\ln k)$ as a function of the inverse (absolute) temperature $(1/T)$. The slope of the plot is

$$E = \frac{R \ln(k_2/k_1)}{1/T_1 - 1/T_2} \tag{4.2}$$

The pre-exponential factor, A, however, as shown before (Tables 3.1 and 3.2), depends on T, both directly and through the diffusion coefficient, D, which is proportional to $T^{1.75}$. Therefore, the values of E derived from the Arrhenius plot should be corrected using the following general relation [7]

$$E_{\text{cor}} = \frac{R \ln(k_2/k_1)}{1/T_1 - 1/T_2} - \frac{nR \ln(T_2/T_1)}{1/T_1 - 1/T_2} \tag{4.3}$$

where n is the exponent of the true power dependence of the A parameter on T.

The second term of Eq. 4.3 can be recast, to within an error of less than 1% for $T_2/T_1 < 1.65$, in the form

$$\frac{nR\ln(T_2/T_1)}{1/T_1 - 1/T_2} = \frac{nR\overline{T}\ln(T_2/T_1)}{(T_2 - T_1)/\overline{T}} \cong nR\overline{T} \tag{4.4}$$

where $\overline{T} = (T_1 \times T_2)^{1/2}$. Thus, Eq. 4.3 transforms to

$$E_{\mathrm{cor}} = E - nR\overline{T} \tag{4.5}$$

For decomposition in vacuum, $n = -0.5$ and if the process occurs in a foreign gas, $n = +0.75$. Accordingly, for $\overline{T} = 1,000\,\mathrm{K}$ the correction amounts to about $+4.2\,\mathrm{kJ\ mol^{-1}}$ in the first case, and to $-6.2\,\mathrm{kJ\ mol^{-1}}$, in the second. Correction of E for temperature also requires correction of the A parameter. Substituting the value of E_{cor} from Eq. 4.5 into Eq. 4.1 yields

$$(\ln A)_{\mathrm{cor}} = \ln A - n \tag{4.6}$$

If these corrections are neglected, the difference between the $\ln A$ parameters measured in vacuum and in a foreign gas would constitute at $1,000\,\mathrm{K}$ about 1.25, and between the E parameters, approximately $10.4\,\mathrm{kJ\ mol^{-1}}$. The majority of researchers using the Arrhenius plot method fail to take these corrections into account, although the final figures for the E parameter are given frequently (see, e.g., [8]) to within a few kJ $\mathrm{mol^{-1}}$, or even a few tenths of kJ $\mathrm{mol^{-1}}$, and the values of $\ln A$, to within an uncertainty of a few tenths of percent.

4.3   The Second-law Method

Application of the second-law method draws on the equation

$$R\ln K_P = \Delta_{\mathrm{r}}S_T^{\circ} - \frac{\Delta_{\mathrm{r}}H_T^{\circ}}{T} \tag{4.7}$$

By measuring K_P at different temperatures and plotting $\ln K_P$ vs $1/T$, one readily finds both parameters, more specifically, $\Delta_{\mathrm{r}}H_T^{\circ}$ from the slope of the straight line and $\Delta_{\mathrm{r}}S_T^{\circ}$ from the intercept of the straight line on the ordinate axis. Quite frequently a simplified (one-parameter) version of this method, based on the use of the Clausius–Clapeyron equation, is used

$$\frac{\mathrm{d}\ln P}{\mathrm{d}T} = \frac{\Delta_{\mathrm{r}}H_T^{\circ}}{RT^2} \tag{4.8}$$

Integration of Eq. 4.8 gives

$$R\ln P = -\frac{\Delta_{\mathrm{r}}H_T^{\circ}}{T} + \mathrm{const} \tag{4.9}$$

To find the value of $\Delta_r H_T^\circ$ by this method, it is necessary to know only the dependence of pressure on temperature rather than the absolute values of P. This is an essential point, because some techniques, in particular, MS and optical absorption spectrometry (atomic and molecular) are capable of determining only quantities proportional to P (the ion current I and absorbance A). In this case, a plot drawn in the $\ln I$ vs $1/T$ or $\ln A$ vs $1/T$ coordinates can yield merely the value of $\Delta_r H_T^\circ$ (from the slope of the straight line), because the intercept of the straight line on the ordinate axis is now an arbitrary constant rather than $\Delta_r S_T^\circ$.

4.4 The Third-law Method

Just as the second-law method, the third-law method is based on use of the relation

$$\Delta_r H_T^\circ = T(\Delta_r S_T^\circ - R \ln K_P) \tag{4.10}$$

The equilibrium constant, K_P, can de expressed through the experimentally determined equilibrium pressure of the gaseous product, P_B. With the use of Eqs. 3.20 and 3.21, Eq. 4.10 can be rewritten as:

$$\Delta_r H_T^\circ = T(\Delta_r S_T^\circ + aR \ln \beta - \nu R \ln P_B) \tag{4.11}$$

for the equimolar decomposition mode and

$$\Delta_r H_T^\circ = T(\Delta_r S_T^\circ + aR \ln \beta - bR \ln P_B^{ext} - aR \ln P_B) \tag{4.12}$$

for the isobaric mode. As seen from these expressions, in order to determine the enthalpy, one has to know, besides the temperature and pressure of the gaseous product, P_B, the entropy, $\Delta_r S_T^\circ$, the stoichiometry of the reaction (a and b coefficients) and, for the isobaric mode, the excess pressure, P_B^{ext}, as well. In contrast to the second-law and Arrhenius plot methods, however, determination of the enthalpy reduces, in this case, to a measurement, in principle, at one temperature only.

Equations 4.11 and 4.12 allow a simplification by excluding the correction term, $aR \ln \beta$, which takes into account the differences in molar masses and stoichiometric coefficients between the products of decomposition. This can be done by replacing the partial pressures $P_A/(a^a M_A^{a/2})$ and $P_B/(b^b M_B^{b/2})$ in Eqs. 3.14 and 3.16 with a generalized quantity $\overline{P}/(f^{1/\nu} \overline{M}^{1/2})$ obeying the condition

$$\frac{P_A^a P_B^b}{a^a M_A^{a/2} b^b M_B^{b/2}} = \frac{\overline{P}^\nu}{f \overline{M}^{\nu/2}} \tag{4.13}$$

where $f = a^a b^b$ and $\overline{M}^\nu = M_A^a M_B^b$. Now Eqs. 4.11 and 4.12 acquire the form

$$\Delta_r H_T^\circ = T(\Delta_r S_T^\circ - \nu R \ln \overline{P}) \tag{4.14}$$

and

$$\Delta_{\mathrm{r}} H_T^\circ = T(\Delta_{\mathrm{r}} S_T^\circ - bR\ln P_{\mathrm{B}}^{\mathrm{ext}} - aR\ln \overline{P}) \tag{4.15}$$

where

$$\overline{P} = \frac{f^{1/\nu}(2\pi\overline{M}RT)^{1/2}}{\gamma M_{\mathrm{R}}} J_\Sigma \tag{4.16}$$

for the case of reactant decomposition in vacuum into the gaseous products A and B, and

$$\overline{P} = \frac{f^{1/\nu}(2\pi\overline{M}RT)^{1/2}}{\gamma b M_{\mathrm{B}}} J_{\mathrm{B}} \tag{4.17}$$

for the case of reactant decomposition in vacuum into the low-volatility product A and gaseous product B.

4.5 Evaluation of the Molar Entropies

The lack of values of $\Delta_{\mathrm{r}} S_T^\circ$, or of tabulated data necessary for their calculation, would seem at first glance to curtail seriously the application of the third-law method. In reality, for most substances, the absolute values of the entropy for standard conditions $(\Delta_{\mathrm{r}} S_{298}^\circ)$ and the corresponding temperature corrections $(S_T^\circ - S_{298}^\circ)$ can be found tabulated in many reference handbooks [4, 9–11]. Nevertheless, for some compounds, even quite common ones, for instance for low-volatility salt molecules in the gas phase, these data are lacking. In these cases, it is sometimes possible to evaluate the entropy from a comparison with the values of $\Delta_{\mathrm{r}} S_T^\circ$ available for similar molecules of other metals. This approach was used, in particular, to evaluate the value of $\Delta_{\mathrm{r}} S_T^\circ$ for the molecules of $Li_2SO_4, CaSO_4$, and $CuSO_4$ [12].

A more general approach for evaluation of the molar entropy, $\Delta_{\mathrm{r}} S_T^\circ/\nu$, was proposed in [5]. In place of the real values of $\Delta_{\mathrm{r}} S_T^\circ/\nu$ for 20 different reactants their averaged value $(148 \pm 17\,\mathrm{J\,mol^{-1}\,K^{-1}})$ was used. This results only in a slight increase (by 2–3%) of the discrepancy between the final results of the determination of $\Delta_{\mathrm{r}} H_T^\circ$ and the expected figures. This approach was subsequently refined in [6]. An analysis of the values of $\Delta_{\mathrm{r}} S_T^\circ/\nu$ performed for 50 different compounds revealed substantial differences between reactants decomposing with the formation of free metal atoms and those undergoing decomposition to metals bound in molecules. As evident from Tables 4.1 and 4.2, the mean value of $\Delta_{\mathrm{r}} S_T^\circ/\nu$ is $136 \pm 9\,\mathrm{J\,mol^{-1}\,K^{-1}}$ in the first case, and $160 \pm 9\,\mathrm{J\,mol^{-1}\,K^{-1}}$ in the second. In both cases, the relative standard deviation is one half of its value for all the 50 reactants.

The potential inherent in this approach is far from being exhausted, so that, in particular, in view of the noticeable differences in the entropy of atomic vapours among some metals, one could propose corrections which would further reduce the scatter of the $\Delta_{\mathrm{r}} S_T^\circ/\nu$ values from their mean figures.

Table 4.1 The molar entropies for CDV reactions at $P_B \cong 10^{-7}$ bar (metal-product is in the atomic form) [4, 9–11]

Reaction	$T(K)$	$\Delta S_T^\circ/\nu^a (\mathrm{J\ mol^{-1}\ K^{-1}})$
$FeO \leftrightarrow Fe(g) + \frac{1}{2}O_2$	1,200	130.0
$CoO \leftrightarrow Co(g) + \frac{1}{2}O_2$	1,100	140.0
$NiO \leftrightarrow Ni(g) + \frac{1}{2}O_2$	925	152.0+
$MgO \leftrightarrow Mg(g) + \frac{1}{2}O_2$	1,600	137.9
$MnO \leftrightarrow Mn(g) + \frac{1}{2}O_2$	1,600	127.3
$Cu_2O \leftrightarrow 2Cu(g) + \frac{1}{2}O_2$	800	128.0
$CdO \leftrightarrow Cd(g) + \frac{1}{2}O_2$	1,300	129.0
$HgO \leftrightarrow Hg(g) + O$	680	129.0
$ZnO \leftrightarrow Zn(g) + O$	1,260	134.1
$CdS \leftrightarrow Cd(g) + \frac{1}{2}S_2$	1,000	122.2−
$CdSe \leftrightarrow Cd(g) + \frac{1}{2}Se_2$	1,000	119.7−
$ZnS \leftrightarrow Zn(g) + \frac{1}{2}S_2$	1,000	133.2
$ZnSe \leftrightarrow Zn(g) + \frac{1}{2}Se_2$	1,000	125.0−
$Be_3N_2 \leftrightarrow 3Be(g) + 1.5N + \frac{1}{4}N_2$	1,600	135.1
$Mg_3N_2 \leftrightarrow 3Mg(g) + 1.5N + \frac{1}{4}N_2$	1,200	130.1
$BN \leftrightarrow B(g) + \frac{1}{2}N_2$	1,800	154.7+
$AlN \leftrightarrow Al(g) + \frac{1}{2}N + \frac{1}{4}N_2$	1,800	148.5+
$GaN \leftrightarrow Ga(g) + \frac{1}{2}N + \frac{1}{4}N_2$	1,200	135.3
$InN \leftrightarrow In(g) + \frac{1}{2}N + \frac{1}{4}N_2$	1,120	138.3
$Si_3N_4 \leftrightarrow 3Si(g) + 2N + N_2$	1,700	155.3+
$NaN_3 \leftrightarrow Na(g) + N + N_2$	300	133.8
$KN_3 \leftrightarrow K(g) + N + N_2$	300	133.6
$Pb(N_3)_2 \leftrightarrow Pb + N + N_2 + N_3$	300	141.9
$AgNO_3(l) \leftrightarrow Ag(g) + NO_2 + \frac{1}{2}O_2$	570	128.5
$AgNO_3 \leftrightarrow Ag(g) + NO_2 + \frac{1}{2}O_2$	480	142.4
Average $\pm s\ (n = 25)$		136 ± 9

^{a} Values $\Delta S_T^\circ/\nu$ outside the interval $136 \pm 9\ \mathrm{J\ mol^{-1}\ K^{-1}}$ are noted by marks: $-$ or $+$

4.6 Precision

As evident from an analysis of thermodynamic data (primarily of the enthalpies of formation and sublimation) listed for several hundreds of substances in a reference book [4], determination of these constants by the third-law method yields values more precise, on the average, by an order of magnitude than those obtained using the second-law method. This can be traced to $\Delta_r H_T^\circ$ depending differently on random and systematic errors in determination of the true reactant temperature and measurement of the variables P, J, or k, a point which becomes obvious when comparing Eqs. 4.10–4.12 with Eq. 4.18 below

$$\Delta_r H_T^\circ = \frac{1}{T_{\min}^{-1} - T_{\max}^{-1}} R \ln \frac{P_{\max}}{P_{\min}} = \frac{T_{\max} T_{\min}}{T_{\max} - T_{\min}} R \ln \frac{P_{\max}}{P_{\min}} \qquad (4.18)$$

Table 4.2 The molar entropies for CDV reactions at $P_B \cong 10^{-7}$ bar (metal product is in the molecule form) [4, 9–11]

Reaction	$T(K)$	$\Delta S_T^\circ/\nu^a (\text{J mol}^{-1}\,\text{K}^{-1})$
$2P(\text{red}) \leftrightarrow P_2(g)$	600	162.3
$6As \leftrightarrow As_4(g) + As_2(g)$	550	157.3
$6Sb \leftrightarrow Sb_4(g) + Sb_2(g)$	650	152.9
$SiO_2 \leftrightarrow SiO(g) + O$	1,800	155.8
$SnO_2 \leftrightarrow SnO(g) + O$	1,240	160.7
$Pb_3O_4 \leftrightarrow 3PbO(g) + O$	700	153.7
$Be(OH)_2 \leftrightarrow BeO(g) + H_2O$	400	169.0
$Mg(OH)_2 \leftrightarrow MgO(g) + H_2O$	530	163.0
$Ca(OH)_2 \leftrightarrow CaO(g) + H_2O$	570	153.5
$Sr(OH)_2 \leftrightarrow SrO(g) + H_2O$	595	151.7
$Ba(OH)_2 \leftrightarrow BaO(g) + H_2O$	600	140.0−
$Zn(OH)_2 \leftrightarrow ZnO(g) + H_2O$	298	168.2
$Cd(OH)_2 \leftrightarrow CdO(g) + H_2O$	298	164.4
$MgCO_3 \leftrightarrow MgO(g) + CO_2$	670	174.8+
$CaMg(CO_3)_2 \leftrightarrow CaO(g) + MgO(g) + 2CO_2$	800	166.0
$CaCO_3 \leftrightarrow CaO(g) + CO_2$	860	158.0
$SrCO_3 \leftrightarrow SrO(g) + CO_2$	910	161.0
$BaCO_3 \leftrightarrow BaO(g) + CO_2$	1,060	142.0−
$MgSO_4 \leftrightarrow MgO(g) + SO_2 + O$	1,010	171.0+
$BaSO_4 \leftrightarrow BaO(g) + SO_2 + O$	1,390	152.0
$Cd(NO_3)_2 \leftrightarrow CdO(g) + 2NO_2 + O$	550	163.0
$Pb(NO_3)_2 \leftrightarrow PbO(g) + 2NO_2 + O$	530	160.0
$Li_2SO_4 \cdot H_2O \leftrightarrow Li_2SO_4(g) + H_2O$	330	175.9+
$CaSO_4 \cdot 2H_2O \leftrightarrow CaSO_4(g) + 2H_2O$	298	159.8
$CuSO_4 \cdot 5H_2O \leftrightarrow CuSO_4(g) + 5H_2O$	298	159.1
Average $\pm s(n = 25)$		160 ± 9

^{a} Values $\Delta S_T^\circ/\nu$ outside the interval 160 ± 9 J mol^{-1} K^{-1} are noted by marks: − or +

Here the quantities $P_{\max}$ and $P_{\min}$ are the pressures corresponding to the maximum and minimum temperatures of the experiment. (When drawing Arrhenius plots, the quantities J or k are used in place of the pressures P). It can be seen that these expressions differ primarily in the presence of an additional factor in Eq. 4.18, namely, of the ratio $T_{\max}/(T_{\max} - T_{\min})$ or $T_{\max}/\Delta T$. Another, less significant difference, lies in the use in Eqs. 4.10–4.12 of one variable, $P_{\min}$ in place of two ($P_{\max}$ and $P_{\min}$).

A simple numerical example can be used to demonstrate this difference. When measuring within a temperature interval from $T_{\min} = 900$ K to $T_{\max} = 1,000$ K (a range fairly typical, for instance, of calcite decomposition), a twofold difference in the magnitude of $P_{\max}/P_{\min}$ (or $k_{\max}/k_{\min}$) will produce an error of 52 kJ mol^{-1} in the second-law and the Arrhenius plot methods. (From Eq. 4.18: $[1,000 \times 900/(1,000 - 900)]R \ln 2 = 51.9$ kJ mol^{-1}). For the same twofold difference in the absolute rate of decomposition from its true value, an error in determination of $\Delta_r H_T^\circ$ by the third-law method (at $T = 900$ K) is only 5.2 kJ mol^{-1}. (From Eq. 4.12: $900R \ln 2 = 5.19$ kJ mol^{-1}.)

Thus, the error inherent in the use of the third-law method is indeed an order of magnitude lower than that provided by the two other methods.

Using the ratio of two independent variables (P_{max} and P_{min}) in Eq. 4.18 in place of one (P_{min}) in Eqs. 4.11 and 4.12 should further increase (by a factor $\sqrt{2}$) the difference in precision. As the number of independent measurements increases above four, the last effect becomes cancelled through averaging of the results. On the whole, however, the impact of this factor on the difference in precision of these methods is not large.

The Ratio $T_{max}/\Delta T$ in Experiments Reported It is instructive to examine the distribution of the number of publications as a function of the value of $T_{max}/\Delta T$ used in the experiments reported. Figure 4.1 is a plot of such a distribution based on the data collected by L'vov [13] from the book by Galwey and Brown [2].

The maximum of this distribution lies at the value $T_{max}/\Delta T = 10$, with an average of $T_{max}/\Delta T$ obtained from the analysis of 220 publications being 16. As can be seen, there are some cases when this ratio and therefore a loss of precision (in comparison with the third-law method) reach values of 30–50. The results of measurements obtained under such conditions certainly inspire very little confidence.

An analysis of publications that have appeared in recent years [5, 12–24] reveals that, where the molar enthalpy (the E parameter) was determined by the third-law method, the random error (relative standard deviation s_r), which
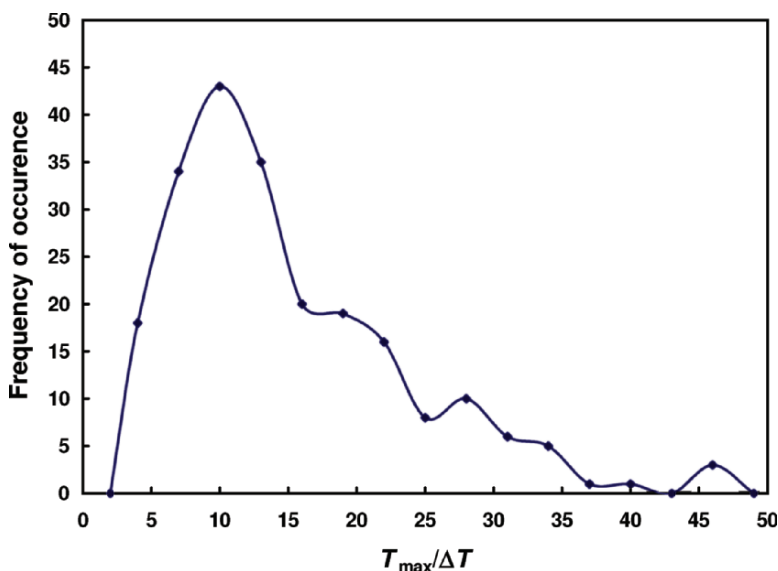

Fig. 4.1 The distribution of publications on the determination of the E parameter by the Arrhenius plot method as a function of $T_{max}/\Delta T$ ratio, in steps of equal increments (0.3). 220 items are included

is a characteristic of the reproducibility of the measurements, turns out to be less than 2%. This figure corresponds to not more than twofold variations of the decomposition rate J. In half of the cases, $s_r < 1\%$. With due account of the random errors typical of the second-law and Arrhenius plot methods, which may reach as high as 10%, the above theoretical estimates of precision appear reasonable enough.

4.7   Accuracy

Besides random variations, the primary variables may undergo systematic deviations which may affect the correctness of the determination of the parameter in question. Such deviations may very often result from an overestimation of the decomposition temperature originating from self-cooling of the reactant (see Chapter 6). The effect of this factor may become particularly pronounced for the upper points of the temperature interval used in measurements by the second-law or Arrhenius plot methods. Assuming the fairly typical conditions mentioned above, namely $T_{\min} = 900\,\mathrm{K}$ to $T_{\max} = 1,000\,\mathrm{K}$ with an error of $10\,\mathrm{K}$ in the estimate of the maximum temperature (i.e., when using $T_{\max} = 990\,\mathrm{K}$ for the calculations) will result in a systematic error in determination of $\Delta_r H_T^\circ$ of 9% in place of only 1% for the third-law method. Thus, just as in the case of random errors, the difference in the magnitude of the systematic error characterizing the third-law method, as opposed to the two other methods, is as large as an order of magnitude.

This theoretical estimate is borne out by the data obtained in the high-vacuum decompositions of the carbonates, hydrates, sulphates, and hydroxides (Chapter 16). In full agreement with theoretical estimates (see Chapter 6), the difference in temperature between the temperature-stabilized heater, say, a crucible and a sample contained in this crucible is, under high-vacuum conditions, a few tens of degrees and may become, in extreme cases, as high as 3% of the heater temperature. In many cases where the second-law and the Arrhenius plot methods are employed, this systematic error would translate into an underestimation of the values of $\Delta_r H_T^\circ$ and E by 15–20%.

Another reason that can account for the systematic differences between the values of $\Delta_r H_T^\circ$ (II), measured by the second-law and Arrhenius plot methods, and those of $\Delta_r H_T^\circ$ (III) measured by the third-law method, is the systematic decrease of the contribution of the condensation energy to the reaction enthalpy with increasing temperature and the ensuing slight increase of $\Delta_r H_T^\circ$ (III) and a substantially larger decrease of $\Delta_r H_T^\circ$ (II). This effect will be considered in detail in Sect. 8.2.

One more typical systematic error that arises in determination of the E parameter with the Arrhenius plot method is the fairly arbitrary choice of kinetic model used to estimate the rate constant k from primary TA measurements. This statement is confirmed by numerous studies generalized, in

particular, in [8]. When invoking the third-law method, the equilibrium pressure of the gaseous product which enters the calculations is unambiguously related to the absolute rate J measured under steady-state decomposition conditions, thus excluding completely such systematic errors.

The uncertainty in the values of the entropy derived from thermochemical data usually does not exceed $1\,\mathrm{J\,mol^{-1}\,K^{-1}}$ and, hence, cannot practically affect the final results of the determination with the third-law method. If, however (in the absence of reliable data), one uses averaged values of $\Delta_\mathrm{r} S_T^\circ / \nu$ known to within $\pm\,9\,\mathrm{J\,mol^{-1}\,K^{-1}}$ (see Sect. 4.5) in the calculation, this factor can no longer be neglected, because the error in determination of the enthalpy becomes as high as 3%. Even in this case, however, this restriction can hardly be a serious obstacle to the use of this method.

4.8 Measurement Time

Application of the third-law method at a single temperature cuts substantially the total measurement time compared to the time expended in using the second-law or Arrhenius plot methods. An experiment conducted at a single temperature takes up about 3–4 h, including the time required for the heating and cooling of the furnace. This does not exceed the time needed for measurements by the fastest non-isothermal TA methods, particularly if the measurements are repeated as a minimum at three different heating rates. There are, however, much longer versions of isothermal and non-isothermal methods. For instance, a measurement of the E parameter by the rate-jump method [25, 26] may take up to a 100 or more hours.

4.9 Conclusions

A comparison of three different methods by which the enthalpy of decomposition reactions can be determined shows the third-law method to excel over the other two in all respects. It is superior in precision, accuracy, and output (productivity). This conclusion finds support in the opinion generally accepted in equilibrium thermochemistry [4]. The question then is why the third-law method has never, until the appearance of publication [5] in 2002, been invoked in studies of decomposition kinetics. Several possible reasons could be proposed.

- The lack of a clear idea of the advantages this method is capable of offering, compared with known methods, as well as the apparent difficulties associated with estimation of the reaction entropy.

- The apparent inapplicability of the method to measurements (by the Arrhenius approach) of rate constants k, which at first glance are not related to the absolute value of equilibrium pressure of the primary product P_{eqp}. However, none of the above reasons can account for the fact that this method is ignored in measurements of the vaporization rate from a free surface (after Langmuir), while it is employed widely in effusion studies (after Knudsen).
- Mechanical extension of the generally accepted concepts of the absence of equilibrium in homogeneous gaseous reactions, in particular, in monomolecular reactions in the low-pressure field [27], to the kinetics of heterogeneous reactions.
- The experimentally observed differences between the decomposition rates of the same compounds from the effusion cells and from the free surface, which led to the conclusion that decomposition reactions should be classed among non-equilibrium processes that do not obey the laws of equilibrium thermodynamics.

The last consideration is possibly the most convincing argument against the use of the third-law method in kinetic studies of solid-state reactions. If the possibility of formation in the course of decomposition of primary gaseous products differing from their equilibrium forms is excluded, the observed differences in the rates have to be assigned to the decomposition mechanism itself. Strangely enough, the possibility of this difference has not yet been recognized, although the assumption of a possible difference in composition between the primary and final products of decomposition was noted by Somorjai and Lester 40 years ago [28] and, furthermore, such difference in composition was clearly observed in decomposition of some metal oxides still earlier [29, 30].

This comment refers, however, to gaseous decomposition products and does not include the extremely broad class of reactions resulting in formation of solid products. In the latter case, a deviation from ideal equilibrium is revealed in congruent vaporization of the reactant rather than in deviation of the chemical composition of the products. Additional quantitative arguments, which support the equilibrium character of decomposition mechanisms, are considered in Part II.

References

1. Brown ME, Dollimore D, Galwey AK (1980) Reactions in the solid state. Elsevier, London
2. Galwey AK, Brown ME (1999) Thermal decomposition of ionic solids. Elsevier, Amsterdam
3. Prodan EA (1986) Inorganic topochemistry. Nauka Tekhnika, Minsk (in Russian)
4. Glushko VP (1978–1982) (ed) Thermodynamic properties of individual substances, Handbook in 4 volumes. Nauka, Moscow (in Russian)

5. L'vov BV (2002) Thermochim Acta 389:199–211
6. L'vov BV (2004) Thermochim Acta 424:183–199
7. L'vov BV, Ryabchuk GN (1981) Zh Analit Khim 36:2085–2096 (in Russian)
8. Brown ME, Maciejewski M, Vyazovkin S, et al. (2000) Thermochim Acta 355:125–143
9. Glushko VP (1965–1982) (ed) Thermodynamic constants of substances, Handbook in 10 volumes. Akad Nauk SSSR, Moscow (in Russian)
10. Kireev VA (1975) Methods of practical calculations in thermodynamics of chemical reactions. Khimiya, Moscow (in Russian)
11. Ryabin VA, Ostroumov MA, Svit TF (1977) Thermodynamic characteristics of substances, Handbook. Khimiya, Leningrad (in Russian)
12. L'vov BV, Ugolkov VL (2003) J Therm Anal Cal 74:697–708
13. L'vov BV (2005) J Therm Anal Cal 79:151–156
14. L'vov BV, Polzik LK, Ugolkov VL (2002) Thermochim Acta 390:5–19
15. L'vov BV, Ugolkov VL (2003) Thermochim Acta 401:139–147
16. L'vov BV, Ugolkov VL (2004) Thermochim Acta 409:13–18
17. L'vov BV, Ugolkov VL (2004) Thermochim Acta 410:47–55
18. L'vov BV, Ugolkov VL (2004) Thermochim Acta 411:73–79
19. L'vov BV, Ugolkov VL, Grekov FF (2004) Thermochim Acta 411:187–193
20. L'vov BV, Ugolkov VL (2004) Thermochim Acta 413:7–15
21. L'vov BV, Ugolkov VL (2004) Thermochim Acta 424:7–13
22. L'vov BV, Ugolkov VL (2005) Russian J Appl Chem 78:379–385
23. L'vov BV, Ugolkov VL (2005) J Therm Anal Cal 82:15–22
24. L'vov BV, Ugolkov VL (2005) Thermochim Acta 438:1–8
25. Nahdi K, Llewellyn P, Rouquerol F, Rouquerol J, et al. (2002) Thermochim Acta 390:123–132
26. Sörensen OT, Rouquerol J (2003) (eds) Sample-controlled thermal analysis. Kluwer Academic, Dordrecht
27. Kondratiev VN, Nikitin EE (1981) Chemical processes in gases. Nauka, Moscow (in Russian)
28. Somorjai GA, Lester JE (1967) Evaporation mechanism of solids. In: Reiss H (ed) Progress in solid state chemistry. Pergamon, Oxford, pp 1–52
29. Harano Y (1961) Nippon Kagaku Zasshi 82:152–155
30. Mitani K, Asakura Y (1965) Bull Chem Soc Japan 38:901–904

Part II

Interpretation and Quantitative Analysis of the Effects and Phenomena Accompanying Thermal Decomposition

Chapter 5
Decomposition Conditions and the Molar Enthalpy

The goal of Part II is to attempt to interpret, in terms of the thermochemical approach developed in this work, some unusual effects and phenomena accompanying the decompositions of solids and melts and to use these results to confirm the correctness of the approach itself. The analysis starts from the most common relationships relating the molar enthalpy to temperature and proceeds further to the reaction mode and stoichiometry.

5.1 Ratio of the Initial Decomposition Temperature to the Molar Enthalpy

Theoretical Consideration The decomposition temperature is an important, if not the most important kinetic parameter used in studies of the decomposition processes. It defines the upper limit of reactant stability and the onset of a decomposition reaction. However, temperature is most commonly used only as an additional factor in determination of the Arrhenius parameters. (For instance, Galwey [1] used an average decomposition temperature in his estimations of A values basing on E parameters, known for various substances.) No quantitative definition of the concept of an initial decomposition temperature has been developed, based on a certain specified value of the decomposition rate J, or on parameters related to it (the rate constant k, or the equilibrium pressure of gaseous products P_B). The detailed interrelation between the decomposition temperature and the molar enthalpy, $\Delta_r H_T^\circ / \nu$ (or E parameter) has also not been considered. Meanwhile, in electrothermal AAS, the proportionality of the initial atomization temperature of an element to the E parameter has been revealed as far back as in the mid 1970s [2].

The expected form of this relationship is based on Eq. 4.11:

$$\Delta_r H_T^\circ = T(\Delta_r S_T^\circ + aR\ln\beta - \nu R\ln P_B) \tag{5.1}$$

Assuming $\beta \cong 1$ for the simplicity of further considerations:

$$\frac{T}{\Delta_r H_T^\circ / \nu} = \frac{1}{\Delta_r S_T^\circ / \nu - R\ln P_B} \tag{5.2}$$

This equation can be used to estimate the ratio of temperature to the molar enthalpy of the process, assuming that the P_B value is defined properly and that the value of molar entropy, $\Delta_r S_T^\circ / \nu$, is known. This

relationship could be considered as a generalization of Trouton's rule, relating the boiling temperature, T_b, and molar enthalpy of evaporation for liquids (see, e.g., [3]). For the boiling temperature at $P_B = 1$ bar, the mean value $\Delta_r S_T^\circ = 86 \pm 20$ J mol^{-1} K^{-1} [4], and the ratio $T_b / \Delta_r H_T^\circ$ is within the limits 9.4–15.2 K mol kJ^{-1} (with the mean value equal to 11.6 K mol kJ^{-1}).

For simple sublimation of solid substances at comparatively low P_B magnitudes, deviations of $T_{sub} / \Delta_r H_T^\circ$ values from the mean should be lower than those for the boiling of liquids, due to the appearance of an additional positive term $(-R \ln P_B)$ in the denominator in Eq. 5.2. This conclusion is confirmed by the calculated values for 37 different substances (see Table 5.1). These substances include some metals and stable binary compounds, known, as it was shown experimentally, for their equilibrium sublimation (i.e., provided that $\alpha_v = 1$). The sublimation temperatures fall within the range from 180 K for ice to 3,020 K for tungsten. Given that $P_B = 10^{-7}$ bar (this value, as will be shown below, corresponds to the initial sublimation temperature), the mean value $\Delta_r S_T^\circ = 144 \pm 17$ J mol^{-1} K^{-1} and the ratio $T_{sub} / \Delta_r H_T^\circ = 3.62 \pm 0.22$ K mol kJ^{-1}. The maximum deviation of the ratio $T_{sub} / \Delta_r H_T^\circ$ from the mean value is only 11% at the sublimation temperature, as compared to that of 25% obtained at the boiling temperature.

Experimental Data for Decomposition Reactions If it is assumed that all decomposition reactions proceed in accordance with the equilibrium laws (but with the formation of primary products which may differ from equilibrium products), then this criterion holds true for other reactions as well.

Tables 5.2 and 5.3 present data, which have been collected by L'vov (see [4] for details and references) from different publications. Table 5.2 presents the results relating to decomposition of 50 different substances to gaseous products, while Table 5.3 summarizes data for 50 other compounds for the process of their decomposition to gaseous and solid products. Despite the differences in methods, techniques, and measurement conditions, the initial decomposition temperatures, T_{in}, correspond, with some minor exceptions, to a partial pressure of the gaseous product of the order of 10^{-7} bar (within the limits of 10-fold deviation in both directions) [4].

The majority of the results presented in these tables have been obtained under isothermal conditions. The only exception are the results obtained using the methods of electrothermal AAS and quadrupole MS. In these latter experiments the mass of a specimen applied onto a graphite heater surface in a form of quasi-monolayer (by means of drying a drop of solution), amounted to several micrograms, so that it was possible to ignore the thermal inhomogeneity of the sample. All experiments were carried out under vacuum or in an inert atmosphere, i.e., in the absence of gaseous products (equimolar decomposition mode). Where there were multiple publications devoted to studies of the same substance, preference was given to the results obtained by more experienced

Table 5.1 $T_{\text{sub}}/\Delta H_T^\circ$ ratio for the sublimation of free metals and simple substances[a] [5]

Reactant	ΔS_T° (J mol^{-1} K^{-1})	T_{sub} (K)	ΔH_T° (kJ mol^{-1})	$T_{\text{sub}}/\Delta H_T^\circ$ (K mol kJ^{-1})
Ag	121.9	1,089	279.4	3.90
B	144.9	2,003	558.6	3.59
Be	123.5	1,245	320.7	3.88
Cd	114.5	447	111.2	4.02
Co	136.1	1,535	414.7	3.70
Cr	138.5	1,419	386.6	3.67
Cu	124.0	1,277	330.8	3.86
Fe	131.0	1,502	398.0	3.77
Mo	143.9	2,340	650.2	3.60
Ni	139.6	1,527	417.7	3.66
Pd	118.2	1,443	364.0	3.96
Pt	141.4	2,005	554.3	3.62
Rh	148.5	1,929	544.9	3.54
Ru	147.3	2,311	650.0	3.56
Si	143.1	1,602	443.8	3.61
Ti	133.2	1,711	457.3	3.74
W	150.2	3,020	858.3	3.52
Zn	115.1	517	128.7	4.02
2I $\leftrightarrow$ I$_2$	151.0	223	63.5	3.51
2Te $\leftrightarrow$ Te$_2$	154.8	558	161.2	3.46
KCl	139.4	779	213.0	3.66
KI	137.0	714	193.5	3.69
LiF	145.2	951	265.4	3.58
NaCl	140.7	804	220.8	3.64
BaF$_2$	165.2	1,229	367.6	3.34
BeF$_2$	160.5	759	223.6	3.39
CaF$_2$	176.3	1,316	408.3	3.22
HgBr$_2$	131.9	316	84.1	3.76
HgCl$_2$	148.7	281	79.4	3.54
HgI$_2$	144.8	321	89.5	3.59
H$_2$O	144.2	180	50.0	3.60
MgF$_2$	167.3	1,235	372.0	3.32
SnCl$_2$	164.2	429	127.8	3.36
SrF$_2$	167.1	1,359	409.2	3.32
ThO$_2$	173.0	2,358	723.9	3.26
ZrO$_2$	168.5	2,418	731.4	3.31
4P(white) $\leftrightarrow$ P$_4$	115.2	236	58.9	4.01
Average $\pm$ s	144 $\pm$ 17			3.62 $\pm$ 0.22

[a] T_{sub} corresponds to the vapour partial pressure of 10^{-7} bar

Table 5.2 T_{in}/E ratio for the decomposition of reactants to gaseous products[a]

Reactant	Sample	Medium	Method	T_{in} (K)	E (kJ mol^{-1})	T_{in}/E (K mol kJ^{-1})
As[b]	Crystal	Vacuum	I-G	550	183	3.01
Sb[b]	Crystal	Vacuum	I-G	650	207	3.14
Al$_2$O$_3$	Sml	Ar	NI-AAS	2,100	638	3.29
BaO	Sml	Ar	NI-AAS	2,200	468	4.70
BeO	Sml	Ar	NI-AAS	2,200	600	3.67
Bi$_2$O$_3$	Sml	Ar	NI-AAS	1,100	245	4.49
CaO	Sml	Ar	NI-AAS	2,000	518	3.86
CdO	Sml	Ar	NI-AAS	800	233	3.43
Cr$_2$O$_3$	Sml	Ar	NI-AAS	1,900	502	3.78
Ga$_2$O$_3$	Sml	Ar	NI-AAS	1,500	427	3.51
HgO	Powder	Vacuum	I-G	650	193	3.36
In$_2$O$_3$	Sml	Ar	NI-AAS	1,300	361	3.60
Li$_2$O	Sml	Ar	NI-AAS	1,400	361	3.88
MgO	Sml	Ar	NI-AAS	1,800	504	3.57
MnO	Sml	Ar	NI-AAS	1,700	450	3.78
PbO	Sml	Ar	NI-AAS	1,100	240	4.58
SrO	Sml	Ar	NI-AAS	2,100	500	4.20
V$_2$O$_3$	Sml	Ar	NI-AAS	2,200	633	3.48
ZnO	Crystal	Vacuum	I-T	1,400	397	3.53
GeO$_2$	Powder	Vacuum	I-MS	1,213	341	3.56
SiO$_2$	Powder	Vacuum	I-MS	1,773	508	3.49
SnO$_2$	Pellet	Vacuum	I-G	1,239	348	3.56
CdS	Crystal	Vacuum	I-G	882	238	3.71
CdSe	Crystal	Vacuum	I-G	957	236	4.06
ZnS	Crystal	Vacuum	I-T	998	258	3.87
ZnSe	Crystal	Vacuum	I-T	952	294	3.24
AlN	Pellet	Vacuum	I-G	1,590	542	2.93
GaN	Crystal	Vacuum	I-T	1,166	305	3.82
InN	Crystal	Vacuum	I-QMS	1,020	336	3.04
UN	Powder	Vacuum	I-R	1,873	526	3.56
Be$_3$N$_2$	Pellet	Vacuum	I-G	1,610	428	3.76
Mg$_3$N$_2$	Pellet	Vacuum	I-T	1,000	238	4.20
KN$_3$	Crystal	Vacuum	I-G	513	144	3.56
NaN$_3$	Crystal	Vacuum	I-G	495	151	3.28
TiN	Powder	Vacuum	I-G	1,987	533	3.73
ZrN	Powder	Vacuum	I-G	2,236	667	3.35
HfC	Pellet	Vacuum	I-G	2,773	778	3.56
TaC	Pellet	Vacuum	I-G	2,973	955	3.11
ThC$_2$	Powder	Vacuum	I-R	2,673	708	3.78
ZrC	Pellet	Vacuum	I-G	2,773	831	3.34

(continued)

Table 5.2 (continued)

LaB_6	Pellet	Vacuum	I-MS	1,993	561	3.55
SrB_6	Pellet	Vacuum	I-M	1,773	410	4.32
ZrB_2	Pellet	Vacuum	I-G	2,173	640	3.40
$BaSO_4$	Crystal	Vacuum	I-T	1,422	384	3.70
HgC_2O_4	Powder	Vacuum	I-G	373	110	3.39
NH_4HCO_3	Pellet	Vacuum	I-G	293	80	3.66
NH_4ClO_4	Pellet	N_2 (reduced)	I-M	653	162	4.03
$CH_2(COOH)_2$	Liquid	Air	I-M	407	136	2.99
Tetryl	Liquid	Air	I-M	484	161	3.01
$NH_3 \cdot NI_3$	Powder	Vacuum	I-G	253	79	3.20

[a] Sml: sub-monolayer; I: isothermal; NI: non-isothermal; G: gravimetric; T: torsion; M: manometric; R: radioactivity; AAS: atomic absorption spectrometry; MS: mass spectrometry; QMS: quadrupole mass spectrometry

[b] As and Sb sublimate in accordance with the reaction: $6M \rightarrow M_4 + M_2$ (Table 9.2)

groups (led by Searcy and Munir, Pavlyuchenko and Prodan, Fesenko and Bolgar, Topley, Jacobs, Galwey, Ingraham, Alcock and Okhotnikov).

The tables contain results for different classes of compounds: from metalloids (As and Sb) and simple binary compounds (oxides, halogens, nitrides, carbides, and borides) to salts of some inorganic and organic acids (nitrates, sulfates, carbonates, permanganates, formates, acetates, and oxalates) and hydrated salts. The tables also include some explosives (azides, ammonium salts, tetryl, metal styphnates, and nitrogen iodide). The initial decomposition temperatures for the above substances fall within the range from 253 K for nitrogen iodide to 2,973 K for TaC.

The magnitude of the ratio $T_{in}/E(K \text{ mol kJ}^{-1})$ for all reactants is very close to the expected (theoretical) value $T_{sub}/\Delta_r H_T^\circ = 3.62 \pm 0.22$ K mol kJ^{-1}. The mean value T_{in}/E is 3.61 ± 0.39 K mol kJ^{-1} for reactants in Table 5.2 and 3.62 ± 0.37 K mol kJ^{-1} for those in Table 5.3. *No difference is observed in the mean values of T_{in}/E for substances that decompose to gaseous products and those that decompose to solid and gaseous products.* The only difference between the experimental values of T_{in}/E and the theoretical (for equilibrium sublimation) value $T_{sub}/\Delta_r H_T^\circ$ is the somewhat higher (by a factor of 1.7) magnitude of the standard deviation from the mean value. This can be explained by random errors in the E parameter determination, by the simplifying assumption $\beta \cong 1$, introduced in the derivation of Eq. 5.2, and by a potential discrepancy between the initial decomposition temperature and the anticipated partial pressure of the gaseous product (10^{-7} bar). (Taking into account all the above-mentioned factors one could expect much higher deviations.)

Table 5.3 T_{in}/E ratio for the decomposition of reactants to gaseous and solid products[a]

Reactant	Sample	Medium	Method	T_{in} (K)	E (kJ mol^{-1})	T_{in}/E (K mol kJ^{-1})
Ag_2O	Powder	Vacuum	I-M	553	151	3.66
Cu_2O	Powder	Vacuum	I-G	900	205	4.39
FeO	Powder	Vacuum	I-G	1,270	331	3.84
NiO	Powder	Ar	I-G	1,180	305	3.87
Pb_3O_4	Powder	Vacuum	I-G	731	188	3.89
AgN_3	Pellet	N_2	I-M	503	151	3.33
PbN_6	Powder	Vacuum	I-M	468	152	3.08
TlN_3	Crystal	Vacuum	I-M	513	149	3.44
Ag_2CO_3	Powder	Vacuum	I-G	420	96	4.38
$CdCO_3$	Powder	Vacuum	I-G	513	151	3.40
$ZnCO_3$	Powder	Vacuum	I-G	523	159	3.29
$MgCO_3$	Powder	Vacuum	I-G	714	192	3.72
$CaMg(CO_3)_2$	Crystal	Vacuum	I-T	824	195	4.23
$CaCO_3$	Crystal	Vacuum	I-G	934	220	4.25
$SrCO_3$	Powder	Vacuum	I-G	888	290	3.06
$BaCO_3$	Powder	Vacuum	I-G	1,215	283	4.29
$NaHCO_3$	Powder	N_2	I-G	383	109	3.51
$AgNO_3$	Sml	Vacuum	NI-QMS	580	167	3.47
$Cd(NO_3)_2$	Sml	Vacuum	NI-QMS	622	183	3.40
$Pb(NO_3)_2$	Sml	Vacuum	NI-QMS	581	145	4.01
$Ca(NO_3)_2$	Powder	Vacuum	I-G	773	229	3.38
$Al_2(SO_4)_3$	Pellet	N_2	I-G	923	268	3.44
$BeSO_4$	Powder	O_2	I-G	875	217	4.03
$CdSO_4$	Powder	N_2	I-G	1,035	289	3.58
$CoSO_4$	Powder	Air	I-G	1,113	315	3.53
$CuSO_4$	Powder	Air	I-G	963	262	3.68
$FeSO_4$	Powder	Air	I-G	949	253	3.75
$MgSO_4$	Powder	Air	I-G	1,193	312	3.82
$NiSO_4$	Pellet	N_2	I-G	1,033	257	4.02
UO_2SO_4	Powder	He	I-G	912	245	3.72
$CsMnO_4$	Crystal	Vacuum	I-G	513	141	3.64
$KMnO_4$	Crystal	Vacuum	I-G	489	165	2.96
$NaMnO_4$	Crystal	Vacuum	I-G	400	128	3.13
$Cu(HCOO)_2$	Powder	Vacuum	I-G	430	146	2.95
$Th(HCOO)_4$	Powder	Ar	I-G	498	150	3.32
$UO_2(HCOO)_2$	Powder	Ar	I-G	538	169	3.18
$Ni(CH_3COO)_2$	Powder	Vacuum	I-G	548	150	3.65
$Ag_2C_2O_4$	Powder	Vacuum	I-G	378	113	3.35

Table 5.3 (continued)

CuC_2O_4	Powder	Vacuum	I-M	521	136	3.83
MnC_2O_4	Powder	Vacuum	I-G	608	180	3.38
NiC_2O_4	Powder	Vacuum	I-G	503	159	3.16
PbC_2O_4	Powder	Vacuum	I-G	582	151	3.85
$Mg(OH)_2$	Crystal	Vacuum	I-G	550	126	4.37
Kaolinite	Powder	Vacuum	I-G	818	225	3.64
$Li_2SO_4 \cdot H_2O$	Crystal	Vacuum	I-QCM	300	87	3.45
Ba-styphnate$\cdot H_2O$	Powder	Vacuum	I-G	542	153	3.54
Pb-styphnate$\cdot H_2O$	Powder	Vacuum	I-G	468	138	3.39
$BaCl_2 \cdot 2H_2O$	Crystal	N_2	I-PP	313	87	3.60
$MgC_2O_4 \cdot 2H_2O$	Crystal	N_2	I-G	425	111	3.83
$CuSO_4 \cdot 5H_2O$	Crystal	Vacuum	I-QCM	260	74	3.51

[a] Sml: sub-monolayer; I: isothermal; NI: non-isothermal; G: gravimetric; T: torsion; M: manometric; PP: periodic photomicrography; QMS: quadrupole mass spectrometry; QCM: quartz crystal microbalance

The statistical distribution of T_{in}/E values for all the 100 reactants is shown in Fig. 5.1 [4]. Each distribution point corresponds to a sum of T_{in}/E values falling within a 0.2-wide interval along the x-axis. The distribution is in good agreement with a Gaussian curve, which confirms the random character of the errors.

Although the decomposition of the majority of reactants listed in Tables 5.2 and 5.3 (as distinct from those in Table 5.1) occurs with some deviation from the completely equilibrium decomposition regime, corresponding to the formation of equilibrium primary products, their decomposition kinetics appear identical. This is observed for all the compounds where the magnitude of the ratio $T_{in}/E = 3.62 \pm 0.38\,\mathrm{K\,mol\,kJ^{-1}}$ or, correspondingly, the magnitude of the molar enthalpy of reaction is $\Delta_r S_T^\circ/\nu = 142 \pm 30\,\mathrm{J\,mol^{-1}\,K^{-1}}$. This conclusion is very important, because it proves that *decomposition reactions for all substances, regardless of the type of products formed (gaseous only or solid and gaseous), proceed according to the equilibrium laws.*

Another important conclusion is that it is possible to use the relationship $T_{in}/E = 3.62 \pm 0.38\,\mathrm{K\,mol\,kJ^{-1}}$ as an approximate estimate of E values from measured values of T_{in} (with a mean relative error of about 10%), and as a validation criterion in the analysis of experimental results. Clearly, this relationship is valid for the equimolar decomposition mode only, and is subject to the requirement that the initial decomposition temperature must correspond to the equilibrium pressure of the gaseous products within the limits of $10^{-8} - 10^{-6}$ bar.
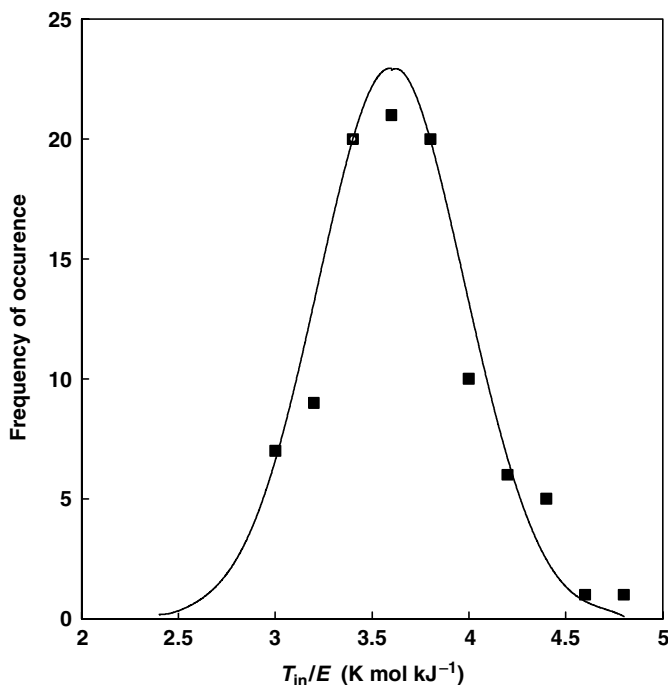
Fig. 5.1 The statistical distribution of T_{in}/E values for all 100 reactants in steps of equal increment (0.2). The curve corresponds to the Gaussian distribution. (Reproduced from [4], with permission.)

5.2   Thermal Desorption and Criteria for its Identification

Matrix Modification Technique   Up to this point, consideration of the mechanisms and kinetics of sublimation and evaporation have been limited to crystalline substances (representing an individual phase). However, the thermodynamic approach used above is not restricted to these processes only. There are some other heterogeneous processes where it can be of use. Among these are, in particular, the processes of heterogeneous catalysis and of the interactions of solid substances with gases and metal vapours. The application of this approach to a mechanism of sample atomization in electrothermal AAS (ET AAS) will be considered further.

The ET AAS technique (see Fig. 5.2) is based on fast evaporation of samples to be analysed in a miniature tube furnace (6–8 mm in diameter and 20–30 mm in length) made of graphite [5]. A light beam from the source of a line spectrum (usually a hollow cathode lamp) passes through this tube and the value of the light absorption by free atoms of analyte is measured. A grating monochromator is used to separate the most sensitive resonance line from the atomic spectrum of the element emitted by the light source.
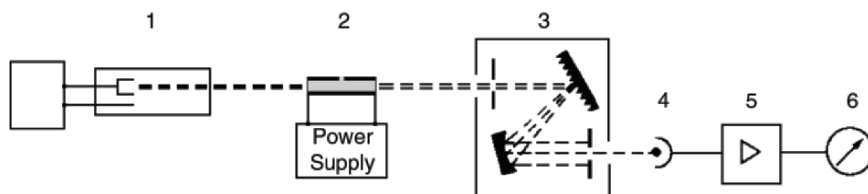
Fig. 5.2 Simplified scheme of an atomic absorption spectrometer with electrothermal atomization of samples: (1) light source (hollow cathode lamp), (2) atomizer (graphite furnace), (3) grating monochromator, (4) photo detector, (5) amplifier; and (6) indicator

Samples in nano- or microgram amounts are introduced into the furnace in a form of solutions. These aliquots (10–30 μL) are dried and, before the atomization, are subjected to a preliminary pyrolysis, which is aimed to remove (evaporate) more volatile matrix components from the sample. To achieve more efficient separation, 1–10 μg of one of the platinum group metals (most often, palladium) is added to the sample in the form of a nitrate solution. This additive serves as a chemical matrix modifier preventing evaporation of the analyte during the pyrolysis stage.

An interpretation of the mechanism of analyte retention on the furnace surface has been one of the most controversial problems in ET AAS for years. Since the first studies in this field in the 1970s, two different mechanisms have been suggested. According to the first one, the adsorption/desorption mechanism, it is supposed that the analyte is distributed on the furnace surface in the form of a monolayer of free atoms or molecules, retained on the surface by means of physical or chemical adsorption forces. According to the second one, the condensation/evaporation mechanism, the sample is distributed in a form of solid microparticles retaining all the thermochemical characteristics of the original (bulk) substance.

Numerous studies have been performed in this field during the last few decades. A non-isothermal method, traditionally used in thermal analysis was applied to measure the rate constants, which were then used in an Arrhenius plot to determine the E parameter. The magnitude of E has been compared with the enthalpies $(\Delta_r H_T^\circ)$ of various possible reactions and this was used to elucidate the actual atomization mechanism. In spite of this, the mechanism of matrix modification, as well as some other evaporation/atomization problems, still remains unrevealed.

Theoretical Consideration Several years ago L'vov [6, 7] attempted to solve this problem in the same way as had been done in the study of decomposition kinetics. That approach was based on the relationship equivalent to Eq. 5.2:

$$\frac{T_{\mathrm{app}}}{E} \cong \frac{1}{\Delta_r S_T^\circ - R \ln P_{\mathrm{app}}} \tag{5.3}$$

This equation relates the initial temperature, T_{app}, of the absorption signal appearance, the parameter E and the atomic vapour pressure, P_{app}, in

the furnace corresponding to this signal. As was shown above, assuming that $P_{\mathrm{app}} = 10^{-7}$ bar and $\Delta_{\mathrm{v}} S_T^\circ = 144 \pm 17\,\mathrm{J\ mol^{-1}\,K^{-1}}$, the ratio T_{app}/E for the evaporation process is $3.62 \pm 0.22\,\mathrm{K\ mol\ kJ^{-1}}$. For desorption of metal atoms located on the surface in the form of a two-dimensional gas, the molar enthalpy change, $\Delta_{\mathrm{d}} S_T^\circ$, should be much lower, because it corresponds to the atom transition from the two-dimensional into a three-dimensional gaseous state. These states differ only in statistical sums (partition functions) for translational motion of atoms, and the difference in entropy may be expressed by the following equation based on the principles of statistical mechanics [8]:

$$\Delta_{\mathrm{d}} S_T^\circ = R(2.5 \ln T + 1.5 \ln M - 1.16487)/3 \qquad (5.4)$$

The mean value of $\Delta_{\mathrm{d}} S_T^\circ$ for desorption of metal atoms with the average molar mass $M = 0.05\,\mathrm{kg\ mol^{-1}}$ at the temperature $T = 1{,}500\,\mathrm{K}$, is $35\,\mathrm{J\ mol^{-1}\,K^{-1}}$. Therefore the mean value of the ratio T_{app}/E for metal atom desorption of $5.9\,\mathrm{K\ mol\ kJ^{-1}}$ is 1.6 times higher than that for metal evaporation. Furthermore, the difference in the magnitudes of $\Delta_{\mathrm{d}} S_T^\circ$ manifests itself in the difference in pre-exponential factors in the Arrhenius equation for these processes. According to theory (see Sect. 3.7) the ratio of the A parameters is:

$$A_{\mathrm{v}}/A_{\mathrm{d}} \;=\; \exp[(\Delta_{\mathrm{v}} S_T^\circ - \Delta_{\mathrm{d}} S_T^\circ)/R] \cong 3 \times 10^5 \qquad (5.5)$$

Instead of a mean value $A_{\mathrm{v}} \cong 3 \times 10^{11}\,\mathrm{s^{-1}}$ (for vaporization) the A_{d} magnitude (for desorption) should be of the order of $10^6\,\mathrm{s^{-1}}$. Application of these two criteria (the T_{app}/E ratio and the absolute A value) to the analysis of the experimental data allows a decision to be made between the two feasible mechanisms and hence to find out the actual mechanism of the entry of atoms into the gas phase.

Experimental Data This method was used to identify the mechanism of analyte retention by a Pd modifier [6]. The experimentally obtained magnitudes of the ratio T_{app}/E for several analytes (in the presence of Pd modifier) were compared with the theoretical values (see Table 5.4).

The magnitudes of T_{app}/E (averaged for all the metals) appeared to be in perfect agreement with the desorption theory: 5.8 ± 0.5 (experiment) and $5.8 \pm 0.1\,\mathrm{K\ mol\ kJ^{-1}}$ (theory). The conclusion was that atoms escape from the surface of solid palladium modifier (the E parameter was measured at temperatures lower than the melting point for Pd) as a result of desorption of single atoms and, thereafter, the mechanism of their retention on palladium on the stage during pyrolysis reduces to dissociative chemisorption. The analyte atoms are adsorbed on the modifier surface in the course of low-temperature decomposition of nitrates or in the process of sample introduction into the furnace in the form of hydrides (see Table 5.4).

In subsequent work by L'vov [7], the results of similar studies for Se, Bi, Sn, and Cr retention on other metals of the platinum group (Pt, Rh, and Ru) as matrix modifiers were analysed. The mean value of the T_{app}/E ratio for

Table 5.4 Experimental and theoretical values of T_{app}/E for the analytes released from solid palladium [6, 7]

Analyte	Sample	T_{app} (K)	E (kJ mol^{-1})	ΔS_T° (J mol^{-1} K^{-1})	T_{app}/E (K mol kJ^{-1})	
					Expt	Theory
Ag	In HNO$_3$	1,778	338 ± 6	39.4	5.3	5.8
As	AsH$_3$	1,693	303 ± 12	37.5	5.6	5.8
Au	In HNO$_3$	1,508	274 ± 10	40.7	5.5	5.7
Bi	BiH$_3$	1,380	251 ± 20	40.4	5.5	5.7
Cd	In HNO$_3$	1,293	218 ± 3	37.8	6.3	5.8
Cu	In HNO$_3$	1,250	192	34.7	6.5	5.9
Se	SeH$_2$	1,465	247 ± 12	36.7	5.9	5.9
Tl	In HNO$_3$	1,709	288 ± 3	41.7	5.9	5.7

all the 11 analyte/modifier combinations (5.9 ± 0.9 K mol kJ^{-1}) was also in a good agreement with the desorption mechanism. A relatively high standard deviation was due to errors in determination of both kinetic parameters and to the deviation of the P_{app} magnitude from its mean value (10^{-7} bar) caused by differences in sensitivity of AAS measurements for Se, Bi, Sn, and Cr.

Based on these and previous results, a conclusion was made [7] that *the mechanism of analyte retention on all metals of the platinum group (at temperatures lower than melting points for these modifiers) amounts to dissociative chemisorption.*

5.3 Impact of the Decomposition Mode and Reaction Stoichiometry on the Molar Enthalpy

Theoretical Conclusions An analysis of the set of Eqs. 3.23–3.30, characterizing the absolute decomposition rates J_B for compounds, which decompose both to gaseous products only and to final solid and gaseous products, reveals, in different experimental conditions (under vacuum and in the presence of a foreign inert gas), some common features. These may be reduced to the following statements.

- The value of the molar enthalpy, $\Delta_r H_T^{\circ}/a$, for the isobaric decomposition mode does not depend on partial pressure of the excess of gaseous product in the system, P_B^{ext}, i.e., for any magnitude of P_B^{ext}:

$$E^i = \Delta H_T^{\circ}/a = \text{const} \tag{5.6}$$

- The decomposition rate in the isobaric mode, J_B^i, other factors being equal, is inversely related to the magnitude $(P_B^{ext})^{b/a}$, i.e.,

$$J_B^i \propto \left(P_B^{ext}\right)^{-b/a} \tag{5.7}$$

- The ratio of the E parameters or molar enthalpies for the isobaric and equimolar decomposition modes satisfies the condition:

$$\frac{E^{\mathrm{i}}}{E^{\mathrm{e}}} = \frac{\nu}{a} = \frac{a+b}{a} \tag{5.8}$$

These theoretical conclusions will be compared below with experimental results using two different classes of compounds, Group IIA metal carbonates and crystalline hydrates, as examples.

5.4 Decomposition of Carbonates in the Presence of CO_2

Introduction to the Problem Specific features of the decomposition of carbonates of alkaline-earth metals in the presence of CO_2 have been studied over the last 70 years in many works. However, no agreement in quantitative and even qualitative interpretation of these features has been achieved [9]. As an illustration, Table 5.5 presents the reported values of the E parameter for decomposition of calcite in the presence of CO_2. As is evident from these data, according to the majority of the studies [10–14], the increase of the CO_2 pressure was accompanied by an increase of the E parameter, and in some cases, its magnitude reached $2,000$–$4,000\,\mathrm{kJ\,mol^{-1}}$. By contrast, in other studies [15–17] the E parameter remained approximately constant, although more than a twofold difference in its absolute value was observed.

Such a scatter in results may be due to experimental errors, and primarily to the use of the Arrhenius plot method in conditions far from optimal when the ratio $T_{\max}/\Delta T$ achieves too high values (see Sect. 4.6). For example, the $T_{\max}/\Delta T$ ratio in work by Zawadski and Bretsznajder [10] was 30, 30, and 100 at CO_2 pressures of 0.026, 0.039, and 0.059 bar, respectively. Even if the rate constants k_2 and k_1 were measured to within an error of 2–3% only, the uncertainty in the determination of the E parameter could reach 200–300%.

Table 5.5 Investigations of the effect of CO_2 pressure on the E parameter for $CaCO_3$ decomposition [9]. (From the data reported in different works.)

Year	Variation of $P_{\mathrm{CO2}}^{\mathrm{ext}}$ (bar)	Point Number	Variation of E $(\mathrm{kJ\,mol^{-1}})$	Measurement Technique[a]	Calculation Method	Ref.
1935	0.0013–0.059	6	186–1,536	Isothermal	Arrhenius plot	[10]
1958	0–0.53	5	160–360	Isothermal	Arrhenius plot	[11]
1960	0.032–0.26	4	708–1,580	Non-isotherm	Arrhenius plot	[12]
1976	1.0	1	565–3,830[b]	Non-isotherm	Arrhenius plot	[13]
1977	0 and 0.05	2	201 and 950	Isothermal	Arrhenius plot	[14]
	0–1.0	3	213–2,142	Non-isotherm		
1985	0.02–0.06	3	310–460	Isothermal	Arrhenius plot	[15]
1995	0.013–0.20	4	191 ± 5	Non-isotherm	Arrhenius plot	[16]
	0.20	1	187	Isothermal		
2002	$4 \times 10^{-6} - 8 \times 10^{-5}$	5	493 ± 5	Isothermal	Third-law	[17]

[a]Non-isotherm: non-isothermal
[b]At different heating rates and sample sizes

Another source of the scatter could be the shortcomings of non-isothermal TA methods [12–14].

Use of the Third-law Method Taking into account the unreliability of these measurements, L'vov and Ugolkov [9] studied the influence of excess CO_2 pressure on the E parameter using the third-law method. In addition to their own measurements of the decomposition rate for $CaCO_3$ and $SrCO_3$ in argon, with the addition of 0.1 bar CO_2, and for $BaCO_3$, with the addition of 0.001 bar CO_2, they used results reported in the literature. Tables 5.6 and 5.7 present the initial data and calculation results for $CaCO_3$ and $SrCO_3$.

As can be seen from Table 5.6, the partial CO_2 pressure varied in different studies within the range of five orders of magnitude, from 3.6×10^{-6} to 0.6 bar. However, the E parameter remained practically the same. The mean value (obtained from 14 independent measurements) is $495 \pm 6 \, \text{kJ mol}^{-1}$. Only two results have been excluded from these calculations. One of them $(468.3 \, \text{kJ mol}^{-1})$ is underestimated, probably due to a catalytic effect of water vapours in the air atmosphere. The other, "overestimated" result $(515.4 \, \text{kJ mol}^{-1}$ at 1,073 K), seems likely to be a consequence of an expected rise of the enthalpy with temperature due to the condensation effect (see Sect. 8.2).

Table 5.6 Values of the E parameter for $CaCO_3$ decomposition in the presence of CO_2 calculated by the third-law method

Medium	$P_{CO_2}^{ext}$ (bar)	T (K)	P_{eqp} (bar)	$\Delta_r S_T^\circ$ (J mol^{-1}K^{-1})	E (kJ mol^{-1})	Ref.
N_2 (dry)	2.0E−1	1,123	4.75E−7	307.2	496.0	[18]
N_2 (dry)	6.0E−1	1,173	9.70E−7	305.8	498.7	[18]
N_2 (dry)	5.4E−1	1,223	5.00E−6	304.2	502.4	[18]
Air	2.4E−1	1,123	8.55E−6	307.2	468.3[a]	[19]
Vacuum	1.0E−4	898	5.10E−8	314.6	493.8	[20]
Vacuum	1.0E−3	983	8.00E−8	311.9	496.6	[20]
Vacuum	1.0E−3	1,006	1.08E−7	311.3	505.1	[20]
Vacuum	1.0E−3	1,073	1.11E−6	308.9	515.4[b]	[20]
He (8 mbar)	3.6E−6	857	2.23E−8	316.1	485.7	[21]
He (8 mbar)	1.5E−5	897	5.60E−8	314.6	489.8	[21]
He (8 mbar)	4.0E−5	935	1.49E−7	313.4	494.0	[21]
He (8 mbar)	5.8E−5	954	2.46E−7	312.8	496.5	[21]
He (8 mbar)	7.8E−5	974	4.86E−7	312.2	498.4	[21]
Ar	1.0E−1	1,100.3	9.05E−7	308.0	487.3	[9]
Ar	1.0E−1	1,071.0	1.30E−7	308.9	492.5	[9]
Ar	1.0E−1	1,070.9	1.80E−7	308.9	489.3	[9]
Average		$1,020 \pm 110$			495 ± 6[c]	

[a]Underestimated because of the possible catalytic effect of H_2O impurity in air
[b]Overestimated because of the strong self-cooling effect in vacuum
[c]The E values in "a" and "b" cases are excluded from calculation

Table 5.7 Values of the E parameter for $SrCO_3$ decomposition in the presence of CO_2 calculated from the literature data [9, 22] by the third-law method

Medium	$P_{CO_2}^{ext}$ (bar)	T (K)	J (kg m^{-2} s^{-1})	P_{eqp} (bar)	$\Delta_r S_T^\circ$ (J mol^{-1} K^{-1})	E (kJ mol^{-1})	Ref.
Vacuum	3.9E−5	1,003	5.92E−7	6.38E−9	318.9	561.9	[22]
Vacuum	2.2E−4	1,053	4.51E−7	4.98E−9	317.0	574.9	[22]
Vacuum	1.3E−3	1,133	4.08E−6	4.67E−8	314.5	577.9	[22]
Argon	1.0E−1	1,131	4.40E−7	5.00E−9	314.6	556.5	[9]
Argon	1.0E−1	1,151	2.30E−7	2.70E−9	313.9	571.6	[9]
Average						569 ± 9	

For $SrCO_3$ (Table 5.7) the difference in $P_{CO_2}^{ext}$ magnitudes was about four orders of magnitude. The rate constants k served as initial data in the paper [22]. They were recalculated as magnitudes of J using Eq. 3.32 and with regard to magnitudes $r_0 = 1.2 \times 10^{-6}$ m (according to estimates given in [22]) and $\rho = 3,700$ kg m^{-3}. The mean value (obtained from five independent measurements) was 569 ± 9 kJ mol^{-1}.

Thus, the molar enthalpy, characterizing the decomposition of carbonates in the presence of excess CO_2 remains unchanged with variations of the CO_2 content within the range of five orders of magnitude for $CaCO_3$ and four orders of magnitude for $SrCO_3$. This supports the first of the three statements (consequences), resulting from the CDV mechanism and the corresponding kinetic equations.

The final values of the molar enthalpy (parameter E) for decomposition of $CaCO_3$, $SrCO_3$, and $BaCO_3$ in the equimolar and isobaric modes are summarized in Table 5.8. The mean value of the ratio E^i/E^e is 1.98 ± 0.03, which coincides with the theoretically expected magnitude of this ratio (the third statement listed above).

Hyperbolic Dependence of the Decomposition rate on the External CO_2 Pressure The results presented in studies [16, 18, 19] confirm the second consequence, which for calcite decomposition in the presence of CO_2 predicts a hyperbolic dependence between the rate and $P_{CO_2}^{ext}$. Data taken from the paper by Hyatt et al. [18] are presented in Fig. 5.3. If we exclude from consideration the rates of $CaCO_3$ decomposition at $900\,^\circ$C in the absence of $CO_2 (P_{CO_2} = 0\,$atm$)$, which are clearly underestimated owing to the self-cooling of the sample caused by the low thermal conductivity of gas and by the

Table 5.8 Experimental values of the E parameter for the decomposition of carbonates in the isobaric [9] and equimolar [17, 23] modes

Carbonate	T (K)		E (kJ mol^{-1})		E^i/E^e	Ref.
	i-mode	e-mode	i-mode	e-mode		
$CaCO_3$	1,020	820	495 ± 6	254 ± 6	1.95	[17]
$SrCO_3$	1,090	908	569 ± 9	285.5 ± 1.3	1.99	[23]
$BaCO_3$	1,249	1,077	605 ± 1	302.1 ± 1.5	2.00	[23]
Average					1.98 ± 0.03	
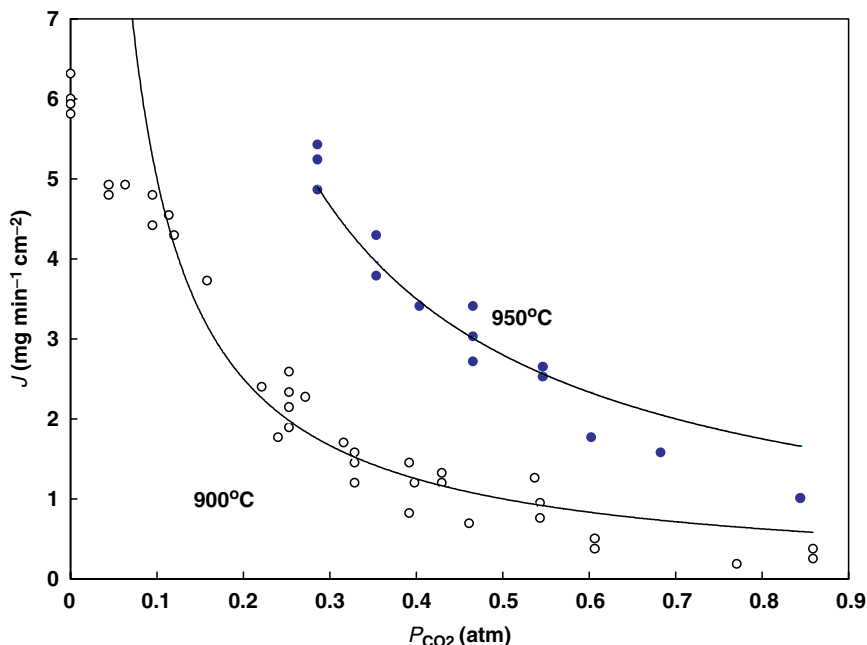
Fig. 5.3 A hyperbolic dependence of the $CaCO_3$ decomposition rate on $P_{CO_2}^{ext}$. Curves correspond to the theory. (Reproduced from [18], with permission.)

high decomposition rate $(\sim 1\,g\,m^{-2}\,s^{-1})$, then the experimental and theoretical results are in very good agreement.

Thus, *the experiments on decomposition of carbonates of alkaline-earth metals in an excess of CO_2 are in excellent agreement with the CDV mechanism and its corresponding kinetic model.* One thus needs to be critical of works reporting a continuous rise of the E parameter with excess CO_2 pressure, in particular, of the results of study [10], a source of the long-lasting misconception in solid-state kinetics, "Zawadski and Bretsznajder rule".

5.5   Dehydration of Crystalline Hydrates in the Presence of H_2O

Selection of Primary Data The thermal dehydrations of crystalline hydrates belong to the vast group of reactions that have been intensively studied and presented in the literature. The long-term kinetics research performed on these reactions has defined, essentially, the main achievements and problems in the field of solid-state reactions. That is why the study of the dependence of the E parameter on the excess pressure of H_2O vapour during the process

of dehydration of crystalline hydrates is of obvious interest. Recent work by L'vov [24] has been devoted to this problem.

The following criteria (with some minor exceptions) have been used in the selection of the primary data, necessary for further analysis:

- The E parameters for both the equimolar and isobaric modes should have been measured and described by the same research group and, preferably, in the same paper.
- Measurements had been performed using isothermal thermogravimetry.
- The determination of E^e values had been carried out in a high vacuum (with continuous pumping).
- The same kinetic model had been used for calculations of the rate constants for different modes.
- Parameters E had been calculated using the Arrhenius plot method.
- Where E^i parameters had been determined at different pressures P_{H_2O}, the result corresponding to the highest P_{H_2O} magnitude was chosen (beyond P_{H2O} magnitudes that are typical for the Topley–Smith effect).

As a result of a thorough analysis of the available literature (monographs, collected papers, conference proceedings, and periodicals) published over the last 45 years, L'vov [24] selected 22 different reactions (see Table 5.9), the kinetics of which had been studied in two different modes, under above-mentioned conditions. The list of reactants includes: 3 layer silicates (clays), 3 hydroxides, 15 hydrates, and 1 anhydrous carbonate (which was included in the table to demonstrate an absence of the effect for anhydrous compounds). The reactants are listed in order of increasing ν/a magnitudes. Analysing the references [25–50] it can be seen that 13 reactants from the 22 were studied during the period 1970–1987 under the leadership of Pavlyuchenko and Prodan (the Institute of General and Inorganic Chemistry at Minsk).

In some cases, the above-mentioned requirements applied to selection of results have not been fulfilled. Magnitudes of E^i and E^e for talc, muscovite, and $Li_2SO_4 \cdot H_2O$ have been obtained by different researchers. For a number of reactants ($Zn(OH)_2$, $LiCl \cdot H_2O$, $Er(HCOO)_3 \cdot 2H_2O$, $NiNa_3P_3O_{10} \cdot 12H_2O$, and $ZnNa_3P_3O_{10} \cdot 12H_2O$) the E^i and E^e parameters were calculated or recalculated by L'vov [24] from the initial data taken from the publications. This was necessary either because of a lack of calculations in the original papers [41, 49], or by obvious discrepancies between the initial data and the calculation results [33, 35, 50]. The reliability of E^i/E^e magnitudes for this group of reactants is apparently lower than for the other reactants, although it is doubtful that the discrepancy with actual values would exceed 10–20%.

Analysis The following conclusions can be drawn from the analysis of the data presented in Table 5.9.

- There is a good correlation between the experimentally obtained magnitudes of E^i/E^e and the theoretical values of ν/a. The magnitude of the

Table 5.9 The kinetic parameters of dehydration reactions in different modes

Reactant	ΔT (K)	a	b	b/a	ν/a	E (kJ mol^{-1}) i-mode	e-mode	E^i/E^e	Δ (%)	P_{H_2O} (mbar)	Refs. i-mode	e-mode
$Na_2CO_3 \cdot 3NaHCO_3$	351–403	4	0	0	1	105	102	1.03	3.0	20	[25]	[25]
$3MgO \cdot 4SiO_2 \cdot H_2O$	1,220–1,295	7	1	0.14	1.14	423	366	1.15	0.6	Zero-grade Ar	[26]	[27]
$K_2O \cdot 3Al_2O_3 \cdot 6SiO_2 \cdot 2H_2O$	1,051–1,101	10	2	0.2	1.2	377	341	1.11	-7.5	Air static	[28]	[27]
$Al_2O \cdot 2SiO_2 \cdot 2H_2O$	663–748	3	2	0.67	1.67	351	213	1.65	-1.0	6	[29]	[29]
$Mg(OH)_2$	543–643	1	1	1	2	238	121	1.97	-1.5	5	[30]	[30]
$Cd(OH)_2$	343–393	1	1	1	2	272	116	2.34	17.0	7	[31]	[32]
$Zn(OH)_2$	348–394	1	1	1	2	209[a]	95	2.20	10.0	18	[33]	[33]
$CaC_2O_4 \cdot H_2O$	382–465	1	1	1	2	281	147	1.91	-4.5	Air dynamic	[34]	[34]
$LiCl \cdot H_2O$	353–373	1	1	1	2	177[b]	98[b]	1.81	-9.5	20	[35]	[35]
$Li_2SO_4 \cdot H_2O$	300–382	1	1	1	2	160	86	1.86	-7.0	Air static	[36]	[37, 38]
$BaCl_2 \cdot H_2O$	318–333	1	1	1	2	151	80	1.89	-5.5	20	[39]	[39]
$Ca(H_2PO_4)_2 \cdot H_2O$	313–373	1	1	1	2	159	67	2.37	18.5	10	[40]	[40]
$Er(HCOO)_3 \cdot 2H_2O$	377–417	1	2	2	3	187[c]	87[c]	2.15	-28.3	11	[41]	[41]
$Y(HCOO)_3 \cdot 2H_2O$	387–407	1	2	2	3	200	82	2.44	-18.7	7	[42]	[42]
$(NH_4)_5P_3O_{10} \cdot 2H_2O$	262–333	1	2	2	3	100	46	2.17	-27.7	1	[43]	[43]
$MnHPO_4 \cdot 3H_2O$	303–375	1	3	3	4	250	57	4.39	9.8	24	[44]	[44]
$Y_2(CO_3)_3 \cdot 4H_2O$	298–453	1	4	4	5	154	35	4.40	-12.0	12	[45]	[45]
$Na_5P_3O_{10} \cdot 6H_2O$	303–370	1	6	6	7	236	59	4.00	-42.9	6	[46]	[46]
$Na_3P_3O_9 \cdot 6H_2O$	260–308	1	6	6	7	264	41	6.44	-8.0	12	[47]	[47]
$La_2(CO_3)_3 \cdot 8H_2O$	270–430	1	8	8	9	515	65	7.92	-12.0	13	[48]	[48]
$NiNa_3P_3O_{10} \cdot 12H_2O$	283–333	1	12	12	13	431[d]	40	10.78	-17.1	18	[49]	[50]
$ZnNa_3P_3O_{10} \cdot 12H_2O$	273–328	1	12	12	13	461[e]	48[e]	9.60	-26.1	20	[50]	[50]

[a] From the data in Fig. 22 [33] at 90°C, 95°C, and 100°C

[b] From the data in Table 1 [35] at 80°C and 85°C for the i-mode and at 95°C and 100°C for the e-mode

[c] From the data in Fig. 3 [41] at 114°C, 124°C, 134°C, and 144°C for the i-mode and from Table 2 at 104°C, 114°C, 124°C, and 144°C for the e-mode

[d] From the data in Fig. 3 [49] at 60°C, 62°C, and 65°C

[e] From the data in Fig. 2 [50] at 0°C and 15°C for the e-mode and at 47°C and 50°C for the i-mode
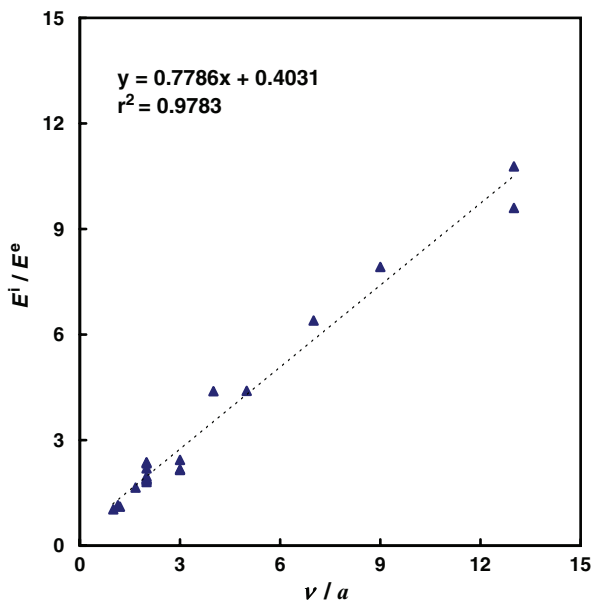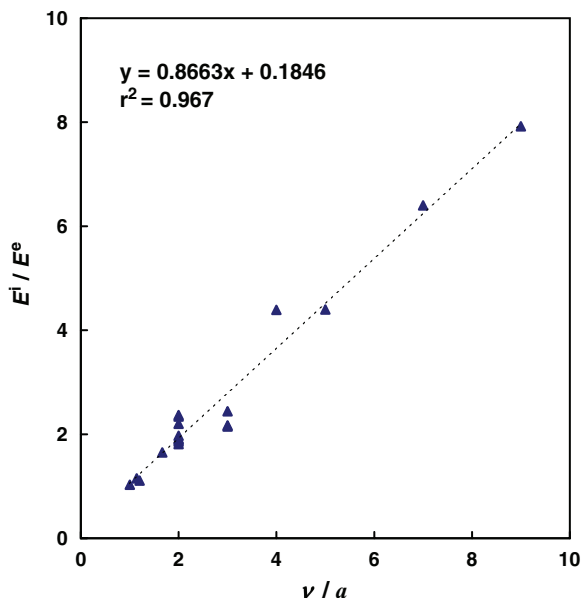
Fig. 5.4 Correlation between the experimental ratios of the Arrhenius parameters E^i/E^e and the theoretical ratios of the stoichiometric coefficients ν/a for all the reactants (see Table 5.9) except for $Na_5P_3O_{10} \cdot 6H_2O$

relative standard deviation, s_r, for all the 22 reactants amounts to 17% only, although for two of them it reaches 28%, and for one, 43%.

- The similar data (excluding one result for $Na_5P_3O_{10} \cdot 6H_2O$ which differs from others most of all), presented in Fig. 5.4 in a graphic form, testify that the correlation coefficient is close to 0.99. However, the slope of the correlation curve is only 0.78. This can be partially explained by underestimation of experimental results for reactants with the ν/a magnitude equal to 13. With the additional exclusion of these points (Fig. 5.5), the slope would increase to 0.87. However, a systematic underestimation of the experimental results on the whole seems obvious. For 16 reactants the results turned out to be lower than expected, and only for 4 reactants, substantially higher. One of the reasons may be the differences in composition of the solid product for different modes. In the presence of H_2O the dehydration of some reactants proceeds via the formation of mono- or dihydrates, whereas in a vacuum anhydrous salts are formed. This was shown, in particular, for $ZnNa_3P_3O_{10} \cdot 12H_2O$ [50] and $NiNa_3P_3O_{10} \cdot 12H_2O$ [49]. The dehydration enthalpy should thus decrease compared to the enthalpy for formation of an anhydrous product.

- To estimate the probability of such a correlation being accidental, it is necessary to calculate the number of statistically independent sectors in a

Fig. 5.5 Correlation between the experimental ratios of the Arrhenius parameters E^i/E^e and the theoretical ratios of the stoichiometric coefficients ν/a for all the reactants (see Table 5.9) except for $Na_5P_3O_{10} \cdot 6H_2O$ and two reactants with $\nu/a = 13$

13-fold variation interval ν/a, with the width $\nu/a \pm 2s$ for each of sectors and $s = 0.17\nu/a$ (2s-criterion for determination of sector independence corresponds to a confidence interval of 95%). Taking into account that the relative rise of width of sectors equals to 1.68, their quantity should be equal to $5(1.68^5 \cong 13)$. The probability of random correlation between E^i/E^e and ν/a is 0.2 for one reactant and $0.2^{22} \cong 4 \times 10^{-16}$ for 22 reactants. Thus, on the whole, this correlation is in no way random in nature.

- The mean value of the E parameter at low dehydration temperatures ($\leq 300\,K$), applicable to eight of the reactants, was $49 \pm 10\,kJ\,mol^{-1}$. This magnitude exceeds the enthalpy of evaporation of free water at $298\,K(\Delta H^\circ_{298} = 44.0\,kJ\,mol^{-1})$. However, for three reactants the E parameter turned out to be lower than $44\,kJ\,mol^{-1}$. This indicates an obvious measurement error, associated, most likely, with the self-cooling effect. If it is assumed that this systematic error affects both parameters, E^e and E^i, equally then their ratio is close to the true value.

- The mechanism of dehydration of layer silicates [51] is believed to differ from the mechanism of dehydration of crystalline hydrates and this has been used to explain the observed differences in parameters E^e (in vacuum) and in decomposition temperatures. This view is reflected, in particular, in the fact that the special term "dehydroxylation" is used in the literature to describe clay dehydration. However, this belief is not justified. As can be

seen from Table 5.9, the increase of molar enthalpy (parameter E^e) for clays is accompanied by an abrupt rise of the coefficient a. This implies that, for instance, for talc to remove one mole of water it is necessary, according to the CDV mechanism, to vaporize, as ballast, seven extra moles of other low-volatility components ($3MgO$ and $4SiO_2$). As a result, both the temperature and molar enthalpy rise considerably (by a factor of 4–8) as compared to these parameters for hydroxides and, especially, for hydrates (for $a = 1$).

Thus, the dehydration of crystalline hydrates in the presence of water, in the same way as the decomposition of carbonates in an excess of CO_2, occurs in agreement with predictions from the CDV mechanism and its corresponding kinetic model.

References

1. Galwey AK (1994) Thermochim Acta 242:259–264
2. Sturgeon RE, Chakrabarti CL, Langford CH (1976) Anal Chem 481:792–1807
3. Pauling L (1970) General chemistry. Freeman, San-Francisco
4. L'vov BV (2002) Thermochim Acta 389:199–211
5. Welz B, Sperling M (1999) Atomic absorption spectrometry. Wiley, Weinheim
6. L'vov BV (2000) Spectrochim Acta B 55:1659–1668
7. L'vov BV (2000) Spectrochim Acta B 55:1913–1919
8. Glushko VP (1978–1982) (ed) Thermodynamic properties of individual substances, Handbook in 4 volumes. Nauka, Moscow (in Russian)
9. L'vov BV, Ugolkov VL (2004) Thermochim Acta 410:47–55
10. Zawadzki J, Bretsznajder S (1935) Z Elektrochem 41:215–223
11. Tagawa H, Sudo F (1958) J Chem Soc Ind Chem Sect 61:946–948
12. Mauras H (1960) Bull Soc Chim France 260–267
13. Gallagher PK, Johnson DW (1976) Thermochim Acta 14:255–261
14. Caldwell KM, Gallagher PK, Johnson DW (1977) Thermochim Acta 18:15–19
15. Maciejewski M, Baldyga J (1985) Thermochim Acta 92:105–108
16. Criado JM, Gonzalez M, Malek J, Ortega A (1995) Thermochim Acta 254:121–127
17. L'vov BV, Polzik LK, Ugolkov VL (2002) Thermochim Acta 390:5–19
18. Hyatt EP, Cutler IB, Wadsworth ME (1958) J Am Ceram Soc 41:70–74
19. Ingraham TR, Marier P (1963) Can J Chem Eng 41:170–173
20. Darroudi T, Searcy AW (1981) J Phys Chem 85:3971–3974
21. L'vov BV (2001) Thermochim Acta 373:97–124
22. Zemtsova ZN, Pavlyuchenko MM, Prodan EA (1971) Vesti AN BSSR Ser Khim No 5:21–26 (in Russian)
23. L'vov BV, Ugolkov VL (2004) Thermochim Acta 409:13–18
24. L'vov BV (2006) J Therm Anal Cal 84:581–587
25. Pavlyuchenko MM, Prodan EA, Kramarenko FG, et al. (1979) Thermal decomposition of inorganic compounds in gaseous atmosphere. In: Prodan EA (ed) Heterogeneous chemical reactions. Nauka Tekhnika, Minsk (in Russian), pp 37–54
26. Ward JR (1975) Thermochim Acta 13:7–14
27. L'vov BV, Ugolkov VL (2005) J Therm Anal Cal 82:15–22
28. Holt B, Cutler IB, Wadsworth ME (1964) Kinetics of the thermal dehydration of hydrous silicates. In: Bradeley WF (ed) Proceedings of 12th National Conference on Clay and Clay Minerals, Atlanta, Georgia. Pergamon, Oxford, pp 55–67

29. Brindley GW, Sharp JH, Patterson JH, Nakahira BN (1967) Am Mineral 52:201–211
30. Zhabrova GM, Gordeeva VA (1960) Kinet Katal (Paper Collection). Akad Nauk SSSR, Moscow (in Russian)
31. Novoselova MYu, Prodan EA, Pavlyuchenko MM, Slyshkina SA (1972) Vesti AN BSSR Ser Khim No 1:10–14 (in Russian)
32. Pavlyuchenko MM, Novoselova MYu, Prodan EA (1969) Vesti AN BSSR Ser Khim No 1:5–10 (in Russian)
33. Pavlyuchenko MM, Prodan EA, Kramarenko FG, et al. (1979) Effect of gaseous phase on the decomposition kinetics of some carbonates and hydroxides. In: Prodan EA (ed) Heterogeneous chemical reactions. Nauka Tekhnika, Minsk (in Russian), pp 54–57
34. Dollimore D, Evans TA, Lee YF, Wilburn FW (1992) Thermochim Acta 198:249–257
35. Pavlyuchenko MM, Borisenko EM, Torgonskaya TI (1971) Dokl AN BSSR 15:322–324 (in Russian)
36. L'vov BV, Ugolkov VL (2005) Russian J Appl Chem 78:379–385
37. Okhotnikov VB, Yakobson BI, Lyakhov NZ (1983) React Kinet Catal Lett 23:125–130
38. Kirdyashkina NA, Okhotnikov VB (1988) React Kinet Catal Lett 36:417–422
39. Lumpkin JA, Perlmutter DD (1995) Thermochim Acta 249:335–349
40. Pavlyuchenko MM, Borisenko EM (1970) Dehydration kinetics of calcium phosphate monohydrate. In: Pavlyuchenko MM, Prodan EA (eds) Heterogeneous chemical reactions. Nauka Tekhnika, Minsk, (in Russian), pp 181–189
41. Masuda Y, Hirata K, Ito Y (1992) Thermochim Acta 203:289–296
42. Masuda Y, Ito Y (1992) J Therm Anal 38:1793–1799
43. Prodan EA, Korzhuev VN, Petrovskaya LI (1981) Vesti AN BSSR Ser Khim No 1:71–75 (in Russian)
44. Samuskevich VV, Prodan EA, Kluy IV (1984) Vesti AN BSSR Ser Khim No 1:47–51 (in Russian)
45. Pavlyuchenko MM, Kokhanovsky VV, Prodan EA (1970) Dehydration kinetics of crystalline hydrate of yttrium carbonate. In: Pavlyuchenko MM, Prodan EA (eds) Heterogeneous chemical reactions. Nauka Tekhnika, Minsk (in Russian), pp 168–180
46. Pavlyuchenko MM, Prodan EA, Lesnikovich LA (1972) Dokl AN BSSR 16:719–722 (in Russian)
47. Prodan EA, Pytlev SI (1985) Vesti AN BSSR Ser Khim No 6:47–52 (in Russian)
48. Pavlyuchenko MM, Samuskevich VV, Prodan EA (1970) Vesti AN BSSR Ser Khim No 6:11–15 (in Russian)
49. Pavlyuchenko MM, Pisyak YaS, Zonov YuG, Prodan EA (1970) Vesti AN BSSR Ser Khim No 1:29–37 (in Russian)
50. Prodan EA, Zonov YuG, Pavlyuchenko MM (1971) Vesti AN BSSR Ser Khim No 2:21–25 (in Russian)
51. Brown ME, Dollimore D, Galwey AK (1980) Reactions in the solid state. Elsevier, London

Chapter 6
The Self-cooling Effect

The role of self-cooling in endothermic decompositions has been discussed in many works. However, only in a few studies [1–3] performed during the period 1930–1950 has this effect been taken into account in measurements of dehydration rates and of the corresponding Arrhenius parameters (E and A). Most of the other researchers assume (often implicitly) that the magnitude of self-cooling is insignificant and may be neglected. Much greater attention has been given to the problem of self-heating during the processes of pyrolysis, carbon gasification, and decomposition of high-energy materials.

L'vov and his colleagues published in 1998 results of their research on the modelling of the temperature distribution in heterogeneous systems and on estimations of the influence of self-cooling on the decomposition parameters for $Mg(OH)_2$ [4] and $Li_2SO_4 \cdot H_2O$ [5]. The difference in temperatures of a furnace and a sample (even in a single crystal form) may reach, in a high vacuum, a few tens of degrees, and, consequently, may be a source of severe errors in the determination of kinetic parameters. The self-cooling effect should be much greater for powder samples.

6.1 The Model for Temperature Calculation

L'vov et al. [4, 5] used the following procedure to model the temperature distribution in a powder sample in the presence of residual air (or foreign gas) and water vapour. The specimen was considered to be composed of horizontal layers of material with the layer thickness equal to a powder grain diameter, so that the modelling could be reduced to a reconstruction of a vertical temperature distribution between the sample layers. (A single crystal sample corresponds to a one-layer specimen.) The furnace temperature above and below the specimen was assumed to be the same so the analysis was limited to consideration of half of this multilayer sample, from a central, zeroth or first layer, up to the nth, outer layer.

If the thermal conductivity at point contacts between grains is neglected and decomposition conditions are assumed to be stationary, a heat balance equation for any ith layer of the sample can be formulated, which connects the amounts of heat expended for decomposition, radiation, and heat conduction of water vapours and residual air, with the heat accumulated from radiation and heat transfer from the neighbouring $(i-1)$th and $(i+1)$th layers:

$$2AT_i^{-1/2}\left[\left(\frac{P_w^2}{4} + B\exp\frac{E}{T_i}\right)^{1/2} - \frac{P_w}{2}\right] + 2CT_i^4$$
$$+ D_wT_i^{-1/2}P_w(T_i - T_{i-1}) + D_aT_i^{-1/2}P_a(T_i - T_{i-1})$$

$$= C(T_{i-1}^4 + T_{i+1}^4) + D_{\mathrm{w}}T_i^{-1/2}P_{\mathrm{w}}(T_{i+1} - T_i)$$
$$+D_{\mathrm{a}}T_i^{-1/2}P_{\mathrm{a}}(T_{i+1} - T_i) \tag{6.1}$$

Here

$$A \equiv \frac{\gamma \Delta_{\mathrm{r}} H_T^\circ}{(2\pi M_{\mathrm{p}} R)^{1/2}} \tag{6.2}$$

$$B \equiv \exp \frac{\Delta S_T^\circ}{R} \tag{6.3}$$

$$C \equiv \varepsilon\sigma \tag{6.4}$$

$$D_{\mathrm{w}} \equiv \frac{\gamma C_{v\mathrm{w}}}{(2\pi M_{\mathrm{w}} R)^{1/2}} \tag{6.5}$$

$$D_{\mathrm{a}} \equiv \frac{\gamma C_{v\mathrm{a}}}{(2\pi M_{\mathrm{a}} R)^{1/2}} \tag{6.6}$$

$$E \equiv -\frac{\Delta_{\mathrm{r}} H_T^\circ}{R} \tag{6.7}$$

As above, $\Delta_{\mathrm{r}} H_T^\circ$ and ΔS_T° are the enthalpy and entropy of the decomposition reaction; P_{w} and P_{a} are the excess partial pressures of water vapour and air; M_{p}, M_{w}, and M_{a} are the molar masses of the product, water and air, respectively; $C_{v\mathrm{w}}$ and $C_{v\mathrm{a}}$ are the molar heat capacities for water and air; ε is the grain surface emittance, and σ is the Stefan–Boltzmann constant. The expression in square brackets corresponds to the partial pressure of product at comparable magnitudes of excess (external) and equivalent (internal) partial pressures of water [5].

Equation 6.1 can be rewritten in a simplified form:

$$C(T_{i+1}^4 - 2T_i^4 + T_{i-1}^4) + (D_{\mathrm{w}}P_{\mathrm{w}} + D_{\mathrm{a}}P_{\mathrm{a}})T_i^{-1/2}(T_{i+1} - 2T_i + T_{i-1})$$
$$= 2AP_{\mathrm{w}}^{-1}T_i^{-1/2}\left[\left(\frac{P_{\mathrm{w}}^2}{4} + B\exp\frac{E}{T_i}\right)^{1/2} - \frac{P_{\mathrm{w}}}{2}\right] \tag{6.8}$$

The following additional boundary conditions can be introduced for the central ($i = 0$ or $i = 1$) coldest layer:

$$T_{i+1} = T_{i-1} \tag{6.9}$$

for an odd total number of layers ($n_{\mathrm{t}} = 2n + 1$) and

$$T_i = T_{i-1} \tag{6.10}$$

for an even number of layers ($n_{\mathrm{t}} = 2n$). Then Eq. 6.8 takes the form:

$$C(T_1^4 - T_0^4) + (D_{\mathrm{w}}P_{\mathrm{w}} + D_{\mathrm{a}}P_{\mathrm{a}})T_i^{-1/2}(T_1 - T_0)$$
$$= AP_{\mathrm{w}}^{-1}T_i^{-1/2}\left[\left(\frac{P_{\mathrm{w}}^2}{4} + B\exp\frac{E}{T_i}\right)^{1/2} - \frac{P_{\mathrm{w}}}{2}\right] \tag{6.11}$$

for an odd number of layers and

$$C(T_2^4 - T_1^4) + (D_w P_w + D_a P_a)T_1^{-1/2}(T_2 - T_1)$$
$$= 2AP_w^{-1}T_1^{-1/2}\left[\left(\frac{P_w^2}{4} + B\exp\frac{E}{T_i}\right)^{1/2} - \frac{P_w}{2}\right] \qquad (6.12)$$

for an even number of layers.

Setting the temperature of the coldest layer (T_0 or T_1), one can determine the temperature of an adjacent layer using determined Eqs. 6.11 and 6.12. The temperatures of all the other layers can be then sequentially using Eq. 6.8. The $(n+1)$-th layer temperature is set to be the same as the furnace temperature. To achieve that, the magnitude of T_0 or T_1 is varied with all the other conditions kept constant.

Software Software to be run on a PC was written in Visual Basic for Windows. A diagram of its algorithm is shown in Fig. 6.1 [5]. After entering all the calculated parameters, namely: furnace temperature, T_f, total number of layers, n_t, water vapour pressure, P_w, foreign gas pressure, P_a, parameters A, B, C, D, E and first-layer temperature, which, in the initial stage may be taken to be equal to $T_f/2$, the temperature of the second layer is calculated by means of an iterative procedure using Eq. 6.12. The T_2 magnitude is a varying parameter, and in the first approximation it is equal to T_1. The iteration process proceeds until the difference between the left (L) and right (R) parts of Eq. 6.12 drops to 10^{-9}. Then the temperatures of all the succeeding layers from T_3 to T_{n+1} are calculated in a similar way, using Eq. 6.8.

The initial temperature for each succeeding layer T_{i+1} is taken to be equal to the preceding layer temperature, T_i. When the calculations are finished, the $(n+1)$-th layer temperature is compared with the furnace temperature. If the condition $|T_f - T_{n+1}| \leq 0.01$ is met, the calculation is considered finished. Otherwise the first-layer temperature is either decreased (if $T_f < T_{n+1}$), or increased (if $T_f > T_{n+1}$) and the calculation is repeated. If the calculation is performed for different pressures of water vapour ($P_{start} \neq P_{end}$), the above described procedure is repeated for each new P_w value, which is varied from $P_{start} = 10^{-5}$ bar to $P_{end} = 10^{-2}$ bar. The results are displayed in the form of graphs and/or tables.

6.2 The Temperature Distribution in Powder Reactants

For an example of the application of the software described above, the temperature distribution in a powder sample of $Mg(OH)_2$ in a high vacuum (in the absence of foreign gas and water vapour), is considered below. The temperature distribution is presented in Fig. 6.2 as a function of the number of layers
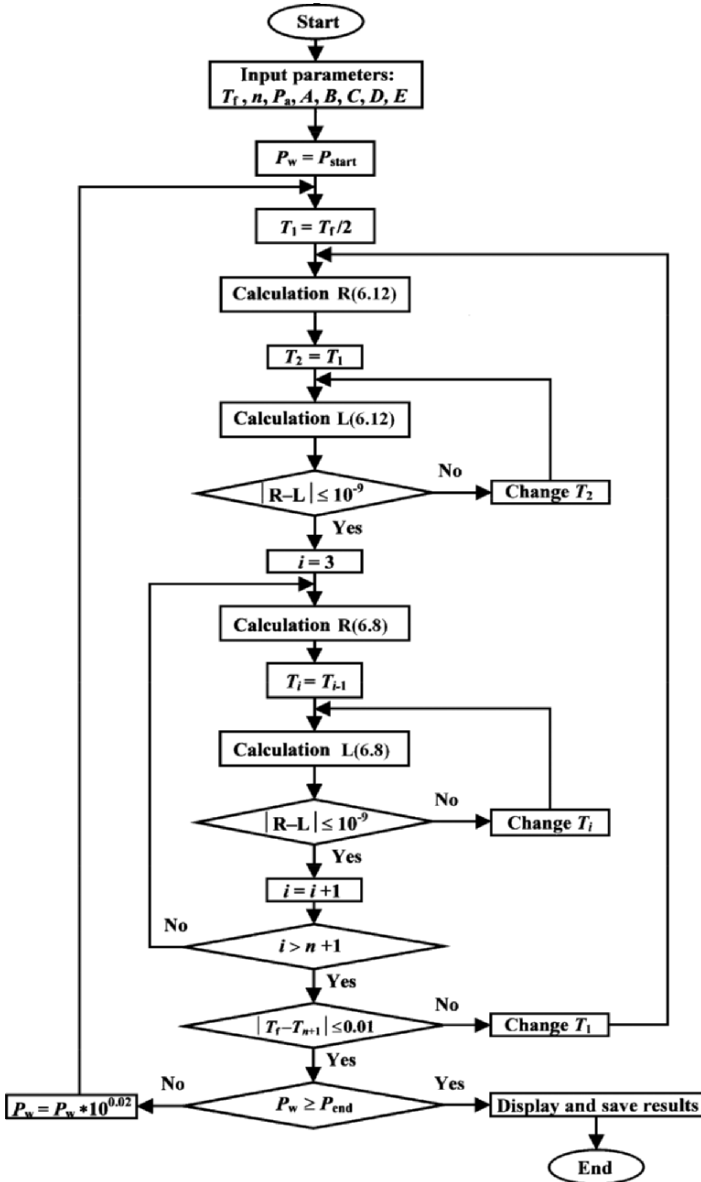
Fig. 6.1 Flow chart of the calculation program
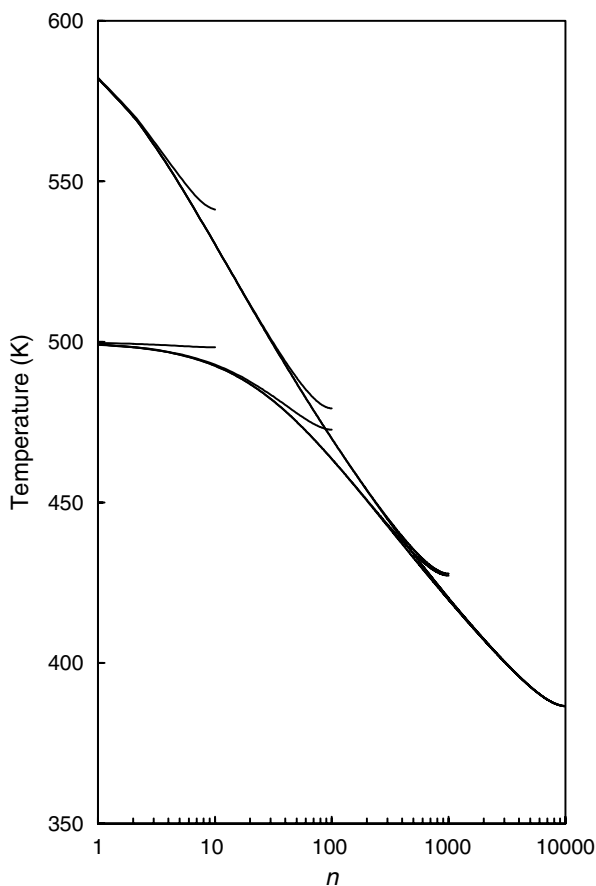
Fig. 6.2 Calculated temperature distribution for a powder sample of $Mg(OH)_2$ in a vacuum at 500 and 600 K furnace temperature for different numbers of layers

n in the powder for two different furnace temperatures (500 and 600 K). The following conclusions can be drawn from an analysis of the calculated data:

- Other factors being equal, the temperature of the outer layer of a powder sample is lower than the surface temperature of a single crystal. For example, if the furnace temperature is 600 K, the surface temperature of $Mg(OH)_2$ powder is 582.0 K, whereas the crystal temperature is 593.2 K.
- The temperature of the outer layer of the powder sample remains practically constant, regardless of the number of layers (for $n > 1$) and is defined by the furnace temperature only.
- The difference in neighbouring layer temperatures decreases monotonically with the distance from the surface.

- The temperature of the central layer of the powder sample depends primarily on the number of layers and for $n > 1,000$ remains practically constant regardless of the furnace temperature. For example, at furnace temperatures of 500 and 600 K the respective central layer temperatures for Mg(OH)$_2$ powder are 472.7 and 479.3 K for $n = 100$; 427.2 and 427.8 K for $n = 1,000$, and 386.6 K for $n = 10,000$.

Parameter n_e An underestimation of the temperature non-uniformity in powder samples will obviously be a source of errors in estimations of their kinetic parameters. To make allowance for this factor L'vov et al. [4] suggested introducing the following parameter into the calculation procedure:

$$n_e \equiv \frac{\sum\limits_{i=0}^{n} T_i^{-1/2} \exp(B/T_i)}{T_n^{-1/2} \exp(B/T_n)} \tag{6.13}$$

This quantity represents an effective number of powder sample layers, which decompose with the same rate as the surface layer. (This value can be determined simultaneously with calculations of the temperature distribution.) As the calculation results show, the n_e magnitude decreases quickly with the furnace temperature rise. At the same time the n_e magnitude is essentially independent of the total number of layers n (for $n > 100$) and is defined by the furnace temperature only.

As an example Fig. 6.3 presents the calculated dependence $n_e = f(T_f)$ for the Mg(OH)$_2$ decomposition (for $n = 1,000$).
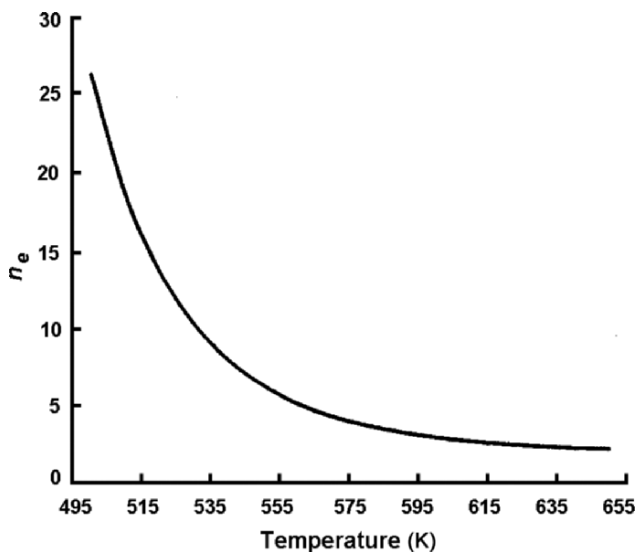
Fig. 6.3 Dependence of the effective number of layers n_e on the furnace temperature for the decomposition of Mg(OH)$_2$ powder in a vacuum (for $n = 1,000$)

Corrected Magnitudes of J and E The corrections to the kinetic parameters J and E, measured without regard to temperature distribution in a powder sample, can now be calculated. For both the parameters, the magnitudes of their deviations from those corresponding to the assumed spatially uniform heating of a sample up to the furnace temperature, are defined, firstly, by a difference in the furnace and sample temperatures, T_f and T_s, and, secondly, by the effective number of layers, involved in the decomposition. Taking both these factors into account, one can calculate the corrected magnitudes of the parameters (or, in other words, magnitudes corrected to conditions of the assumed isothermal heating) from the following expressions [4]:

$$J_{cor} = \frac{P(T_f)n}{P(T_s)n_e} J_{expt} \qquad (6.14)$$

and

$$E_{cor} = \frac{(1/T_f' - 1/T_f'')E_{expt} + R\ln(n_e'/n_e'')}{(1/T_s' - 1/T_s'')} \qquad (6.15)$$

Parameters marked by one or two primes are those for low and high temperature, respectively. Parameters marked by a subscript "expt" are the initial (experimental) values of the kinetic parameters. The magnitudes of $P(T_f)$ and $P(T_s)$ correspond to the equilibrium pressure of gaseous product for the corresponding temperatures (water vapour for magnesium hydroxide decomposition).

Interpretation of Unusual Effects Modelling of the temperature distribution has allowed, for the first time, some unusual effects observed for powder decomposition to be explained quantitatively. One of these is associated with an independence of the overall decomposition rate on the powder mass, which seems to be inexplicable at first thought. However, when the self-cooling of the sample is taken into account, this effect seems obvious. Irrespective of the total number of layers, i.e., of the powder mass, the effective number of layers n_e, involved in the decomposition process should remain practically constant (the height of powder filling is assumed to be much less than its diameter).

Another unusual effect associated with temperature non-uniformity in decomposing powder samples of $CaCO_3$ had been described by L'vov et al. [6]. Periodic variations in the absolute decomposition rate appear during the course of decomposition (Fig. 6.4). This effect becomes more marked with an increase in the decomposition temperature and, hence, of the degree of thermal non-uniformity. The initial data for calculations of the absolute rate were obtained by Maciejewski (see [6]) for further usage in an interlaboratory study of kinetic data obtained by means of commonly accepted calculation methods [7]. These kinetic data were measured by means of a Mettler 2000C thermoanalyser during decomposition in a vacuum (5×10^{-8} bar) of $CaCO_3$
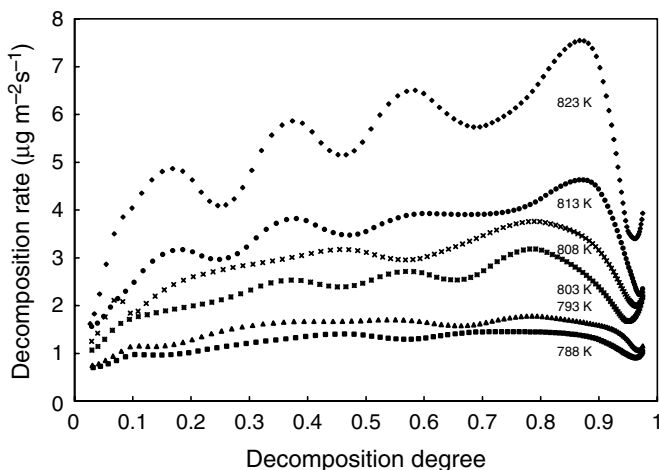
Fig. 6.4 The rate of decomposition of $CaCO_3$ powder as a function of the decomposition degree at different temperatures

powder samples of mass 10 mg in a Pt-Rh crucible 6.3 mm in diameter. The mean radius of the particles was 7.5 μm. Quantitative analysis [6] showed that the number of observed oscillations (4) appeared to be comparable, although twice as low, as the calculated number of layers ($n_{1/2} = 8$) of a powder sample.

This allowed L'vov et al. [6] to admit that, at sufficiently loose packing of spherical particles, the two neighbouring layers of the powder sample heat up from the container walls in a similar way. Only after complete decomposition of these layers does the decomposition of the next two succeeding layers begin, including initial stages of nucleation and acceleration. However, a discrepancy between the number of layers and that of oscillations may also be due to an error in determination of the mean size of the particles. If the particle radius was 9.5 μm instead of 7.5 μm, the number of layers would decrease from 8 to 4.

6.3   Experimental Evaluation of Self-cooling

Method With the exception of installation of a thermocouple between two alum crystals pressed up together [1–3], no simple and reliable methods for the experimental determination of the magnitude of self-cooling in a decomposing solid existed until recent years. Verification of the above calculations was thus difficult. The situation changed for the better only very recently with the appearance of third-law methodology in TA [8].

In contrast to the second-law method, for the third-law method the influence of self-cooling manifests itself in overestimation of the E parameter. This is evident from Eqs. 4.10–4.12. Therefore, the ratio of these two values measured by different methods is a very sensitive indicator of self-cooling.

If the only cause of overestimation of the experimental values E_{expt}, calculated by the third-law method, is the self-cooling effect, then its magnitude can be easily determined. If it is also assumed that the E magnitude at the lower temperature is free of this effect (i.e., that the sample temperature, T_s, is equal to the furnace temperature, T_f) and corresponds to the true value of the E parameter, E_{true}, then it becomes possible to determine the actual value of sample temperature for any higher decomposition temperature. This temperature is equal to:

$$T_s = T_f \frac{E_{\text{true}}}{E_{\text{expt}}} \tag{6.16}$$

if a small systematic decrease of both thermodynamic parameters ($\Delta_r S_T^\circ$ and $\Delta_r H_T^\circ$) with a temperature rise is neglected. Therefore, the difference, $\Delta T = T_s - T_f$, actually corresponds to the magnitude of the self-cooling of the sample at the higher temperature of the experiment, assuming $\Delta T = 0$ at its lower temperature.

The above assumption, that self-cooling is the only cause of overestimation of the experimental values E_{expt}, is valid only for reactants decomposing to gaseous products. For decompositions with formation of a solid product, there is an additional reason for overestimation related to the condensation effect (Sect. 8.2). Therefore, it is more appropriate to call this combined effect the *apparent self-cooling effect.*

Effect of a Solid Product on Self-cooling The self-cooling effect is more noticeable for compounds decomposing with formation of solid products, as can be seen from a comparison of the results listed in Tables 9.2 and 9.3 below. In contrast to a group of reactants decomposing with formation of gaseous products only (Table 9.2), where only 4 of the 21 compounds (SnO_2, GaN, Be_3N_2, and Mg_3N_2) differ in values of the E parameter measured with the second-law and third-law methods, such a difference is observed for 16 of the 20 reactants in Table 9.3.

This difference can be easily explained. For formation of solid product on the reactant surface, heating of the sample in a high vacuum by radiation (for example, from the walls of an alumina container) occurs through an intermediate product layer, for example, CaO for the $CaCO_3$ decomposition. This means that the effective value of the emittance for heat transfer from the container walls to the calcite crystal covered by a CaO layer, is the product of the corresponding coefficients for the four surfaces: Al_2O_3, CaO (outward side), CaO (inward side), and $CaCO_3$. (The residual thermal conductivity through point contacts between $CaCO_3$ crystal and CaO nanoparticles is neglected.) If

it is assumed that the emittance, ε, is the same for all the surfaces and equal to 0.3, then their product or the resulting emittance, ε^*, should be close to 0.01.

Impact of Self-cooling and Condensation Effects on the E Parameters The initial data for the analysis below were taken from the literature (Table 6.1). The list of reactants in this table includes two groups of compounds, the first of which decompose to gaseous products, and the second, to solid and gaseous products. Except for the $CaCO_3$ decomposition [6], all other reactions were investigated in works of Searcy and his colleagues [9–13], and Okhotnikov et al. [14–17]. All the experiments were performed in a high vacuum.

Table 6.1 contains the values of molar enthalpies for these reactions at the minimum and maximum temperatures of the experiments, which were calculated by L'vov using the third-law method (E_{min}^{III} and E_{max}^{III}), and the molar enthalpies determined experimentally in the original works by the second-law method (E^{II}) and also their calculated values. The following Eq. 6.17 was used for calculations:

$$E^{II} = \frac{E_{min}^{III}/T_{min} - E_{max}^{III}/T_{max}}{1/T_{min} - 1/T_{max}} \tag{6.17}$$

This equation, which can be derived from Eq. 4.2, is strictly valid if a small decrease of the entropy change with a temperature increase is neglected. As can be seen from Eq. 6.17, equality of the molar enthalpies determined by the second- and third-law methods ($E^{II} = E^{III}$) can be reached if $E_{min}^{III} = E_{max}^{III}$. Analysis of the data listed in Table 6.1 yields the following conclusions.

- The ratio $E_{max}^{III}/E_{min}^{III}$ for all the reactants except for $Li_2SO_4 \cdot H_2O$ [14] varies in the range 1.01–1.06 (the average value is 1.032). At the same time, the ratio $E_{min}^{III}/E_{expt}^{II}$ varies in the range 1.14–2.12 (the average value is 1.38). Therefore, a rather small increase of E^{III} values with temperature produces a large decrease of E^{II} values. The calculated values of E^{II} are in a good agreement with the experimental data. This fact supports the validity of the correlation between E^{II} and E^{III} values described by Eq. 6.17

- The ratio $E_{min}^{III}/E_{expt}^{II}$ for the reactants decomposed to gaseous products (the average value is 1.16) is significantly lower than that for the reactants decomposed to solid and gaseous products (the average value is 1.57). This difference is related to the apparent self-cooling effect, i.e., with the true self-cooling effect and the additional effect of condensation. The problem of how to estimate the impact of these factors on the $E_{min}^{III}/E_{expt}^{II}$ ratio separately remains unsolved.

- In conformity with the above theoretical estimations (Sects. 6.1–6.3), the temperature difference between the temperature-controlled heater and a sample in a high vacuum amounts to a few tens of degrees (e.g., 20–30 K for the first three reactants in Table 6.1). This systematic error in combination with the condensation effect manifests itself in a considerable (up to 15–50%) underestimation of E parameters when the second-law method is used.

Table 6.1 Impact of self-cooling and the condensation effects on the E parameters measured by the second- and third-law methods

Decomposition Reaction	T (K)		E^{III} (kJ mol^{-1})		$E^{III}_{max}/E^{III}_{min}$	E^{II} (kJ mol^{-1})		$E^{III}_{min}/E^{II}_{expt}$	Ref.
	Min.	Max.	Min.	Max.		Expt	Calc.		
$Be_3N_2 \leftrightarrow 3Be(g) + 1.52N + 0.24N_2$	1,610	1,880	486	493	1.01	428	444	1.14	[9]
$SnO_2 \leftrightarrow SnO(g) + O$	1,270	1,485	411	418	1.02	351	370	1.17	[10]
$GaN \leftrightarrow Ga(g) + 0.42N + 0.29N_2$	1,166	1,428	356	366	1.03	305	311	1.17	[11]
$BaCO_3 \leftrightarrow BaO(g)_\downarrow + CO_2$	1,076	1,232	299	318	1.06	168	168	1.78	[12]
$CaCO_3 \leftrightarrow CaO(g)_\downarrow + CO_2$	863	948	266	273	1.03	191	195	1.40	[6]
$1/2CaMg(CO_3)_2 \leftrightarrow 1/2CaO(g)_\downarrow + 1/2MgO(g)_\downarrow + CO_2$	824	900	246	258	1.05	116	116	2.12	[13]
$Li_2SO_4 \cdot H_2O \leftrightarrow Li_2SO_4(g)_\downarrow + H_2O$	348	433	104	115	1.11	50.6	59	2.06	[14]
$Li_2SO_4 \cdot H_2O \leftrightarrow Li_2SO_4(g)_\downarrow + H_2O$	315	363	108	112	1.04	84.9	82	1.27	[15]
$CaSO_4 \cdot 2H_2O \leftrightarrow CaSO_4(g)_\downarrow + 2H_2O$	288	357	97.6	101	1.03	82.8	83	1.18	[16]
$CuSO_4 \cdot 5H_2O \leftrightarrow CuSO_4(g)_\downarrow + 5H_2O$	255	303	88.0	89.8	1.02	74.5	78	1.18	[17]

References

1. Smith ML, Topley B (1931) Proc Roy Soc A134:224–245
2. Cooper MM, Garner WE (1940) Proc Roy Soc A174:487–503
3. Anous MM, Bradley RS, Colvin J (1951) J Chem Soc 3348–3354
4. L'vov BV, Novichikhin AV, Dyakov AO (1998) Thermochim Acta 315:135–143
5. L'vov BV, Novichikhin AV, Dyakov AO (1998) Thermochim Acta 315:169–179
6. L'vov BV, Polzik LK, Ugolkov VL (2002) Thermochim Acta 390:5–19
7. Brown ME, Maciejewski M, Vyazovkin S, et al. (2000) Thermochim Acta 355:125–143
8. L'vov BV (2002) Thermochim Acta 389:199–211
9. Hoenig CL, Searcy AW (1967) J Am Ceram Soc 50:460–466
10. Hoenig CL, Searcy AW (1966) J Am Ceram Soc 49:128–134
11. Munir ZA, Searcy AW (1965) J Chem Phys 42:4223–4228
12. Basu TK, Searcy AW (1976) J Chem Soc Faraday Trans I 72:1889–1895
13. Powell EK, Searcy AW (1978) J Am Ceram Soc 61:216–221
14. Modestov AN, Poplaukhin PV, Lyakhov NZ (2001) J Therm Anal Cal 65:121–130
15. Kirdyashkina NA, Okhotnikov VB (1988) React Kinet Catal Lett 36:417–422
16. Okhotnikov VB, Petrov SE, Yakobson BI, Lyakhov NZ (1987) Reactivity of Solids 2:359–372
17. Okhotnikov VB, Lyakhov NZ (1984) J Solid State Chem 53:161–167

Chapter 7
The Topley–Smith Effect

7.1 Historical Background

An abnormal change of the dehydration rate, J, of crystalline hydrates with an increase of water vapour pressure, P_w, was discovered by Topley and Smith (T–S) in 1931 [1] in their studies of the dehydration rate of $MnC_2O_4 \cdot 2H_2O$. In contrast to the expected monotonous decrease of the rate with increasing P_w, the dehydration rate, on reaching a certain critical pressure (about 0.1 Torr), begins to increase, passes through a maximum (about 1 Torr), and then decreases (Fig. 7.1).

Since then, the T–S effect has been observed in a few dozens of crystalline hydrates [1–17] (see Table 7.1 [3]). Frost et al. [5–8] in the 1950s and Bertrand et al. [11–13] in the 1970s made the most important contributions to studies of this effect. However no generally accepted explanation of this phenomenon has been developed till now, that would be able to interpret the shape of the curve $J = f(P_w)$ and specific features of the effect under varying measurement conditions: temperature, sample mass, powder grain size, presence of foreign gases, etc. Among three or four mechanisms suggested by different researchers, the most popular one is a mechanism of product recrystallization in the presence of H_2O, suggested by Volmer and Seydel [4]. This mechanism implies the formation, during the recrystallization process, of additional channels, cracks and pores between product grains, which facilitate water vapour removal from the reaction zone and, as a result, the rate of dehydration increases.
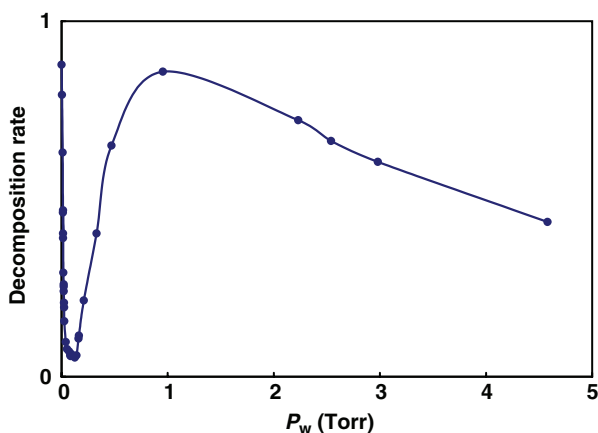
Fig. 7.1 The Topley–Smith effect. The dehydration rate of $MnC_2O_4 \cdot 2H_2O$ at 76° C in the presence of water vapour. (Reproduced from [2], with permission.)

Table 7.1   Studies of the Topley–Smith effect [2]

Reactant	Product	$T(^\circ C)$	Grain Diameter (μm)	P_w (Torr) Min.	P_w (Torr) Max.	Ref. and Year of Publication
$MnC_2O_4 \cdot 2H_2O$	MnC_2O_4	76		0.1	1.0	[1] 1931
$MnC_2O_4 \cdot 2H_2O$	MnC_2O_4	76	88	0.125	0.96	[3] 1935
$MnC_2O_4 \cdot 2H_2O$	MnC_2O_4	60		0.061	0.26	[4] 1937
$ZnSO_4 \cdot 6H_2O$	$ZnSO_4 \cdot H_2O$	45	310–420	0.8	1.55	[5] 1951
$CuSO_4 \cdot 5H_2O$	$CuSO_4 \cdot H_2O$	40	310–420	0.3	3.4	[6] 1953
$MnSO_4 \cdot 5H_2O$	$MnSO_4 \cdot H_2O$	40	310–420	1.1	3.0	[7] 1955
$ZnSO_4 \cdot 7H_2O$	$ZnSO_4 \cdot H_2O$	40	310–420	1.5[a]	4.0	[7] 1955
$FeSO_4 \cdot 7H_2O$	$FeSO_4 \cdot H_2O$	60	310–420	6	8	[7] 1955
$Ni(NO_3)_2 \cdot 7H_2O$	$Ni(NO_3)_2 \cdot 2H_2O$	50	310–420	2.5	2.9	[7] 1955
$MgSO_4 \cdot 7H_2O$	$MgSO_4 \cdot H_2O$	40	310–420	5	7	[7] 1955
$NiSO_4 \cdot 6H_2O$	$NiSO_4 \cdot H_2O$		310–420			[7] 1955
$MgSO_4 \cdot 7H_2O$	$MgSO_4 \cdot H_2O$	40	310–420	4	15	[8] 1956
$CoCl_2 \cdot 6H_2O$	$CoCl_2 \cdot H_2O$	30	310–420		0.7	[8] 1956
$CaSO_4 \cdot 0.5H_2O$	$CaSO_4$	140	64–75	5	17	[9] 1970
$CaC_2O_4 \cdot H_2O$	CaC_2O_4	120	120–150	0.5	1	[10] 1970
$CuSO_4 \cdot 5H_2O$	$CuSO_4 \cdot H_2O$	31		0.4	1.3	[11] 1972
$Li_2SO_4 \cdot H_2O$	Li_2SO_4	86	90–100	1.7	2	[12] 1974
$MgSO_4 \cdot 7H_2O$	$MgSO_4 \cdot 2H_2O$	86	< 63	8	30	[12] 1974
$CuSO_4 \cdot 5H_2O$	$CuSO_4 \cdot 3H_2O$	52	63–90	1	6	[12] 1974
$CuSO_4 \cdot 3H_2O$	$CuSO_4 \cdot H_2O$	54	< 40	0.2	3	[12] 1974
$NaB_4O_5(OH)_4 \cdot 8H_2O$	$NaB_4O_5(OH)_4$	38	63–90	5	12	[12] 1974
$CuSO_4 \cdot 5H_2O$	$CuSO_4 \cdot 3H_2O$	45	15–20	1	3	[13] 1978
$MgC_2O_4 \cdot 2H_2O$	MgC_2O_4	114	120–150	0.5	2	[14] 1978
$Zn(HCO_2)_2 \cdot 2H_2O$	$Zn(HCO_2)_2$	100	160–250		0.7	[15] 1989
$Er(HCO_2)_3 \cdot 2H_2O$	$Er(HCO_2)_3$	124	250–310		0.5	[16] 1992
$BaCl_2 \cdot 2H_2O$	$BaCl_2 \cdot H_2O$	44	53–63	0.7	1.2	[17] 1995

[a] Two minima and two maxima were observed at 0.2 and 0.7 Torr, and 1.5 and 4.0 Torr

The model suggested by Bertrand et al. [11–13] assumed the existence of a spatial gradient of temperature in the reaction zone. In this model the abnormal rise of the dehydration rate with P_w was attributed to the increase of heat transfer from the furnace to the self-cooled reactant. Model calculations and experiments on the evaporation and condensation of ethanol and water vapours provided a convincing proof of this mechanism. In the experiments [13], the temperature of the evaporating liquids turned out to be much lower than that of the heater. For instance, for ethanol the difference from the thermostat temperature (300 K) was as much as 45 K or 15%. However, this model remained unclaimed during the following 20 years of studies on the T–S effect. Such a considerable difference in temperatures between the crystalline hydrate and the furnace seemed improbable to the majority of researchers.

7.2 Modelling of the Topley–Smith Effect for $Li_2SO_4 \cdot H_2O$

For modelling of the T–S effect, L'vov et al. [3] used the software described in Sect. 6.1 and parameters listed in Table 7.2.

The calculation results are shown below in a graphic form. As may be deduced from the shape of the curves $J = f(P_w)$ in Figs. 7.2 and 7.3, the P_w rise from 10^{-5} to 10^{-2} bar leads to the rate increase and the appearance of maxima on the curves, which is in complete agreement with experimental observations. This is due to the increase in the thermal conductivity of water vapour which results in a decrease of self-cooling. The T–S effect becomes more marked with a rise of T_f and n, which is also in good correspondence with the experimental data [12, 13] and, in particular, with an intensification of the effect with the decrease of powder grain size [13].

Nevertheless, the comparison of calculation curves $J = f(P_w)$ presented in Figs. 7.2 and 7.3 with the experimental curve in Fig. 7.1 reveals also some inherent differences in their shapes. Firstly, over the initial part of the experimental curve the decomposition rate decreases with P_w rise, and a minimum is formed. Secondly, the decrease of dehydration rate after the maximum occurs much faster than in the calculations, so that the maximum on the experimental curves $J = f(P_w)$ is sharper.

The cause of the first of these differences is probably due to a presence of residual air in the reaction system. This air participates in the heat transfer and, therefore, in a decrease of self-cooling. Given that $P_w < P_a$, addition of water vapour should result in a rate decrease only. This assumption is confirmed by the curves in Fig. 7.4, which were calculated for the same temperature (380 K) as those in Fig. 7.3, but with due account for the presence of air with pressures of $10^{-4}, 3 \times 10^{-4}$ and 10^{-3} bar. The initial decrease of dehydration rate is absent in experiments on the dehydrations of $CoCl_2 \cdot 6H_2O$ [8], $Zn(HCO_2)_2 \cdot 2H_2O$ [15] and $Er(HCO_2)_3 \cdot 2H_2O$ [16], so that experimental

Table 7.2 Parameters used in the calculations of the Topley–Smith effect [3]

Parameter	Symbol	Value
Molar mass of $Li_2SO_4 \cdot H_2O$	M_r	$0.124 \, \text{kg mol}^{-1}$
Molar mass of Li_2SO_4	M_p	$0.106 \, \text{kg mol}^{-1}$
Molar mass of H_2O	M_w	$0.018 \, \text{kg mol}^{-1}$
Molar mass of air (N_2)	M_a	$0.028 \, \text{kg mol}^{-1}$
Enthalpy of dehydration reaction	$\Delta_r H_{298}^{\circ}$	$193.8 \, \text{kJ mol}^{-1}$
Entropy of dehydration reaction	ΔS_{298}°	$350.5 \, \text{J mol}^{-1} \, \text{K}^{-1}$
Molar heat capacity of air	C_{va}	$20.8 \, \text{J mol}^{-1} \, \text{K}^{-1}$
Molar heat capacity of H_2O vapour	C_{vw}	$27.4 \, \text{J mol}^{-1} \, \text{K}^{-1}$
Emittance	ε	0.62
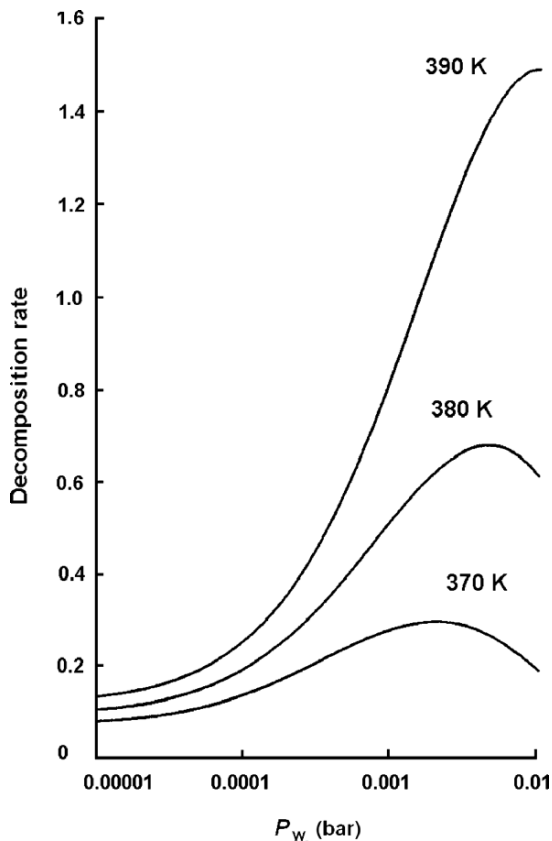
Fig. 7.2 Shapes of the calculated curves $J = f(P_w)$. Decomposition rate (g m^{-2}s^{-1}) of Li$_2$SO$_4 \cdot$ H$_2$O powder ($n = 10$) as a function of partial pressure of H$_2$O vapour at various temperatures. (Reproduced from [3], with permission.)

curves are more similar to the calculation curves presented in Figs. 7.2 and 7.3, rather than to those in Fig. 7.4.

According to molecular physics [18], an increase in thermal conductivity with vapour pressure should occur only until the average free-path length, λ, of the H$_2$O molecules approaches that of the distance between powder grains. The dependence of the magnitude of λ on the molecular radius, r, and the concentration, N, is [18]:

$$\lambda = \frac{1}{4\sqrt{2}\pi r^2 N} \tag{7.1}$$

The radii of the H$_2$O and N$_2$ molecules are about the same and equal to $r = 1.75 \times 10^{-10}$ m [18]. After inserting this magnitude into Eq. 7.1 and substituting the molecular concentration N for pressure (in bars) and temperature,
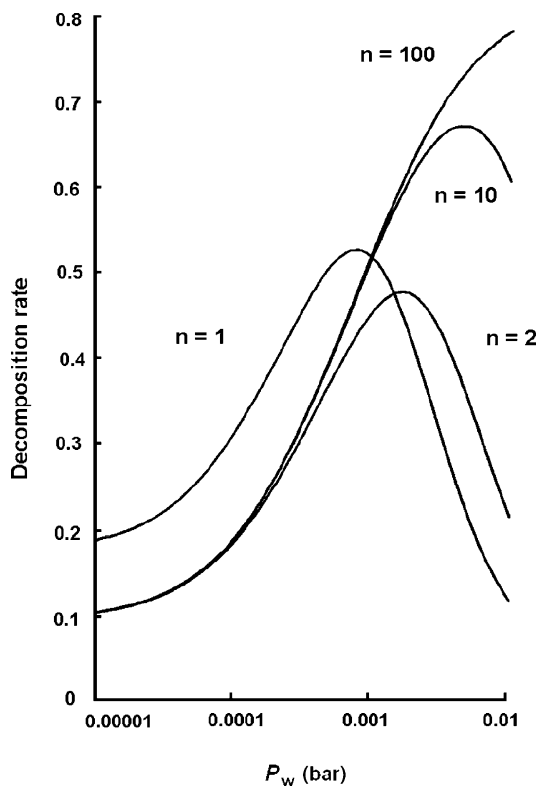
Fig. 7.3 Shapes of the calculated curves $J = f(P_w)$. Decomposition rate (g m^{-2} s^{-1}) of Li$_2$SO$_4$ · H$_2$O monocrystal ($n = 1$) and Li$_2$SO$_4$ · H$_2$O powder ($n = 2$, 10 and 100) as a function of partial pressure of H$_2$O vapour at $T_f = 380$ K. (Reproduced from [3], with permission.)

a final expression, common for both H$_2$O and N$_2$ molecules, has the form:

$$\lambda = 2.5 \times 10^{-10} T/P \tag{7.2}$$

Most probably the second of above-mentioned differences is due to the fact that the average free-path length of H$_2$O molecules at the maximum of the curve $J = f(P_w)$ becomes equal to the distance between powder layers. This distance may be taken to be approximately equal to half of the powder grain diameter $(d/2)$, whence it follows that:

$$\lambda_{\max} \cong d/2 \tag{7.3}$$

Figure 7.5 presents curves $J = f(P_w)$ (in logarithmic and linear scale), calculated assuming that $P_a = 10^{-3}$ bar and that the thermal conductivity increases up to $P_w = 2 \times 10^{-3}$ bar (1.52 Torr) at the expense of H$_2$O vapour. For P_w magnitudes higher than 2×10^{-3} bar the thermal conductivity was assumed
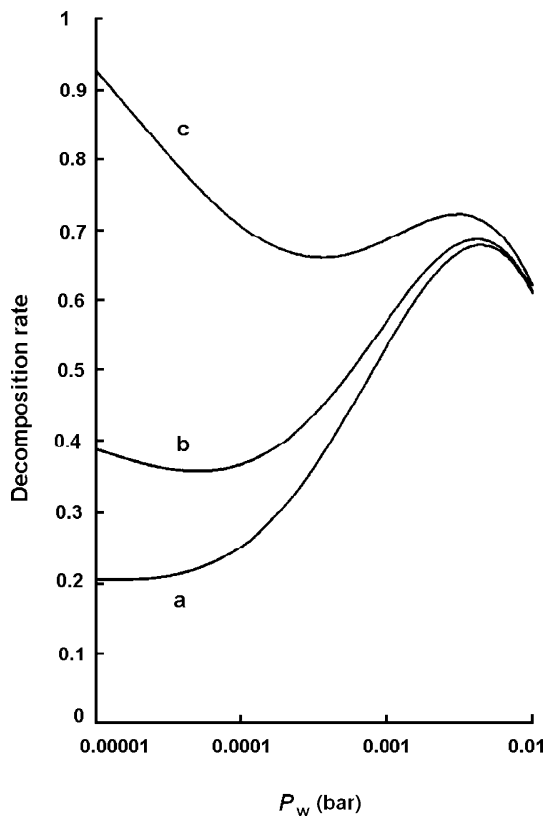
Fig. 7.4 Shapes of the calculated curves $J = f(P_w)$. Decomposition rate (g m^{-2} s^{-1}) of Li$_2$SO$_4 \cdot$H$_2$O powder ($n = 10$) as a function of partial pressure of H$_2$O vapour at $T_f = 380$ K for different partial pressures of air (P_a): (a) 10^{-4} bar, (b) 3×10^{-4} bar and (c) 10^{-3} bar. (Reproduced from [3], with permission.)

to be constant. As can be seen, after passing the maximum the rate drops more sharply, and the maximum itself becomes more profound. (Due to the powder polydispersity in real conditions, the boundary corresponding to the attainment of maximal thermal conductivity may be fuzzy.)

The above mechanism responsible for the formation of the maximum permits the fairly broad variation in the values of $(P_w)_{max}$, which correspond to the maxima in the $J = f(P_w)$ curves, observed for different crystalline hydrates, and in some cases also the differences between the values of $(P_w)_{max}$ found for the same crystalline hydrate (see Table 7.1) to be explained.

The extreme values of $(P_w)_{max}$, which are 0.26 Torr for MnC$_2$O$_4 \cdot$2H$_2$O [4] and 30 Torr for MgSO$_4 \cdot$4H$_2$O [12], correspond, according to Eq. 7.2, to the values of λ_{max} and, hence, of the grain radius, $d/2$, equal, respectively, to 240 and 2.3 μm. For some reactants, the values of λ_{max} calculated using Eq. 7.2
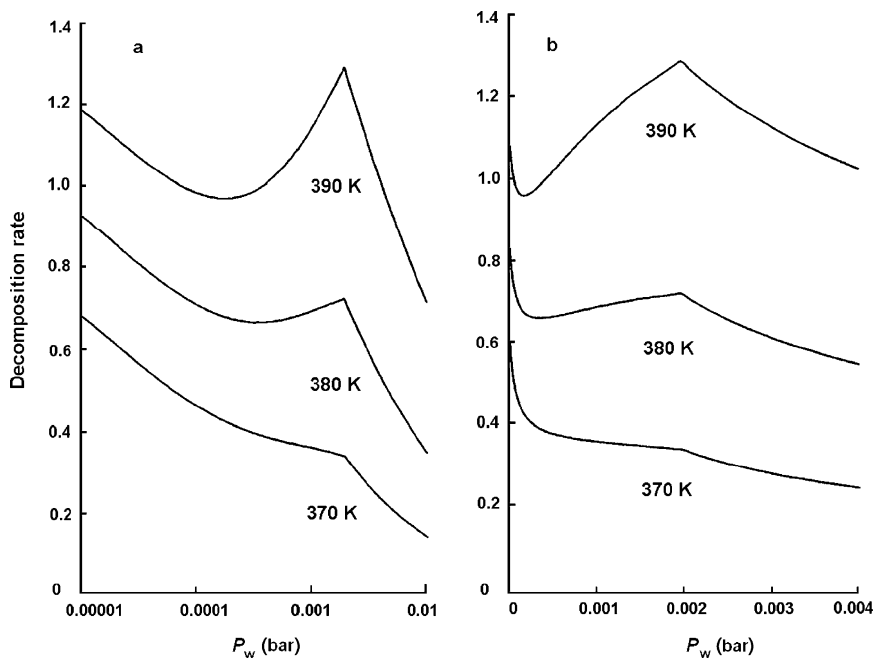
Fig. 7.5 Shapes of the calculated curves $J = f(P_w)$. Decomposition rate (g m^{-2} s^{-1}) of $Li_2SO_4 \cdot H_2O$ powder ($n = 10$) as a function of partial pressure of H_2O vapour at $P_a = 10^{-3}$ bar on (a) logarithmic and (b) linear scales. (Reproduced from [3], with permission.)

agree fairly satisfactorily (within a factor two) with the average grain radii quoted in the corresponding publications: $MnC_2O_4 \cdot 2H_2O$ [13], $CoCl_2 \cdot 6H_2O$ [18], $CaC_2O_4 \cdot H_2O$ [10], $LiSO_4 \cdot H_2O$ [12], $CuSO_4 \cdot 3H_2O$ [12], $CuSO_4 \cdot 5H_2O$ [13], $MgC_2O_4 \cdot 2H_2O$ [14], $Zn(HCO_2)_2 \cdot 2H_2O$ [15], $Er(HCO_2)_3 \cdot 2H_2O$ [16] and $BaCl_2 \cdot 2H_2O$ [17]. At the same time the calculations were found to disagree strongly with experiment for some reactants. For $ZnSO_4 \cdot 6H_2O$ [5], $CuSO_4 \cdot 5H_2O$ [6], $MnSO_4 \cdot 4H_2O$ [7], $ZnSO_4 \cdot 7H_2O$ [7], $FeSO_4 \cdot 7H_2O$ [7], $Ni(NO_3)_2 \cdot 7H_2O$ [7], $MgSO_4 \cdot 7H_2O$ [7, 8], $MgSO_4 \cdot 4H_2O$ [12] and $NaB_4O_5(OH)_4 \cdot 8H_2O$ [12], the calculated values of λ_{max} were found to lie below the grain radius by an order of magnitude. This is possibly due to the fact that the sizes quoted in the papers relate to the starting (undecomposed) powder grains. As a result of the formation of smaller particles during the course of decomposition, the distance between grains in the reactant/product mixture decreases.

In summary, *modelling of the $T - S$ effect not only confirmed the abnormal change of dehydration rate in the presence of water vapour, but also allowed various specific features of this phenomenon to be explained, in particular, an enhancement of the effect with increasing temperature and with decreasing powder grain size.*

7.3   Modelling of the Topley–Smith Effect for $CaCO_3$

Until recently, the T–S effect had been observed for crystalline hydrates only and, hence, was associated with peculiarities of the dehydration reactions. Modelling of the T–S effect for $CaCO_3$ considered below has been stimulated by the results of Darroudi and Searcy [19], who studied the influence of additions of 10^{-6}–10^{-3} bar of CO_2 on the $CaCO_3$ decomposition at different temperatures. In the figures of their work [19] at 983, 1,006 and 1,073 K one can observe a well-defined curvature or even the appearance of a maximum on the curves $J = f(P_{CO_2})$. As an illustration, Fig. 7.6 presents experimental data obtained at 1,006 K.

   To prove the possibility of the appearance of a T–S effect L'vov [20] modelled the curve $J = f(P_{CO_2})$ for decomposition of single crystals of $CaCO_3$, using the same software as had been used for dehydration reactions. The heat spent for decomposition was assumed to be compensated in part at the expense of heater radiation and thermal conductivity of the excess CO_2 present in the reactor. The result of modelling [20] under these conditions (1,000 K) was that the T–S effect could be observed only when the emittance ε became lower than 0.02 (Fig. 7.6). At higher magnitudes of ε the maximum disappears and only a small distortion of the $J = f(P_{CO_2})$ curve is observed. The self-cooling effect appears to be insignificant and, thus, some increase of $CaCO_3$ temperature
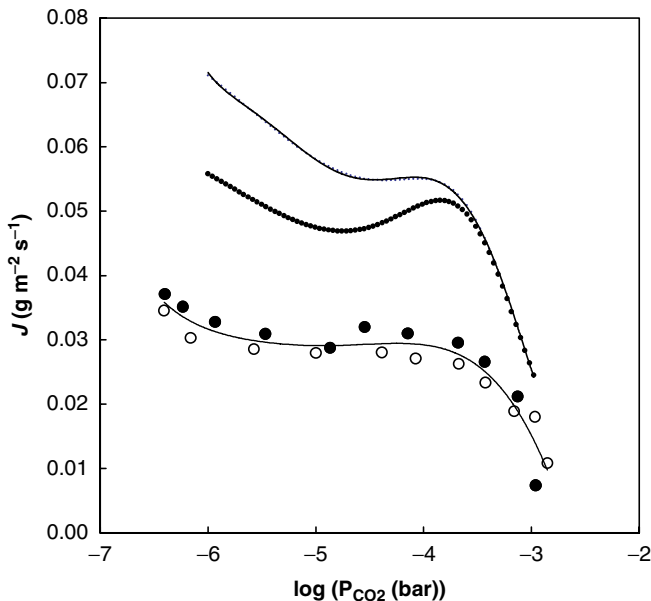
Fig. 7.6 The Topley–Smith effect for $CaCO_3$. Two sets of experimental data (points) were taken from [19], with permission. Theoretical curves were calculated for different emittance factors: (above) 0.002 and (below) 0.0015

with the rise of CO$_2$ pressure is compensated by the suppressing effect of CO$_2$ (in the isobaric regime) on the decomposition rate.

The relatively low magnitude of the emittance in experiments described by Darroudi and Searcy [19] is confirmed by consideration of the experimental conditions used. To decrease the temperature gradient and to interaction of CO$_2$ with the tungsten heater, a platinum cylinder, 3 cm in diameter and 10 cm high, was placed around the sample. As a result, the sample was heated by emission from platinum and the magnitude of ε was only 0.10 [22] or even 0.08 [23]. Taking into account the formation of a product layer (CaO) on the CaCO$_3$ surface, the resulting emittance ε^* (considering the successive thermal emission from the platinum surface to the CaO surface and from that to the CaCO$_3$ surface) was unlikely to be higher than 0.01–0.02.

The shapes of theoretical and experimental curves in Fig. 7.6 are very similar. In line with the calculations, a maximum and curvature are observed on the curves at a pressure of 10^{-4} bar. The difference in the calculated and experimental values of the absolute decomposition rate is not more than twofold. Taking into account the simplifications used in the calculation model and measurement errors, the agreement is excellent.

Another important conclusion that can be drawn from the analysis of the results in [19] is an explanation of the apparent differences in behaviour of the decomposition rate of CaCO$_3$ in the presence of CO$_2$ reported by different researchers (a hyperbolic variation in [23–25] and close to linear in [19]). This is, once again, due to the effect of intense self-cooling of the sample in a high vacuum. Instead of the expected 100-fold decrease of decomposition rate as the pressure changes in the range from 10^{-6} to 10^{-4} bar CO$_2$, its magnitude holds practically constant [19]. Only at CO$_2$ pressures exceeding 10^{-4} bar (used in papers [23–25]), does the increase of thermal conductivity, compensating for the depressing effect of CO$_2$, stop and the dependence of the decomposition rate of CaCO$_3$ on CO$_2$ approaches hyperbolic behaviour.

Self-cooling in a High Vacuum To prove the above conclusion, it is possible to estimate the value of self-cooling for the calcite decomposition in the experiments by Darroudi and Searcy [19]. Recall that as the CO$_2$ pressure was increased from 10^{-6} to 10^{-4} bar the decomposition rate of CaCO$_3$ at 1,006 K held practically constant. This means that the suppressing influence of CO$_2$ on the decomposition rate J was compensated for by differences in temperature of the CaCO$_3$ crystals. Using Eq. 3.26 for reactant decomposition in the isobaric mode, the equality of the rates, $J_1 = J_2$, can be expressed in the following way (the differences in magnitudes of the pre-exponential factors for J_2 and J_1 at T_2 and T_1 are neglected):

$$\left(\frac{P_2}{P_1}\right)^{b/a} = \exp\left(\frac{\Delta_r H_T^\circ}{aRT_1} - \frac{\Delta_r H_T^\circ}{aRT_2}\right) \tag{7.4}$$

Here $P_1 = 10^{-6}$ bar and $P_2 = 10^{-4}$ bar, T_1 and T_2 are reactant temperatures corresponding to these pressures. After taking the logarithm:

$$\frac{1}{T_1} = \frac{1}{T_2} + \frac{bR}{\Delta_r H_T^\circ} \ln(P_2/P_1) \tag{7.5}$$

For the decomposition temperature T_2 to be equal to the furnace temperature, i.e., 1,000 K and the enthalpy value $\Delta H_{1000}^\circ / b \cong 500\,\mathrm{kJ\,mol^{-1}}$, $T_1 \cong 929$ K. This is 71 K lower than the furnace temperature. The magnitude obtained is consistent with ΔT magnitudes (78, 25 and 44 K for $BaCO_3$, $CaCO_3$ and $CaMg(CO_3)_2$, respectively), measured by the third-law method (Table 6.1).

7.4 Conclusions

The most important result of Chaps. 6 and 7 devoted to self-cooling and to observations of the T–S effect, is the unexpectedly high magnitude of self-cooling. This manifests itself not only in a surprisingly high thermal inhomogeneity of powders, but also in temperatures of single crystals which in specific (extreme) experimental conditions may differ from the furnace temperature by a few tens of degrees.

The T–S effect becomes apparent under extreme conditions of such kind. The temperature for experiments on the T–S effect is chosen to be much higher than temperatures typical for usual experiments on the decomposition kinetics in the absence of an excess of gaseous product. For crystalline hydrates this excess of temperature may reach 30–50 K, and for calcium carbonate, 100–150 K. This is because the decomposition in the isobaric mode is slower than in the equimolar mode. However, for initial points of the T–S curve corresponding to the absence of gaseous product or to a very low pressure of this gaseous product, this temperature is obviously much higher than the optimal value. That is why self-cooling appears to be well above the common value.

Historically the underestimation of the role and magnitude of the self-cooling effect in kinetic studies of thermal decomposition has turned out to be one of the most important reasons which hindered interpretation of the T–S effect and, to some extent, the compensation effect, and promoted some misconceptions [19, 26–28], based on the confidence in infallibility of the second-law method in determination of thermochemical parameters (the enthalpy and entropy for decomposition reactions).

References

1. Topley B, Smith ML (1931) Nature 128:302
2. Topley B, Smith ML (1935) J Chem Soc 321–325
3. L'vov BV, Novichikhin AV, Dyakov AO (1988) Thermochim Acta 315:169–179

4. Volmer M, Seydel G Z. (1937) Phys Chem A179:153–171
5. Frost GB, Moon KA, Tompkins EH (1951) Can J Chem 29:604–632
6. Frost GB, Campbell RA (1953) Can J Chem 31:107–119
7. Wheeler RC, Frost GB (1955) Can J Chem 33:546–561
8. Ford RW, Frost GB (1956) Can J Chem 34:591–599
9. Ball MC, Urie RG (1970) J Chem Soc A 528–530
10. Dollimore D, Jones TE, Spooner P (1970) J Chem Soc A 2809–2812
11. Lallemant M, Bertrand G, Watelle-Marion G (1972) C R Acad Sci Paris 275:519
12. Bertrand G, Lallemant M, Watelle-Marion G (1974) J Inorg Nucl Chem 36:1303–1309
13. Bertrand G, Lallemant M, Mokhlisse A, Watelle-Marion G (1978) J Inorg Nucl Chem 40: 819–824
14. Dollimore D, Heal GR, Mason J (1978) Thermochim Acta 24:307–314
15. Masuda Y, Nagagata K (1989) Thermochim Acta 155:255–261
16. Masuda Y, Hirata K, Ito Y (1992) Thermochim Acta 203:289–296
17. Lumpkin JA, Perlmutter DD (1995) Thermochim Acta 249:335–349
18. Kikoin AK, Kikoin IK (1976) Molecular physics. Nauka, Moscow (in Russian)
19. Darroudi T, Searcy AW (1981) J Phys Chem 85:3971–3974
20. L'vov BV (2002) Thermochim Acta 386:1–16
21. Kikoin IK (1976) (ed) Tables of physical constants. Atomizdat, Moscow (in Russian)
22. Svet DYa (1968) Objective methods of high temperature pyrometry for continuum radiation. Nauka, Moscow (in Russian)
23. Criado JM, Gonzalez M, Malek J, Ortega A (1995) Thermochim Acta 254:121–127
24. Hyatt EP, Cutler IB, Wadsworth ME (1958) J Am Ceram Soc 41:70–74
25. Ingraham TR, Marier P (1963) Can J Chem Eng 41:170–173
26. Beruto D, Searcy AW (1974) J Chem Soc Faraday Trans I 70:2145–2153
27. Powell EK, Searcy AW (1980) Met Trans B11:427–432
28. Beruto DT, Searcy AW, Kim MG (2004) Thermochim Acta 424:99–109

Chapter 8
Impact of Vapour Condensation on the Reaction Enthalpy

8.1 The Contribution of Condensation Energy to the Reaction Enthalpy

The τ Coefficient According to the CDV mechanism, for the decomposition of compound R into gaseous products A and B and the subsequent condensation of the low-volatility component A

$$R(s) \leftrightarrow aA(g) + bB(g) \rightarrow aA(s) + bB(g)$$
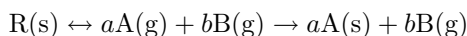
an additional term $\tau a\Delta_c H_T^\circ(A)$ should be introduced into calculation of the decomposition enthalpy. This term takes into account the partial transfer of condensation energy to the reactant. The transfer coefficient τ, corresponds to the part of the energy $a\Delta_c H_T^\circ(A)$, returned to the reactant. Thus:

$$\Delta_r H_T^\circ = a\Delta_f H_T^\circ(A) + b\Delta_f H_T^\circ(B) - \Delta_f H_T^\circ(R) + \tau a\Delta_c H_T^\circ(A)$$
$$= \Delta_v H_T^\circ + \tau a\Delta_c H_T^\circ(A) \tag{8.1}$$

Here $\Delta_v H_T^\circ$ is the enthalpy of the initial evaporation process. Hence it follows that:

$$\tau = \frac{\Delta_r H_T^\circ - \Delta_v H_T^\circ}{a\Delta_c H_T^\circ(A)} = \frac{\nu E - \Delta_v H_T^\circ}{a\Delta_c H_T^\circ(A)} \tag{8.2}$$

Originally the coefficient τ was introduced into the CDV mechanism as an adjustable parameter aimed to connect the E parameter with the enthalpy of an assumed reaction [1]. It was supposed [2] that, in the majority of cases, the condensation energy would be distributed equally among solid phases of the reactant and product, so that the coefficient τ would be equal to 0.50. However, as became evident later, when the coefficients τ had been determined for a sufficient number of reactants, this is not true [3].

Correlation between the τ Coefficient and Thermodynamic Features of the Low-volatility Product An analysis of variations of the coefficient τ for 16 different compounds, studied by L'vov and Ugolkov [3–6], allowed these magnitudes to be connected with the oversaturation of the vapour of the low-volatility component at the moment of decomposition. The complete list of these reactants is presented in Table 8.1.

This dependence, having a correlation coefficient (r^2) equal to 0.866 can be described by the following equation (Fig. 8.1):

$$\tau_1 = 0.339 \log c_1 + 0.028 \tag{8.3}$$

111

Table 8.1 Dependence of the τ coefficient on the energy of condensation and the oversaturation degree of low-volatility product at the decomposition temperature (with consideration of the refinements and supplements noted in Part III)

Reactant	Product	T^a (K)	P_∞ (bar)	c_1	c_2	τ	Ref.
BN	B	1,790	1.9E−09	1.03	3.63	0.044	[3]
AgNO$_3$	Ag	472	1.7E−25	17.1	4.28	0.259	Sect. 16.11
SrCO$_3$	SrO	1,456	4.1E−13	4.7	3.83	0.334	Sect. 16.14
Cd(NO$_3$)$_2$	CdO	563	5.1E−23	14.6	4.27	0.394	Sect. 16.11
MgSO$_4$	MgO	1,000	2.8E−24	15.9	4.33	0.412	[3]
CaCO$_3$	CaO	1,200	3.2E−21	12.8	4.20	0.449	[3]
Ba(OH)$_2$	BaO	600	6.2E−29	20.5	4.40	0.496	[4]
Cd(OH)$_2$	CdO	400	7.9E−36	27.4	4.67	0.441	[4]
MgCa(CO$_3$)$_2$	MgO + CaO	824	2.6E−36	27.9	4.52	0.449	[5]
MgCO$_3$	MgO	800	1.6E−32	24.1	4.55	0.536	[3]
Sr(OH)$_2$	SrO	600	6.4E−42	33.5	4.77	0.586	[4]
Zn(OH)$_2$	ZnO	400	9.8E−51	42.3	4.94	0.572	[4]
Mg(OH)$_2$	MgO	500	3.0E−57	48.8	4.96	0.585	[4]
Ca(OH)$_2$	CaO	600	2.1E−50	42.0	4.95	0.632	[4]
Li$_2$SO$_4 \cdot$ H$_2$O	Li$_2$SO$_4$	300	4.5E−58	49.6	4.84	0.656	[1, 6]
Be(OH)$_2$	BeO	400	3.4E−88	79.8	5.42	0.724	[4]

^{a} Temperature that corresponds to $P_{\mathrm{eqp}} \cong 2 \times 10^{-8}$ bar

where $c_1 \equiv \log(P_{\mathrm{eqp}}/P_\infty)$. Here P_{eqp} and P_∞ are equilibrium and saturated pressures of the low-volatility product, respectively.

This correlation can be improved considerably if AgNO$_3$, Cd(NO$_3$)$_2$, Cd(OH)$_2$, and MgCa(CO$_3$)$_2$ are excluded from the list of reactants. These reactants have the lowest values of the τ coefficient. The reason for excluding these compounds is that, because of their relatively low decomposition temperatures, self-cooling effects may result in their τ magnitudes being underestimated. Figure 8.2 presents the corresponding results. The approximating

$\tau = 0.339 \log c_1 + 0.028$

$r^2 = 0.8406$
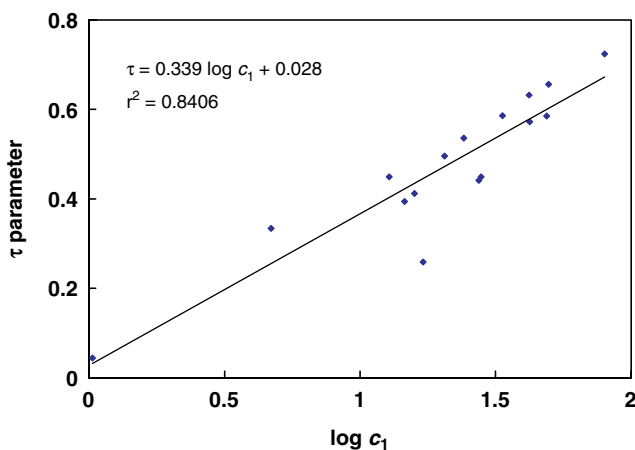
Fig. 8.1 Approximation of the τ coefficient by Eq. 8.3
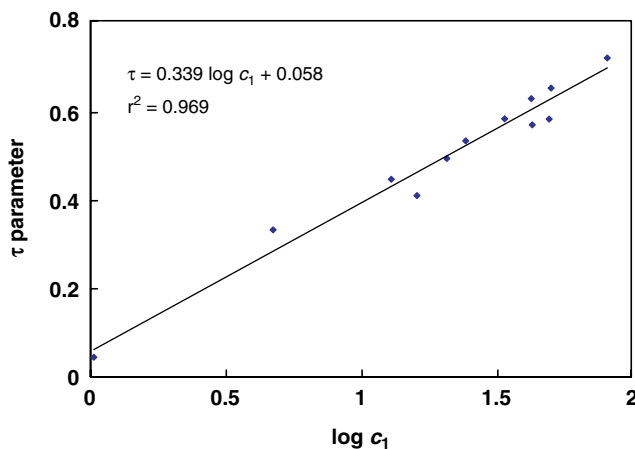
Fig. 8.2 Approximation of the τ coefficient by Eq. 8.4

function then takes the form:

$$\tau_1 = 0.339 \log c_1 + 0.058 \tag{8.4}$$

and $r^2 = 0.969$.

Another possible way of describing the correlation between the τ coefficient and the thermodynamic characteristics of the low-volatility product has been suggested in [4]. The approximating function for all the 16 compounds has the following form (Fig. 8.3):

$$\tau_2 = 0.353 c_2 - 1.127 \tag{8.5}$$

A reduced value of the condensation energy, $c_2 \equiv \ln[-\Delta_c H_T^\circ/(RT)]$, is used here as a controlling parameter instead of the vapour oversaturation, $c_1 \equiv \log(P_{eqp}/P_\infty)$. The correlation coefficient, as compared to that in equation (8.3) rose from 0.866 to 0.883. The correlation between τ and c_2 may be improved further (up to $r^2 = 0.919$), if a quadratic polynomial [7] (Fig. 8.4) is used:

$$\tau_2 = -0.1182(c_2)^2 + 1.3862 c_2 - 3.359 \tag{8.6}$$

In general, the correlation revealed is a very important step in the development of this approach. Firstly, a very unusual relation occurs between the condensation energy transfer (τ coefficient) and vapour oversaturation, P_{eqp}/P_∞, of the low-volatility product. As can be seen from Eq. 8.3 this relation is doubly logarithmic, and thus, it is very weak. (For Eq. 8.5, besides the logarithmic relationship $c_2 \equiv \ln[-\Delta_c H_T^\circ/(RT)]$, account must be taken of an additional logarithmic relation of the reduced value of condensation enthalpy $\Delta_c H_T^\circ/(RT)$ with P_∞.) Variation of P_∞ from 4.1×10^{-13} bar for $SrCO_3$ to 3.4×10^{-88} bar for $Be(OH)_2$ (within 75 orders of magnitude) produces only

$$\tau = 0.353c_2 - 1.127$$
$$r^2 = 0.883$$
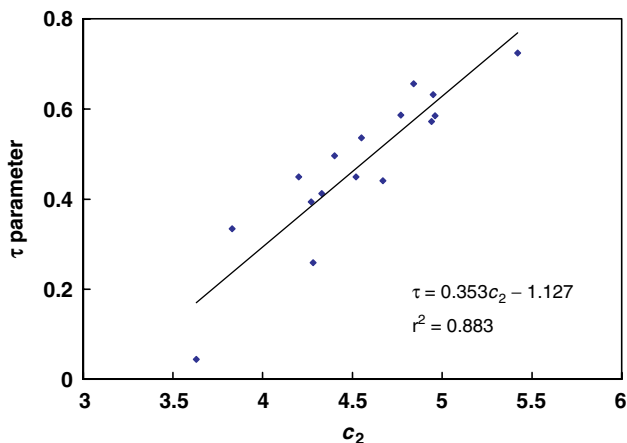
Fig. 8.3 Approximation of the τ coefficient by Eq. 8.5

about a twofold increase in τ magnitude (from 0.33 to 0.72). The correlation revealed may become a key point in the understanding of the mechanism of condensation energy transfer.

Secondly, the discovered correlation (in the form of the semi-empirical dependences presented above) may be used for theoretical calculations of decomposition kinetics and for thermochemical analysis of the composition of primary reaction products, which is one of the final goals of this research (see Chapter 9).

$$\tau = -0.118c_2^2 + 1.386c_2 - 3.359$$
$$r^2 = 0.919$$
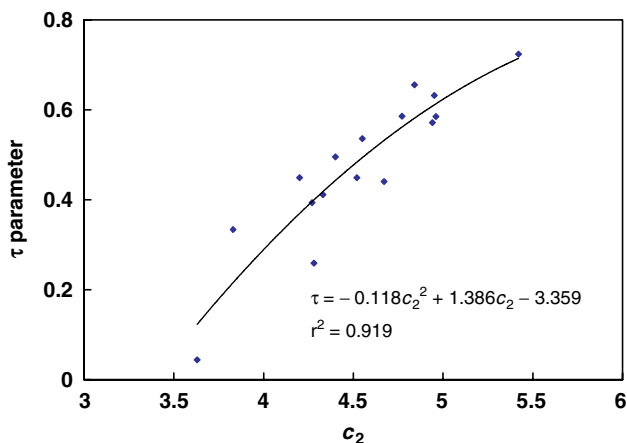
Fig. 8.4 Approximation of the τ coefficient by Eq. 8.6

8.2 Increase of Reaction Enthalpy with Temperature

Another unexpected consequence of this condensation energy transfer is the enthalpy rise with temperature. The magnitude of oversaturation, which determines the condensation energy transfer to reactant, decreases with a rise in temperature. That is why the contribution of the condensation energy to the enthalpy, owing to the decrease in the τ coefficient (and, to a lesser degree, to the condensation energy itself) should decrease. As a result, *instead of the ordinary small decrease of enthalpy with temperature rise, its magnitude should increase.*

As an example, Table 8.2 presents calculated and experimental data for the decomposition of $CaCO_3$. Equation 8.4 has been used in estimations of the coefficient τ. As can be seen from the table, the temperature rise from 900 to 1,200 K is accompanied by an increase in the magnitude of $\Delta_r H_T^\circ$ by about 50 kJ mol^{-1}, instead of the expected decrease of 10 kJ mol^{-1}, which considerably exceeds the measurement error. Theoretical results are confirmed quite well by experiments. (Additional results for the decompositions of $CaCO_3$ and $SrCO_3$, supporting this effect, are presented in Sect. 16.14.)

It is difficult to overestimate the significance of this effect. First of all, it provides a convincing proof of the fact of condensation energy transfer to the reactant and supports the validity of the calculations of reaction enthalpies for compounds decomposing with the formation of a low-volatility product. Secondly, it points to the need to revise the main causes of systematic underestimation of results obtained in measurements with the second-law and Arrhenius plot methods. In addition to self-cooling, the condensation effect is also among these causes. Moreover, while the self-cooling effect can be eliminated or reduced by choosing the appropriate experimental conditions, the condensation effect cannot, in principle, be eliminated.

An increase of the true value of $\Delta_r H_T^\circ$ with temperature decreases the slope of the ln K_P = f(1/T) plot and, therefore, the value of the E parameter measured by the second-law and Arrhenius plot methods. As an example, a contribution of the condensation effect into the E parameter for the decomposition of $CaCO_3$ can be considered. The averaged experimental magnitudes of K_P at 970 and 1,215 K (see Sect. 16.14), measured in the isobaric mode, in atmospheric air (0.04% CO_2) and in pure CO_2, are equal to 3×10^{-11}

Table 8.2 Calculated and experimental values of the enthalpy change for the decomposition of $CaCO_3$

T (K)	$\Delta_v H_T^\circ$ (kJ mol^{-1})	$-\Delta_c H_T^\circ$ (kJ mol^{-1})	P_∞ (bar)	c_1[a]	τ_1	$\Delta_r H_T^\circ$(kJ mol^{-1}) Theory	Expt
900	840.6	669.5	6.7E−31	22.5	0.516	495	487 ± 5
1,000	837.3	667.8	5.1E−27	18.6	0.487	512	500 ± 7
1,100	834.0	666.3	7.5E−24	15.4	0.458	529	515 ± 1
1,200	830.0	664.7	3.2E−21	12.8	0.430	544	535 ± 5

[a] $c_1 = \log(P_{eqp}/P_\infty)$, where $P_{eqp} = 2 \times 10^{-8}$ bar

and $1.2 \times 10^{-7} \, \text{bar}^2$, respectively. The value of E parameter measured by the second-law method should be equal to $332 \, \text{kJ mol}^{-1}$. This value is 35–40% lower than the $\Delta_r H_T^\circ$ magnitudes, measured at the same temperatures by the third-law method (Table 8.2). The difference obtained is probably somewhat overestimated due to an uncertainty of the measured values K_P. However, *the decisive contribution of the condensation effect in the systematic underestimation of E parameters, measured by the second-law and Arrhenius plot methods, is indisputable.* Some additional results confirming this effect (for the decomposition of $SrCO_3$) are presented in Sect. 16.14.

8.3 Reactant Melting and Decomposition Enthalpy

Silver and Cadmium Nitrates Studies of the decomposition rates for solid and liquid (melted) reactants are of the top most importance for verification of the CDV mechanism. Measurements of such kind have been recently described by L'vov and Ugolkov [11] for the decompositions of the anhydrous nitrates of silver and cadmium. Melting temperatures for these salts are equal to 483 and 633 K, respectively. The final results of these experiments (with an allowance for some corrections mentioned in Sect. 16.11) are presented in Table 8.3.

As can be seen from Table 8.3, regardless of the difference in temperatures, the decomposition rates for $AgNO_3$ and $Cd(NO_3)_2$ in the solid and molten states appear to be about the same. (With a temperature difference of 100 K, a rate increase by 2–3 orders of magnitude could be expected.) For some reason the decompositions of the solid reactants slow down after their melting. The magnitude of the molar enthalpy (parameter E) rises by about $20 \, \text{kJ mol}^{-1}$.

These observations are contradictory to the popular opinion that melting should result in faster decomposition of the reactant [12]. This opinion is based on the following reasonable assumptions: "Reasons why reactions of solids may proceed more rapidly in a molten zone than within a crystalline reactant, include: (i) relaxation of the regular stabilizing intercrystalline forces; (ii) establishment of a favorable configuration for chemical change may be possible due to mobility in a liquid but inhibited within a rigid crystal structure, and (iii) the influences of intermediates and impurities may be greater (or different) in a molten phase" [12].

Table 8.3 Kinetic parameters for the decomposition of solid and melted nitrates in a vacuum [11]

Nitrate	T (K)	Primary Products	$J(\text{kg m}^{-2}\,\text{s}^{-1})$	$E(\text{kJ mol}^{-1})$
$AgNO_3(s)$	472	$Ag(g)_\downarrow + NO_2 + 1/2 O_2$	3E−7	146.6 ± 0.4
$AgNO_3(l)$	574	$Ag(g) + NO_2 + 1/2 O_2$	8E−7	165.5 ± 0.8
$Cd(NO_3)_2(s)$	563	$CdO(g)_\downarrow + 2NO_2 + O$	7E−6	177.5 ± 1.0
$Cd(NO_3)_2(l)$	660	$CdO(g) + 2NO_2 + O$	9E−6	198.1 ± 0.8

These arguments, although seeming reasonable, are too general and not yet supported by experiments. Meanwhile, the decelerating influence of melting has a very simple explanation and can be interpreted quantitatively within the framework of the CDV mechanism. A partial transfer of condensation energy $(\tau a \Delta_c H_T^\circ)$ to a solid reactant during the decomposition process causes the decrease of the reaction enthalpy and the increase of the rate. In the absence of such a zone and such a transfer for a molten reactant $\tau = 0$, and the reaction enthalpy is higher than that for a solid reactant.

As will be shown in Sect. 16.11, the experimental results for both nitrates agree with the theoretical calculations.

Calcium Nitrate The results of similar experiments for $Ca(NO_3)_2$ by Ettarh and Galwey [13] are also in a full agreement with the above approach. The melting point for $Ca(NO_3)_2$ is 836 K. The E parameters measured in [13] for solid (774–820 K) and melted nitrate (229 ± 10 and 315 ± 20 kJ mol^{-1}), agree with thermochemical calculations of the molar enthalpy (234 and 318 kJ mol^{-1}) for the corresponding reactions:

$$Ca(NO_3)_2(s) \leftrightarrow CaO(g)_\downarrow + 2NO_2 + O \qquad (8.7)$$

$$Ca(NO_3)_2(l) \leftrightarrow CaO(g) + 2NO_2 + O \qquad (8.8)$$
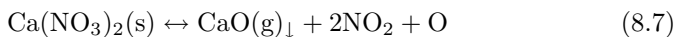
The calculated value, $\tau a \Delta_c H_T^\circ / \nu = 84$ kJ mol^{-1} [11], practically coincides with the experimentally obtained difference in parameters E for melted and solid nitrates, i.e., to 86 kJ mol^{-1}.

Thus, *the decelerating influence of melting on the rate of reactant decomposition is in complete agreement with the CDV mechanism.* It is doubtful that any other explanation of this unusual effect can be found within the framework of commonly accepted views.

References

1. L'vov BV (1991) Evaporation, thermal dissociation, carbothermal reduction and thermal decomposition of substances. A general approach to the theoretical calculation of kinetics. XXVII CSI, Bergen, Norway. Book of Abstracts A-5.2
2. L'vov BV (1998) Thermochim Acta 315:145–157
3. L'vov BV, Ugolkov VL (2004) Thermochim Acta 411:73–79
4. L'vov BV, Ugolkov VL (2004) Thermochim Acta 413:7–15
5. L'vov BV, Ugolkov VL (2003) Thermochim Acta 401:139–147
6. L'vov BV, Ugolkov VL (2003) J Therm Anal Cal 74:697–708
7. L'vov BV (2004) Thermochim Acta 424:183–189
8. Darroudi T, Searcy AW (1981) J Phys Chem 85:3971–3974
9. Powell EK, Searcy AW (1978) J Am Ceram Soc 61:216–221
10. Gordon RS, Kingery WD (1967) J Am Ceram Soc 50:8–14
11. L'vov BV, Ugolkov VL (2004) Thermochim Acta 424:7–13
12. Galwey AK, Brown ME (1999) Thermal decomposition of ionic solids. Elsevier, Amsterdam
13. Ettarh C, Galwey AK (1996) Thermochim Acta 288:203–219

Chapter 9
Thermochemical Analysis of the Composition of the Primary Products

Introduction Starting in 1981 [1], L'vov and his colleagues tried to interpret the experimental parameter E in the Arrhenius equation as the molar enthalpy, $\Delta_r H_T^\circ / \nu$, of the desired decomposition reaction. However, it did not affect the traditional interpretation of the parameter E. One of the potential reasons for mistrust of this approach could be due to the unreliability of E values measured by the traditional Arrhenius plot method. As an illustration, a comment by Vyazovkin [2] can be quoted: "The comparison of theoretical values of the activation energy with the experimental ones may itself present a considerable challenge as the reported values tend to be widely different."

With the beginning of application of the third-law method in 2002, the situation has been significantly improved. As a rule, the measurement error for the parameter E is lower than 2–3 kJ mol^{-1}. Approximately the same error applies to theoretical calculations of the molar enthalpy, $\Delta_r H_T^\circ / \nu$. To date, reliable data on E parameters have been accumulated for several classes of substances [3–14]. Most of them (for oxides, nitrides, hydroxides, nitrates, sulfates, and carbonates) have been obtained by L'vov and his colleagues (see Part III). For other reactants (P, As, Sb, azides, higher oxides, sulfides, selenides, ZnTe, and Be$_3$N$_2$) the primary experimental data reported in the literature (Part III) were used for calculations of the E parameter by the third-law method.

Method In accordance with the general concept of the approach, based on the CDV mechanism, the goal of thermochemical analysis is to find out the composition of the primary decomposition products, for which the magnitude of the reaction molar enthalpy is taken to be the E value. The fundamental difference between the commonly accepted approach and the thermochemical approach is illustrated schematically in Fig. 9.1.

For the decompositions of solid substances to gaseous products only, the desired parameters are the chemical form and relative contents of different gaseous products. For decompositions to both solid and gaseous products, the main difference from the equilibrium composition is due to the congruent dissociative evaporation of the reactant. For example, for hydroxides and carbonates the only difference is in the decomposition of these compounds to gaseous oxides and in their subsequent condensation. The corresponding gaseous products (H$_2$O and CO$_2$) are in their equilibrium form. For some reactants, the difference from the equilibrium composition may additionally manifest itself in a different chemical form and/or in the content of some gaseous components. For example, as is shown below, the decomposition of
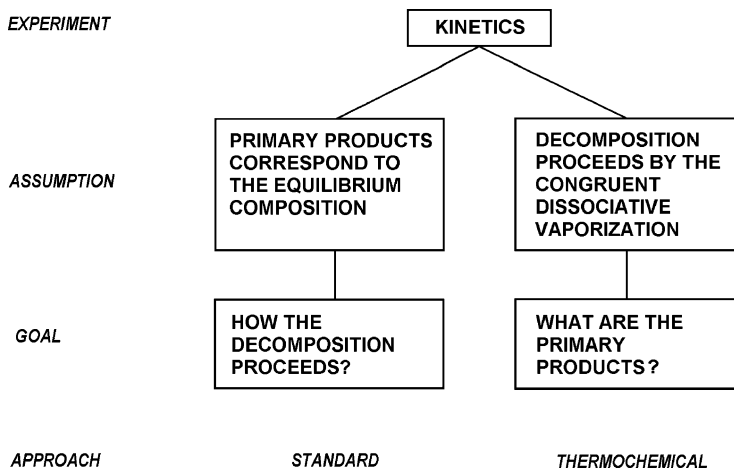
Fig. 9.1 Basic distinction between the standard and thermochemical approaches to studying decomposition mechanisms

some sulfates and nitrates proceeds until the dissociation of these compounds to atomic oxygen (instead of the equilibrium O_2).

As an illustration, Table 9.1 presents data for the comparison of experimentally obtained magnitudes of molar enthalpies for AlN, measured by means of the third-law method, with the results of thermochemical calculations of these magnitudes for the similar reactions (having close $\Delta_r H_T^\circ/\nu$ values). The relative content of atomic and molecular nitrogen (N and N_2) was used as a varying parameter. Calculations via the third-law method have been carried out in accordance with Eqs. 3.19 and 3.20. As can be seen from the table, the equality of the experimental and calculated magnitudes of $\Delta_r H_T^\circ/\nu$ is best fulfilled for the reaction: $AlN \leftrightarrow Al(g) + 0.42N + 0.29N_2$. The variation of the stoichiometric coefficient ν by 0.01 causes a noticeable discrepancy in $\Delta_r H_T^\circ/\nu$ magnitudes, which is greater than the calculation error ($< 1\,\text{kJ mol}^{-1}$).

Final Results of Analysis All the available data are collected in Tables 9.2 and 9.3. Table 9.2 contains the corresponding thermodynamic and kinetic data for 21 reactants, decomposing to gaseous products only, while Table 9.3

Table 9.1 Effect of the reaction stoichiometry on the experimental and calculated values of the molar enthalpy [14]

Deduced Reaction	ν	$\Delta S_T^\circ/\nu$ (J mol^{-1} K^{-1})	$\Delta_r H_T^\circ/\nu$ (kJ mol^{-1})	
			Third-law[a]	Deduced
$AlN \leftrightarrow Al(g) + 0.5N_2$	1.5	151.2	488.3	423.1
$AlN \leftrightarrow Al(g) + 0.40N + 0.30N_2$	1.70	149.5	489.1	486.1
$AlN \leftrightarrow Al(g) + 0.42N + 0.29N_2$	1.71	149.4	488.9	488.9
$AlN \leftrightarrow Al(g) + 0.44N + 0.28N_2$	1.72	149.3	488.8	491.6
$AlN \leftrightarrow Al(g) + N$	2.0	146.7	479.3	557.1

[a]At $P_{\text{eqp}} = 5.1 \times 10^{-7}$ bar and $T = 1,785\,\text{K}$

Table 9.2 Thermochemical parameters for the decompositions of reactants to gaseous products

Deduced Reaction	ν	T (K)	$\Delta S^\circ_T/\nu$ (J mol^{-1} K^{-1})	$\Delta_r H^\circ_T/\nu$ (kJ mol^{-1})	E (kJ mol^{-1}) Third-law[a]	Second-law
$2P(red) \leftrightarrow P_2$	1	600	162.3	175	192　191	218
$6As \leftrightarrow As_4 + As_2$	2	550	157.3	164	189　190	180–183
$6Sb \leftrightarrow Sb_4 + Sb_2$	2	650	152.9	215	214　219	207
$SnO_2 \leftrightarrow SnO + O$	2	1,239	160.7	416	413　412	351[b]
$HgO \leftrightarrow Hg + O$	2	681	128.8	201	188　193	162–241
$ZnO \leftrightarrow Zn + O$	2	1,400	133.3	363	373　377	180–428
$CdS \leftrightarrow Cd + \tfrac{1}{2}S_2$	1.5	1,000	122.2	220	218　232	210[b]
$CdSe \leftrightarrow Cd + \tfrac{1}{2}Se_2$	1.5	1,000	119.7	213	210　226	234[b]
$ZnS \leftrightarrow Zn + \tfrac{1}{2}S_2$	1.5	1,108	133.2	263	255　258	258–266[b]
$ZnSe \leftrightarrow Zn + \tfrac{1}{2}Se_2$	1.5	1,000	125.0	251	239　250	294[b]
$ZnTe \leftrightarrow Zn + \tfrac{1}{2}Te_2$	1.5	900	117.3	214	214　231	246[b]
$AlN \leftrightarrow Al + 0.42N + 0.29N_2$	1.71	1,785	149.3	489	490　466	542
$GaN \leftrightarrow Ga + 0.42N + 0.29N_2$	1.71	1,264	144.4	363	362　351	305
$InN \leftrightarrow In + 0.32N + 0.34N_2$	1.66	1,015	138.7	308	308　305	336
$Be_3N_2 \leftrightarrow 3Be + 1.52N + 0.24N_2$	4.76	1,600	135.0	486	479　481	428
$Mg_3N_2 \leftrightarrow 3Mg + 1.52N + 0.24N_2$	4.76	1,200	130.1	337	337　344	238
$Si_3N_4 \leftrightarrow 3Si + 1.8N + 1.1N_2$	5.9	1,700	155.5	501	503　470	480
$NaN_3 \rightarrow Na + 0.86N + 1.07N_2$	2.93	603	134.3	168	168　169	144–197
$KN_3 \leftrightarrow K(g) + 0.73N + 1.135N_2$	2.86	524	134.6	152	152　153	130–205
$AgNO_3(l) \leftrightarrow Ag + NO_2 + \tfrac{1}{2}O_2$	2.5	574	128.5	168	166　170	167–174
$Cd(NO_3)_2(l) \leftrightarrow CdO + 2NO_2 + O$	4	660	152.5	204	198　203	186

[a] Left-hand value corresponds to $\Delta S^\circ_T/\nu$ listed in this table, and right-hand value, to the average value $\Delta S^\circ_T/\nu$: 136 or 160 J mol^{-1} K^{-1}
[b] Our estimation

Table 9.3 Thermochemical parameters for the decomposition of reactants to solid and gaseous products

Deduced Reaction	ν	T (K)	$\Delta_v H_T^\circ$ (kJ mol^{-1})	$-\Delta_c H_T^\circ$ (kJ mol^{-1})	τ_1	$\Delta S_T^\circ/\nu$ (J mol^{-1} K^{-1})	$\Delta_r H_T^\circ/\nu$ (kJ mol^{-1})	E (kJ mol^{-1}) Third-law[a]		Second-law
$BN \leftrightarrow B(g)_\downarrow + \tfrac{1}{2}N_2$	1.5	1,800	$808.2_{1,800}$	$560.2_{1,800}$	0.047	$154.7_{1,800}$	521	529	495	329
$Pb(N_3)_2 \leftrightarrow Pb(g)_\downarrow + 2.36N + 1.82N_2$	5.18	520	827.2_{300}	193.8_{500}	0.298	138.2_{300}	149	152	151	125–159
$Pb_3O_4 \leftrightarrow 3PbO(g)_\downarrow + O$	4	780	1139.1_{780}	833.7_{800}	0.178	150.8_{800}	248	220	227	188^{b}
$Be(OH)_2 \leftrightarrow BeO(g)_\downarrow + H_2O$	2	400	796.9_{400}	743.4_{400}	0.672	169.0_{400}	149	130	126	115
$Mg(OH)_2 \leftrightarrow MgO(g)_\downarrow + H_2O$	2	535	710.4_{500}	632.2_{500}	0.600	163.9_{500}	166	171	169	126–134
$Ca(OH)_2 \leftrightarrow CaO(g)_\downarrow + H_2O$	2	570	778.3_{600}	674.1_{600}	0.578	152.6_{600}	194	178	182	145–174
$Sr(OH)_2 \leftrightarrow SrO(g)_\downarrow + H_2O$	2	590	706.6_{600}	579.3_{600}	0.544	151.3_{600}	196	186	191	126
$Ba(OH)_2 \leftrightarrow BaO(g)_\downarrow + H_2O$	2	610	556.1_{600}	415.5_{600}	0.472	140.3_{600}	180	178	190	63
$Zn(OH)_2 \leftrightarrow ZnO(g)_\downarrow + H_2O$	2	400	508.4_{300}	455.4_{300}	0.579	168.2_{300}	122	125	122	95
$Cd(OH)_2 \leftrightarrow CdO(g)_\downarrow + H_2O$	2	385	400.8_{300}	340.1_{300}	0.515	164.4_{300}	113	127	125	95–116
$AgNO_3 \leftrightarrow Ag(g)_\downarrow + NO_2 + \tfrac{1}{2}O_2$	2.5	470	430.7_{470}	283.9_{500}	0.446	142.8_{470}	122	147	142	142
$Cd(NO_3)_2 \leftrightarrow CdO(g)_\downarrow + 2NO_2 + O$	4	560	841.9_{600}	335.5_{600}	0.422	161.9_{600}	175	178	177	177
$MgSO_4 \leftrightarrow MgO(g)_\downarrow + SO_2 + O$	3	1,006	$1262.6_{1,000}$	$631.3_{1,000}$	0.435	$171.3_{1,000}$	329	334	323	312–343
$BaSO_4 \leftrightarrow BaO(g) + SO_2 + O$	3	1,400	$1237.3_{1,400}$	$399.5_{1,400}$	0	$152.7_{1,400}$	412	421	431	384
$MgCO_3 \leftrightarrow MgO(g)_\downarrow + CO_2$	2	670	728.1_{700}	630.9_{700}	0.496	174.3_{700}	208	219	209	176
$\tfrac{1}{2}CaMg(CO_3)_2 \leftrightarrow \tfrac{1}{2}CaO(g)_\downarrow + \tfrac{1}{2}MgO(g)_\downarrow + CO_2$	2	810	815.3_{800}	650.9_{800}	0.518	164.5_{800}	239	254	250	192
$CaCO_3 \leftrightarrow CaO(g)_\downarrow + CO_2$	2	910	840.6_{900}	669.4_{900}	0.403	157.3_{900}	285	250	252	205
$SrCO_3 \leftrightarrow SrO(g)_\downarrow + CO_2$	2	910	805.6_{900}	566.9_{900}	0.256	161.1_{900}	330	284	283	279
$BaCO_3 \leftrightarrow BaO(g)_\downarrow + CO_2$	2	1,080	$645.2_{1,100}$	$406.0_{1,100}$	0.240	$137.6_{1,200}$	274	304	328	226
$Li_2SO_4 \cdot H_2O \leftrightarrow Li_2SO_4(g)_\downarrow + H_2O$	2	300	446.6_{300}	388.0_{300}	0.602	175.9_{300}	106	96	91	86

[a] Left-hand value corresponds to $\Delta S_T^\circ/\nu$ listed in this table, and right-hand value, to the average values of $\Delta S_T^\circ/\nu$: 136 or 160 J mol^{-1} K^{-1}

[b] Our estimation
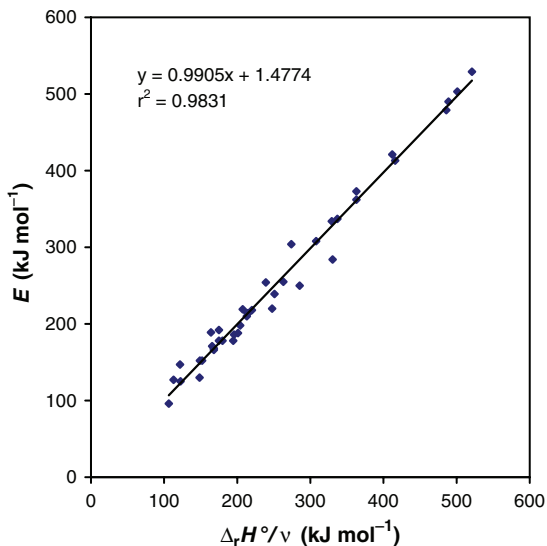
Fig. 9.2 Correlation between the experimental values of the E parameter measured by the third-law method and the calculated values of the molar enthalpy $\Delta_r H_T^\circ / \nu$ (precise calculations)

contains the data for 20 reactants decomposing to both solid and gaseous products. (The bibliography for the experimental results listed in these tables is given in Chapter 16.)

The results presented in [3–14] have been corrected for refinements of the calculation scheme (see Part III). The transfer coefficient τ_1, included in Table 9.3 was calculated using Eq. 8.3. The E parameters for all reactants were calculated by the third-law method using two schemes: the precise scheme (using the $\Delta_r S_T^\circ / \nu$ magnitudes, given in the table) and the approximate scheme (using averaged magnitudes of $\Delta_r S_T^\circ / \nu$: 136 or 160 J mol^{-1} K^{-1}).

The correlation between the experimentally obtained magnitudes E calculated by the third-law method and magnitudes of the molar enthalpy, $\Delta_r H_T^\circ / \nu$, for assumed reactions is presented in Fig. 9.2 for the precise calculation and in Fig. 9.3 for the approximate calculation.

The difference between the precise and approximate calculation schemes for the parameter E is insignificant. The precise scheme gives a higher linear correlation coefficient (0.99 instead of 0.95 for the approximate calculation). The average values of the relative standard deviations of the ratio $(\Delta_r H_T^\circ / \nu)/E$ from 1 are 7.0% and 7.6%, respectively.
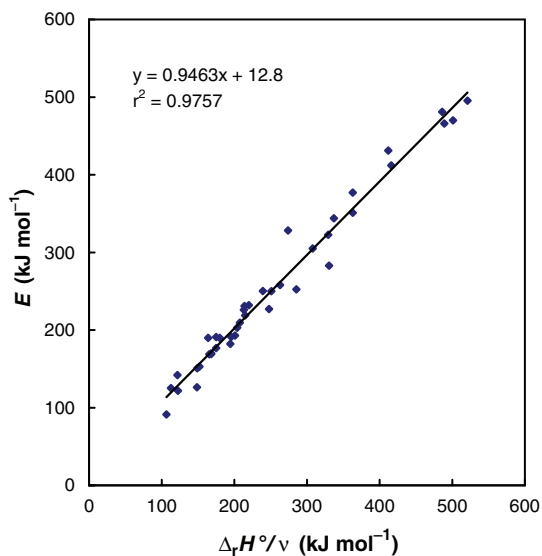
Fig. 9.3 Correlation between the experimental values of the E parameter measured by the third-law method and the calculated values of the molar enthalpy $\Delta_r H_T^\circ/\nu$ (approximate calculations)

References

1. L'vov BV, Ryabchuk GN (1981) Zh Analit Khim 36:2085–2096 (in Russian)
2. Vyazovkin S (2002) Anal Chem 74:2749–2762
3. L'vov BV (2002) Thermochim Acta 389:199–211
4. L'vov BV, Polzik LK, Ugolkov VL (2002) Thermochim Acta 390:5–19
5. L'vov BV, Ugolkov VL (2003) Thermochim Acta 401:139–147
6. L'vov BV, Ugolkov VL (2004) Thermochim Acta 409:13–18
7. L'vov BV, Ugolkov VL (2004) Thermochim Acta 410:47–55
8. L'vov BV, Ugolkov VL (2004) Thermochim Acta 411:73–79
9. L'vov BV, Ugolkov VL Grekov FF (2004) Thermochim Acta 411:187–193
10. L'vov BV, Ugolkov VL (2004) Thermochim Acta 413:7–15
11. L'vov BV, Ugolkov VL (2004) Thermochim Acta 424:7–13
12. L'vov BV (2004) Thermochim Acta 424:183–189
13. L'vov BV, Ugolkov VL (2005) Russian J Appl Chem 78:379–385
14. L'vov BV, Ugolkov VL (2005) Thermochim Acta 438:1–8

Chapter 10
Effect of the Reactant Crystal Structure on the Composition of the Primary Decomposition Products

As can be seen from Tables 9.2 and 9.3, for many reactants the composition of the primary gaseous products (oxygen and nitrogen) differs from the equilibrium composition. These products are released, completely or partially, in the form of free atoms. This phenomenon is of remarkable theoretical and practical interest. Some general features of this phenomenon, related to the decompositions of oxides, nitrides and, to some extent, of phosphorus, arsenic, and antimony, are described below.

10.1 Oxides

Historical Background The fact that some oxides decompose with the formation in the primary stage of free atomic oxygen is well known. Over 40 years ago Harano [1] showed (using the colour change of MoO_3 oxide from pale yellow to light blue), that during the decomposition of ZnO, HgO, CuO, and PtO_2 in vacuum, oxygen is partially released in the form of atoms. Later [2, 3] a similar effect was discovered for the decomposition of lead oxide (Pb_3O_4). These studies stimulated research on the decomposition kinetics of Group IIB oxides (ZnO, CdO, and HgO) by L'vov and Ugolkov [4] towards identification of the actual content of O and O_2 in the primary products. For the sake of completeness, cadmium oxide was included in this study, although the equilibrium composition of the products (Cd and O_2) formed during its decomposition had been proved unambiguously [5]. Good agreement of the E parameters and the molar enthalpies for the decomposition of ZnO and HgO to atomic oxygen (Table 9.2), as well as the absence of any decelerating effect of O_2-additives on their decomposition, led to the conclusion that the dissociative evaporation of both oxides proceeds with the formation of atomic oxygen.

Analysis The first attempt to explain the difference in the decomposition mechanisms for CdO, on the one hand, and for ZnO and HgO, on the other, undertaken in [4], was based on an analysis of interatomic spacings O–O in the corresponding crystals. Their estimation was carried out using the software (PowderCell Program), developed by Kraus and Nolze [6], and tables [7]. An analysis showed that the minimum spacing in the series ZnO, CdO, and HgO varies as 2.60, 3.34, and 3.50 Å. This is considerably larger than the

interatomic distance in the O_2 molecule (1.21 Å). This means that differences in the decomposition mechanisms are due to other factors.

To study this problem in more detail, L'vov et al. [4] collected all the available data on the evaporation mechanisms for 23 different oxides (and two sulfates) and compared them with the crystal structures of these substances. When these compounds were divided into two groups in accordance with the form of the oxygen in the primary decomposition products, clear-cut differences in their crystal structures were revealed (Table 10.1).

All the oxides decomposing with the release of molecular oxygen (excluding PbO) belong to the cubic (I) system. The decompositions of all the other compounds having a system other than cubic (II, III, IIIa, IV, and V) results in the formation of atomic oxygen. The release of molecular oxygen in the decomposition of PbO may be due to it having the shortest O–O interatomic spacing (1.98 Å) compared to all the other oxides.

The obvious deduction is that there is an interrelation between these differences and the structural symmetry. One could assume that the crucial role belongs here to the local symmetry in the positions of the O-atoms. Fragments

Table 10.1 The crystal structures and evaporation mechanisms for some oxides and sulfates

Oxide	System[a]	Space Group	Minimum O–O Distance (Å)	Primary Product
Li_2O	I	225	2.31	O_2
Cu_2O	I	224	3.68; 4.25	O_2
Ag_2O	I	224	4.09; 4.72	O_2
MgO	I	225	2.98	O_2
CaO	I	225	3.39	O_2
SrO	I	225	3.63	O_2
CdO	I	225	3.34	O_2
MnO	I	225	3.14	O_2
FeO	I	225	3.06	O_2
CoO	I	225	3.01	O_2
NiO	I	225	2.95	O_2
PbO	II	129	1.98	O_2
CaO_2	II	139	4.62	O
SrO_2	II	139	3.55	O
BaO_2	II	139	5.12	O
GeO_2	II	136	2.86	O
SnO_2	II	136	3.19	O
Pb_3O_4	II	135	3.28	O
SiO_2	III	182	2.91	O
PtO_2	IIIa	164	2.74	O
ZnO	III	186	2.60	O
HgO	IV	62	3.50	O
$MgSO_4$	IV	63	2.47	O
$BaSO_4$	IV	62	2.44	O
CuO	V	15	2.62	O

[a]I: cubic; II: tetragonal; III: hexagonal; IIIa: trigonal; IV: rhombic; and V: monoclinic
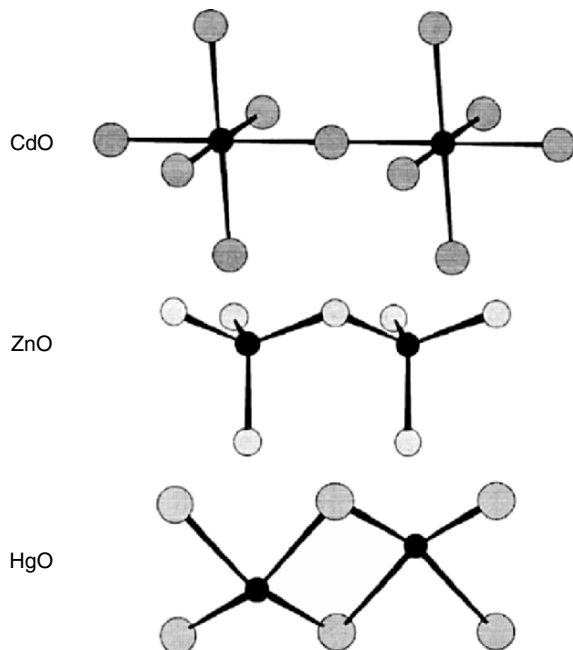
Fig. 10.1 Fragments of a crystal structure for CdO, ZnO, and HgO. Large and small circles represent, respectively, atoms of metals and oxygen

of the structure shown in Fig. 10.1 illustrate the difference in the symmetry of the O-atoms in the crystal structures of CdO, ZnO, and HgO. For oxides with higher symmetry and a close to isotropic neighbourhood, the dissociative evaporation results in the release of molecules. Oxygen atoms residing in low-symmetry positions leave their sites without recombination. Presumably, some differences exist in the electronic structure of these atoms that are responsible for the recombination mechanism. These preliminary conclusions are undoubtedly worthy of further investigation and comparison with decomposition peculiarities of other compounds.

10.2   Nitrides

Historical Background   A regularity fairly close to the one considered above has been discovered in studies of the decompositions of metal nitrides [8–12]. The analysis of the stoichiometry of the primary products formed during the decompositions of nitrides was based on early works [8–11] on the kinetic data available in the literature, in particular, on the results of the determination of vaporization coefficients. The reliability of these data, especially for Langmuir

measurements, was not high. That is why the proportion of atomic and molecular nitrogen in the decomposition products in [8–11] varied within a factor of 1.5.

The goal of the latter work [12] relating to this topic was to measure the free-surface evaporation enthalpy for the group of nitrides (Mg_3N_2, BN, AlN, GaN, InN, and Si_3N_4) using the third-law method. It was anticipated that, similarly to many other cases, this should raise the accuracy and precision of experimental data considerably and, thus, the reliability of the final conclusions.

Analysis From comparison of the data obtained with the results of thermodynamic calculations (e.g., see Table 9.1 for AlN) the reactions best corresponding to the decomposition kinetics have been found. The final results of this research, including the analysis of data available in the literature [13–19], with due account for some corrections specified in Sect. 16.6, are summarized in Table 10.2. The following conclusions can be drawn from their analysis.

- First of all, considerable differences in decomposition schemes for nitrides of cubic and hexagonal modifications are apparent. All cubic nitrides decompose with the release of molecular nitrogen only, while all hexagonal nitrides form atomic nitrogen in amounts from 32% to 76%. The first part of this regularity is in a full conformity with the decomposition mechanism for oxides. However, the decompositions of hexagonal nitrides are somewhat different. Recall that the decompositions of all oxides having a system other than cubic, proceeds with the release of oxygen in the form of free atoms only, rather than in the form of an O/O_2 mixture.
- No correlation was observed between the reaction stoichiometry and the minimum interatomic spacing N–N, which was determined in the same way as for oxides, using the software [6] and tables [7]. Moreover, the minimum N–N spacing for AlN and GaN (3.1 Å) is shorter than that for InN (3.5 Å), regardless of the higher content of free N-atoms in the primary decomposition products for the first two nitrides (42% instead of 32% for InN). Therefore, the commonly used explanation of a low vaporization coefficient for some nitrides [15], based on the difference of the interatomic distance for a free molecule N_2(1.07 Å) from the much longer spacings (2.5–3.5 Å) between the closest nitrogen atoms in the crystal lattices of nitrides, is incorrect.
- For two pairs of nitrides of a similar composition (Be_3N_2/Mg_3N_2 and AlN/GaN) the stoichiometry of the products turns out to be completely identical, regardless of considerable differences in the decomposition temperatures (1,600/1,200 K and 1,800/1,300 K). Apparently, the decomposition stoichiometry does not depend on temperature. However, due to unknown reasons, the stoichiometry of the decomposition of InN differs noticeably from that of AlN and GaN.

Table 10.2 The decomposition mechanisms of nitrides in a vacuum vs their crystal structures [21]

Deduced Reaction	$b/(b+2c)^a$ (%)	Sample[b]	System	Space Group	N-N Minimum Distance (Å)	T (K)	$\Delta_r H^\circ_T/\nu$ (kJ mol^{-1})			Ref.
							Second Law	Third Law	Deduced	
$Be_3N_2 \leftrightarrow 3Be(g) + 1.5N + 0.25N_2$	75	Pressed pellet	III	194	2.84	1,600	428	486	479	[13]
$Mg_3N_2 \leftrightarrow 3Mg(g) + 1.5N + 0.25N_2$	75	Pressed pellet	III[c]	194	3.29	1,200	238	302	336	[14]
		Pellet				1,231	350	334	336	[12]
$h\text{-}AlN \leftrightarrow Al(g) + 0.42N + 0.29N_2$	42	Pressed pellet	III	186	3.07	1,800	494[d]	502	489	[15]
		Pellet				1,785		490	489	[12]
$h\text{-}GaN \leftrightarrow Ga(g) + 0.42N + 0.29N_2$	42	MOCVD film	III	186	3.17	1,300	379	361	363	[16]
		Pressed pellet				1,300	305	350	363	[17]
		Pellet				1,264		362	363	[12]
$InN \leftrightarrow In(g) + 0.32N + 0.34N_2$	32	Polycrystal	III	186	3.51	1,100	336	305	307	[16]
		Pellet				1,015		308	308	[12]
$\alpha, \beta\text{-}Si_3N_4 \leftrightarrow 3Si(g) + 1.8N + 1.1N_2$	45	Powder	III	159; 176	2.82; 2.79	1,713	480[d]	480	503	[18]
		Pellet				1,700		502	503	[12]
$c\text{-}BN \leftrightarrow B(g)_\downarrow + 0.5N_2$	0	Pressed pellet	I	216	2.56	1,800	329[d]	541	539	[15]
		Pellet				1,800		527	539	[12]
$c\text{-}AlN \leftrightarrow Al(g) + 0.5N_2$	0	MOCVD film	I	216	3.09	1,300	414	397	427	[16]
$c\text{-}GaN \leftrightarrow Ga(g) + 0.5N_2$	0	MBE film	I	216	3.09	900	261	305	284	[19]

[a] Content of atomic nitrogen species in the reaction $M_a N_{b+2c} \leftrightarrow aM(g) + bN + cN_2$
[b] MOCVD: metal organic chemical vapor deposition; MBE: molecule beam epitaxy
[c] Polymorphous transition from the cubic (α) to hexagonal (β) structure for Mg_3N_2 at 823 K has been observed in [20] and supported in [21]
[d] Calculated in this work on the basis of experimental data reported in original publications

10.3 Phosphorous, Arsenic, and Antimony

Historical Background An extremely low evaporation rate for red phosphorus, as compared to that for white phosphorus, was reported for the first time by Melville and Gray in 1936 [21]. The vapour pressure measured by the Langmuir method at $578\,\mathrm{K}$ was found to be equal to 1.3×10^{-9} bar [22]. Melville and Gray [21] supposed that this was due to the absence of structural units of the P_4-type for red phosphorus and, as a result, it evaporated in the form of P_2 molecules. Research into this anomaly was continued later by Brewer and Kane [23], who concluded that, even if evaporation of red phosphorus in the form of P_2 molecules was assumed, the vaporization coefficient appears to be lower than 1. In these studies [22, 23] a low evaporation rate for arsenic and antimony had been noted as well. Rosenblatt et al. [24] measured the molar enthalpies and entropies of free-surface evaporation for arsenic and antimony and confirmed the previous results. The low vaporization coefficient, according to Rosenblatt et al. [24], is, similarly to phosphorus, due to the absence of M_4-fragments in the crystal structure of these metals and the difficulty of their formation via the variation of initial interatomic spacings and angles. None of the researchers mentioned above tried to compare the experimentally obtained magnitudes of the thermochemical parameters with calculations to identify the primary evaporation products.

Analysis Such an attempt was undertaken by L'vov and Novichikhin [8] in 1997. The results of this comparison are presented in Table 10.3. The discrepancy in $\Delta_r H_T^\circ$ magnitudes for red phosphorus is most probably due to an overestimation of the experimentally obtained magnitude ($218\,\mathrm{kJ\,mol^{-1}}$), reported in [23].

   Estimation of the $\Delta_r H_T^\circ$ magnitude by the third-law method basing on the data obtained in [21], gives the magnitude 192–$212\,\mathrm{kJ\,mol^{-1}}$ (see Sect. 16.1). As can be seen, all of the low evaporation rates can be explained by a partial (for As and Sb) and complete (for P) evaporation of these elements in the form of binary molecules (M_2) instead of the more thermodynamically stable M_4 molecules.

Table 10.3 The crystal structures and the mechanisms of vaporization of phosphorus, arsenic and antimony

Deduced Reaction	System[a]	T (K)	$\Delta_r H_T^\circ$ (kJ mol^{-1})		Ref.
			Expt	Deduced [9]	
$4P(\text{white}) \leftrightarrow P_4$	I	298	59	59	[22]
$2P(\text{red}) \leftrightarrow P_2$	VI	600	218	175	[23, 25]
$6As \leftrightarrow As_4 + As_2$	IIIa	550	180; 183	177	[23–25]
$6Sb \leftrightarrow Sb_4 + Sb_2$	IIIa	650	207	214	[24]

[a] I: cubic; VI: triclinic; and IIIa: trigonal

Comparison of the decomposition products with the crystal structures of the corresponding substances shows that the equilibrium composition of products is observed only for white phosphorus, having the cubic structure. For elements with structures other than cubic, evaporation occurs with the formation (partial or complete) of binary molecules. Thus, *the distinctive feature of crystals with cubic structure to sublime with the formation of equilibrium primary products manifests itself for all the substances considered above: oxides, nitrides and white phosphorus.*

References

1. Harano Y (1961) Nippon Kagaku Zasshi 82:152–155
2. Malinin GV, Tolmachev YuM, Yadrintsev VB (1968) Zh Neorg Khim 13:1746–1749 (in Russian)
3. Malinin GV, Tolmachev YuM, Brach BYa (1972) Vestnik LGU 4:126–129 (in Russian)
4. L'vov BV, Ugolkov VL, Grekov FF (2004) Thermochim Acta 411:187–193
5. Gilbert IGF, Kitchener JA (1956) J Chem Soc 3919–3921
6. Kraus W, Nolze G (1996) J Appl Cryst 29:301–303
7. International crystal structure data (1996) Gmelin Institute, Karlsruhe
8. L'vov BV, Novichikhin AV (1997) Thermochim Acta 290:239–251
9. L'vov BV (2001) Thermochim Acta 373:97–124
10. L'vov BV (2002) Thermochim Acta 389:199–211
11. L'vov BV (2004) Thermochim Acta 424:183–189
12. L'vov BV, Ugolkov VL (2005) Thermochim Acta 438:1–8
13. Hoenig CL, Searcy AW (1967) J Am Ceram Soc 50:460–466
14. Blank BAH, Searcy AW (1968) J Phys Chem 72:2241–2243
15. Dreger LH, Dadape VV, Margrave JL (1962) J Phys Chem 66:1556–1559
16. Ambacher O, Brandt MS, Dimitrov R, et al. (1996) J Vac Sci Technol B 14:3532–3542
17. Munir ZA, Searcy AW (1965) J Chem Phys 42:4223–4228
18. Ryklis EA, Bolgar AS, Fesenko VV (1969) Poroshkovaya Metallurgiya 73:92–96 (in Russian)
19. Brandt O, Yang Hui, Ploog KH (1996) Phys Rev B 54:4432–4435
20. Mitchell DW (1949) Ind Eng Chem 41:2027–2031
21. Melville HW, Gray SC (1936) Trans Faraday Soc 32:271, 1017, 1026
22. Nesmeyanov AnN (1961) Vapour pressure of chemical elements. Akad Nauk SSSR, Moscow (in Russian)
23. Brewer L, Kane JS (1955) J Phys Chem 59:105–109
24. Rosenblatt GM, Lee P-K, Dowell MB (1966) J Chem Phys 45:3454–3455
25. Somorjai GA, Lester JE (1967) Evaporation mechanism of solids. In: Reiss H (ed) Progress in solid state chemistry. Pergamon, Oxford, pp 1–52

Chapter 11
Vaporization Coefficients

Definition The vaporization coefficient, α_v, is usually defined as the ratio of the actual flow of gaseous decomposition product J to the flow $J_{\max}$ coming from an effusion cell, in which, it is assumed, decomposition products are in an ideal equilibrium with the reactant. For many substances, as found from comparative Knudsen–Langmuir TG measurements, $\alpha_v \ll 1$, i.e., their free-surface decomposition proceeds much more slowly than would be expected from effusion observations. It is a common practice to explain this discrepancy by a multistage character of the evaporation process, by surface relief peculiarities or by impurities and defects (imperfections) in the reactant lattice.

Analysis L'vov and Novichikhin [1] were the first to relate this effect to the difference between the actual decomposition scheme and the supposed scheme of decomposition directly to equilibrium products (as in an effusion cell). Initial gasification of all of the products, including low-volatility components (metals or metal oxides) is assumed, followed by partial or complete release of gaseous products in a chemical form different from the equilibrium composition.

The contributions of these factors to the decomposition coefficient are presented separately for reactants decomposing to gaseous products only (Table 11.1) and to gaseous and solid products (Table 11.2). Reactants are listed in order of decreasing coefficient α_v. The coefficients were determined from the experimentally obtained magnitudes of the equilibrium pressures P_{eqp} for the primary evaporation products found by means of the third-law method (see Chapter 16), and from theoretically calculated equilibrium pressures P_{eq} for the final (equilibrium) products. Analysis of these data yielded the following conclusions.

- The variation of α_v magnitudes in both cases is extraordinarily wide: from 1 to 10^{-25} for the first group and from 10^{-3} to 10^{-29}, in the second group. If the anomalously low magnitudes of vaporization coefficients for azides and oxalates are excluded, then the average value of α_v for the first group of reactants is about 10^{-3}, while that for the second group is about 10^{-6}.
- The anomalously low magnitudes of α_v for the azides and the oxalates (10^{-10} to 10^{-29}) are related to exothermic properties of these compounds (they are explosives). However, because their decompositions result in the formation of primary products differing from the equilibrium products, they turn out to be fairly stable around room temperature.
- A wide variety of materials having α_v coefficients equal or very close to 1, should be assigned to the first group of substances, which evaporate to gaseous products only. Besides the solids listed in Table 5.1 (metals, halogenides and ice), which sublime without changes of the chemical form of the

Table 11.1 The vaporization coefficients for reactants decomposing into gaseous products[a]

Reactant	T (K)	Primary Products	P_{eqp}	Equilibrium Products	P_{eq} (bar)	α_v
SiO_2	1,800	$SiO + O$	1.1E−07	$SiO + 1/2O_2$	2.2E−07	5E−01
SnO_2	1,287	$SnO + O$	3.2E−09	$SnO + 1/2O_2$	4.9E−07	7E−02
Sb	650	$Sb_4 + Sb_2$	9.8E−10	Sb_4	3.0E−08	3E−02
GeO_2	1,323	$GeO + O$	1.5E−07	$GeO + 1/2O_2$	2.0E−05	1E−02
h-AlN	1,800	$Al + 0.42N + 0.29N_2$	4.1E−07	$Al + 1/2N_2$	4.1E−05	1E−02
ZnO	1,250	$Zn(g) + O$	6.6E−09	$Zn + 1/2O_2$	7.3E−07	9E−03
As	550	$As_4 + As_2$	1.6E−07	As_4	9.9E−05	2E−03
Be_3N_2	1,600	$3Be + 1.52N + 0.24N_2$	2.7E−09	$3Be + N_2$	2.7E−06	1E−03
h-GaN	1,300	$Ga + 0.42N + 0.29N_2$	9.0E−08	$Ga + 1/2N_2$	2.3E−04	4E−04
InN	1,000	$In + 0.32N + 0.34N_2$	1.5E−09	$In + 1/2N_2$	6.6E−06	2E−04
Si_3N_4	1,700	$3Si + 1.8N + 1.1N_2$	4.5E−08	$3Si + 2N_2$	2.5E−05	2E−05
P (red)	600	P_2	2.3E−07	P_4	2.3E−02	1E−05
Mg_3N_2	1,200	$3Mg + 1.52N + 0.24N_2$	1.3E−08	$3Mg + N_2$	1.7E−03	8E−06
HgO	700	$Hg + O$	3.0E−08	$Hg + 1/2O_2$	1.9E−01	2E−07
NaN_3	600	$Na + 0.86N + 1.07N_2$	2.4E−08	$Na(l) + 3/2N_2$	1.6E+06	2E−14
KN_3	530	$K + 0.72N + 1.14N_2$	1.1E−08	$K(l) + 3/2N_2$	6.2E+05	2E−14
HgC_2O_4	424	$Hg + CO + CO_2 + O$	1E−07	$Hg(l) + 2CO_2$	5E+16	2E−24

[a] P_{eqp} and P_{eq} are equilibrium pressure for the primary and eventual products, respectively

Table 11.2 Vaporization coefficients for reactants decomposing into solid and gaseous products[a]

Reactant	T (K)	Primary Products	P_{eqp} (bar)	Equilibrium Products	P_{eq} (bar)	α_v
$BaSO_4$	1,397	$BaO(g)_\downarrow + SO_2 + O$	3.9E−08	$BaO(s) + SO_2 + 1/2O_2$	2.4E−06	2E−02
$Ba(OH)_2$	600	$BaO(g)_\downarrow + H_2O$	6.3E−09	$BaO(s) + H_2O$	2.8E−06	2E−03
Pb_3O_4	784	$3PbO(g)_\downarrow + O$	1.7E−07	$3PbO(s) + 1/2O_2$	1.2E−04	1E−03
$BaCO_3$	903	$BaO(g)_\downarrow + CO_2$	9E−08	$BaO(s) + CO_2$	1E−04	9E−04
Kaolinite	750	$Al_2O_3(g)_\downarrow + 2SiO_2(g)_\downarrow + 2H_2O$	3.8E−08	$Al_2O_3(s) + 2SiO_2(s) + 2H_2O$	1E−04	4E−04
$SrCO_3$	908	$SrO(g)_\downarrow + CO_2$	1E−08	$SrO(s) + CO_2$	6E−05	1E−04
$Sr(OH)_2$	600	$SrO(g)_\downarrow + H_2O$	5.7E−09	$SrO(s) + H_2O$	1.3E−04	4E−05
$MgSO_4$	1,006	$MgO(g)_\downarrow + SO_2 + O$	5.4E−09	$MgO(s) + SO_2 + 1/2O_2$	1.7E−04	3E−05
$CaMg(CO_3)_2$	820	$MgO(g)_\downarrow + CaO(g)_\downarrow + 2CO_2$	4E−08	$MgO(s) + CaO(s) + 2CO_2$	6E−03	7E−06
$Ca(OH)_2$	600	$CaO(g)_\downarrow + H_2O$	4.7E−08	$CaO(s) + H_2O$	7.2E−03	7E−06
$CaCO_3$	903	$CaO(g)_\downarrow + CO_2$	3E−08	$CaO(s) + CO_2$	7E−03	4E−06
$CuSO_4 \cdot 5H_2O$	273	$CuSO_4(g)_\downarrow + 5H_2O$	1.2E−09	$CuSO_4(s) + 5H_2O$	1.0E−03	1E−06
$CuSO_4 \cdot 5H_2O$	273	$CuSO_4(g)_\downarrow + 5H_2O$	1.2E−09	$CuSO_4(s) + 5H_2O$	1.0E−03	1E−06
$Cd(NO_3)_2$	563	$CdO(g)_\downarrow + 2NO_2 + O$	3.9E−08	$CdO(s) + 2NO_2 + 1/2O_2$	4.8E−02	8E−07
Talc	1,285	$3MgO(g)_\downarrow + 4SiO_2(g)_\downarrow + H_2O$	4.0E−07	$3MgSiO_3(s) + SiO_2(s) + H_2O$	1E−00	4E−07
$AgNO_3(l)$	573	$Ag(g) + NO_2 + 1/2O_2$	5.8E−09	$Ag(s) + NO_2 + 1/2O_2$	3.3E−02	2E−07

(continued)

Table 11.2 (continued)

Reactant	T (K)	Primary Products	P_{eqp} (bar)	Equilibrium Products	P_{eq} (bar)	α_v
$Cd(NO_3)_2(l)$	657	$CdO(g) + 2NO_2 + O$	5.6E−08	$CdO(s) + 2NO_2 + 1/2O_2$	3.5E−00	2E−08
$Cd(OH)_2$	400	$CdO(g)_\downarrow + H_2O$	1.0E−08	$CdO(s) + H_2O$	8.6E−01	1E−08
$CaSO_4 \cdot 2H_2O$	288	$CaSO_4(g)_\downarrow + 2H_2O$	3.9E−10	$CaSO_4(s) + 2H_2O$	4.0E−02	1E−08
$Li_2SO_4 \cdot H_2O$	300	$Li_2SO_4(g)_\downarrow + H_2O$	8.7E−10	$Li_2SO_4(s) + H_2O$	9.6E−02	9E−09
$Mg(OH)_2$	535	$MgO(g)_\downarrow + H_2O$	4.6E−09	$MgO(s) + H_2O$	9.2E−01	5E−09
$Zn(OH)_2$	400	$ZnO(g)_\downarrow + H_2O$	2.5E−08	$ZnO(s) + H_2O$	1.6E+01	2E−09
$MgCO_3$	686	$MgO(g)_\downarrow + CO_2$	3E−08	$MgO(s) + CO_2$	3E+01	1E−09
$Be(OH)_2$	400	$BeO(g)_\downarrow + H_2O$	9.3E−09	$BeO(s) + H_2O$	1.20E+01	8E−10
PbC_2O_4	532	$Pb(g)_\downarrow + 2CO + 1/2O_2$	1E−07	$PbO(s) + CO + CO_2$	5E+02	2E−10
MnC_2O_4	651	$Mn(g)_\downarrow + 2CO + 1/2O_2$	1E−07	$MnO(s) + CO + CO_2$	4E+03	3E−11
NiC_2O_4	568	$Ni(g)_\downarrow + CO + CO_2 + 1/2O_2$	1E−07	$Ni(s) + 2CO_2$	2E+05	5E−12
$Sr(N_3)_2$	390	$Sr(g)_\downarrow + 0.5N + 2.75N_2$	1.5E−04	$Sr(s) + 3N_2$	2.90E+08	5E−13
$Ca(N_3)_2$	350	$Ca(g)_\downarrow + 0.5N + 2.75N_2$	1.5E−03	$Ca(s) + 3N_2$	5.80E+09	3E−13
$Ba(N_3)_2$	400	$Ba(g)_\downarrow + 0.74N + 2.63N_2$	8.1E−06	$Ba(s) + 3N_2$	3.90E+07	2E−13
TlN_3	520	$Tl(g)_\downarrow + 1.14N + 0.93N_2$	3.1E−06	$Tl(s) + 3/2N_2$	5.4E+16	6E−23
$Ag_2C_2O_4$	363	$2Ag(g)_\downarrow + CO + CO_2 + 1/2O_2$	1E−07	$2Ag(s) + 2CO_2$	1E+17	1E−24
$AgN_3(l)$	530	$Ag(g) + 1.14N + 0.93N_2$	4.7E−07	$Ag(s) + 3/2N_2$	1.40E+19	3E−26
$Pb(N_3)_2$	520	$Pb(g)_\downarrow + 2.36N + 1.82N_2$	7.1E−09	$Pb(s) + 3N_2$	3.10E+20	2E−29

[a] P_{eqp} and P_{eq}: equilibrium pressure for the primary and eventual products, respectively

initial reactant, oxides (Table 10.1), nitrides (Table 10.2), sulfides, selenides, and tellurides (Table 16.15), having cubic crystal structures, belong to the same group.

• As distinct from the first group, all the substances of the second group, decomposing ultimately to solid and gaseous products, have vaporization coefficients much lower than 1. This is primarily due to the gaseous (non-equilibrium) aggregate state of the main decomposition product. For some reactants (azides, oxalates, nitrates, and sulfates) it may be also caused by the difference of the chemical form of the primary gaseous products from the equilibrium products. The average value of α_v, calculated from the results in Tables 11.1 and 11.2 (excluding azides and oxalates) has a magnitude close to 10^{-5} and characterizes the difference of the actual decomposition rates of substances from the rates calculated for reactants decomposing directly to equilibrium products. (It is difficult to imagine how the world would change if the majority of substances, both natural and synthetic, did decompose to equilibrium products, i.e., 100,000 times faster.)

Misconception and its Interpretation The low magnitudes of the vaporization coefficients for many substances ($\ll 10^{-6}$) are in conflict with the widespread opinion that the magnitude of α_v varies for different compounds within the limits from 1 to 10^{-6} [2]. This misconception is actually due to the limitations (ultimate capabilities) of the effusion method, which is used for estimations of the maximum decomposition rate or of the equilibrium pressure of the product. The ratio of the equilibrium pressure inside the cell, P_{eq}, to the effusion pressure, P_{eff}, is governed by [3]:

$$\frac{P_{eq}}{P_{eff}} \cong 1 + \frac{s_{eff} W_C}{s_0} \tag{11.1}$$

where s_{eff} and s_0 are the areas of the effusion outlet and of the evaporation surface (cross section of the cell), respectively, and W_C is the Clausing factor. To measure the P_{eff} magnitude with an error of less than 10%, it is necessary to satisfy the condition: $P_{eq}/P_{eff} \leq 1.1$, or

$$\alpha_v \geq 10 \frac{s_{eff} W_C}{s_0} \tag{11.2}$$

Taking into account that the magnitude of W_C varies within the range 0.2–0.4 and $s_{eff}/s_0 > 10^{-5}$ [3], one can conclude that α_v should be greater than 10^{-5} to provide a correct measurement of the equilibrium pressure. Otherwise the pressure inside the effusion cell would not reach equilibrium.

References

1. L'vov BV, Novichikhin AV (1997) Thermochim Acta 290:239–251
2. Dettorre JF, Knorr TG, Hall EH (1966) Evaporation processes. In: Powell CF, Oxley JH, Blocher JM (eds) Vapour deposition. Wiley, New York, pp 62–101
3. Nesmeyanov AnN (1961) Vapour pressure of chemical elements. Akad Nauk SSSR, Moscow (in Russian)

Chapter 12
The Kinetic Compensation Effect

Definition By definition [1, p.130], "the compensation effect refers to the behaviour pattern in which a rise in E_a (which will decrease the rate of reaction at any particular temperature) is partially or completely offset by an increase in A". In many cases the variation of these parameters corresponds to the equation:

$$\ln A = a + bE \tag{12.1}$$

where a and b are some constants. Once this phenomenon was observed by Zawadski and Bretsznajder [2] in 1935 in their studies of the $CaCO_3$ decomposition at various CO_2 pressures, this effect became a subject for numerous research works. However, till now, no theory exists that provides a convincing explanation of its mechanism.

Analysis Equation 12.1 is in fact the Arrhenius equation, written in logarithmic form, in which constants a and b correspond to magnitudes $\ln k$ and $1/(RT)$. That is why the satisfaction of Eq. 12.1 for a set of measurements at close values of rate constants and temperatures signifies the validity of the Arrhenius equation, i.e., it is possible to represent any point in the plane $\ln k = f[1/(RT)]$ by a set of interconnected parameters, $\ln A$ and E. An alternative description of the compensation effect is the availability of the so-called isokinetic temperature, T_θ, corresponding to the same reaction rate for different sets of $\ln A$ and E.

The real problem is the interpretation of the physical nature of the Arrhenius parameters and their interrelation under varying experimental conditions. In particular, an explanation needs to be provided for the increase in both of these parameters in the presence of an excess of gaseous product in the reactor. In the framework of traditional representations this problem remains unsolved. In particular, the transition state theory characterizes the A and E parameters as independent parameters. As compared to this approach, the CDV concept has evident advantages.

Different Decomposition Modes As follows from the above kinetic equations (Sect. 3.6), the presence of a gaseous product in the reactor should cause variations of the A and E parameters in full conformity with Eq. 12.1. This can be shown using the example of the decomposition of a binary substance into two products in the equimolar and isobaric modes, when one of the products (A) is a low-volatility one.

Taking into account Eqs. 3.23–3.30 and the equality of rate constants ($\ln k^e = \ln k^i$) it can be shown that:

$$\frac{\Delta S_T^\circ}{2R} - \frac{\Delta_r H_T^\circ}{2RT_\theta} = -\ln P_B^{ext} + \frac{\Delta S_T^\circ}{R} - \frac{\Delta_r H_T^\circ}{RT_\theta} \tag{12.2}$$

Table 12.1 Isokinetic temperatures corresponding to different (equimolar and isobaric) modes of decomposition under the condition $P_B^{ext} = 1\,\text{Torr} = 0.0013\,\text{bar}$

Reactant	Products	$\Delta_r H_T^{\circ,a}$ (kJ mol^{-1})	ΔS_T° (J mol^{-1} K^{-1})	T_θ (K)
$CaCO_3$	$CaO(g)_\downarrow + CO_2$	$498.2_{1,200}$	$305.0_{1,200}$	1,200
$Mg(OH)_2$	$MgO(g)_\downarrow + H_2O$	351.0_{600}	322.9_{600}	810
$Li_2SO_4 \cdot H_2O$	$Li_2SO_4(g)_\downarrow + H_2O$	193.8_{298}	350.5_{298}	420

^{a} The condensation energy transfer to the reactant was taken into account in the calculation of the reaction enthalpy ($\tau = 0.5$ for $CaCO_3$ and 0.6 for two other reactants)

(if the difference in the molar masses of the products is neglected) and after rearranging Eq. 12.2:

$$T_\theta = \frac{\Delta_r H_T^{\circ}}{\Delta S_T^{\circ} - 2R \ln P_B^{ext}} \tag{12.3}$$

Equation 12.3 can be used for calculations of isokinetic temperatures corresponding to different decomposition modes. Table 12.1 presents as an example of the calculated results for the decompositions of $CaCO_3$, $Mg(OH)_2$, and $Li_2SO_4 \cdot H_2O$ under the condition: $P_B^{ext} = 1\,\text{Torr}$. The experimentally obtained magnitudes of T_θ for $CaCO_3$ (1,244 and 1,250 K [3]) and $Li_2SO_4 \cdot H_2O (\sim 400\,\text{K}$ [3]) are close to theoretical values (1,200 and 420 K, respectively).

Different decomposition modes are probably the most common cause for spreads of the parameters A and E, as well as for the appearance of a kinetic compensation effect. When the primary gaseous products differ from the equilibrium products (being, for instance, in the form of O or N atoms) and when the isobaric mode is practically unattainable (so-called irreversible decomposition), different researchers obtain very similar and reproducible magnitudes of the parameters A and E. This is true, in particular, for the decompositions of the alkali metal permanganates ($KMnO_4$, $RbMnO_4$, and $CsMnO_4$), for which the parameter E obtained in different works varied within narrow limits from 140 to 170 kJ mol^{-1} [3]. It may be suggested that, for the above reactants, by analogy with $BaSO_4$ (of the same crystal structure) oxygen is released in the form of free atoms. If this is the case, these reactants can be used as kinetics "standards" insensitive to the surrounding atmosphere (vacuum, inert gas, or air).

Other Factors The difference in the decomposition mode is not the only cause of the spread. Some additional factors are listed below. Among these are: (1) differences in the mathematical models used for the initial processing of the experimental data; (2) differences in the kinetic parameters for the periods of induction, acceleration, and deceleration; (3) the self-cooling effect and its dependence upon particle sizes, sample mass, crucible geometry, and surrounding medium (vacuum or the presence of inert gas), and (4) differences in heating rates for non-isothermal methods. Within the framework of the CDV concept, the influences of factors (1) and (4) are excluded and potential differences in kinetic parameters caused by factors (2) and (3) can be theoretically calculated, or at least, estimated, as has been demonstrated in [4, 5].

On this basis, it is necessary to agree with the Galwey's remark [6] that "the detection of a compensation effect should no longer be reported as an 'interesting' kinetic result but recognized as a demonstration of serious inadequacies in the experimental and/or computational methods used for the data collection and interpretation."

References

1. Galwey AK, Brown ME (1999) Thermal decomposition of ionic solids. Elsevier, Amsterdam
2. Zawadzki J, Bretsznajder S (1935) Z Elektrochem 41:215–223
3. Galwey AK, Brown ME (1997) Thermochim Acta 300:107–115
4. L'vov BV, Novichikhin AV, Dyakov AO (1998) Thermochim Acta 315:135–143
5. L'vov BV (2000) Thermochim Acta 364:99–109
6. Galwey AK (2004) Thermochim Acta 413:139–183

Chapter 13
Conclusions

Confirmation of the CDV Mechanism The most important result following from the analysis of the material presented in Parts I and II of this book is the confirmation of the CDV mechanism, which provides the basis for the thermochemical approach. The major arguments confirming this mechanism are listed in Table 13.1. Some of the arguments result from the effects discovered experimentally, and some are predicted from theory. Among the latter are: the increase of the reaction enthalpy with temperature (for decompositions with formation of a solid product); the deceleration of the decomposition rate during reactant melting, and the peculiarities of the A and E parameters in the isobaric mode of decomposition.

Most of these arguments (items 6–13) have a rigorous quantitative character and their correctness is verified by good agreement of experimental and theoretical results. No qualitative and especially quantitative interpretations of these regularities based on any other known approaches are available, and an appearance of an alternative theory capable of explaining all of these features is highly unlikely.

Table 13.1 Main arguments for the CDV mechanism

No.	Argument	Section
1	Direct MS observation of the primary products of decomposition	2.3
2	Effect of vapour oversaturation of the low-volatility product and the mechanism of formation of germ nuclei	2.4
3	Acceleration stage as a result of condensation of the low-volatility product in the reaction interface	2.4
4	Nucleus position on the reactant surface	2.5
5	Vapour oversaturation and structure of the product (crystal size)	2.6
6	Invariance of the E^i parameter under the pressure of gaseous product	5.3; 5.4
7	$E^i/E^e = (a+b)/a$ in the equimolar and isobaric decomposition modes	5.3–5.5
8	The retardation effect of the gaseous product: $A^i \propto (P_B)^{-b/a}$	5.3; 5.4
9	Modelling of the Topley–Smith effect	7.2; 7.3
10	Increase of the decomposition enthalpy with T (for reactions with solid product formation)	8.2
11	Increase of the decomposition enthalpy with reactant melting	8.3
12	$E^e(\text{expt}) = \Delta_r H_T^o/\nu$ (theory) for a large group of reactants	9
13	Interpretation of the vaporization coefficient α_v	11

Contribution of ET AAS and Quadrupole MS A substantial (if not the major) contribution to the development of thermochemical approach, in general, has been made by investigations in the fields of AAS and quadrupole MS (QMS). The corresponding studies, in which new effects have been discovered, are

listed in Table 13.2. This table contains also the studies of their theoretical interpretation that has lead, eventually, to the development of some novel concepts, methods, and mechanisms, considered in this book [1–16].

Table 13.2 Contribution of flame and electrothermal AAS and QMS to the kinetics of solid-state reactions

Experimental Background	Year	Ref.	Method/Mechanism Evolved	Year	Ref.
Dissociative vaporization of Al_2O_3 aerosol in flames	1966	[1]	The Langmuir single-particle vaporization equation was used for the rate calculation	1966	[1]
Constancy of the T_{app}/E ratio for different analytes in ET AAS	1975 1976	[2] [3]	Evaluation of the molar entropy and enthalpy values for decomposition reactions	1978 2002	[4] [5]
Decrease of the slope of the Arrhenius plots with temperature	1976	[3]	Equimolar and isobaric modes of decompositions were proposed	1984	[6]
ET AAS studies of atomization of metal oxides	1981	[7]	Method for the determination of the absolute decomposition rate	1981	[7]
Observation of Al spikes in graphite furnaces	1981	[8]	Gaseous carbide mechanism of oxide reduction by carbon	1982	[9]
ET QMS observation of low-volatility products	1983 1987	[10] [11]	Congruent dissociative vaporization mechanism	1990	[12]
ET AAS studies of Pd-modifier action	1989 1994	[13] [14]	Mechanism of chemisorption of analytes on Pd modifier	2000	[15] [16]

The gaseous carbide mechanism of oxide reduction by carbon, noted in the table but left out of consideration in this book, is in many ways close to the CDV mechanism. It will suffice to mention that both mechanisms involve gasification of reactants. About 30 articles by L'vov and colleagues published during the period 1981–2000 are devoted to studies of this mechanism (see [17, 18] for a list of these papers). Nevertheless, this mechanism was excluded from consideration owing to the author's wish to focus on the main subject of this monograph.

Basic achievements The proposed thermochemical approach to the kinetics of solid and melt decompositions rested on the CDV mechanism revealed the interconnection of two traditional, but distinct, scientific approaches (after Arrhenius and after Knudsen–Langmuir). Some unusual or mysterious phenomena (including misconceptions), revealed or formed during the more than a one-hundred-year period of studies in these traditional fields, have been interpreted. The most significant achievements are the explanation of the mechanism of the nucleation and growth of nuclei and the interpretation of such effects as localization of the decomposition process, the Topley–Smith effect, the difference between the rates of decomposition under effusion (after Knudsen) and free-surface (after Langmuir) conditions, a decrease in the decomposition rate upon melting of the reactant, differences in the crystalline structure

of the solid product versus temperature, and the effect of gaseous products and foreign gases on the decomposition rate. Finally, based on the third-law method, a simple and reliable methodology has been suggested, aimed to measure the enthalpies of decompositions with the accuracy, precision and efficiency exceeding considerably the same features for the usual methodology based on the second-law and Arrhenius plot methods.

Unresolved Problems Against the background of above listed achievements, there are still some unanswered questions that appear in the course of the research. These include, in particular, the mechanism of condensation energy transfer from a low-volatility product to a reactant, and the influence of the symmetry of the reactant crystal structure on the composition of the gaseous decomposition products. It would be worthwhile to perform a more thorough analysis of the dependence of the τ coefficient and the sizes of the condensate particles on the vapour oversaturation of the low-volatility product, as well as of the relative contributions of the condensation and self-cooling effects to the underestimation of enthalpies determined by the second-law and Arrhenius plot methods.

The thermochemical approach to kinetic studies is in the stage of development, as compared to the commonly used approaches. This explains the insufficiency and, in some cases, a rather low reliability of the obtained data to answer the above listed questions and to draw final conclusions on the decomposition mechanisms for certain substances. Independent verification and/or comparative experiments are required to confirm or disprove the results obtained. Information presented in Part III of this book may be helpful for further development of such studies. Part III is devoted to the technique of isothermal thermogravimetry and contains the primary results of kinetic measurements, and their detailed discussion, for a few dozens of substances. Results of these measurements have been partly discussed in a generalized form in Part II.

References

1. L'vov BV (1966) Atomic absorption spectral analysis. Nauka, Moscow (in Russian)
2. Johnson DC, Sharp BL, West TS, Dagnall RM (1975) Anal Chem 47:1234–1240
3. Sturgeon RE, Chakrabarti CL, Langford CH (1976) Anal Chem 48:1792–1807
4. L'vov BV (1978) Spectrochim Acta B 33:153–193
5. L'vov BV (2002) Thermochim Acta 389:199–211
6. L'vov BV, Fernandes GHA (1984) Zh Analit Khim 39:221–231 (in Russian)
7. L'vov BV, Ryabchuk GN (1981) Zh Analit Khim 36:2085–2096 (in Russian)
8. L'vov BV (1981) XII Mendeleev Congress on General and Applied Chemistry Proceedings, Part I. Nauka, Moscow (in Russian), p 286
9. L'vov BV, Savin AS (1982) Zh Analit Khim 37:2116–2124 (in Russian)
10. Sturgeon RE, Mitchell DF, Berman SS (1983) Anal Chem 55:1059–1064
11. Dressler MS, Holcombe JA (1987) Spectrochim Acta B 42:981–994

12. L'vov BV (1990) Zh Analit Khim 45:2144–2153 (in Russian)
13. Sturgeon RE, Willie SN, Sproule GI, Robinson PT, Berman SS (1989) Spectrochim Acta B 44:667–682)
14. Liang Y-Z, Ni Z-M (1994) Spectrochim Acta B 49:229–241
15. L'vov BV (2000) Spectrochim Acta B 55:1659–1668
16. L'vov BV (2000) Spectrochim Acta B 55: 1913–1919
17. L'vov BV, Vasilevich AA, Dyakov AO, Lam JW, Sturgeon R (1999) J Anal At Spectrosc 14:1019–1024
18. L'vov BV, Dyakov AO, Vasilevich AA, Lam JW, Sturgeon R (2000) J Anal At Spectrosc 15: 115–120

Part III

Thermal Decomposition of Individual Substances

Chapter 14
Instruments for Thermogravimetric Measurements

Valery L. Ugolkov
Physics and Chemistry of Nanosized Systems,
Institute of Silicate Chemistry, St. Petersburg
199155, Russia

Thermogravimetric analysis (TGA or TG) is one of the most widely used methods of TA. With this method, changes in the sample mass, maintained in a specified atmosphere, can be monitored during heating, cooling, or being kept at a constant temperature. For most reactants, the sample mass decreases as a result of evaporation of the adsorbed or chemically bound water, pyrolysis of organic substances, and decomposition or evaporation of the material. For some samples in some atmospheres, the sample mass increases owing to, e.g., oxidation of metals to oxides or carbonation of oxides.

Thermal analysers used for studying thermal decomposition include a high-sensitivity balance, a temperature-controlled furnace, a unit for evacuation and control of the atmosphere in the furnace, and a control and data recording system. There are many monographs dealing with the theoretical problems of TA, including TG [1], and providing schematic diagrams and designs of devices [2–4]. Therefore, only a brief description will be given of two models of thermal analysers, STA 429 and STA 449 (Netzsch), used in their experimental studies by L'vov and Ugolkov.

The STA 429 thermal analyser has a unit with a mechanical beam balance. The specific feature of this balance is that, as the sample mass changes, a constant position of the crucible is ensured by a special unit consisting of a compensation electromagnet and a beam position sensor. The unit operates as follows. As the sample mass changes, the balance beam starts to deviate from the equilibrium position. The sensor, a ferromagnetic core rigidly coupled with the balance beam, starts to change its position inside a stationary induction coil. The induction current arising in the process is transmitted as a steering command to the power-feed circuit of the electromagnet. The power of the electromagnet is varied, compensating for the shift of the beam balance and returning it to the initial position. With this measurement scheme, the use of electronics makes it possible to maintain a virtually constant position of the crucible in the internal space of the furnace, which, in turn, ensures the constancy of the crucible temperature in the isothermal measurements. The sample mass can vary from 2.5 mg to 2.5 g.

The balance is hermetically connected to the lower part of the furnace so as to ensure the free movement of the vertical holding rod with the sample, resting

upon the sample beam, on the one hand, and to reliably separate the internal volume of the furnace from the external atmosphere, on the other hand. The internal cavity of the furnace is confined by a cylindrical corundum protective shield 32 mm in diameter and 270 mm high, separating the silicon carbide furnace heater from the sample and serving to make the internal temperature field of the furnace uniform. From the outside, the heater is protected by a heat-insulating sheath and a metallic housing cooled by a fan. At the maximum furnace temperature of 1,700°C, the consumed power is 2 kW.

To reduce the heat loss, the lower aperture of the protective cylindrical shield is covered by horizontal corundum heat reflectors. This unit efficiently separates the heated upper part of the furnace from the connection with the balance compartment. The protective shields allow the temperature of the lower part of the furnace to be kept within 100°C even at the maximum temperature in the furnace (1,700°C). Furthermore, the connection with the balance compartment is cooled with distilled water whose temperature is maintained at 20.0 ± 0.1°C by a circulating thermostat.

All the mechanical part of the balance, with the beam, set of weights, beam position sensor and compensation electromagnet, is enclosed in a thick-walled metallic chamber, which allows evacuation of the balance and beam cavity (of total volume of about 40 L) to a pressure of 4×10^{-4} bar with a mechanical rotary pump and to 4×10^{-8} bar with an additional diffusion pump. The evacuation can be performed either before starting the heating or during the course of the measurements. The gas distribution system allows the furnace space to be filled with various gases. Both static and dynamic atmospheres can be provided in the furnace, and two gases can be introduced in a preset ratio.

The STA 449 thermal analyser uses a Sartorius piezoelectric analytical balance unit. A specific feature of this balance is its high sensitivity, with the above-described principle of "stationary balance" preserved. The sample mass is up to 5 g. The balance operation is based on the piezoelectric effect of a quartz crystal. Depending on the load applied to the crystal, the magnitude of the electric signal, taken from the opposite faces of the crystal, changes. To protect the balance mechanism from the corrosive effect of decomposition products, the balance is arranged in a housing of volume about 1.5 L, which is temperature-controlled with running water, and the housing cavity can be purged with an inert gas. The internal volume of the furnace is about 200 mL and it can be purged independently with either an individual gas or a mixture of two gases in a preset ratio.

The advantage of the piezoelectric balance is that the considerably higher measurement sensitivity provides a mass resolution of about 0.1 μg, against 25 μg for the mechanical balance. Owing to the smaller size of the balance, its temperature control is simpler, and the overall size of the thermal analyser is appreciably smaller. The mass of a fully equipped STA 429 thermal analyser is about 450 kg, and that of a STA 449 analyser, 120 kg (Fig. 14.1).

Fig. 14.1 A view of the STA 449 instrument

In both devices, the temperature in the range from 20°C to 1,700°C is measured with Pt–PtRh(10%) thermocouples. The temperature control involves feedback based on the comparison of the attained and preset temperatures. When setting the programme, the operator can vary the duration of the heating electric pulse and the time intervals between the moments of temperature comparison.

Both thermal analysers are equipped with replaceable sample holders allowing various combinations of measurements depending on the task: a TG holder for monitoring the variation of the sample mass in the range from 20°C to 1,700°C; a TG + DTA holder for monitoring the mass variation and thermal effects for samples weighing from 50 to 500 mg in the interval from 20°C to 1,700°C; and a TG + DSC holder for monitoring the mass variation and enthalpies of transformations for samples weighing from 1 to 50 mg in the range from 20°C to 1,400°C. The mass ranges are the same for both devices.

Figure 14.2 shows an example of the decomposition measurement of a 6 mg talc crystal in air with isothermal heating at 978°C, recorded with an STA 449 thermal analyser.
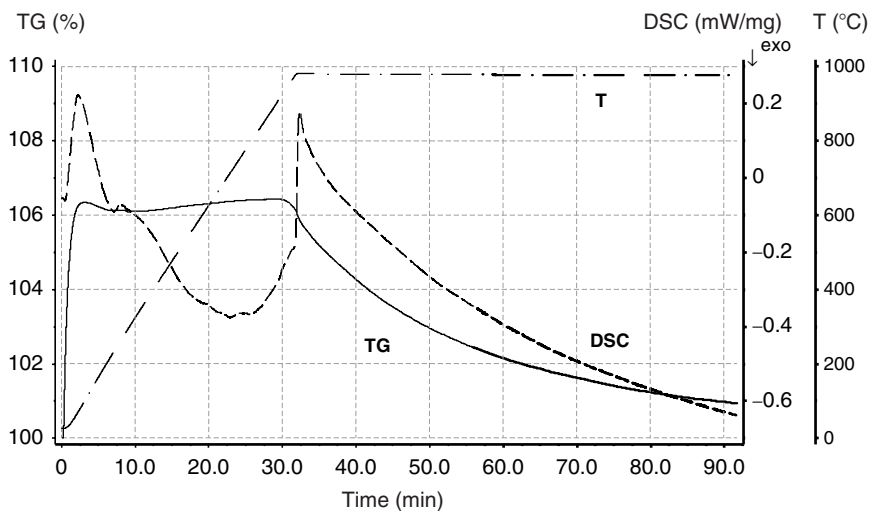
Fig. 14.2 TG and DSC curves for the decomposition of a monocrystal of talc in an atmosphere of air under isothermal conditions at $978°C$ obtained with an STA 449 instrument

A great advantage of the thermal analysers under consideration is the high accuracy of setting the heating temperature and its stable maintenance for several hours (with the deviations from the mean value being within $0.1–0.2°C$). However, as applied to isothermal TG measurements, both these thermal analysers have certain shortcomings: significant and irreproducible baseline drift reaching $0.05–0.07\,\mu g\,s^{-1}$, lack of reliable devices for measuring the gas pressure in the furnace in the range $10^{-3}-1$ bar, and the relatively long time required to cool the furnace (up to $2–3\,h$), which restricts the number of runs that can be done within a workday.

References

1. Šesták J (1984) Thermophysical properties of solids. Their measurements and theoretical thermal analysis. Academia, Prague
2. Boldyrev VV (1958) Methods for investigation of the kinetics of thermal decomposition of solids. Tomsk University Press, Tomsk (in Russian)
3. Wendland WW (1986) Thermal analysis, 3rd edn. Wiley, New York
4. Brown ME (2001) Introduction to thermal analysis: techniques and applications, 2nd edn. Kluwer Academic, Dordrecht

Chapter 15
Measurement Conditions and Procedures for Isothermal Thermogravimetric Studies

As follows from the consideration of the third-law method (Chapter 4), its use for determining the reaction enthalpy requires estimation of the equivalent pressure P_{eqp} of the gaseous product under the conditions of free-surface vaporization of the reactant. This, in turn, involves determination of the absolute rate of decomposition J (kg m^{-2} s^{-1}) and, hence, of the effective surface area of the decomposing sample. This problem, as applied to crystals, powders, and melts, is discussed below.

15.1 Evaluation of the Absolute Rate of Decomposition

Crystals For crystals, or pressed materials with a very low porosity, the effective surface area can be readily determined from the known sample geometry. It is convenient to use for this purpose an optical microscope with a scale and magnification of 20–30. The absolute rate of decomposition is evaluated by dividing the change in sample mass per unit time, $\Delta m / \Delta t$, measured under isothermal conditions, by the area of the external surface of the crystal at the instant of the measurement s_m, i.e.,

$$J_c = \frac{\Delta m / \Delta t}{s_m} \tag{15.1}$$

For samples of a cubic shape and similarly for spherical particles, s_m should decrease with an increase in the degree of decomposition α, in accordance with the "contracting sphere" equation:

$$s_m = s_0 (1 - \alpha)^{2/3} \tag{15.2}$$

where s_0 is the initial surface area of the crystal. Equation 15.2 was used by Roginsky and Schultz [1] to characterize the reaction kinetics during steady-state decomposition with the aim of taking into account the deceleration caused by a decrease in the area of the crystal surface. Taking into account Eq. 15.2, Eq. 15.1 can be presented in the form:

$$J_c = \frac{\Delta m / \Delta t}{s_0 (1 - \alpha)^{2/3}} \tag{15.3}$$

As an example of the evaluation of the absolute rate, data for decomposition of a $CaCO_3$ crystal in air are given in Table 15.1 (this procedure is discussed in detail in Sects. 15.4 and 15.5).

Table 15.1 Absolute rate of $CaCO_3$ decomposition in air at 995 K (crystal mass: 20 mg and $s_0 = 27\,mm^2$)

Time (min)	10	20	30	40	50	60	70	80	90	100
$\Delta m/m(\%)$	2.07	2.02	1.94	1.86	1.79	1.72	1.66	1.60	1.54	1.48
$\Delta m/\Delta t$ (µg s^{-1})	0.687	0.670	0.643	0.617	0.594	0.570	0.551	0.531	0.511	0.491
$\Delta\alpha$	0.047	0.046	0.044	0.042	0.041	0.039	0.038	0.036	0.035	0.034
α_m	0.110	0.157	0.201	0.243	0.284	0.323	0.361	0.397	0.432	0.466
$(1-\alpha_m)^{2/3}$	0.925	0.892	0.861	0.831	0.800	0.771	0.742	0.714	0.686	0.658
J_c (mg m^{-2} s^{-1})	27.5	27.8	27.7	27.5	27.5	27.4	27.5	27.5	27.6	27.6

Some comments to Table 15.1 need to be given. The initial parameter, automatically recorded by the device, is the sample mass loss ($\Delta m/m$, %) in a chosen time interval between the signal readings (Δt). Usually this time interval is 5 or 10 min. From these data, the quantities $\Delta m/\Delta t$(µg s^{-1}) and $\Delta\alpha = (\Delta m/m)/(bM_B/M_R)$ were calculated, where M_B and M_R are the molar masses of the gaseous product and reactant, respectively. The quantity α_m is calculated by summation of the $\Delta\alpha$ values over the period preceding the given measurement, taking into account the preliminary loss $\Delta\alpha_0$ in the time from the start of heating the furnace to the start of the measurements. It can be seen that, over a 100 min decomposition period (during which α increases from 0.11 to 0.47), J_c remains essentially constant and equal to $(2.76 \pm 0.01) \times 10^{-5}$ kg m^{-2} s^{-1}. The enthalpy of the reaction, calculated by Eqs. 3.16 and 4.12 taking into account the quantities $P_B^{ext} = 4 \times 10^{-4}$ bar, $\beta = 0.886$ and $\Delta_r S_{995}^\circ = 311.5$ J mol^{-1} K^{-1}, is 497.8 kJ mol^{-1}.

Powders Estimation of the effective surface area of powders with an indeterminate number and size of particles is a complicated problem. This quantity can, in principle, be determined by the BET method. However, decomposition of a powder is not uniform in space. Because of self-cooling, internal layers of powdered samples are heated more weakly than the surface layers and, therefore, make a lower contribution to the total decomposition effect.

A theoretical simulation of the powder decomposition rate was attempted by L'vov et al. [2, 3] in 1998 (Chapter 6). Later L'vov and Ugolkov [4] continued these theoretical and experimental studies with dolomite crystals and powders of various particle sizes. Calculations performed for powders with varied numbers of layers ($n = 10$ and 100), emittance coefficients ε (from 0.01 to 1), and residual air pressures in the reactor (10^{-4} and 10^{-7} bar) showed that the differences in the particle size and powder mass do not noticeably affect the temperature distribution and the effective number of powder layers n_e (see Sect. 6.3) decomposing at the same rate as does the surface layer. Furthermore, it was found that the decomposition rates of crystals and powders with the same external surface area and ε coefficients ranging from 0.01 to 0.3 should differ by a factor of no more than 2.

An experimental check of these conclusions showed that the apparent absolute rate of decomposition of powders $(J_p{}^*)$, related to the external surface area of a powder pellet, is always higher than that of crystals (J_c). It was also found that the difference between the decomposition rates is independent of temperature, residual air pressure in the reactor, sample mass and powder particle size. The mean value of $J_p{}^*/J_c$ was 2.8 ± 0.4. This value somewhat exceeds the theoretical estimate, which may be due to the rough external surface of the powder. Evidently, the area of a pimpled surface formed by spherical particles should be at least twice that of the flat surface.

Thus, the true absolute rate of decomposition of powders (J_p) is evaluated by dividing the change in sample mass per unit time, $\Delta m/\Delta t$, measured under isothermal conditions, by the external surface area of a powder pellet at the instant of measurement, s_m, *multiplied by a factor of* 2.8, i.e.,

$$J_p = \frac{\Delta m/\Delta t}{2.8 s_m} \tag{15.4}$$

For a pellet whose diameter, d, exceeds its thickness, h, by an order of magnitude, a decrease in the surface area, s_m, with an increase in the degree of decomposition, α, is mainly determined by a decrease in the pellet thickness (i.e., in the lateral surface area). Hence,

$$s_m = s_0 - (s_0 - \pi d^2/2)\alpha \tag{15.5}$$

The initial data and results of calculating the absolute rate of decomposition of $CaCO_3$ powder in air using Eqs. 15.4 and 15.5 are given in Table 15.2. The dimensions d and h were 5.7 and 0.4 mm, respectively, so that $s_0 = 58.2\,mm^2$.

As seen from the table, during an 80 min decomposition period in which α increases from 0.216 to 0.665, the variations of J_p do not exceed 1%, with the mean value $J_p = (6.14 \pm 0.04) \times 10^{-6}\,kg\,m^{-2}\,s^{-1}$. Thus, Eq. 15.5 allows the variation of the surface area of a powder pellet in the course of decomposition to be taken into account quite adequately.

The enthalpy of the reaction, calculated by Eqs. 3.16 and 4.12, taking into account the quantities $P_B^{ext} = 4 \times 10^{-4}$ bar, $\beta = 0.886$ and $\Delta_r S_{970}^\circ = 312.3\,J\,mol^{-1}\,K^{-1}$, is $498.4\,kJ\,mol^{-1}$, which virtually coincides with the value

Table 15.2 Absolute rate of $CaCO_3$ decomposition in air at 970 K (powder mass: 20 mg and $s_0 = 58.2\,mm^2$)

Time (min)	10	20	30	40	50	60	70	80	90	100
$\Delta m/m$ (%)	2.94	2.87	2.85	2.82	2.84	2.83	2.80	2.76	2.68	2.59
$\Delta m/\Delta t$ ($\mu g\,s^{-1}$)	0.98	0.96	0.95	0.94	0.95	0.94	0.93	0.92	0.89	0.86
$\Delta\alpha$	0.067	0.065	0.065	0.064	0.064	0.064	0.064	0.063	0.061	0.059
$\alpha_m{}^a$	0.216	0.281	0.346	0.410	0.474	0.538	0.602	0.665	0.726	0.785
$s_m{}^b$ (mm^2)	56.7	56.2	55.7	55.3	54.8	54.3	53.9	53.4	53.0	52.6
J_p ($mg\,m^{-2}\,s^{-1}$)	6.17	6.10	6.09	6.07	6.19	6.18	6.16	6.15	6.00	5.84

a Based on $\Delta\alpha_0 = 0.149$
b s_m (mm^2) $= s_0 - (s_0 - 51.0)\alpha$

of $497.8 \, \text{kJ mol}^{-1}$ found above for a $CaCO_3$ crystal. This fact once again confirms the correctness of the empirical factor 2.8 in Eq. 15.4.

Melts A similar scheme for measuring the absolute rate of decomposition was applied to melts. To prevent spillage of the melt over the crucible surface in the course of heating, the reactant was taken as a 1:1 mixture with a neutral Al_2O_3 powder. After melting of the reactant, this mixture preserves the structure of the Al_2O_3 powder, so that the *absolute rate of decomposition of the melt can be evaluated in the same way as described above for powders.* This calculation scheme was applied in [5] to $AgNO_3$ and $Cd(NO_3)_2$ melts. The absolute rates obtained for mixtures of $AgNO_3$ and Al_2O_3 at different component ratios (1:1 and 1:5) were equal, confirming the correctness of this approach.

It is also appropriate to use mixtures of a reactant and a neutral Al_2O_3 powder for reactants that undergo a phase transition before reaching the measurement temperature, so that the size of a pellet prepared from the individual reactant may decrease relative to the initial size (as an example, see Table 16.57). The size of the mixed pellet remains constant.

15.2 Choice of the Decomposition Temperature

The choice of the temperature is governed by the conditions of reliable measurement of the primary signal, $\Delta m / \Delta t$. The lower limit of measuring this signal depends on the stability of the analyser baseline. According to experimental estimates, with the devices, STA 429 and STA 449, the variations in blank experiments reach 0.05–$0.07 \, \mu\text{g s}^{-1}$. Therefore, it is desirable that the measured signal should exceed at least 0.2–$0.3 \, \mu\text{g s}^{-1}$ (overestimation of the signal by a factor of 1.3 leads to underestimation of the determined enthalpy by $-RT \ln 1.3$, i.e., by $-2.2 \, \text{kJ mol}^{-1}$ at $1{,}000 \, \text{K}$).

The upper limit of the signal is determined by ensuring the steady-state decomposition mode for a period of 30–40 min required for the measurement. The corresponding values of $\Delta m / \Delta t$ are usually 2–$3 \, \mu\text{g s}^{-1}$. This limit depends to some extent on the ratio of the mass of volatile decomposition products to the total sample mass (bM_B / M_R). If only gaseous decomposition products are formed, the upper limit of the decomposition rate can be increased. However, in this case, the temperature difference between the sample (especially if it is a powder) and the crucible increases, which may lead to ejection of the sample from the crucible. Thus, the optimal range for measuring the primary signals is relatively narrow, typically from 0.3 to $3 \, \mu\text{g s}^{-1}$. The equivalent pressures of decomposition products corresponding to these rates are usually about $10^{-7} - 10^{-6} \, \text{bar}$.

15.3   Choice of the Residual Pressure of Gas in the Reactor (Equimolar Mode)

The free-surface vaporization condition means the absence of any diffusion limitations to the removal of gaseous products from the surface of a decomposing substance. This is usually provided by maintaining a high vacuum in the reactor ($\leq 10^{-7}$ bar). However, in many cases, this measure is excessive. The permissible pressure of a foreign (inert) gas in the reactor can be readily estimated by comparing the decomposition rate in a high vacuum with that in the presence of an inert gas, described by a one-dimensional Langmuir diffusion Eq. 3.8

$$J = \frac{\gamma M D P_{\text{eq}}}{zRT}$$

where D is the diffusion coefficient of a gaseous product in an inert gas, and z is the distance from the evaporation surface to the outlet where the concentration of molecules decreases to zero. The presence of an inert gas can be neglected if

$$\frac{\gamma M D P_{\text{eq}}}{zRT} \geq \frac{\gamma M P_{\text{eq}}}{(2\pi MRT)^{1/2}} \tag{15.6}$$

This means that

$$D \geq z \left(\frac{RT}{2\pi M} \right)^{1/2} \tag{15.7}$$

If it is taken into account that [6]

$$D \cong D_0 \frac{P_0}{P} \left(\frac{T}{T_0} \right)^{1.8} \tag{15.8}$$

where $P_0 = 1$ bar, $T_0 = 273$ K, and $D_0 \cong 2 \times 10^{-5}$ m^2 s^{-1} (for the diffusion of O_2, CO, CO_2, and H_2O in argon, air or nitrogen [6]), and assuming that $M = 0.05$ kg mol^{-1} and $z = 4$ mm $= 4 \times 10^{-3}$ m (height of the crucible with the sample), then the permissible pressure P of an inert gas in a reactor can be estimated from the relationship

$$P \leq 4 \times 10^{-8} T^{1.3} \tag{15.9}$$

It follows from Eq. 15.9 that $P \cong 3 \times 10^{-4}$ bar at 1,000 K and 2×10^{-4} bar at 700 K. *This permits the use of only a mechanical pump to ensure the free-surface vaporization conditions.* For example, the dolomite decomposition rates at 800 K and residual air pressure in the reactor of 2×10^{-4} and 8×10^{-8} bar virtually coincide: 2.3×10^{-5} and 1.8×10^{-5} kg m^2 s^{-1} [4] (the slightly higher rate in a low vacuum is most probably due to weaker self-cooling).

Limitations   Despite apparent advantages (simpler evacuation and weaker self-cooling), a low vacuum (about 10^{-4} bar) cannot be used in the equimolar mode of decomposition if the equivalent pressure of the gaseous product is

comparable with, or lower than the pressure of this component in the residual air. This primarily concerns substances decomposing with the release of N_2 and/or O_2. The content of other possible gaseous products in the residual air in the reactor is considerably lower: within 10^{-8}–10^{-7} bar for CO_2 and about 10^{-6} bar for H_2O vapour; the latter value, however, is comparable with the equivalent pressure. Therefore, measurements in a low vacuum can give insufficiently reliable results when studying dehydration, and essentially incorrect results when studying decompositions of oxides and nitrides (and also other compounds decomposing with the release of O_2 or N_2). However, *in studying the decompositions of sulfides, selenides, tellurides, and carbonates, the use of a low vacuum is quite justified.* In particular, experiments on the decomposition of dolomite [4] and of Mg, Ca, Sr, and Ba carbonates [7–9] were performed in a low vacuum.

15.4 Decomposition in the Presence of the Gaseous Product (Isobaric Mode)

The above limitations concern the equimolar decomposition mode. For the isobaric decomposition mode and for the corresponding measurements and calculations, the pattern is different. The major requirement of the isobaric mode of measurements is the need to determine the excess pressure of the gaseous product in the reactor at the instant of the measurements. Depending on the reaction type (number of stable gaseous decomposition products), the ranges of permissible variation of the pressures of the gaseous product and foreign gas are different. Two different situations can be distinguished.

Reactions Yielding Two or More Stable Gaseous Products In this case, the excess pressure of one of the gaseous products can be increased to a level not exceeding 10^{-4} bar. At higher pressures, diffusion limitations to the removal of the second gaseous product arise, and the calculation using the Hertz–Langmuir equation (under the free-surface vaporization conditions) becomes inadequate. Thus, the excess pressure of the gaseous product should be in the range from 10^{-6} to 10^{-4} bar. The maximum pressure of foreign (inert) gases is also limited to 10^{-4} bar.

Reactions Yielding a Single Stable Gaseous Product The isobaric mode becomes more attractive when applied to decompositions yielding a single stable gaseous product. Here the excess pressure of the gaseous product can be varied without limit (it can even exceed the atmospheric pressure), because the other products (low-volatility or reactive intermediate species such as, e.g., free O or N atoms) occur in the non-equilibrium state and, irrespective of the presence of a gas, should instantaneously condense with the formation of a solid phase or recombine into stable molecules. The pressure of a foreign gas can also be varied without limit.

Advantages of this procedure are elimination or minimization of the reactant self-cooling in the course of the decomposition, simpler measurement procedures with a foreign gas atmosphere, and the possibility of varying the decomposition temperature in a wide range by varying the excess pressure of the gaseous product. The only complication is that it is necessary to estimate and control the excess pressure of the gaseous product at the instant of measurement.

This reasoning is valid only for congruent dissociative vaporization when all the primary decomposition products, in accordance with Eqs. 3.20 and 3.21, obey the laws of equilibrium thermodynamics. If this is so, then the enthalpies determined in a high vacuum (equimolar mode) by Eq. 3.20 and in an atmosphere of foreign gases (isobaric mode) by Eq. 3.21 should be equal. Their comparison is of much interest for confirming or refuting the CDV mechanism.

15.5 Decomposition of Hydrates in Air and Carbonates in Argon and Air

Among reactions yielding a single stable gaseous product are the dehydrations of hydrates and the decompositions of carbonates. L'vov and Ugolkov recently published a series of papers on the kinetics of decomposition of these compounds in various modes [4, 7–11]. All the experiments in a vacuum were performed with an STA 429 thermal analyser. The measurements were performed under isothermal conditions with continuous evacuation of the furnace chamber to a pressure of $n \times 10^{-8}$ bar. Experiments on the dehydration of $Li_2SO_4 \cdot H_2O$, kaolinite, muscovite, and talc [10, 11] in the isobaric mode were performed in air. The partial vapour pressure of H_2O was estimated with a digital thermohygrometer (relative humidity) and from the known saturated vapour pressure of H_2O (see Appendix, Table A6) at the ambient air temperature. Experiments on the decompositions of carbonates were performed in argon with an addition of CO_2 (0.1 bar for $CaCO_3$ and $SrCO_3$, and 0.001 bar for $BaCO_3$) [9].

In principle, as shown in Sects. 15.1 and 16.13, the kinetics of the carbonate decompositions can also be studied in air. The only shortcoming of this procedure is that the CO_2 content can vary over its minimum concentration (0.038%) in a relatively wide range (up to 0.1% in towns). However, if a mean value for the CO_2 content, 0.060%, is taken, the maximum error in the enthalpy determination, brought about by this variation, should not exceed $4 \, kJ \, mol^{-1}$.

The averaged results of these studies are given in Tables 15.3 and 15.4. For all the compounds, the enthalpies determined in a high vacuum are fairly close to those determined in an atmosphere of foreign gases (at similar temperatures),

Table 15.3 The reaction enthalpies for the decompositions of carbonates measured by the third-law method in a vacuum and in argon (with an addition of CO_2)

Reactant	Sample	$\Delta_r H_T^\circ$ (kJ mol^{-1})		Difference (%)	Ref.
		Vacuum	Argon		
$CaCO_3$	Crystal	540 ± 4	490 ± 3	9.2	[7–9]
$SrCO_3$	Powder	572 ± 9	564 ± 11	1.4	[7–9]
$BaCO_3$	Powder	611 ± 11	605 ± 1	1.0	[7–9]

Table 15.4 The dehydration enthalpies measured by the third-law method in a vacuum and air (with regard to the refinements noted in Sects. 15.9 and 15.10)

Reactant	Sample	$\Delta_r H_T^\circ$ (kJ mol^{-1})		Difference (%)	Ref.
		Vacuum	Air		
$Li_2SO_4 \cdot H_2O$	Crystal	210 ± 2	192 ± 2	9.2	[10]
$Al_2O_3 \cdot 2SiO_2 \cdot 2H_2O$	Powder	$1,058 \pm 6$	978 ± 16	8.2	[10]
$K_2O \cdot 3Al_2O_3 \cdot 6SiO_2 \cdot 2H_2O$	Crystal	$3,949 \pm 40$	$3,506 \pm 19$	12.6	[10]
$3MgO \cdot 4SiO_2 \cdot H_2O$	Crystal	$2,817 \pm 10$	$2,612 \pm 16$	7.8	[10, 11]

but always exceed them. The differences in $\Delta_r H_T^\circ$ for powder samples are 1–8%, but for crystals they are 8–13%, significantly exceeding the random scatter (about 1–2%).

The results obtained are fully consistent with the CDV mechanism. Systematically lower values of $\Delta_r H_T^\circ$ in an atmosphere of foreign gases confirm the expected trend that *the decreased self-cooling effect should make the measurements in an atmosphere of foreign gases more reliable compared to high-vacuum measurements.*

Unfortunately, ambient air is unsuitable as an atmosphere for studying decomposition of metal hydroxides because of the presence of approximately 0.04% CO_2 which reacts with metal oxides with partial formation of thermally stable carbonates. This conclusion was checked [10] by the example of the dehydration of $Mg(OH)_2$ (brucite). The rate of its decomposition in air at 650 K appeared to be 20–30 times lower than the calculated decomposition rate in a CO_2-free atmosphere ($MgCO_3$ formed in the process starts to decompose above 650 K even in a vacuum).

15.6 Equilibrium Constant for Reactions with Three or More Decomposition Products

Previously (Sects. 3.4 and 3.5) a scheme was considered for calculating the partial pressures of products and equilibrium constants of decomposition reactions yielding two products. For the formation of three or more products, consideration of the decomposition congruence is more complicated.

For a reaction of the general form

$$R(s/l) \leftrightarrow aA(g)_\downarrow + bB(g) + cC(g) \tag{15.10}$$
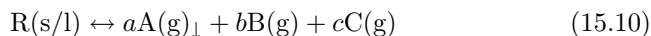
the dependence of the partial pressures of the products on the overall decomposition rate, J_Σ, is given by the set of Eqs. 15.11–15.13:

$$P_A = \frac{a(2\pi M_A RT)^{1/2} J_\Sigma}{\gamma(bM_B + cM_C)} \tag{15.11}$$

$$P_B = \frac{b(2\pi M_B RT)^{1/2} J_\Sigma}{\gamma(bM_B + cM_C)} \tag{15.12}$$

$$P_C = \frac{c(2\pi M_C RT)^{1/2} J_\Sigma}{\gamma(bM_B + cM_C)} \tag{15.13}$$

The factor in parentheses in the denominator of these equations corresponds to the molar mass of the gaseous decomposition products. If no solid products are formed, it is equal to the molar mass of the reactant, M_R.

The equilibrium constant of reaction (15.10) can be calculated from the partial pressure of any product in accordance with the equations

$$K_P(A) = \frac{(P_A)^\nu}{\delta_A} \tag{15.14}$$

$$K_P(B) = \frac{(P_B)^\nu}{\delta_B} \tag{15.15}$$

$$K_P(C) = \frac{(P_C)^\nu}{\delta_C} \tag{15.16}$$

In turn, the coefficient δ, in accordance with the congruence condition, taking into account the apparent equality $K_P(A) = K_P(B) = K_P(C)$, is calculated by the following set of equations:

$$\delta_A = (\beta_B^A)^b (\beta_C^A)^c \tag{15.17}$$

$$\delta_B = (\beta_A^B)^a (\beta_C^B)^c \tag{15.18}$$

$$\delta_C = (\beta_A^C)^a (\beta_B^C)^b \tag{15.19}$$

where

$$\beta_B^A = \frac{a}{b} \left(\frac{M_A}{M_B} \right)^{1/2} \tag{15.20}$$

$$\beta_C^A = \frac{a}{c} \left(\frac{M_A}{M_C} \right)^{1/2} \tag{15.21}$$

$$\beta_{\mathrm{A}}^{\mathrm{B}} = \frac{b}{a} \left(\frac{M_{\mathrm{B}}}{M_{\mathrm{A}}} \right)^{1/2} \tag{15.22}$$

$$\beta_{\mathrm{C}}^{\mathrm{B}} = \frac{b}{c} \left(\frac{M_{\mathrm{B}}}{M_{\mathrm{C}}} \right)^{1/2} \tag{15.23}$$

$$\beta_{\mathrm{A}}^{\mathrm{C}} = \frac{c}{a} \left(\frac{M_{\mathrm{C}}}{M_{\mathrm{A}}} \right)^{1/2} \tag{15.24}$$

$$\beta_{\mathrm{B}}^{\mathrm{C}} = \frac{c}{b} \left(\frac{M_{\mathrm{C}}}{M_{\mathrm{B}}} \right)^{1/2} \tag{15.25}$$

References

1. Roginsky S, Schultz E (1928) Z phys Chem A138:21–41; Ukr Khim Zh 3:177–207 (in Russian)
2. L'vov BV, Novichikhin AV, Dyakov AO (1998) Thermochim Acta 315:135–143
3. L'vov BV, Novichikhin AV, Dyakov AO (1998) Thermochim Acta 315:169–179
4. L'vov BV, Ugolkov VL (2003) Thermochim Acta 401:139–147
5. L'vov BV, Ugolkov VL (2004) Thermochim Acta 424:7–13
6. Kikoin IK (1976) (ed) Tables of physical constants. Atomizdat, Moscow (in Russian)
7. L'vov BV, Polzik LK, Ugolkov VL (2002) Thermochim Acta 390:5–19
8. L'vov BV, Ugolkov VL (2004) Thermochim Acta 409:13–18
9. L'vov BV, Ugolkov VL (2004) Thermochim Acta 410:47–55
10. L'vov BV, Ugolkov VL (2005) Russ J Appl Chem 78:379–385
11. L'vov BV, Ugolkov VL (2005) J Therm Anal Cal 82:15–22

Chapter 16
Sublimation and Decomposition Reactions

16.1 Non-metals (phosphorus)

Introduction Sublimation of white and red phosphorus has been examined in numerous studies summarized in [1]. Of particular interest is the enormous difference between the evaporation rates of white and red phosphorus, reaching 6–7 orders of magnitude according to the existing estimates [2–4]. The low-vapour pressure of red phosphorus was attributed, in all these studies, to complicated removal of phosphorus in the form of the most stable tetrahedral P_4 molecules from the surface of triclinic red phosphorus containing no such fragments in the crystal structure. In 1997, L'vov and Novichikhin [5] compared the experimental (measured by the second-law method) and calculated enthalpies of vaporization and concluded that vaporization of red phosphorus occurs with the formation of P_2 rather than P_4 molecules (see Sect. 10.3).

Results and Discussion This conclusion is also confirmed by the data given below, obtained by the third-law method. The thermodynamic functions required to determine the enthalpy are given in Table 16.1. Only one paper published by Melville and Gray [2] 70 years ago was found, in which the equivalent pressure of red phosphorus was measured under the free-surface vaporization conditions (after Langmuir). The vapour pressure in this study was determined in the range 578–673 K from the mass of the vapour condensate (Table 16.2).

The quantities $\Delta_r H_T^\circ$ determined from these data by the third-law method were compared in the same table with the calculated $\Delta_r H_T^\circ$ values for the reaction

$$2P(s, red) \leftrightarrow P_2(g) \tag{16.1}$$

Comparison of the data given in Table 16.2 shows that the difference between the experimental and calculated values at various temperatures reaches 10–20%. Nevertheless, this agreement can be considered as satisfactory, taking into account the poor reproducibility of the initial data [2].

For comparison, the enthalpy and entropy of vaporization of white phosphorus at 600 K in accordance with the reaction

$$4P(s, \text{ white}) \leftrightarrow P_4(g) \tag{16.2}$$

are $47.3 \, \text{kJ mol}^{-1}$ and $86.0 \, \text{J mol}^{-1} \, \text{K}^{-1}$, respectively. Hence, the equilibrium vapour pressure over white phosphorus at 600 K should reach 2.4 bar, exceeding by 9 orders of magnitude the experimental vapour pressure over red phosphorus.

Table 16.1 Values of the thermodynamic functions for phosphorus [6, 7]

Species	T (K)	$\Delta_f H_T^\circ$ (kJ mol^{-1})	S_T° (J mol^{-1} K^{-1})
P(s, red)	600	−10.5	39.3
P(s, white)	600	8.5	61.3
P$_2$(g)	600	153.9	241.7
P$_4$(g)	600	81.3	331.2
P(s, red)	700	−7.6	43.3
P$_2$(g)	700	157.6	247.2
P$_4$(g)	700	89.2	343.4

Table 16.2 Vapour pressure above red phosphorus under conditions of its free-surface vaporization [2] and the enthalpy of reaction (16.1)

T (K)	P_{eqp} (bar)	$\Delta_r S_T^\circ$ (J mol^{-1} K^{-1})	$\Delta_r H_T^\circ$ (kJ mol^{-1})	
			Theory	Expt
578	1.3E−9	163.7	175.4	192.0
623	4.8E−9	162.5	174.4	200.5
623	4.7E−9	162.5	174.4	200.6
623	3.6E−9	162.5	174.4	201.9
673	1.2E−8	161.3	173.4	210.6
673	8.5E−9	161.3	173.4	212.5

16.2   Metalloids (Arsenic, Antimony)

Introduction Arsenic and antimony, like red phosphorus, vaporize more slowly than expected from their thermochemical properties. L'vov and Novichikhin [5], based on the results obtained by Rosenblatt et al. [8], attributed this difference to the fact that both elements vaporize, not in the form of the most stable molecules As$_4$ and Sb$_4$, but with detachment of two molecules from the surface:

$$6As(s) \leftrightarrow As_4(g) + As_2(g) \qquad (16.3)$$
$$6Sb(s) \leftrightarrow Sb_4(g) + Sb_2(g) \qquad (16.4)$$
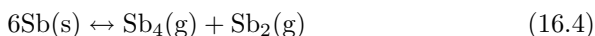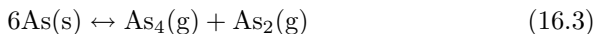
The refined results of this thermochemical analysis are given below. The thermodynamic functions required for the calculation are given in Table 16.3, and the theoretically calculated and experimentally measured enthalpies of the corresponding reactions, in Table 16.4.

Results and Discussion The initial data for calculating the enthalpy by the third-law method were the equivalent pressures measured for both elements under the free-surface vaporization conditions (after Langmuir) in [8]. The quantities $\Delta_r H_T^\circ$ were also determined in [8] by the second-law method. Table 16.4 shows that the results obtained by the second- and third-law methods are quite consistent. The agreement between the calculated and

Table 16.3 Values of the thermodynamic functions for arsenic and antimony [6, 7]

Species	T (K)	$\Delta_f H_T^\circ$ (kJ mol^{-1})	S_T° (J mol^{-1} K^{-1})	Species	T (K)	$\Delta_f H_T^\circ$ (kJ mol^{-1})	S_T° (J mol^{-1} K^{-1})
As(s)	500	5.1	48.7	Sb(s)	600	7.9	62.0
As$_2$(g)	500	201.0	260.9	Sb$_2$(g)	600	250.2	282.8
As$_4$(g)	500	159.8	370.9	Sb$_4$(g)	600	230.0	409.3
As(s)	600	7.8	53.4	Sb(s)	700	10.7	66.2
As$_2$(g)	600	204.7	267.6	Sb$_2$(g)	700	254.0	288.5
As$_4$(g)	600	168.0	385.7	Sb$_4$(g)	700	238.2	423.0

Table 16.4 Vapour pressure above arsenic and antimony under conditions of their free-surface vaporization [2] and the molar enthalpies of reactions (16.3) and (16.4)

Element	T (K)	P_{eqp} (bar)	$\Delta_r S_T^\circ/\nu$ (J mol^{-1} K^{-1})	$\Delta_r H_T^\circ/\nu$ (kJ mol^{-1})		
				Theory	Second-law	Third-law
As(s)	550	6.6E−10	168.1	164.0	183 ± 6	189.1
Sb(s)	650	1.3E−09	158.6	215.2	207 ± 9	213.7

Table 16.5 Calculated (theory) and experimental values of vaporization coefficients for P(red), As and Sb

Element	T (K)	Primary Products	P_{eqp} (bar)	Equilibrium Products	P_{eq} (bar)	α_v		Ref.
						Theory	Expt	
P(s, red)	600	P$_2$	2.3E−07	P$_4$	2.3E−02	1E−05	1E−06	[3]
As(s)	550	As$_4$ + As$_2$	1.6E−07	As$_4$	9.9E−05	2E−03	5E−04	[3]
Sb(s)	650	Sb$_4$ + Sb$_2$	9.8E−10	Sb$_4$	3.0E−08	3E−02	2E−01	[8]

experimental data was very good for Sb and satisfactory for As. The 12–15% discrepancy may be caused by errors in the thermodynamic functions. According to Kireev [9], $\Delta_f H_{600}^\circ$ of the As$_2$ molecule is 233.1 rather than 204.7 kJ mol^{-1}. If so, the calculated enthalpy will increase to 178.2 kJ mol^{-1} and the discrepancy will decrease to 3–6%.

The discrepancies between the calculated and experimental vaporization coefficients of P, As, and Sb do not exceed an order of magnitude (Table 16.5), which is quite acceptable taking into account the experimental errors. The correlation between the composition of products formed in vaporization of phosphorus, arsenic and antimony, and the crystal structures of these elements was discussed in Sect. 10.3.

16.3   Oxides

Introduction Decomposition of oxides with the release of atomic oxygen was apparently the first revealed case where the composition of primary decomposition products deviated from the equilibrium composition. More than 40 years ago, using the colour changes during the reaction of MoO$_3$ with atomic

oxygen (pale yellow MoO_3 transforms into blue Mo_3O_8 in accordance with the reaction $3MoO_3 + O \rightarrow Mo_3O_8 + O_2$), Mitani and Harano [10] showed that, during the decompositions of ZnO, HgO, CuO, and PtO_2 in a vacuum, oxygen is partially released in the atomic form. The same property was later discovered for Fe_2O_3, MnO_2, and Co_3O_4 [11]. A similar effect was also revealed by Malinin et al. [12] in the decomposition Pb_3O_4, from the characteristic blackening of the platinum crucible walls. (Strange though it may seem, these facts still remain unnoticed when discussing specific features of vaporization of the above-mentioned oxides [13, 14]).

Results and Discussion The first attempt of a thermochemical analysis of the mechanism of HgO vaporization was made by L'vov [15]. The initial experimental data were those obtained by Derbinsky et al. [16] and Pavlyuchenko [17] on the decomposition of HgO in a vacuum, in oxygen, and in the presence of mercury vapour. Analysis of primary data from Derbinsky et al. [16], made by L'vov [15], showed that mean molar enthalpy (parameter E) of vaporization of five different HgO samples at $T > 650\,K$ was $193 \pm 8\,kJ\,mol^{-1}(n = 8)$ in a vacuum and $201.7 \pm 3\,kJ\,mol^{-1}(n = 3)$ in O_2. These values are consistent with the theoretical value $E = 200.8\,kJ\,mol^{-1}$ for the reaction

$$HgO(s) \leftrightarrow Hg(g) + O \qquad (16.5)$$

and differ essentially from the value of $101.5\,kJ\,mol^{-1}$ for the reaction

$$HgO(s) \leftrightarrow Hg(g) + \tfrac{1}{2}O_2 \qquad (16.6)$$
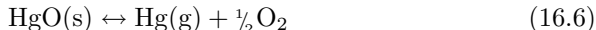
There are additional arguments in favour of Reaction 16.5. Above all, molecular oxygen does not affect the quantity E compared to the vacuum [16]. On the other hand, when HgO was decomposed in the presence of mercury vapour (800 Torr), the decomposition temperature increased by $130°C$ and E, to $430\,kJ\,mol^{-1}$ [17]. In the latter case, the theoretically expected value of E should be twice that for a vacuum, i.e., about $400\,kJ\,mol^{-1}$.

The mechanisms of decomposition of zinc and mercury oxides were further studied in [18]. The rates of vaporization of ZnO and HgO in a vacuum were measured with the aim of subsequent thermochemical analysis of the decomposition products by the third-law method. The thermodynamic functions required for the calculation are given in Table 16.6, and the conditions and results of the experiments, in Table 16.7. In this book, as compared to [18], the refined calculation scheme was used: the condition of congruent vaporization was taken into account and the molar enthalpy (parameter E) was calculated using Eq. 4.14.

Also, variation of the surface area of a powder pellet in the course of decomposition (see Sect. 15.1) was taken into account with Eq. 15.5 instead of Eq. 15.2. These refinements ultimately led to a slight increase in the final values of E. The mean value of E for HgO was $187.5 \pm 0.3\,kJ\,mol^{-1}$, which is 7% lower than that given by the thermochemical calculation ($201\,kJ\,mol^{-1}$), whereas

Table 16.6 Values of the thermodynamic functions for ZnO and HgO and products of their decompositions [6, 9]

Species	T	$\Delta_f H_T^\circ$	S_T°	Species	T	$\Delta_f H_T^\circ$	S_T°
	(K)	(kJ mol^{-1})	(J mol^{-1} K^{-1})		(K)	(kJ mol^{-1})	(J mol^{-1} K^{-1})
ZnO(s)	1,200	−305.6	111.7	HgO(s)	600	−75.5	105.7
Zn(g)	1,200	149.3	189.8	Hg(g)	600	67.8	189.5
O$_2$(g)	1,200	38.4	249.9	O$_2$(g)	600	17.9	226.3
O(g)	1,200	272.5	190.5	O(g)	600	260.0	176.0
ZnO(s)	1,300	−300.1	116.1	HgO(s)	700	−69.9	114.2
Zn(g)	1,300	151.4	191.5	Hg(g)	700	69.8	192.5
O$_2$(g)	1,300	42.0	252.8	O$_2$(g)	700	21.2	231.4
O(g)	1,300	274.6	192.2	O(g)	700	262.1	179.2

Table 16.7 The experimental conditions and results of determination of the molar enthalpies of vaporization of ZnO ($m_0 = 20$ mg) and HgO ($m_0 = 40$ mg) by the third-law method ($s_0 = 57.3$ mm^2)

Oxide	P_{air}	T	α_m	$\Delta m/\Delta t$	J^a	P_{eqp}	$\Delta_r S_T^\circ/\nu$	$\Delta_r H_T^\circ/\nu$
	(bar)	(K)		(μg s^{-1})	(kg m^{-2} s^{-1})	(bar)	(J mol^{-1} K^{-1})	(kJ mol^{-1})
ZnO	5E−08	1255.3	0.018	0.220	1.37E−06	7.75E−09	134.1	363.3
ZnO	5E−08	1255.5	0.005	0.073	4.56E−07	2.58E−09	134.1	374.8
ZnO	5E−08	1255.4	0.005	0.100	6.25E−07	3.54E−09	134.1	371.5
ZnO	5E−04	1257.6	0.001	0.052	3.30E−07	1.87E−09	134.1	378.8
ZnO	5E−04	1257.2	0.002	0.061	3.80E−07	2.15E−09	134.1	377.2
HgO	5E−04	681.0	0.055	1.82	1.15E−05	1.27E−08	129.0	187.2
HgO	5E−04	711.0	0.212	6.28	3.98E−05	4.46E−08	128.7	187.8

$^a J = (\Delta m/\Delta t)/(2.8\ s_0)$

for ZnO (373 ± 6 kJ mol^{-1}) it exceeds the calculated value (363 kJ mol^{-1}) by 3%. The latter discrepancy can be attributed to an error in the measurement of the initial $\Delta m/\Delta t$ values, which were below the level of reliable measurement (about 0.2 μg s^{-1}). Only one measurement was an exception (0.220 μg s^{-1}); the corresponding value of $E = 363$ kJ mol^{-1} coincides with the calculated value.

A comparison of the vaporization kinetics of ZnO and HgO in pure nitrogen and in air, made in [18], revealed no differences in the rates, which confirms the above assumption that oxygen is released in the form of free atoms (if oxygen were released in the molecular form, the difference would reach two orders of magnitude).

The calculated vaporization coefficients of both oxides are given in Table 16.8. The considerably lower coefficient α_v for HgO is due to the lower vaporization temperature, at which the relative content of atomic oxygen deviates from the equilibrium content more strongly. On the whole, *the thermochemical analysis reliably confirms the mechanism of dissociative vaporization of ZnO and HgO with the release of atomic oxygen.* The correlation between the composition of the primary products and the crystal structure of both oxides was discussed in Sect. 10.1.

Table 16.8 Calculated values of the vaporization coefficients for zinc and mercury oxides

Oxide	T (K)	Primary Products	P_{eqp} (bar)	Equilibrium Products	P_{eq} (bar)	α_v
ZnO	1,250	$Zn(g) + O$	6.6E−09	$Zn(g) + \frac{1}{2}O_2$	7.3E−07	9E−03
HgO	700	$Hg(g) + O$	3.0E−08	$Hg(g) + \frac{1}{2}O_2$	1.9E−01	2E−07

16.4 Higher oxides

Introduction Higher oxides of Group IV metals (SiO_2, GeO_2, and SnO_2), according to many studies, in particular, [14, 19–23], are characterized by relatively low vaporization coefficients. Therefore, taking into account the release of atomic oxygen in decomposition of Pb_3O_4 [12], one can assume that this is due to decomposition of all these oxides with the release of oxygen in the form of free atoms. Using published data on the vaporization of SnO_2 from a free surface (after Langmuir) and an effusion cell (after Knudsen) [22], and also the results of recent studies of L'vov and Ugolkov (unpublished) of the dissociative vaporization of Pb_3O_4, the experimental enthalpies are compared with their calculated values for the alternative schemes of decomposition with the release of free oxygen in the form of O_2 molecules or of O atoms only. For SiO_2 and GeO_2, primary data on the rates of free-surface vaporization are lacking. Therefore, the consideration below is restricted to a comparison of the vaporization coefficients, calculated assuming the decomposition of the oxides to atomic and molecular oxygen, with the experimental values of α_v given in [19, 20, 23]. The thermodynamic functions required for the calculations are given in Table 16.9.

Decomposition of SnO_2 Data on the dissociative sublimation of SnO_2 from an effusion cell (after Knudsen) and a free surface (after Langmuir), obtained by Hoenig and Searcy [22], are given in Fig. 16.1 and Table 16.10. Also presented are the molar enthalpies of the assumed processes that were determined by L'vov, using data from Hoenig and Searcy [22], by the second-law method (Fig. 16.1) and by the third-law method and thermochemical calculations (Table 16.10). Comparison of these results allows the following conclusions.

- The results of effusion measurements are in excellent agreement with the results of a thermochemical calculation for the dissociative decomposition of SnO_2 to $SnO + 1/2O_2$. The mean molar enthalpy measured by the third-law method ($397.0 \pm 1.8\,\text{kJ mol}^{-1}$) is very close to the averaged value of $\Delta_r H_T^\circ / \nu$ for the thermochemical calculation ($393.8 \pm 0.8\,\text{kJ mol}^{-1}$). The value measured by the second-law method, $390.3\,\text{kJ mol}^{-1}$, is slightly (by $<1\%$) lower than the thermochemical value.

Table 16.9 Values of the thermodynamic functions for SiO_2, GeO_2, SnO_2, Pb_3O_4, and the products of their decompositions [6]

Species	T (K)	$\Delta_f H_T^\circ$ (kJ mol^{-1})	S_T° (J mol^{-1} K^{-1})	Species	T (K)	$\Delta_f H_T^\circ$ (kJ mol^{-1})	S_T° (J mol^{-1} K^{-1})
$SiO_2(s)$	1,800	−805.4	160.1	$O(g)$	1,400	272.4	193.7
$SiO(g)$	1,800	−46.1	272.7	$SnO_2(s)$	1,600	−475.6	174.3
$O_2(g)$	1,800	51.7	264.7	$SnO(g)$	1,600	68.9	291.5
$O(g)$	1,800	280.7	198.9	$O_2(g)$	1,600	44.3	260.3
$GeO_2(s)$	1,500	−454.6	180.1	$O(g)$	1,600	276.5	196.5
$GeO(g)$	1,500	4.9	279.4	$Pb_3O_4(s)$	700	−642.0	372.8
$O_2(g)$	1,500	40.6	258.0	$PbO(s)$	700	−198.2	110.7
$O(g)$	1,500	274.5	195.1	$PbO(g)$	700	82.2	269.5
$SnO_2(s)$	1,200	−509.7	149.8	$O_2(g)$	700	12.5	231.4
$SnO(g)$	1,200	54.0	280.7	$O(g)$	700	257.7	179.2
$O_2(g)$	1,200	29.8	249.9	$Pb_3O_4(s)$	800	−620.1	402.1
$O(g)$	1,200	268.2	190.5	$PbO(s)$	800	−192.1	118.3
$SnO_2(s)$	1,400	−492.8	162.8	$PbO(g)$	800	85.8	274.4
$SnO(g)$	1,400	61.4	286.5	$O_2(g)$	800	15.8	235.8
$O_2(g)$	1,400	37.0	255.5	$O(g)$	800	259.8	182.0
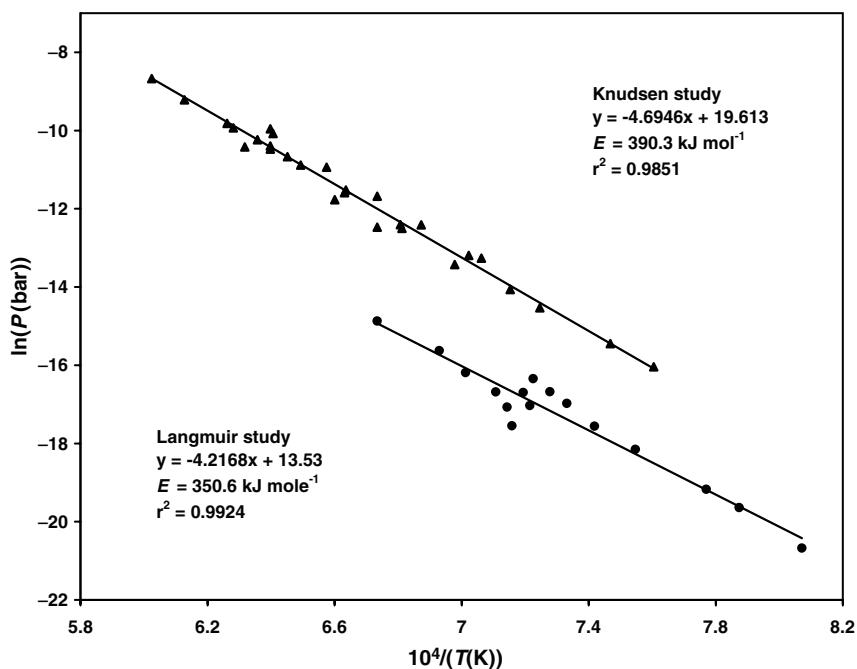
Fig. 16.1 Results of Knudsen and Langmuir [22] evaporation studies of SnO_2 and the molar enthalpies of the corresponding sublimation reactions calculated by the second-law method

Table 16.10 Experimental data on sublimation of SnO_2 in Langmuir and Knudsen studies [22] and the molar enthalpies calculated by the third-law method

Study	Primary Products	T (K)	$P(O_2)$ (bar)	$\Delta_r S_T^\circ$ (J mol⁻¹ K⁻¹)	$\Delta_r H_T^\circ / \nu$ (kJ mol⁻¹)		Difference (%)
					Expt	Theory[a]	
Knudsen	$SnO + \frac{1}{2}O_2$	1,315	1.08E−07	253.3	397.4	394.8	0.7
	$SnO + \frac{1}{2}O_2$	1,339	1.95E−07	252.8	397.6	394.6	0.8
	$SnO + \frac{1}{2}O_2$	1,380	4.88E−07	251.9	398.5	394.2	1.1
	$SnO + \frac{1}{2}O_2$	1,433	1.48E−06	250.7	399.5	393.9	1.4
	$SnO + \frac{1}{2}O_2$	1,468	3.72E−06	250.0	397.3	393.6	0.9
	$SnO + \frac{1}{2}O_2$	1,508	9.25E−06	249.5	396.2	393.4	0.7
	$SnO + \frac{1}{2}O_2$	1,550	2.33E−05	249.3	395.0	393.0	0.5
	$SnO + \frac{1}{2}O_2$	1,592	4.86E−05	247.5	394.2	392.5	0.4
Langmuir	$SnO + O$	1,239	1.05E−09	320.6	411.6	415.5	−0.9
	$SnO + O$	1,270	2.96E−09	320.0	410.6	415.1	−1.1
	$SnO + O$	1,287	4.72E−09	319.6	410.8	414.8	−1.0
	$SnO + O$	1,325	1.31E−08	318.8	411.2	414.3	−0.7
	$SnO + O$	1,348	2.36E−08	318.8	411.7	414.0	−0.6
	$SnO + O$	1,364	4.23E−08	318.2	409.6	413.8	−1.0
	$SnO + O$	1,386	5.72E−08	317.6	408.7	413.5	−1.2
	$SnO + O$	1,384	7.97E−08	317.8	408.0	413.5	−1.3
	$SnO + O$	1,374	4.02E−08	318.0	416.6	413.7	0.7
	$SnO + O$	1,397	5.60E−08	318.8	414.5	413.3	0.3
	$SnO + O$	1,400	2.40E−08	317.4	425.5	413.3	3.0
	$SnO + O$	1,390	3.85E−08	317.6	421.1	413.4	1.9
	$SnO + O$	1,407	5.69E−08	317.2	418.3	413.2	1.2
	$SnO + O$	1,426	9.30E−08	316.8	417.8	412.9	1.2
	$SnO + O$	1,443	1.63E−07	316.6	415.9	412.7	0.8
	$SnO + O$	1,485	3.48E−07	315.8	418.1	412.2	1.4

[a]Thermochemical calculation

- In the dissociative vaporization of SnO_2 from a free surface, the expected primary products are SnO and O. This assumption is confirmed by agreement between the molar enthalpies measured by the third-law method and determined by thermochemical calculation (Table 16.10). The averaged values of $\Delta_r H_T^\circ/\nu$ are 414.4 ± 4.9 and $413.7 \pm 0.9\,kJ\,mol^{-1}$, respectively. However, the value of $350.6\,kJ\,mol^{-1}$ found by the second-law method (see Fig. 16.1) is significantly (by 18%) underestimated. This result is not unexpected, taking into account the fact that the measurement results obtained using the second-law method (and method of Arrhenius plots) are influenced by the self-cooling effect in the course of free-surface vaporization. The extent of the underestimation is comparable to that (10–30%) observed when the second-law method was applied to measuring $\Delta_r H_T^\circ/\nu$ for the dissociative decomposition (to gaseous products) of other compounds, in particular, Be, Mg, and Ga nitrides (see Sect. 16.6).

It is noteworthy that all the measurements in question were performed within a short period (1965–1968) in the same laboratory (headed by Searcy). These results show that *it is not appropriate to use the second-law method when studying the free-surface vaporization of compounds in a high vacuum.*

Decomposition of Pb_3O_4 L'vov and Ugolkov have measured recently the absolute rates of decomposition of Pb_3O_4 in a low vacuum (about 10^{-4} bar) with an STA 429 thermal analyser. An additional problem in calculating the enthalpies of alternative decomposition pathways of Pb_3O_4, compared to SnO_2, is the formation of a low-volatility product, PbO(s). To calculate the transfer coefficient τ, Eq. 8.4 was used. Table 16.11 shows that both decomposition pathways are characterized by a noticeable discrepancy (8–10%) between the experimental and theoretical values. The use of other schemes for calculating τ leads to an increase in the difference between the compared quantities for the first of the reactions. Therefore, the mechanism of this reaction requires further study. In particular, the release of oxygen in the form of a mixture of O and O_2 cannot be ruled out.

Table 16.11 The initial data and results of determination of the decomposition enthalpy of Pb_3O_4 by the third-law method

Products	T (K)	J^a (kg m^{-2} s^{-1})	$\overline{P}$ (bar)	$\Delta_r S_T^\circ$ (J mol^{-1} K^{-1})	$\Delta_r H_T^\circ$ (kJ mol^{-1}) Expt	Theory[b]
$3PbO(g)_\downarrow + O$	784.0	1.69E−06	1.66E−07	605.2	881.6	955.3
$3PbO(g)_\downarrow + O$	773.4	1.39E−06	1.36E−07	606.4	875.6	955.3
$3PbO(g)_\downarrow + 1/2O_2$	784.0	1.69E−06	2.04E−07	541.1	775.6	703.5
$3PbO(g)_\downarrow + 1/2O_2$	773.4	1.39E−06	1.68E−07	542.2	770.4	703.5

[a] $J = (\Delta m/\Delta t)/(2.8\,s_0)$, where $s_0 = 56.4\,mm^2$
[b] With the use of $\tau = 0.220$ calculated by Eq. (7.4), $\Delta_c H_{780}^\circ = 278.4\,kJ\,mol^{-1}$ and $\Delta_v H_{780}^\circ = 1139.1$ and $887.3\,kJ\,mol^{-1}$ for the first and second reactions

Table 16.12 Calculated (theory) and experimental values of the vaporization coefficients for some higher oxides

Oxide	T (K)	Primary Products	P_{eqp} (bar)	Equilibrium Products	P_{eq} (bar)	α_v Theory	α_v Expt	Ref.
SiO_2	1,800	$SiO(g) + O$	1.1E−07	$SiO(g) + \frac{1}{2}O_2$	2.2E−07	5E−01	4E−02	[20]
GeO_2	1,473	$GeO(g) + O$	4.7E−06	$GeO(g) + \frac{1}{2}O_2$	4.0E−04	1E−02	6E−02	[23]
SnO_2	1,380	$SnO(g) + O$	3.2E−08	$SnO(g) + \frac{1}{2}O_2$	4.9E−07	7E−02	1E−01	[22]
Pb_3O_4	784	$3PbO(g)_\downarrow + O$	1.7E−07	$3PbO(s) + \frac{1}{2}O_2$	1.2E−04	1E−03		

Vaporization Coefficients The calculated and experimental vaporization coefficients for all the above-mentioned oxides are listed in Table 16.12. The calculated vaporization coefficients of GeO_2 and SnO_2 are somewhat lower than those measured by the Knudsen and Langmuir methods; for SiO_2 the pattern is opposite. However, these discrepancies do not exceed an order of magnitude and are most likely caused by experimental errors. Therefore, one can conclude with confidence that the *decomposition of all the higher oxides of Group IV metals under the free-surface vaporization conditions occurs with the release of oxygen in the atomic form.* This conclusion is consistent with the crystal structures of these oxides, which are other than cubic (see Sect. 10.1).

16.5   Sulfides, Selenides, and Tellurides

Introduction The vaporization of cadmium and zinc sulfides, selenides, and tellurides has been thoroughly examined in many studies [24–30]. The authors of these papers report that the vaporization coefficients of these compounds are in the range 0.1–0.3, which suggests that, not only the most stable diatomic molecules, but also free S, Se, and Te atoms can be detached from the surface in the course of vaporization. Using the primary data from [24–30], the corresponding molar enthalpies are compared with the values calculated for the equilibrium vaporization scheme. The thermodynamic functions given in Table 16.13 were used in the calculations. The final results are presented in Table 16.14.

Results and Discussion The differences between the actual and theoretically calculated molar enthalpies are seen to be insignificant. The largest discrepancy, 9–12 kJ mol^{-1} (about 4%), is observed for ZnS and ZnSe. This is comparable with the scatter of the experimental data given for the same compounds (CdS and CdSe) in different papers. Therefore, there are no grounds to attribute the observed discrepancies to deviation of the product composition from the equilibrium composition. This conclusion is, on the whole, consistent with the general features of the effect of the crystal structure on the decomposition products (see Chapter 9).

Table 16.13 Values of the thermodynamic functions for CdS, CdSe, ZnS, ZnSe, ZnTe, and products of their decompositions [6, 7, 9, 31]

Species	T (K)	$\Delta_f H_T^\circ$ (kJ mol^{-1})	S_T° (J mol^{-1} K^{-1})	Species	T (K)	$\Delta_f H_T^\circ$ (kJ mol^{-1})	S_T° (J mol^{-1} K^{-1})
CdS(s)	1,000	−119.4	134.9	ZnS(s)	1,000	−155.8	121.6
Cd(g)	1,000	126.4	182.8	Zn(g)	1,000	145.1	186.1
S$_2$(g)	1,000	162.5	270.7	ZnSe(s)	1,000	−127.7	146.8
S(g)	1,000	297.1	195.0	ZnTe(s)	900	−82.5	162.4
CdSe(s)	1,000	−102.7	151.5	Zn(g)	900	143.0	183.9
Se$_2$(g)	1,000	171.9	296.4	Te$_2$(g)	900	189.9	308.8
Se(g)	1,000	242.6	203.0	Te(g)	900	204.2	205.5

Table 16.14 The initial data and results of determination of the vaporization enthalpies for CdS, CdSe, ZnS, ZnSe, and ZnTe by the third-law method

Vaporization Products	System	T (K)	$\overline{P}$ (bar)	$\Delta_r S_T^\circ/\nu$ (J mol^{-1} K^{-1})	$\Delta_r H_T^\circ/\nu$ (kJ mol^{-1}) Expt	$\Delta_r H_T^\circ/\nu$ (kJ mol^{-1}) Theory	Ref.
Cd + 1/2S$_2$	I	993	1.1E−05	122.2	215.6	218.0	[24]
Cd + 1/2S$_2$	I	1,000	7.9E−06	122.2	219.9	218.0	[25]
Cd + 1/2Se$_2$	I	1,000	5.0E−05	119.7	202.0	210.0	[26]
Cd + 1/2Se$_2$	I	1,000	1.3E−05	119.7	213.1	210.0	[27]
Zn + 1/2S$_2$	III	1,108	3.5E−06	133.2	263.3	254.8	[24]
Zn + 1/2S$_2$	III	1,000	1.4E−07	133.2	264.4	254.8	[28]
Zn + 1/2Se$_2$	I	1,000	2.6E−07	125.0	251.0	239.2	[29]
Zn + 1/2Te$_2$	I	900	5.0E−07	117.3	214.1	213.6	[30]

Presumably, all the compounds, except ZnS, have a cubic zinc blende structure (I) at the vaporization temperatures. The ZnS crystals, as noted in [28], had a hexagonal wurtzite structure (III). To bring the calculated value in agreement with the experimental molar enthalpy ($263.8\,\text{kJ mol}^{-1}$), the following vaporization scheme needs to be assumed:

$$\text{ZnS(s)} \leftrightarrow \text{Zn(g)} + 0.42\text{S}_2 + 0.16\text{S} \tag{16.7}$$
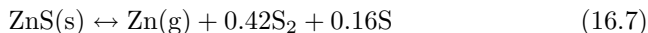
The calculated molar enthalpy of this reaction is $263.7\,\text{kJ mol}^{-1}$. However, the product composition differs insignificantly from the equilibrium composition, and therefore this interpretation is hardly reliable.

16.6 Nitrides

Introduction The development, manufacture, and application of light-emitting diodes and semiconductor lasers, operating in the infrared, red, and green ranges, stimulated recently a search for materials exhibiting such properties in the blue and ultraviolet ranges. Hexagonal nitrides such as AlN, GaN, and InN are of interest in this respect. Knowledge of the conditions

and mechanism of their decomposition is extremely important for the manufacture of films, the production of articles, and their operation at elevated temperatures. The decomposition mechanism of nitrides is also of considerable scientific interest. The vaporization coefficients of the majority of nitrides are very low, despite their congruent vaporization with the formation (except BN) of gaseous products only.

Numerous papers published in the past four decades have dealt with the vaporization of nitrides (see, e.g., [32–41]). L'vov et al. [42] summarized the published data and the results of their own measurements of the vaporization kinetics of a large group of nitrides (Mg_3N_2, AlN, GaN, InN, Si_3N_4, and BN). As a result, certain correlations between the vaporization of nitrides and features of their crystal structures were revealed. The results given below are based on data presented in [42].

Experimental The vaporization rates were measured in [42] with an STA 429 thermal analyser in a high vacuum (5×10^{-8} bar) with continuous evacuation of the system. The experiments were performed with high-purity powders of Mg_3N_2 (99.5%), GaN (99.99%), and InN (99.99%) (all Aldrich), Si_3N_4 of H-1 grade (Stark), and AlN and BN of unknown origin. To prevent ejection of samples from the crucible in the course of their intense decomposition, some nitrides (Mg_3N_2, GaN, and InN) were mixed with high-purity Al_2O_3 powder. Powder samples weighing from 5 to 30 mg were placed in an alumina crucible and manually pressed (under a pressure of about $1\,kg\,mm^{-2}$) into flat pellets. The total (external) surface area of the pellet was calculated from its thickness and diameter.

Results and Discussion To determine the molar enthalpy, the third-law method and the thermodynamic functions given in Table 16.15 were used. The experimental conditions and results obtained are given in Table 16.16. In contrast to L'vov et al. [42], the surface area of the powder pellet was taken into account with Eq. 16.5, and generalized Eqs. 4.14, 4.16, and 4.17 were used when determining the molar enthalpy. These refinements led to slight changes in the molar enthalpy but did not affect the composition of the vaporization products except Mg_3N_2, for which the stoichiometric content of atomic nitrogen increased from 1.50N to 1.52N.

The decomposition of c-BN deserves a special discussion. Among the nitrides considered in this book, this is the only nitride decomposing with the formation of a solid product, boron. Its decomposition can be described by the reaction

$$c\text{-BN(s)} \leftrightarrow B(g) + \tfrac{1}{2}N_2 \rightarrow B(s) + \tfrac{1}{2}N_2 \qquad (16.8)$$
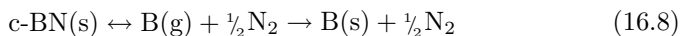
However, the kinetics of the c-BN decomposition are determined only by the first decomposition step. Partial transfer of the condensation energy to the reactant can be neglected, because the equivalent pressure of boron for reaction (16.8) at 1,800 K exceeds the saturated pressure of the metal by only an

Table 16.15 Values of thermodynamic functions for some nitrides and products of their decomposition [6, 9, 39, 40]

Species	T (K)	$\Delta_f H_T^\circ$ (kJ mol^{-1})	S_T° (J mol^{-1} K^{-1})	Species	T (K)	$\Delta_f H_T^\circ$ (kJ mol^{-1})	S_T° (J mol^{-1} K^{-1})
c-AlN(s)	1,300	−274.2	83.2	h-GaN(s)	1,200	−112.7[b]	101.9[a]
Al(g)	1,300	350.7	195.3	Ga(g)	1,200	294.6	204.5
N$_2$(g)	1,300	31.5	236.8	N$_2$(g)	1,200	28.1	234.1
N(g)	1,300	493.5	183.8	N(g)	1,200	491.4	182.1
h-AlN(s)	1,700	−254.1	96.7	h-GaN(s)	1,300	−107.1[b]	106.2[b]
Al(g)	1,700	359.0	200.9	Ga(g)	1,300	296.8	206.3
N$_2$(g)	1,700	45.5	246.2	InN(s)	1,000	−90.6[a]	106.0[a]
N(g)	1,700	501.8	189.4	In(g)	1,000	257.0	201.5
h-AlN(s)	1,800	−248.9	99.6	N$_2$(g)	1,000	21.5	228.1
Al(g)	1,800	361.1	202.1	N(g)	1,000	487.3	178.3
N$_2$(g)	1,800	48.9	248.2	InN(s)	1,100	−84.5[a]	111.6[a]
N(g)	1,800	503.9	190.6	In(g)	1,100	259.7	204.1
c-BN(s)	1,800	−187.5[a]	82.7	N$_2$(g)	1,100	24.8	231.2
B(s)	1,800	36.1	44.9	N(g)	1,100	489.3	180.3
B(g)	1,800	596.3	190.7	Mg$_3$N$_2$(s)	1,200	−353.8	246.0
Be$_3$N$_2$(s)	1,600	−436.5	215.4	Mg(g)	1,200	165.7	177.5
Be(g)	1,600	357.3	171.1	Mg$_3$N$_2$(s)	1,300	−340.8	256.3
N$_2$(g)	1,600	41.9	244.0	Mg(g)	1,300	167.8	179.1
N(g)	1,600	499.7	188.1	Si$_3$N$_4$(s)	1,700	−576.6	308.1
c-GaN(s)	900	−128.7[b]	86.5[b]	Si(g)	1,700	479.7	204.9
Ga(g)	900	287.6	197.8				
N$_2$(g)	900	18.2	224.6				

[a] From [39]
[b] From [40]

order of magnitude. Nevertheless, this assumption may be responsible for a 2% discrepancy between the experimental and theoretical values of $\Delta_r H_T^\circ/\nu$ (Table 16.16).

The experimental conditions and results [42] of determining the molar enthalpies of vaporization of hexagonal nitrides Be$_3$N$_2$, Mg$_3$N$_2$, AlN, GaN, InN, and Si$_3$N$_4$ and of cubic nitrides BN, AlN, and GaN, on the basis of data from [32–38], are given in Table 16.17. The theoretical values of $\Delta_r H_T^\circ/\nu$ for Mg$_3$N$_2$, BN, AlN, GaN, InN, and Si$_3$N$_4$ were taken from Table 16.16. The theoretical molar enthalpy of vaporization of Be$_3$N$_2$ was obtained from comparison with the experimental value calculated in [42] from data of Hoenig and Searcy [32]. The theoretical values of $\Delta_r H_T^\circ/\nu$ for cubic nitrides BN, AlN, and GaN correspond to the equilibrium reactions with the dissociation of the nitrides to molecular nitrogen.

Table 16.17 presents also the $\Delta_r H_T^\circ/\nu$ values determined in the papers cited by the second-law method. These values are less reliable than those determined by the third-law method and are lower in seven cases out of ten. The difference in the $\Delta_r H_T^\circ/\nu$ values for BN reaches 60%. This systematic underestimation may be attributing to the self-cooling effect, which is particularly pronounced

Table 16.16 Initial data [42] and the results of determination of the vaporization enthalpy for some nitrides by the third-law method

Deduced Reaction	T (K)	s_0 (mm^2)	α_m	$\Delta m/\Delta t$ (μg s^{-1})	J (kg m^{-2}s^{-1})	$\overline{P}$ (bar)	ν	$\Delta_\mathrm{r}S_T^\circ/\nu$ (J mol^{-1} K^{-1})	$\Delta_\mathrm{r}H_T^\circ/\nu$ (kJ mol^{-1}) Expt	Theory
Mg$_3$N$_2$ $\leftrightarrow$ 3Mg(g) + 1.52N + 0.24N$_2$	1,261	47.4	0.369	0.987	7.44E−06	5.75E−08	4.76	129.8	338.5	336.8
Mg$_3$N$_2$ $\leftrightarrow$ 3Mg(g) + 1.52N + 0.24N$_2$	1,232	47.4	0.206	0.540	4.07E−06	3.11E−08	4.76	130.0	337.2	336.9
Mg$_3$N$_2$ $\leftrightarrow$ 3Mg(g) + 1.52N + 0.24N$_2$	1,201	47.4	0.143	0.234	1.76E−06	1.33E−08	4.76	130.1	337.3	337.1
BN $\leftrightarrow$ B(g)$_\downarrow$ + 1/2N$_2$	1,800	60.0	0.016	0.51	3.04E−06	6.43E−08	1.5	154.7	526.3	538.8
BN $\leftrightarrow$ B(g)$_\downarrow$ + 1/2N$_2$	1,799	60.0	0.013	0.43	2.56E−06	5.42E−08	1.5	154.7	528.6	538.8
AlN $\leftrightarrow$ Al(g) + 0.42N + 0.29N$_2$	1,784	61.8	0.046	5.53	3.20E−05	2.37E−07	1.71	149.4	492.8	488.9
AlN $\leftrightarrow$ Al(g) + 0.42N + 0.29N$_2$	1,785	61.8	0.066	6.90	3.99E−05	2.96E−07	1.71	149.4	489.8	488.9
GaN $\leftrightarrow$ Ga(g) + 0.42N + 0.29N$_2$	1,268	50.6	0.070	1.49	1.05E−05	4.25E−08	1.71	144.4	362.0	363.1
GaN $\leftrightarrow$ Ga(g) + 0.42N + 0.29N$_2$	1,256	45.7	0.042	0.53	4.14E−06	1.67E−08	1.71	144.5	368.5	363.2
GaN $\leftrightarrow$ Ga(g) + 0.42N + 0.29N$_2$	1,277	50.5	0.20	2.09	1.48E−05	6.00E−08	1.71	144.4	361.0	363.0
GaN $\leftrightarrow$ Ga(g) + 0.42N + 0.29N$_2$	1,257	50.5	0.030	1.33	9.41E−06	3.79E−08	1.71	144.5	360.2	363.2
GaN $\leftrightarrow$ Ga(g) + 0.42N + 0.29N$_2$	1,256	50.5	0.037	1.35	9.55E−06	3.84E−08	1.71	144.5	359.8	363.2
GaN $\leftrightarrow$ Ga(g) + 0.42N + 0.29N$_2$	1,266	45.7	0.046	1.41	1.10E−05	4.45E−08	1.71	144.4	361.0	363.1
GaN $\leftrightarrow$ Ga(g) + 0.42N + 0.29N$_2$	1,267	45.7	0.046	1.20	9.38E−06	3.79E−08	1.71	144.4	363.0	363.1
InN $\leftrightarrow$ In(g) + 0.32N + 0.34N$_2$	1,028	54.6	0.070	0.137	8.96E−07	2.48E−09	1.66	138.6	311.8	307.5
InN $\leftrightarrow$ In(g) + 0.32N + 0.34N$_2$	1,008	54.6	0.040	0.131	8.57E−07	2.35E−09	1.66	138.7	306.3	307.7
InN $\leftrightarrow$ In(g) + 0.32N + 0.34N$_2$	1,009	54.6	0.035	0.126	8.24E−07	2.26E−09	1.66	138.7	307.0	307.7
Si$_3$N$_4$ $\leftrightarrow$ 3Si(g) + 1.8N + 1.1N$_2$	1,700	61.8	0.020	1.34	7.74E−06	5.29E−08	5.9	155.3	500.8	503.2
Si$_3$N$_4$ $\leftrightarrow$ 3Si(g) + 1.8N + 1.1N$_2$	1,699	61.8	0.019	1.29	7.45E−06	5.09E−08	5.9	155.3	501.1	503.2

Table 16.17 The initial data [32–38] and results of determination of the molar enthalpies for nitride decompositions by the second- and third-law methods

Deduced Decomposition Reaction	Sample[a]	T (K)	$\overline{P}$ (bar)	ν	$\Delta_r S^\circ_T/\nu$ (J mol^{-1} K^{-1})	$\Delta_r H^\circ_T/\nu$ (kJ mol^{-1})			Ref.
						Second-law	Third-law	Theory	
Be$_3$N$_2$ ↔ 3Be(g) + 1.52N + 0.24N$_2$	Tablet	1,600	1.50E−09[b]	4.76	135.0	428	486	478.6	[32]
Mg$_3$N$_2$ ↔ 3Mg(g) + 1.52N + 0.24N$_2$	Tablet	1,200	4.60E−07[b]	4.76	130.1	238[c]	302	337.1	[33]
h-AlN ↔ Al(g) + 0.42N + 0.29N$_2$	Tablet	1,762	1.45E−07	1.71	149.5	494[c]	494	489.0	[34]
h-GaN ↔ Ga(g) + 0.42N + 0.29N$_2$	MOCVD film	1,300	1.00E−07	1.71	143.9	379	361	362.8	[35]
h-GaN ↔ Ga(g) + 0.42N + 0.29N$_2$	Tablet	1,300	1.01E−07[b]	1.71	143.9	305	361	362.8	[36]
InN ↔ In(g) + 0.32N + 0.34N$_2$	Film	1,100	5.40E−08	1.66	137.9	336	305	306.8	[35]
Si$_3$N$_4$ ↔ 3Si(g) + 1.8N + 1.1N$_2$	Powder	1,713	2.90E−07	5.9	155.2	480[c]	480	503.1	[37]
c-BN ↔ B(g)$_\downarrow$ + 1/2N$_2$	Tablet	1,800	2.40E−08	1.5	154.7	329[c]	541	538.8	[34]
c-AlN ↔ Al(g) + 1/2N$_2$	MOCVD film	1,300	1.20E−08	1.5	153.7	414	397	427.1	[35]
c-GaN ↔ Ga(g) + 1/2N$_2$	MBE film	900	1.20E−10	1.5	149.1	261	305	283.6	[38]

[a] MOCVD: metal organic chemical vapour deposition; MBE: molecule beam epitaxy

[b] $\overline{P}$ value is reduced by a factor of 2.8 to take into account the tablet porosity

[c] Calculated in this work from experimental data presented in original publications

for BN because of the formation of a boron layer on the reactant surface and a decrease in the resulting emittance ε^* (see Sect. 6.3). Even after exclusion of this result, the mean standard deviation is as high as 13%. Apparently, use of the $\Delta_{\mathrm{r}} H_T^{\circ}/\nu$ values, measured by the second-law method for evaluating the stoichiometry of the reactions occurring in the course of vaporization, leads to unreliable results.

The $\Delta_{\mathrm{r}} H_T^{\circ}/\nu$ values for AlN, GaN, InN, Si_3N_4, and BN, measured by the third-law method, show much better agreement with the theoretical values taken from Table 16.17. The standard deviation is as low as 3.2%. The value of $\Delta_{\mathrm{r}} H_T^{\circ}/\nu = 302\,\mathrm{kJ}\,\mathrm{mol}^{-1}$ for Mg_3N_2, obtained from the data reported in [33], is apparently underestimated. This is seen from the comparison with the value of $\Delta_{\mathrm{r}} H_T^{\circ}/\nu = 305\,\mathrm{kJ}\,\mathrm{mol}^{-1}$, measured in [33] for vaporization of Mg_3N_2 from a Knudsen cell. The molar enthalpy measured under the free-surface vaporization conditions (after Langmuir) cannot be lower than the enthalpy measured under equilibrium conditions. The conclusions following from the whole set of data given in Tables 16.16 and 16.17 and the correlation revealed between the product compositions and the crystal structures of the nitrides were discussed in Sect. 10.2.

Table 16.18 presents the theoretical and experimental vaporization coefficients for the hexagonal nitrides. The discrepancy between the experimental and theoretical values does not exceed an order of magnitude (except Mg_3N_2 for which, as noted above, the experimental value of α_{v} [33] is apparently overestimated because of error in the determination of the vaporization rate), which seems to be quite acceptable.

Table 16.18 Calculated (theory) and experimental values of the vaporization coefficients for some nitrides

Nitride	T (K)	Primary Products	P_{eqp} (bar)	Equilibrium Products	P_{eq} (bar)	α_{v} Theory	α_{v} Expt	Ref.
Be_3N_2	1,600	$3Be(g) + 1.52N + 0.24N_2$	2.7E−09	$3Be(g) + N_2$	2.7E−06	1.0E−03	1.0E−04	[32]
Mg_3N_2	1,200	$3Mg(g) + 1.52N + 0.24N_2$	1.3E−08	$3Mg(g) + N_2$	1.7E−03	7.8E−06	3.0E−03	[33]
h-AlN	1,800	$Al(g) + 0.42N + 0.29N_2$	4.1E−07	$Al(g) + 1/2N_2$	4.1E−05	1.0E−02	3.5E−03	[34]
h-GaN	1,300	$Ga(g) + 0.42N + 0.29N_2$	9.0E−08	$Ga(g) + 1/2N_2$	2.3E−04	3.9E−04		
InN	1,000	$In(g) + 0.32N + 0.34N_2$	1.5E−09	$In(g) + 1/2N_2$	6.6E−06	2.3E−04		
Si_3N_4	1,700	$3Si(g) + 1.8N + 1.1N_2$	4.5E−08	$3Si(g) + 2N_2$	2.5E−05	1.8E−05	1.0E−04	[37]

16.7 Azides

Introduction The interest in studying the mechanism and kinetics of thermal decomposition of inorganic azides is due to their unique properties determined by the azide group and to important applications of these compounds as explosives, sources of pure nitrogen and potential photographic materials. Furthermore, because of their chemical and structural simplicity, azides are a convenient model system for studying the kinetics of solid-state reactions. Despite long and active studies [43–46], many specific features of decomposition of these compounds and concomitant phenomena (in particular, the mechanism of UV emission) remain poorly understood. An attempt to interpret some specific features of the decomposition of azides by thermochemical analysis of the reaction kinetics was made in 1997 by L'vov [47]. The results presented below were obtained using the same approach, but with an improved calculation procedure taking the metal condensation into account and involving the third-law method for determining the molar enthalpies of the reactions.

Results and Discussion The thermodynamic functions of azides and their decomposition products, used in the subsequent calculations, are given in Table 16.19, and the results of the determination of the molar enthalpies and the corresponding decomposition schemes, in Tables 16.20 and 16.21.

Some comments on the calculations should be noted. The molar enthalpies of decomposition of sodium, potassium, barium, and lead azides that were calculated by the third-law method are given in Table 16.20. The initial data for these calculations were the absolute decomposition rates J of these azides, measured in [49–51]. The results obtained for NaN_3 and $Pb(N_3)_2$ at different temperatures and in different studies show good agreement. In Table 16.21, these results are compared with the averaged molar enthalpies measured for these and some other azides by the second-law method (the initial values of

Table 16.19 Values of the thermodynamic functions for some azides and products of their decompositions at 298 K [6, 31, 48]

Species	$\Delta_f H^\circ_{298}$ (kJ mol^{-1})	S°_{298} (J mol^{-1}K^{-1})	Species	$\Delta_f H^\circ_{298}$ (kJ mol^{-1})	S°_{298} (J mol^{-1}K^{-1})
$AgN_3(s)$	310.6	115.5	$Pb(N_3)_2(s)$	483.5	170.1
$Ag(g)$	284.9	172.9	$Pb(g)$	195.1	175.3
$Ba(N_3)_2(s)$	−22.2	165.2	$Sr(N_3)_2(s)$	7.1	159.0
$Ba(g)$	179.0	170.1	$Sr(g)$	160.5	164.5
$Ca(N_3)_2(s)$	46.0	145.3	$TlN_3(s)$	233.6	125.9
$Ca(g)$	177.8	154.3	$Tl(g)$	180.8	180.9
$KN_3(s)$	−1.3	104.0	$N(g)$	472.7	153.2
$K(g)$	89.0	160.2	$N_2(g)$	0	191.5
$NaN_3(s)$	21.3	96.9	$N_3(g)$	436.0	223.0
$Na(g)$	107.5	153.6			

Table 16.20 The initial data [49–51] and results of determination of the molar enthalpies of azide decompositions by the third-law method

Azide	Primary Products	ν	T (K)	J (mol m^{-2} s^{-1})	$\bar{P}$ (bar)	$\Delta_r S^\circ_{298}/\nu$ (J mol^{-1} K^{-1})	E (kJ mol^{-1})	Ref.
NaN$_3$	Na(g) + 0.86N + 1.07N$_2$	2.93	603	1.3E−04	3.3E−08	134.3	167	[49]
NaN$_3$	Na(g) + 0.86N + 1.07N$_2$	2.93	573	1.8E−05	5.0E−09	134.3	168	[49]
KN$_3$	K(g) + 0.73N + 1.135N$_2$	2.86	524	2.8E−05	7.5E−09	134.6	152	[50]
Ba(N$_3$)$_2$	Ba(g)$_\downarrow$ + 0.74N + 2.63N$_2$	4.37	388	5.1E−05	1.4E−08	142.4	114	[50]
Pb(N$_3$)$_2$	Pb(g)$_\downarrow$ + 2.36N + 1.82N$_2$	5.18	543	8.8E−05	3.1E−08	138.2	153	[50]
Pb(N$_3$)$_2$	Pb(g)$_\downarrow$ + 2.36N + 1.82N$_2$	5.18	500	6.6E−06	2.2E−09	138.2	152	[51]

Table 16.21 Reaction schemes and the molar enthalpies for azide decompositions measured by the second- and third-law methods

Azide	Primary Products	ν	T (K)	$b/(b+2c)$ (%)	System	$-\Delta_c H^\circ_T$ (kJ mol^{-1})	τ_2	E (kJ mol^{-1}) Third-law	Second-law^a	$\Delta_v H^\circ_T/\nu$ (kJ mol^{-1}) Expt	Theory
NaN$_3$	Na(g) + 0.86N + 1.07N$_2$	2.93	600	28.7	IIIa	0	0	168	168($n=4$)	168	168
KN$_3$	K(g) + 0.73N + 1.135N$_2$	2.865	530	24.3	II	0	0	152	162($n=4$)	152	152
AgN$_3$(l)^b	Ag(g) + 0.94N + 1.03N$_2$	2.97	530	31.3	IV	0	0		140($n=3$)	140	140
TlN$_3$	Tl(g)$_\downarrow$ + 1.14N + 0.93N$_2$	3.07	520	38.0	IV	180.8	0.17		149($n=1$)	159	159
Ca(N$_3$)$_2$	Ca(g)$_\downarrow$ + 0.54N + 2.73N$_2$	4.27	350	9.0	IV	177.8	0.35		78($n=2$)	93	92
Sr(N$_3$)$_2$	Sr(g)$_\downarrow$ + 0.52N + 2.74N$_2$	4.26	390	8.7	IV	160.5	0.25		84($n=1$)	93	94
Ba(N$_3$)$_2$	Ba(g)$_\downarrow$ + 0.74N + 2.63N$_2$	4.37	400	12.3	V	179.0	0.29	114	103($n=3$)	126	126
Pb(N$_3$)$_2$	Pb(g)$_\downarrow$ + 2.36N + 1.82N$_2$	5.18	520	39.3	IV, V, VI	195.1	0.21	152	145($n=3$)	160	160

^{a} Average values from n independent results collected in [47] from different works
^{b} Melting point of AgN$_3$ is 523 K

the molar enthalpies are given in [47]). The crystal systems of the azides are also indicated in Table 16.21.

The further scheme for calculating the composition of the primary products for sodium and potassium azides, decomposing to gaseous products only, and for the silver azide melt was the same as for the nitrides (see above). The composition was determined by choosing the decomposition scheme for which the molar enthalpy would fit the experimental value. For the other azides, decomposing to the solid metal and a mixture of atomic and molecular nitrogen, the molar enthalpy for one or another product composition needs to be compared to the experimental value, taking into account a partial contribution of the heat of condensation, $\Delta_c H_T^\circ$. For this purpose, the $\tau \Delta_c H_T^\circ / \nu$ quantity was subtracted from the experimental value of E. Their difference $(E - \tau \Delta_c H_T^\circ / \nu)$ corresponds to the molar enthalpy, $\Delta_v H_T^\circ / \nu$, of a hypothetical reaction of vaporization of the azides with the formation of gaseous products, without taking the condensation into account. The quantity $\tau \Delta_c H_T^\circ / \nu$ ranged from $-8 \, \text{kJ mol}^{-1}$ for $Pb(N_3)_2$ to $-14 \, \text{kJ mol}^{-1}$ for $Ca(N_3)_2$. The transfer coefficient τ was calculated by Eq. 7.6 approximating the dependence $\tau_2 = f(c_2)$. When selecting the experimental values of E, the values obtained by the third-law method (Table 16.20) were preferred.

Conclusions The data in Table 16.21 allow the following conclusions.

- The experimental values of the molar enthalpy, obtained by the second- and third-law methods, differ by no more than $10 \, \text{kJ mol}^{-1}$, which is within the scatter of the $\Delta_r H_T^\circ / \nu$ values measured by the second-law method in different studies.
- The fraction of atomic nitrogen $b/(b + 2c)$, where b and c are the stoichiometric coefficients for atomic and molecular nitrogen in the reaction products, varies for different azides in a wide range, from 9% to 39%. Nevertheless, a certain correlation can be seen between the composition of the products, on the one hand, and the stoichiometries and crystal structures of the azides, on the other. For AgN_3 and TlN_3, $b/(b+2c) = 34.6\% \pm 4.7\%$, and for $Ca(N_3)_2$ and $Sr(N_3)_2$, it is as low as $8.8\% \pm 0.2\%$. All these azides have a rhombic structure. For the azides NaN_3 and KN_3 having similar stoichiometry but different crystal structures, the $b/(b + 2c)$ magnitudes are also similar $(26.5\% \pm 2.2\%)$; their difference is within the measurement error.
- For the azides $Ba(N_3)_2$ and $Pb(N_3)_2$, having similar stoichiometry but crystallizing in different systems, the difference is much more significant: $b/(b + 2c)$ is 12.3% and 39.3%, respectively. However, for lead azide, the primary decomposition pathway might be different [47]: $Pb(N_3)_2 \leftrightarrow Pb(g) + N + N_2 + N_3$. The molar enthalpy of this reaction is $155 \, \text{kJ mol}^{-1}$, which is consistent with the experimental value of $160 \, \text{kJ mol}^{-1}$. The feasibility of this reaction pathway indirectly follows from features of the crystal structure of α-$Pb(N_3)_2$ [47]. This modification is the only stable form of

this azide at temperatures exceeding 160°C. As shown in [48], in the crystal structure of this modification there are four crystallographically nonequivalent azide groups with different interatomic distances N(1)–N(2) and N(2)–N(3). In two out of the four groups, these distances are shorter than in the neutral N_3 molecule (1.181 Å). This fact indirectly suggests that a half of nitrogen atoms can be released in the form of N_3 molecules, and the other half, in the form of $N + N_2$. This assumption requires further study.

Other Observations The assumption that azides decompose with partial release of nitrogen in the form of free atoms is confirmed by L'vov [47] by direct mass-spectrometric analysis of the primary decomposition products of NaN_3. Analysis of the initial mass-spectrometric patterns reported by Walker [49], taking into account partial dissociation of N_2 molecules in the ionizing chamber of a quadrupole mass spectrometer, and the differences in the ionization cross sections of N and N_2 and in the solid angles of the inlet of these species into the ionizing chamber, showed that the ion current ratio $I(N^+)/I(N_2^+)$ in Walker's experiments [49] was 0.86, which is consistent with the estimate based on thermochemical data (Table 16.21).

Partial release of nitrogen in the form of free atoms accounts, not only for the thermal stability of azides, but also for certain phenomena that accompany the decomposition, as first noted by L'vov [47]. Among such unusual phenomena are the formation of NO_2 in the decomposition of AgN_3 in the presence of oxygen, noted in [52]. Apparently, this product can be formed by the direct reaction $N + O_2 \rightarrow NO_2$.

Another effect, discovered by Audubert [53] approximately 70 years ago, is strong UV emission in the Vegart–Kaplan molecular band, observed in the course of azide decomposition. This band with peaks at 198, 215, 230, and 240 nm, (also observed in the spectra of auroras) originates from the $A^3\Sigma_u^+ \rightarrow X^1\Sigma_g$ transition in excited N_2^* molecules. Based on the results of independent studies by Kondratiev and Nikitin [54], L'vov [47] suggested that the emission in the Vegart–Kaplan band is caused by the recombination of free nitrogen atoms in accordance with the scheme $N + N \rightarrow N_2^* \rightarrow N_2 + h\nu$. In the decompositions of $Ca(N_3)_2$ and $Ba(N_3)_2$, the UV emission is considerably weaker than in decompositions of KN_3, NaN_3, AgN_3, and $Pb(N_3)_2$. This fact is consistent with the difference in the fraction of atomic nitrogen in the decomposition products formed from these azides.

The calculated decomposition coefficients for all the examined azides are given in Table 16.22. As expected, for azides as typical high-energetic substances, the α_v values ($10^{-13} - 10^{-29}$) are considerably lower than the values typical of other compounds.

Table 16.22 Theoretical values of the vaporization coefficients of azides

Azide	T (K)	Primary Products	P_{eqp} (bar)	Equilibrium Products	P_{eq} (bar)	α_{v}
NaN$_3$	600	Na(g) + 0.86 N + 1.07N$_2$	2.4E−08	Na(g) + 1.5N$_2$	1.6E+06	1.5E−14
KN$_3$	530	K(g) + 0.73N + 1.135N$_2$	1.1E−08	K(g) + 1.5N$_2$	6.2E+05	1.8E−14
AgN$_3$(l)	530	Ag(g) + 0.94N + 1.03N$_2$	4.7E−07	Ag(s) + 1.5N$_2$	1.4E+19	3.4E−26
TlN$_3$	520	Tl(g)$_\downarrow$ + 1.14N + 0.93N$_2$	3.1E−06	Tl(s) + 1.5N$_2$	5.4E+16	5.8E−23
Ca(N$_3$)$_2$	350	Ca(g)$_\downarrow$ + 0.54N + 2.73N$_2$	1.5E−03	Ca(s) + 3N$_2$	5.8E+09	2.5E−13
Sr(N$_3$)$_2$	390	Sr(g)$_\downarrow$ + 0.52N + 2.74N$_2$	1.5E−04	Sr(s) + 3N$_2$	2.9E+08	5.1E−13
Ba(N$_3$)$_2$	400	Ba(g)$_\downarrow$ + 0.74N + 2.63N$_2$	8.1E−06	Ba(s) + 3N$_2$	3.9E+07	2.1E−13
Pb(N$_3$)$_2$	520	Pb(g)$_\downarrow$ + 2.36N + 1.82N$_2$	7.1E−09	Pb(s) + 3N$_2$	3.1E+20	2.3E−29

16.8 Hydroxides

Introduction Dehydrations of metal hydroxides are attractive model reactions for basic studies of the kinetics of solid-state reactions and these reactions are widely used for the commercial production of metal oxides [45]. However, as shown in the recent paper by L'vov and Ugolkov [55], available data on the reaction mechanisms and kinetics are inconsistent. For example, the parameter E for the dehydration of Mg(OH)$_2$, reported in different papers, varies from 53 to 372 kJ mol^{-1}. One of the factors responsible for the large scatter of the E values estimated from Arrhenius plots is the low precision and accuracy of this method, especially as applied to decomposition to gaseous and solid products. The results obtained in [55] by the third-law method, as indicated below, are much more reliable.

Experimental The experiments by L'vov and Ugolkov [55] were performed with an STA 429 thermal analyser using high-purity powders prepared in a laboratory by precipitation of Be, Sr, Ba, Zn, and Cd hydroxides from aqueous solutions and commercial hydroxides of Ca and Mg. The compositions of all the samples were preliminarily checked by their decomposition in the dynamic heating mode. The sample mass was 20 mg for Be(OH)$_2$, 40 mg for Mg(OH)$_2$, and 30 mg for all the other hydroxides. Differences between the results presented below and those reported in [55] are due to the fact that the variation of the surface area of the powder pellet has been taken into account with Eq. 15.5, and the vaporization congruence, through coefficient β. The measurements were performed with continuous evacuation to a residual pressure of $(4–9) \times 10^{-8}$ bar.

   The thermodynamic functions used in the calculations are given in Table 16.23. The initial data and results of determining the molar enthalpy, in accordance with general scheme

$$\text{M(OH)}_2(\text{s}) \leftrightarrow \text{MO(g)} + \text{H}_2\text{O} \rightarrow \text{MO(s)} + \text{H}_2\text{O} \qquad (16.9)$$
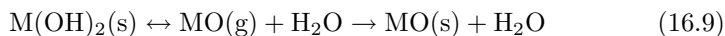
Table 16.23 Values of the thermodynamic functions for some hydroxides and the products of their decompositions [6, 31]

Function[a]	Species	T (K)				
		298	400	500	600	700
$\Delta_f H_T^\circ$	Zn(OH)$_2$(s)	−645.4				
	ZnO(s)	−350.6				
	ZnO(g)	104.8				
	Cd(OH)$_2$(s)	−561.5				
	CdO(s)	−259.0				
	CdO(g)	81.1				
	Be(OH)$_2$(s)		−898.2	−889.3		
	BeO(s)		−606.4	−602.7		
	BeO(g)		137.0	140.1		
	Mg(OH)$_2$(s)			−906.1	−895.9	
	MgO(s)			−593.0	−588.3	
	MgO(g)			39.2	43.1	
	Ca(OH)$_2$(s)			−966.6	−956.2	
	CaO(s)			−625.7	−620.7	
	CaO(g)			49.9	53.4	
	Sr(OH)$_2$(s)			−945.1	−934.2	
	SrO(s)			−580.8	−575.6	
	SrO(g)			7.2	3.7	
	Ba(OH)$_2$(s)				−904.6	−894.9[b]
	BaO(s)				−532.7	−527.3
	BaO(g)				−117.2	−113.6
	H$_2$O(g)	−241.8	−238.3	−234.9	−231.3	−227.6
S_T°	Zn(OH)$_2$(s)	77.0				
	ZnO(s)	43.6				
	ZnO(g)	224.7				
	Cd(OH)$_2$(s)	93.0				
	CdO(s)	54.8				
	CdO(g)	233.0				
	Be(OH)$_2$(s)		67.0	86.7		
	BeO(s)		22.5	30.6		
	BeO(g)		206.3	213.2		
	Mg(OH)$_2$(s)			109.5	128.0	
	MgO(s)			48.6	57.1	
	MgO(g)			230.9	238.0	
	Ca(OH)$_2$(s)			132.5	151.4	
	CaO(s)			62.0	71.1	
	CaO(g)			237.1	243.6	
	Sr(OH)$_2$(s)			144.8	164.6	
	SrO(s)			80.2	89.6	
	SrO(g)			247.7	254.3	
	Ba(OH)$_2$(s)				192.0	207.0[b]
	BaO(s)				107.2	115.5
	BaO(g)				259.6	265.1
	H$_2$O(g)	188.7	198.7	206.4	212.9	218.6

[a] $\Delta_f H_T^\circ$ and S_T° values are in kJ mol^{-1} and J mol^{-1} K^{-1} respectively
[b] At 681.5 K (melting point)

Table 16.24 The initial data [55] and results of determination of the enthalpies for decompositions of some hydroxides by the third-law method

Hydroxide	T (K)	s_0 (mm^2)	α_m	s_m (mm^2)	$\Delta m/\Delta t$ (μg s^{-1})	J^a (kg m^{-2} s^{-1})	P_{eqp} (bar)	β	K_P (bar^2)	$\Delta_r S_T^{\circ\,b}$ (J mol^{-1} K^{-1})	$\Delta_r H_T^{\circ}$ (kJ mol^{-1})
Be(OH)$_2$	406.5	81.5	0.245	74.0	0.770	3.71E−06	1.05E−08	0.849	1.30E−16	337.8	260.9
Be(OH)$_2$	397.0	81.5	0.186	75.8	0.535	2.52E−06	7.03E−09	0.849	5.82E−17	338.2	257.7
Be(OH)$_2$	396.0	81.5	0.204	75.3	0.538	2.55E−06	7.11E−09	0.849	5.96E−17	338.2	256.9
Mg(OH)$_2$	510.4	77.9	0.026	77.2	0.104	4.81E−07	1.95E−09	0.668	5.69E−18	327.4	335.6
Mg(OH)$_2$	535.2	77.9	0.033	77.0	0.260	1.21E−06	5.00E−09	0.668	3.74E−17	326.0	342.8
Mg(OH)$_2$	536.7	77.9	0.059	76.3	0.260	1.22E−06	5.06E−09	0.668	3.83E−17	326.0	343.6
Ca(OH)$_2$	602.3	69.8	0.083	68.2	0.815	4.27E−06	2.13E−08	0.567	8.00E−16	305.2	357.9
Ca(OH)$_2$	572.0	70.7	0.004	70.6	0.315	1.59E−06	7.74E−09	0.567	1.06E−16	307.0	350.6
Ca(OH)$_2$	572.8	70.7	0.022	70.3	0.377	1.92E−06	9.32E−09	0.567	1.53E−16	307.0	349.3
Sr(OH)$_2$	592.3	65.4	0.100	64.0	0.101	5.64E−07	3.39E−09	0.417	2.76E−17	303.4	367.5
Sr(OH)$_2$	592.3	65.4	0.011	65.2	0.113	6.19E−07	3.72E−09	0.417	3.32E−17	303.4	366.6
Ba(OH)$_2$	617.9	63.6	0.395	58.6	0.362	2.21E−06	1.52E−08	0.343	6.74E−16	279.4	352.1
Ba(OH)$_2$	607.5	63.6	0.324	59.5	0.315	1.89E−06	1.29E−08	0.343	4.86E−16	280.0	348.2
Zn(OH)$_2$	398.1	68.1	0.344	62.2	0.648	3.72E−06	1.70E−08	0.470	6.15E−16	336.4	249.9
Zn(OH)$_2$	388.4	68.1	0.223	64.3	0.453	2.52E−06	1.14E−08	0.470	2.76E−16	336.4	246.3
Cd(OH)$_2$	382.0	64.5	0.053	63.8	0.070	3.92E−07	2.01E−09	0.374	1.08E−17	328.8	249.7
Cd(OH)$_2$	388.9	64.5	0.056	63.7	0.098	5.49E−07	2.85E−09	0.374	2.17E−17	328.8	251.9

^{a} $J = (\Delta m/\Delta t)/(2.8 s_m)$

^{b} $\Delta_r S_T^{\circ}$ values for Zn(OH)$_2$ and Cd(OH)$_2$ correspond to 298 K, whereas $\Delta_r S_T^{\circ}$ values for all other hydroxides correspond to the temperatures of experiments (see Table 15.23)

are listed in Table 16.24. The temperature dependences of the thermodynamic functions of $Zn(OH)_2$ and $Cd(OH)_2$ are not tabulated, and therefore the values for 298 K ($\Delta_f H^\circ_{298}$ and S°_{298}) were used.

Results and Discussion Tables 16.24, 16.25, and 16.26 allow the following conclusions.

- The measurement results show good reproducibility due to the use of the third-law method. The relative standard deviation never exceeds 1%.
- The mean T/E ratio (3.2 ± 0.2 K mol kJ^{-1}) is in agreement with the theoretical value (see Sect. 5.1).
- The transfer coefficients τ calculated from Eq. 8.1:

$$\Delta_r H^\circ_T = a\Delta_f H^\circ_T(A) + b\Delta_f H^\circ_T(B) - \Delta_f H^\circ_T(R) + \tau a\Delta_c H^\circ_T(A) =$$
$$= \Delta_v H^\circ_T + \tau a\Delta_c H^\circ_T(A)$$

where $\Delta_v H^\circ_T$ is the enthalpy of dissociative vaporization of a hydroxide (without taking the oxide condensation into account) and $\Delta_c H^\circ_T(A)$ is the enthalpy of condensation of the oxide, vary from 0.44 for $Cd(OH)_2$ to 0.72 for $Be(OH)_2$, which, in accordance with the approximation, Eq. 8.5, is consistent with the variation of c_2. The ratio $(\tau+1.127)/(0.353c_2) = 0.99\pm0.03$.

Table 16.25   Values of the τ parameter for the hydroxide decompositions

Hydroxide	T	$\Delta_r H^\circ_T$	$\Delta_v H^\circ_T$	$\Delta_c H^\circ_T$	c_2[a]	τ	$\dfrac{\tau + 1.127}{0.353c_2}$
	(K)	(kJ mol^{-1})	(kJ mol^{-1})	(kJ mol^{-1})			
$Be(OH)_2$	400	258.5	796.9	-743.4	5.42	0.724	0.968
$Mg(OH)_2$	500	340.7	710.4	-632.2	4.96	0.585	0.978
$Ca(OH)_2$	600	352.6	778.3	-674.1	4.95	0.632	1.006
$Sr(OH)_2$	600	367.0	706.6	-579.3	4.77	0.586	1.017
$Ba(OH)_2$	600	350.2	556.1	-415.5	4.40	0.496	1.045
$Zn(OH)_2$	400	248.1	508.4	-455.4	4.94	0.572	0.974
$Cd(OH)_2$	400	250.8	400.8	-340.1	4.67	0.441	0.951

[a] $c_2 \equiv \ln(-\Delta_c H^\circ_T/RT)$

Table 16.26   The molar enthalpies for the decomposition of hydroxides measured by different methods

Hydroxide	$\Delta_r H^\circ_T/\nu$ (kJ mol^{-1})		Procedure[a]	Ref.
	Third-law [55]	Arrhenius Plot		
$Be(OH)_2$	129.3 ± 1.1	115	I-TG, powder	[56]
$Mg(OH)_2$	170.3 ± 2.2	$126-134$	I-TG, crystal	[57]
$Ca(OH)_2$	176.3 ± 2.4	$145-174$	I-TG, powder	[58]
$Sr(OH)_2$	183.5 ± 0.3	126	NI-TG, powder	[59]
$Ba(OH)_2$	175.1 ± 1.4	63	NI-TG, powder	[59]
$Zn(OH)_2$	124.1 ± 1.2	95	I-TG, powder	[60]
$Cd(OH)_2$	125.4 ± 0.8	$95-116$	I-TG, powder	[61]

[a] I-TG: isothermal TG; NI-TG: non-isothermal TG. In all cases: vacuum

Table 16.27 Calculated values of the vaporization coefficients for the hydroxide decompositions

Hydroxide	T (K)	Primary Products	P_{eqp} (bar)	Equilibrium Products	P_{eq} (bar)	α_v
Be(OH)$_2$	400	BeO(g)$_\downarrow$ + H$_2$O	9.3E−09	BeO(s) + H$_2$O	1.2E+01	7.9E−10
Mg(OH)$_2$	535	MgO(g)$_\downarrow$ + H$_2$O	4.6E−09	MgO(s) + H$_2$O	9.2E−01	5.0E−09
Ca(OH)$_2$	600	CaO(g)$_\downarrow$ + H$_2$O	4.7E−08	CaO(s) + H$_2$O	7.2E−03	6.5E−06
Sr(OH)$_2$	600	SrO(g)$_\downarrow$ + H$_2$O	5.7E−09	SrO(s) + H$_2$O	1.3E−04	4.3E−05
Ba(OH)$_2$	600	BaO(g)$_\downarrow$ + H$_2$O	6.3E−09	BaO(s) + H$_2$O	2.8E−06	2.2E−03
Zn(OH)$_2$	400	ZnO(g)$_\downarrow$ + H$_2$O	2.5E−08	ZnO(s) + H$_2$O	1.6E+01	1.6E−09
Cd(OH)$_2$	400	CdO(g)$_\downarrow$ + H$_2$O	1.0E−08	CdO(s) + H$_2$O	8.6E−01	1.2E−08

- Comparison of the data obtained in [55] with the most reliable published data (Table 16.26) shows that the results obtained from Arrhenius plots are systematically underestimated. This fact can be attributed to the inherent drawbacks of the second-law and Arrhenius plot methods, associated with the effects of the product condensation (see Sect. 8.2) and self-cooling, on the results.

Table 16.27 presents the calculated vaporization coefficients for hydroxides. Decomposition of Be(OH)$_2$ is characterized by the lowest $\alpha_v : 8 \times 10^{-10}$.

16.9 Clays

Introduction Layered silicates, in particular, clays, are of great interest to industry as versatile raw materials. Data on the thermal dehydrations of these materials are required for choosing optimal conditions for their use and preparation of new products. Among different types of clays (kaolinite, muscovite and talc) considered below, kaolinite has been studied in more detail. Nevertheless, even for kaolinite the main features of dehydration remain poorly understood. Above all, the parameters, E, measured by different researchers, are essentially inconsistent [62–69]. In the absence of water vapour, they vary from 159 [62], 172 [67], and 182 kJ mol^{-1} [63] to 213 [66] and 233 kJ mol^{-1} [69]. Still larger discrepancies are observed for the process performed in the presence of water vapour. According to [65], at $P_{H2O} \cong 1$ bar $E = 490$ kJ mol^{-1}, and according to [66], at $P_{H2O} = 6$ and 60 mbar $E = 352$ and 469 kJ mol^{-1}. Anthony and Garn [68] observed an increase in E from 261 to 1,060 kJ mol^{-1} with an increase in P_{H2O} from 0.4 to 3.2 bar. The opposite effect, i.e., a decrease in E in the presence of water vapour, was noted by Toussaint et al. [64], who obtained $E = 105$ kJ mol^{-1} at $P_{H2O} = 6$ mbar, and by Nahdi et al. [69], who measured $E = 188$ kJ mol^{-1} at $P_{H2O} = 5$ mbar.

The observed discrepancies in the values of E are most likely caused by imperfect methods of their determination. In this context, it is not surprising

that, until recently, there was no common view on the dehydration mechanism and effect of water vapour on the dehydration rate.

Experimental The kinetics and mechanism of the dehydration of kaolinite, muscovite, and talc was studied by L'vov and Ugolkov within the framework of the CDV mechanism [70]. The main goal of that study was determination of the enthalpy of decomposition by the third-law method in a high vacuum (equimolar mode) and in the presence of water vapour (isobaric mode). In the isobaric mode, the measurements were performed in air, to eliminate or minimize the effect of self-cooling on the results (see Sect. 15.4).

Experiments were performed with analytically pure-grade kaolinite powder, crystalline muscovite, and talc in the form of mica. The powder (20 mg) was placed in an alumina crucible 4 mm high and 5.7 mm in diameter and manually pelletized. The surface area of rectangular pieces of muscovite and talc (0.2–0.5 mm thick, side length 3–4 mm) was estimated with an MPB-2 optical microscope ($\times 24$).

Measurements in a vacuum were performed with an STA 429 thermal analyser, and those in air, with STA 429 and 449 thermal analysers. The partial water-vapour pressure in air was estimated from the relative humidity (measured with a hygrometer) and tabulated pressures of saturated water vapour at the temperatures in the room (see Appendix, Table A6).

The enthalpy was calculated by the scheme taking into account the condition of congruent vaporization (Sect. 16.6). The thermodynamic functions for kaolinite, muscovite, and talc and of their decomposition products at 298 K are given in Table 16.28. However, published data on the temperature dependences of the enthalpies and entropies of the reactants are lacking. Therefore, to estimate the molar entropies of the reactions the approximation $\Delta_r S_T^\circ / \nu = 160 \pm 9 \text{ J mol}^{-1}\text{K}^{-1}$, valid for reactants decomposing to metal-containing products in the molecular form, was used. The number of moles of the primary decomposition products ν is determined by the reactant stoichiometry and is 5, 12, and 8 for kaolinite, muscovite, and talc, respectively. Therefore, $\Delta_r S_T^\circ$ is equal to 800, 1,920, and 1,280 J mol^{-1}K^{-1}, respectively.

Results and Discussion The conditions of measuring and results of determining the enthalpy of dehydration of kaolinite, muscovite, and talc are given in Tables 16.29–16.31, and the averaged enthalpies and molar enthalpies in various decomposition modes, in Table 16.32. These data allow the following conclusions.

- The enthalpies measured in a high vacuum ($n \times 10^{-8}$ bar) are 6–8% higher than those measured at atmospheric pressure. This is due to self-cooling, which leads to overestimation of the enthalpies measured by the third-law method. As expected, in a low vacuum (10^{-4} bar) the difference is somewhat less pronounced (6% instead of 8% for kaolinite).

Table 16.28 Values of thermodynamic functions for kaolinite, muscovite, talc, and the products of their decomposition at 298 K [6, 31]

Species	$\Delta_f H_{298}^{\circ}$ (kJ mol^{-1})	S_{298}° (J mol^{-1}K^{-1})
$Al_2O_3 \cdot 2SiO_2 \cdot 2H_2O(s)$	−4098.6	203.1
$Al_2O_3(s)$	−1675.7	50.9
$Al_2O_3(g)$	−550.4	313.5
$SiO_2(s)$	−910.7	41.5
$SiO_2(g)$	−322.1	228.6
$H_2O(g)$	−241.8	188.7
$K_2O \cdot 3A_2O_3 \cdot 6SiO_2 \cdot 2H_2O(s)$	−11965.4	612.8
$K_2O(s)$	−361.7	96.0
$K_2O(g)$	−74.1	286.4
$3MgO \cdot 4SiO_2 \cdot H_2O(s)$	−5916.6	261.2
$MgO(s)$	−601.5	27.0
$MgO(g)$	32.3	213.2

- The similarity of the results of the enthalpy determination in various decomposition modes (taking into account the 6–8% difference caused by self-cooling) is in agreement with the CDV mechanism and the calculation scheme based on it.
- The relative standard deviation of the results from the mean value is less than 1–2% (Table 16.32), confirming the high precision of determinations by the third-law method. When averaging the results, the results of determination in a vacuum, and also the less reliable values of $\Delta_r H_T^{\circ}$ corresponding to the primary signals $\Delta m/\Delta t$ less than 0.1 µg s^{-1}, were rejected.
- The enthalpy tends to increase with temperature, especially for kaolinite, which is apparently due to the condensation effect (Sect. 8.2).
- Because of the lack of published thermodynamic functions of reactants at high temperatures, it is impossible to calculate the water-vapour pressure reliably for equilibrium reactions. A rough estimation using the thermodynamic functions at 298 K gives the water-vapour pressure close to 10^{-4} bar at 750 K for kaolinite and 1 bar at 1,285 K for talc. As seen from comparison with data in Tables 16.30 and 16.32, these values correspond to decomposition coefficients α_v of about 4×10^{-4} for kaolinite and 4×10^{-7} for talc.
- The mean value of E for the decomposition of kaolinite in the absence of water vapour, determined in various studies from Arrhenius plots (159 [62], 172 [67], 182 [63], 213 [66], and 233 kJ mol^{-1} [69]), is 192 ± 30 kJ mol^{-1}, being consistent with, but considerably less precise than the value of 196 ± 4 kJ mol^{-1} found in [70] by the third-law method. From the values of E measured in the presence of water vapour, the closest to the value reported in [70], 326 ± 5 kJ mol^{-1}, are the values of 352 and 377 kJ mol^{-1} found in [66] at 6 and 18 mbar of H_2O.

Table 16.29 The experimental conditions and results of determination of the dehydration enthalpies for kaolinite ($Al_2O_3 \cdot 2SiO_2 \cdot 2H_2O$) by the third-law method

Sample	Instrument	P_a (bar)	P_w^{ext} (bar)	T (K)	s_0 (mm^2)	α_m^a	s_m (mm^2)	$\Delta m/\Delta t$ (µg s^{-1})	J^b (kg m^{-2} s^{-1})	P_{eqp} (bar)	K_P^c (bar^5)	$\Delta_r H_T^\circ$ (kJ mol^{-1})
Powder	STA 429	6E–8	6E–10	661.9	61.8	0.14	60.3	0.063	3.73E–07	2.59E–09	4.60E–42	1,053
Powder	STA 429	6E–8	6E–10	672.6	61.8	0.16	60.1	0.083	4.93E–07	3.45E–09	1.93E–41	1,062
Powder	STA 429	8E–5	1.2E–6	673.2	61.8	0.08	60.9	0.147	8.62E–07	6.02E–09	1.25E–35	988
Powder	STA 429	8E–5	1.2E–6	673.8	61.8	0.08	60.9	0.111	6.51E–07	4.55E–09	5.38E–36	994
Powder	STA 429	8E–5	1.2E–6	674.6	61.8	0.13	60.4	0.108	6.39E–07	4.47E–09	5.10E–36	995
Powder	STA 429	1	1.4E–2	715.0	61.8	0.15	60.2	0.062	3.68E–07	2.65E–09	1.45E–28	953
Powder	STA 429	1	1.4E–2	728.8	61.8	0.22	59.4	0.137	8.23E–07	5.99E–09	1.67E–27	957
Powder	STA 449	1	7.9E–3	750.0	58.7	0.25	56.8	0.422	2.65E–06	1.96E–08	1.86E–26	969
Powder	STA 449	1	7.7E–3	770.0	58.2	0.46	54.9	0.568	3.70E–06	2.76E–08	4.96E–26	989

^{a} Decomposition degree at the instant of measurement
^{b} $J = (\Delta m/\Delta t)/(2.8\ s_m)$
^{c} At $\delta = 0.0252$

Table 16.30 The experimental conditions and results of determination of the dehydration enthalpies for muscovite single-crystals ($K_2O \cdot 3Al_2O_3 \cdot 6SiO_2 \cdot 2H_2O$) by the third-law method

Instrument	P_a (bar)	P_w^{ext} (bar)	T (K)	m (mg)	s_0 (mm^2)	α_m [a]	s_m (mm^2)	$\Delta m/\Delta t$ (μg s^{-1})	J [b] (kg m^{-2} s^{-1})	P_{eqp} (bar)	K_P^c (bar^{12})	$\Delta_r H_T^\circ$ (kJ mol^{-1})
STA 429	8E$-$8	8E$-$10	1,070	10.6	99.3	0.75	39.4	0.023	5.84E$-$07	1.03E$-$08	2.00E$-$90	3,912
STA 429	4E$-$8	4E$-$10	1,084	10.2	74.5	0.60	40.4	0.019	4.70E$-$07	8.35E$-$09	1.61E$-$91	3,986
STA 429	1	9.8E$-$3	1,051	16.5	93.6	0.17	82.7	0.100	1.21E$-$06	2.11E$-$08	2.45E$-$71	3,459
STA 429	1	7.5E$-$3	1,051	13.1	110	0.48	71.1	0.054	7.59E$-$07	1.33E$-$08	2.43E$-$73	3,499
STA 449	1	7.6E$-$3	1,070	9.30	64.7	0.40	46.0	0.090	1.96E$-$06	3.45E$-$08	3.35E$-$69	3,478
STA 429	1	5.2E$-$3	1,081	13.7	103	0.40	73.3	0.113	1.54E$-$06	2.73E$-$08	3.23E$-$70	3,534
STA 449	1	9.0E$-$3	1,101	9.21	65.3	0.23	54.9	0.212	3.86E$-$06	6.91E$-$08	3.48E$-$66	3,515
STA 429	1	8.4E$-$3	1,101	18.1	97.3	0.50	61.3	0.162	2.64E$-$06	4.73E$-$08	7.86E$-$68	3,549

[a] The decomposition degree at the instant of measurement

[b] $J = (\Delta m/\Delta t)/s_m$, where $s_m = s_0(1 - \alpha_m)^{2/3}$

[c] At $\delta = 7.11E{-}06$

Table 16.31 The experimental conditions and results of determination of the dehydration enthalpies for single-crystals of talk ($3MgO \cdot 4SiO_2 \cdot H_2O$) by the third-law method

Instrument	P_a (bar)	P_w^{ext} 9bar)	T (K)	m (mg)	s_0 (mm²)	α_m [a]	s_m (mm²)	$\Delta m/\Delta t$ (µg s⁻¹)	J [b] (kg m⁻² s⁻¹)	P_{eqp} (bar)	K_P [c] (bar⁸)	$\Delta_r H_T^\circ$ (kJ mol⁻¹)
STA 429	8E−8	8E−10	1248.2	16.6	58.0	0.52	35.6	0.182	5.11E−06	9.74E−08	2.08E−51	2,809
STA 429	8E−8	8E−10	1258.8	15.0	55.3	0.55	32.5	0.184	5.66E−06	1.08E−07	4.76E−51	2,824
STA 449	1	1.4E−2	1220.7	6.01	37.2	0.35	27.9	0.053	1.90E−06	3.58E−08	1.94E−47	2,654
STA 449	1	1.2E−2	1220.7	8.03	47.1	0.33	36.1	0.070	1.94E−06	3.65E−08	2.22E−47	2,653
STA 429	1	9.9E−3	1250.5	13.3	49.3	0.41	34.7	0.099	2.85E−06	5.44E−08	3.62E−46	2,689
STA 449	1	1.3E−2	1250.7	5.88	34.6	0.46	22.9	0.063	2.75E−06	5.24E−08	2.79E−46	2,692
STA 449	1	1.1E−2	1250.7	6.66	42.2	0.53	25.5	0.076	2.98E−06	5.68E−08	4.90E−46	2,686
STA 429	1	9.9E−3	1275.0	10.8	35.8	0.37	26.3	0.462	1.76E−05	3.38E−07	1.30E−40	2,606
STA 449	1	1.1E−2	1275.0	12.9	39.2	0.34	29.7	0.584	1.97E−05	3.78E−07	2.83E−40	2,597
STA 449	1	8.9E−3	1294.8	15.2	69.8	0.16	62.2	1.63	2.62E−05	5.08E−07	2.24E−39	2,615
STA 449	1	8.4E−3	1294.8	13.8	73.7	0.30	58.1	1.23	2.12E−05	4.11E−07	5.09E−40	2,631

[a] The decomposition degree at the instant of measurement

[b] $J = (\Delta m/\Delta t)/s_m$, where $s_m = s_0(1 - \alpha_m)^{2/3}$

[c] At $\delta = 3.89E{-}06$

Table 16.32 Average values of the reaction enthalpy and the E parameter for the equimolar and isobaric modes of clay decompositions

Reactant	Primary Products of Decomposition	T (K)	$\Delta_r H_T^\circ$ (kJ mol^{-1})	E (kJ mol^{-1}) e-mode	i-mode
Kaolinite	$Al_2O_3(g)_\downarrow + 2SiO_2(g)_\downarrow + 2H_2O$	750	978 ± 16	196 ± 4	326 ± 5
Muscovite	$K_2O(g)_\downarrow + 3Al_2O_3(g)_\downarrow + 6SiO_2(g)_\downarrow + 2H_2O$	1,100	$3,506 \pm 19$	292 ± 2	351 ± 2
Talc	$3MgO(g)_\downarrow + 4SiO_2(g)_\downarrow + H_2O$	1,285	$2,612 \pm 16$	327 ± 2	373 ± 2

- The parameters E found in [70] for muscovite and talc in the isobaric mode (351 and 373 kJ mol^{-1}) are consistent with the E^i values (376 and 423 kJ mol^{-1}) reported in [71, 72].

The data discussed in this section show that the *effect of water vapour on the decomposition kinetics of clays is in full agreement with the CDV mechanism and is quite similar to the effect of water on the kinetics of decomposition of metal hydroxides and crystalline hydrates.* Therefore, the wide use of the term "dehydroxylation" (see, e.g., [64–69]), as applied to dehydration of clays, provokes obvious objections. The cause of the large differences between the decomposition temperatures of hydroxides and hydrates, on the one hand, and clays, on the other, was discussed in Sect. 5.5.

16.10   Hydrates

Introduction Hydrates of metal salts undoubtedly played a leading part in the history of the kinetics of solid-state reactions. Particularly noteworthy are the first observations of the dehydration of crystalline hydrates, made by Faraday after scratching the crystal surface (Chapter 1), and the anomalous acceleration of the dehydrations of some crystalline hydrates in the presence of water vapour, discovered by Topley and Smith (Chapter 7).

Localization of reactions and appearance of decomposition patterns, specific features of formation of crystalline and X-ray amorphous dehydration products, nucleation, self-cooling – these are only a few examples of research subjects for crystalline hydrates [43, 45]. Recently the interest in dehydration kinetics was expressed in an attempt (unfortunately, unsuccessful) to use the dehydration of $Li_2SO_4 \cdot H_2O$ as a kinetics standard [73].

The studies of dehydration processes by L'vov and his colleagues during the last decade gave some additional important results. The primary products of the low-temperature dehydration of $Cu(NO_3)_2 \cdot 3H_2O$ were identified by quadrupole mass spectrometry [74]; the congruent mechanism of dehydration was confirmed for $Li_2SO_4 \cdot H_2O$ [75]; the T–S effect was interpreted [76];

Table 16.33 Values of the thermodynamic functions for some hydrates and the products of their decompositions [6, 31]

Species	$\Delta_f H^\circ_{298}$ (kJ mol^{-1})	S°_{298} (J mol^{-1} K^{-1})	Species	$\Delta_f H^\circ_{298}$ (kJ mol^{-1})	S°_{298} (J mol^{-1} K^{-1})
$Li_2SO_4 \cdot H_2O(s)$	−1736.4	146.4	$CaSO_4(g)$		296.2[b]
$Li_2SO_4(s)$	−1436.0	114.0	$CuSO_4 \cdot 5H_2O(s)$	−2279.4	300.4
$Li_2SO_4(g)$	−1048.0[a]	309.5[b]	$CuSO_4(s)$	−770.9	109.2
$CaSO_4 \cdot 2H_2O(s)$	−2024.8	194.1	$CuSO_4(g)$		311.3[b]
$CaSO_4(s)$	−1434.5	107.0	$H_2O(g)$	−241.8	188.7

[a] By estimation [86]
[b] By estimation [77]

the extent of self-cooling was measured [77], and the third-law method was applied to determine the enthalpies of dehydration of crystalline hydrates in air [78]. The specific features of dehydration of crystalline hydrates in various modes were used in [79] to prove the CDV mechanism.

Below, only the data concerning the determination of the enthalpies of dehydration of $Li_2SO_4 \cdot H_2O$, $CaSO_4 \cdot 2H_2O$, and $CuSO_4 \cdot 5H_2O$ by the third-law method [77, 78] and published data [80–85] are presented. One of problems for hydrates is the lack of reliable values of thermodynamic functions for salt molecules in the gaseous state. The entropies given in Table 16.33 were found in [77] by comparing the known entropies of the molecules of Na, K, Rb, and Cs sulphates with the entropies of the corresponding oxides. The mean difference, S°_{298} (sulphate) − S°_{298}(oxide) = 76.7 ± 5.2 J mol^{-1} K^{-1}, was used to estimate the entropies of the Li_2SO_4, $CaSO_4$, and $CuSO_4$ molecules.

Experimental The measurement conditions and the molar enthalpies of dehydration of $Li_2SO_4 \cdot H_2O$, $CaSO_4 \cdot 2H_2O$, and $CuSO_4 \cdot 5H_2O$, determined by the third-law method from the results of measurements by L'vov and Ugolkov [77, 78] and other published data [80–85], are given in Tables 16.34 and 16.35. The measurements in [77, 78] were performed with an STA 429 thermal analyser. The $Li_2SO_4 \cdot H_2O$ crystals (analytically pure grade) were grown under laboratory conditions. Open alumina crucibles 4.0 mm high, with an inside diameter of 5.7 mm were used. The surface areas of the crystals were estimated with an MPB-2 optical microscope (×24). Measurements with $Li_2SO_4 \cdot H_2O$ crystals were performed in a vacuum (equimolar mode) and in air (isobaric mode). The water-vapour content was estimated from digital hygrometer readings (relative humidity) and the saturated vapour pressure of H_2O at a given air temperature in the room.

In [80–85], measurements were performed with a laboratory-made precision thermal balance. In all cases, single crystals of the reactants were used. In [81–85], to improve the thermal contact between the crystal and the cylindrical

Table 16.34 Experimental conditions and the results of determination of the molar enthalpy of dehydration of $Li_2SO_4 \cdot H_2O$ by the third-law method [77, 78]

Sample	P_a (bar)	P_w^{ext} (bar)	T (K)	m_0 (mg)	s_0 (mm²)	α_m [a]	s_m [b] (mm²)	$\Delta m/\Delta t$ (μg s⁻¹)	J (kg m⁻² s⁻¹)	P_{eqp} (bar)	K_P [c] (bar²)	$\Delta_r S_T^\circ/\nu$ (J mol⁻¹ K⁻¹)	$\Delta_r H_T^\circ/\nu$ (kJ mol⁻¹)
Powder	8E−08	8E−10	342.9	40	68.9	0.52	60.0	1.000	5.95E−06	5.94E−08	6.61E−15	174.4	106.3
Powder	8E−08	8E−10	335.6	40	68.9	0.14	66.4	0.820	4.41E−06	4.36E−08	4.35E−15	174.7	104.8
Crystal	5E−07	5E−09	326.9	10.4	27.9	0.12	25.6	0.052	2.03E−06	1.98E−08	9.68E−16	175.0	104.2
Crystal	5E−07	5E−09	327.4	12.7	29.5	0.13	26.9	0.059	2.19E−06	2.14E−08	1.13E−15	175.0	104.1
Crystal	1	1.1E−02	350.9	49.5	141	0.02	139	0.047	3.38E−07	3.41E−09	9.27E−11	174.1	96.7
Crystal	1	9.4E−03	351.7	29.7	42.4	0.01	42.1	0.024	5.70E−07	5.76E−09	1.34E−10	174.1	96.8
Crystal	1	9.9E−03	352.0	10.3	39.2	0.03	38.4	0.028	7.29E−07	7.37E−09	1.80E−10	174.1	94.2
Crystal	1	1.1E−02	360.1	13.9	31.7	0.14	28.7	0.118	4.11E−06	4.21E−08	1.14E−09	173.9	95.7
Crystal	1	8.9E−03	360.9	12.1	29.5	0.16	26.3	0.147	5.59E−06	5.72E−08	1.26E−09	173.8	95.0
Crystal	1	1.4E−02	376.4	9.7	40.4	0.34	30.6	0.374	1.22E−05	1.28E−07	4.42E−09	173.3	96.5
Crystal	1	1.3E−02	382.0	15.1	26.0	0.30	20.5	0.719	3.51E−05	3.69E−07	1.19E−08	173.1	98.0

[a] The decomposition degree at the instant of measurement

[b] The surface area at the instant of measurement calculated with the formulas $s_m = s_0 - (s_0 - 51.0)\alpha_m$ for powders and $s_m = s_0(1 - \alpha_m)^{2/3}$ for crystals

[c] At $\beta = 0.405$

Table 16.35 The experimental conditions and results of determination of the reaction enthalpy for the dehydrations of $Li_2SO_4 \cdot H_2O$, $CaSO_4 \cdot 2H_2O$, and $CuSO_4 \cdot 5H_2O$ by the third- and second-law methods [80–85]

Hydrate	T (K)	P_{eqp} (bar)	$\ln K_P$[a]	$\Delta_r S^\circ_{298}/\nu$ (J mol^{-1} K^{-1})	$\Delta_r H^\circ_T/\nu$ (kJ mol^{-1}) Third-law	Second-law	Ref.
$Li_2SO_4 \cdot H_2O$	300	5.32E−10	−41.8	175.9	104.9	87.1 ± 0.8	[81]
$Li_2SO_4 \cdot H_2O$	315	1.04E−09	−40.5	175.3	108.2	84.9 ± 0.8	[84]
$Li_2SO_4 \cdot H_2O$	348	2.74E−07	−29.3	174.2	103.0	50.6	[85]
$CaSO_4 \cdot 2H_2O$	288	3.98E−10	−64.6	159.8	97.6	82.8 ± 1.6	[83]
$CuSO_4 \cdot 5H_2O$	273	9.58E−10	−125.1	159.1	90.8	76.2	[80]
$CuSO_4 \cdot 5H_2O$	255	2.08E−10	−134.3	159.1	88.0	74.5 ± 0.8	[82]

[a] At $\beta = 0.405$, 0.728 and 1.678 for $Li_2SO_4 \cdot H_2O$, $CaSO_4 \cdot 2H_2O$, and $CuSO_4 \cdot 5H_2O$

holder, the lower and lateral surfaces of the crystal were coated with an In–Ga eutectic mixture. All the measurements were performed under isothermal conditions in a high vacuum.

Results and Discussion The data in Tables 16.34 and 16.35 allow the following conclusions.

- The molar enthalpies of dehydration of $Li_2SO_4 \cdot H_2O$ in a vacuum, found in [77, 78] and determined from data of [81, 84, 85], virtually coincide. The mean values of $\Delta_r H^\circ_T/\nu$ were 104.9 ± 1.0 and 105.4 ± 2.6 kJ mol^{-1}, respectively, exceeding by approximately 9 kJ mol^{-1} the mean value of $\Delta_r H^\circ_T/\nu$ for the series of measurements in air (96.1 ± 0.8 kJ mol^{-1} [78]). This difference is apparently associated with the self-cooling of the samples in a vacuum.
- For the same reason, the molar enthalpies measured in a vacuum by the second-law method (86.0 ± 1.1 kJ mol^{-1} [81, 84]) appear to be approximately 10 kJ mol^{-1} lower than the enthalpies measured in air. The value of $\Delta_r H^\circ_T/\nu = 50.6$ kJ mol^{-1} [83], obtained for $Li_2SO_4 \cdot H_2O$ at high decomposition temperatures (348–433 K), is still more underestimated. Apparently, the condensation effect is added here to the self-cooling effect. The molar enthalpies determined for $CaSO_4 \cdot 2H_2O$ and $CuSO_4 \cdot 5H_2O$ by the second- and third-law methods differ to approximately the same extent.
- From the thermodynamic functions given in Table 16.33, the transfer coefficient τ, defined (see Sect. 8.1) as $\tau = (\Delta_r H^\circ_T - \Delta_v H^\circ_T)/a\Delta_c H^\circ_T$, can be calculated. Insertion of $\Delta_r H^\circ_{298} = 192.2$ kJ mol^{-1}, $\Delta_v H^\circ_{298} = 446.6$ kJ mol^{-1} and $\Delta_c H^\circ_{298} = -388.0$ kJ mol^{-1} in this equation gives $\tau = 0.656$. This value coincides with the value of $\tau_2 = 0.655$ at 300 K, calculated from approximating Eq. 7.5, where $c_2 \equiv \ln[-\Delta_c H^\circ_T/(RT)]$.

The calculated vaporization coefficients of the hydrates studied are listed in Table 16.36. For $Li_2SO_4 \cdot H_2O$ and $CaSO_4 \cdot 2H_2O$, α_v is about 10^{-8}, and for $CuSO_4 \cdot 5H_2O$, about 10^{-6}.

Table 16.36 Theoretical values of the vaporization coefficients for some hydrates

Hydrate	T (K)	Primary Products	P_{eqp} (bar)	Equilibrium Products	P_{eq} (bar)	α_v
$Li_2SO_4 \cdot H_2O$	300	$Li_2SO_4(g)_\downarrow + H_2O$	8.7E−10	$Li_2SO_4(s) + H_2O$	9.6E−02	9.1E−09
$CaSO_4 \cdot 2H_2O$	288	$CaSO_4(g)_\downarrow + 2H_2O$	3.9E−10	$CaSO_4(s) + 2H_2O$	4.0E−02	9.8E−09
$CuSO_4 \cdot 5H_2O$	273	$CuSO_4(g)_\downarrow + 5H_2O$	1.2E−09	$CuSO_4(s) + 5H_2O$	1.0E−03	1.2E−06

16.11 Nitrates

Introduction The kinetics and mechanisms of the decompositions of nitrates have been discussed in several extensive reviews [45, 87, 88]. During the last 25 years, metal nitrates have been thoroughly studied by electrothermal AAS and quadrupole MS (see Sects. 2.3 and 2.7). In the course of these studies, the CDV mechanism was discovered [89] and the composition of the primary decomposition products of Ag, Cd, Cu, and Pb nitrates was determined [90]. A recent TG study of the effect of reactant melting on the decomposition rate [91] confirmed the CDV mechanism (Sect. 8.3). The above-mentioned results are considered in part in this section.

Figures 16.2 and 16.3 show the mass- spectrometric patterns [90] characterizing the composition of the primary decomposition products on heating of microgram amounts of $AgNO_3$ and $Cd(NO_3)_2$ at a rate of about $1\,K\,s^{-1}$ on tantalum (Fig. 16.2) and graphite (Fig. 16.3) platforms. The quadrupole mass spectrometer described in Sect. 2.3 (Fig. 2.1) was used. Detailed quantitative analysis of the data obtained led to the following conclusions [90].

- The major decomposition pathway is as follows:

$$AgNO_3(s/l) \leftrightarrow Ag(g)_\downarrow + NO_2 + 1/2O_2$$
$$Cd(NO_3)_2(s/l) \leftrightarrow CdO(g)_\downarrow + 2NO_2 + 1/2O_2$$
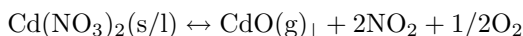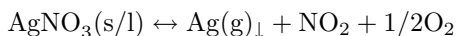
  The decomposition is accompanied by partial vaporization of the unchanged initial nitrates. L'vov and Novichikhin [90] noted the absence of the expected O_2^+ signal in the mass spectrum of the decomposition products of $Cd(NO_3)_2$ and suggested that oxygen is released in some form other than O_2.
- The content of volatile and low-volatility products, calculated taking into account the isotopic composition of the elements and the ionization cross sections of the components, indicates that the decomposition is congruent.
- In the course of low-temperature decomposition of the nitrates, approximately half of the low-volatility product (Ag or CdO) condenses on the platform surface. This is confirmed, in particular, by the fact that the sum of the intensities of low-temperature peaks of CdO^+, $CdNO_3^+$, and Cd^+ in decomposition of $Cd(NO_3)_2$ is close to the intensity of the high-temperature peak of Cd^+ in the decomposition of CdO (Fig. 16.3). A similar conclusion was reached for the decompositions of nickel and lead nitrates (Figs. 2.3 and 2.4).
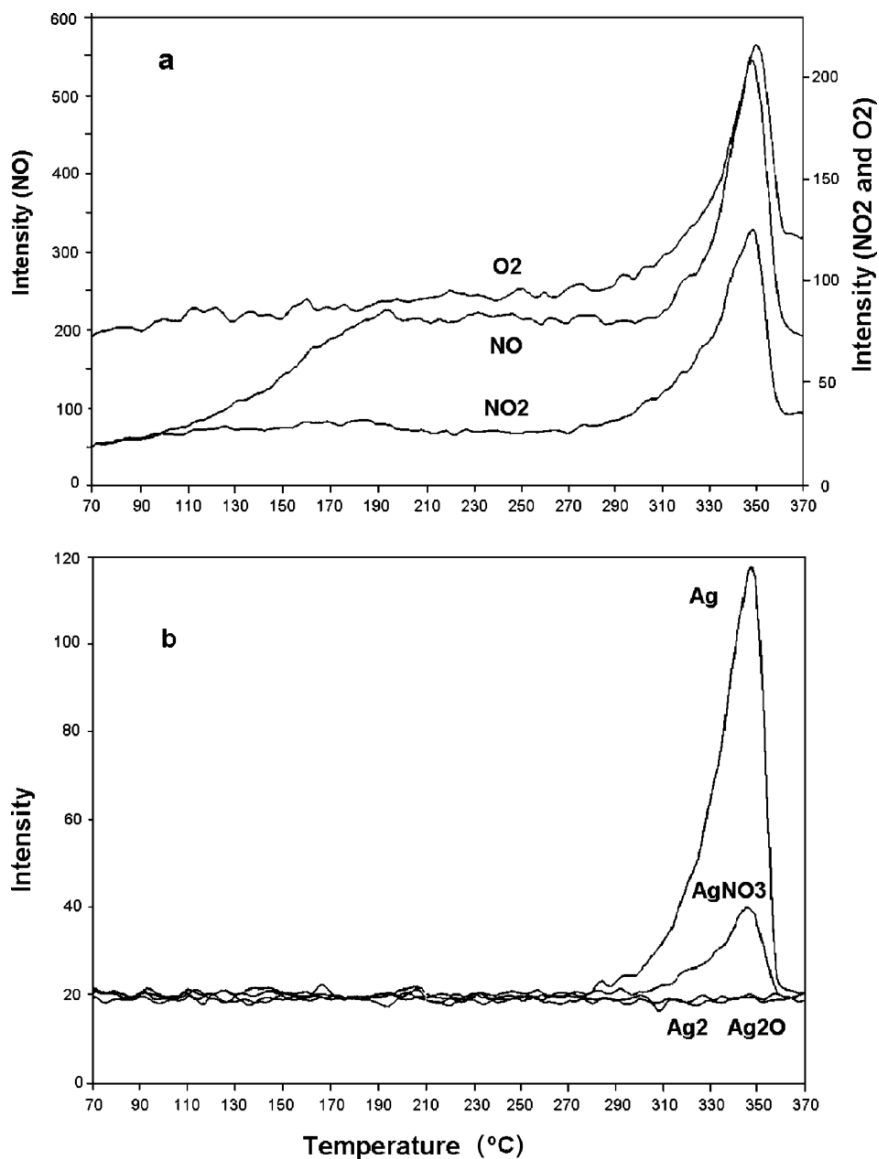
Fig. 16.2 Mass intensity signals in the process of heating $(1\,\mathrm{K\,s^{-1}})$ of 16 µg of $AgNO_3$ on a tantalum platform: (a) ions of volatile products, (b) ions of low-volatility products [90]

Experimental The recent study by L'vov and Ugolkov [91] mainly concerned the TG determination of the molar enthalpies of decomposition of solid and molten silver and cadmium nitrates by the third-law method. The rates of $Cd(NO_3)_2$ decomposition in pure nitrogen and in air were also measured.
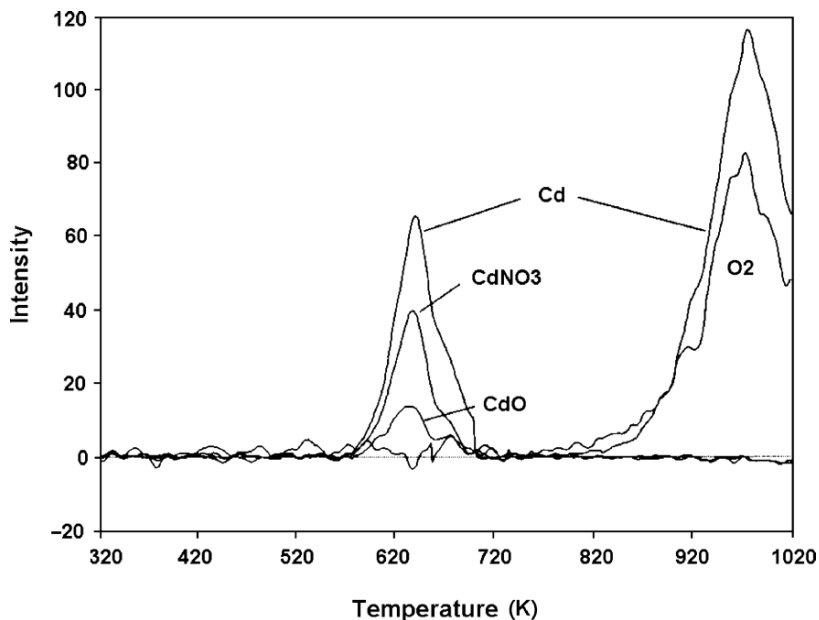
Fig. 16.3 Mass intensity signals in the process of heating $(1\,\mathrm{K}\,\mathrm{s}^{-1})$ of 8μg of $Cd(NO_3)_2$ on a graphite platform [90]

These experiments were aimed at revealing the chemical form of oxygen released in the course of the decomposition. If the primary decomposition product is O_2, then the presence of oxygen in the reactor (at a pressure of about 0.21 bar) should decelerate the process by a factor of $2,100^{1/6} \cong 3.6$ as compared to the atmosphere of nitrogen containing about 10^{-4} bar of O_2 (see Sect. 3.6). If the primary decomposition product is atomic oxygen, then the presence of O_2 in the reactor should not affect the decomposition rate.

The experiments involving determination of the molar enthalpy were performed with an STA 429 thermal analyser in a vacuum $(10^{-7} - 10^{-8}$ bar$)$ under the same conditions as those described above (Sect. 16.10). The reactants were high-purity $AgNO_3$ and $Cd(NO_3)_2$ powders. The sample mass was 20 mg. In the experiments with molten nitrates, the powders of the nitrates were mixed with Al_2O_3 (see Sect. 15.1) prior to heating, to prevent spillage of the melt over the crucible walls. The thermodynamic functions used in the calculations are given in Table 16.37.

Results and Discussion The results of the majority of experiments are given in Table 16.38, and some results of these studies are summarized in Tables 16.39 and 16.40. They allow the following conclusions.

Table 16.37 Values of the thermodynamic functions for some nitrates and the products of their decompositions [6, 31, 88]

Function[a]	Species	T (K)			
		400	500	600	700
$\Delta_f H_T^\circ$	AgNO$_3$(s/l)	−114.1	−88.2	−75.4	
	Ag(s)	2.6	5.2	7.9	
	Ag(g)	287.0	289.1	291.2	
	Cd(NO$_3$)$_2$(s/l)		−421.1[b]	−400.9[b]	−360.9[b]
	CdO(s)		−248.0	−242.9	−237.5
	CdO(g)		88.0[b]	91.6[b]	95.2[b]
	NO$_2$(g)	38.1	42.4	46.9	51.6
	O$_2$(g)	3.0	6.1	9.2	12.5
	O(g)		253.5	255.6	257.7
S_T°	AgNO$_3$(s/l)	171.1	227.1	250.5	
	Ag(s)	50.2	55.9	60.9	
	Ag(g)	179.0	183.4	187.4	
	Cd(NO$_3$)$_2$(s/l)		287.1[b]	323.9[b]	386.4[b]
	CdO(s)		79.7	90.0	98.3
	CdO(g)		250.8[b]	257.3[b]	262.8[b]
	NO$_2$(g)	251.5	260.8	269.0	276.4
	O$_2$(g)	213.8	220.6	226.3	231.4
	O(g)		172.1	176.0	179.2

[a] $\Delta_f H_T^\circ$ and S_T° values are in kJ mol^{-1} and J mol^{-1}K^{-1}, respectively
[b] High-temperature increments for the corresponding Ba species are used [6]

- Comparative measurements of the absolute decomposition rates of Cd(NO$_3$)$_2$ in nitrogen and in air gave essentially the same results. The $J(N_2)/J(air)$ ratio at 680 ± 1 K, determined from three replicate runs, appeared to be 0.9 ± 0.1, whereas for the release of molecular oxygen this ratio should be equal to 3.6. This fact means that, in contrast to the commonly accepted interpretation, the decomposition of cadmium nitrate can be described by the reaction

$$Cd(NO_3)_2(s/l) \leftrightarrow CdO(g)_\downarrow + 2NO_2 + O \qquad (16.10)$$

This conclusion is fully consistent with the assumption made by L'vov and Novichikhin [90], who found no O$_2^+$ signal in the mass spectrum of Cd(NO$_3$)$_2$ decomposition products and suggested that oxygen was released in a form other than O$_2$.

- Table 16.38 shows that the absolute decomposition rates of molten silver nitrate diluted with Al$_2$O$_3$ powder in 1:1 and 1:5 ratios are virtually identical. That is, a threefold difference in the concentration of AgNO$_3$ in Al$_2$O$_3$ does not affect the decomposition rate. This fact means that the initial distribution of the molten reactant throughout the bulk of the pellet at any concentration of the melt reproduces the morphology of the solid sample (structure of Al$_2$O$_3$ powder). Correspondingly, the geometric factor (2.8) introduced in calculations of the absolute rates for powder pellets is equally applicable to melts distributed in these pellets.

Table 16.38 The experimental conditions and results of determination of the molar enthalpies for $AgNO_3$ and $Cd(NO_3)_2$ decompositions by the third-law method (the melting points of these nitrates are 483 and 633 K, respectively) [91]

Nitrate	T (K)	s_0 (mm²)	α_m	$\Delta m/\Delta t$ (μg s⁻¹)	J^a (kg m⁻² s⁻¹)	P_{NO_2} (bar)	δ	$\ln K_P$	$\Delta_r S_T^\circ$ (J mol⁻¹ K⁻¹)	$\Delta_r H_T^\circ/\nu$ (kJ mol⁻¹)
$AgNO_3(s)$	472.5	58.2	0.071	0.059	3.65E−07	2.65E−09	1.011	−50.11	357.1	146.2
$AgNO_3(s)$	472.0	58.2	0.017	0.047	2.89E−07	2.11E−09	1.011	−50.69	357.1	147.0
$AgNO_3(s)$	471.8	58.2	0.016	0.050	3.07E−07	2.25E−09	1.011	−50.54	357.1	146.7
$AgNO_3(l)^b$	573.5	61.8	0.185	0.130	7.76E−07	6.06E−09	1.011	−47.98	321.3	165.2
$AgNO_3(l)^b$	574.5	61.8	0.187	0.100	5.97E−07	4.67E−09	1.011	−48.63	321.3	166.8
$AgNO_3(l)^b$	574.2	61.8	0.180	0.124	7.40E−07	5.79E−09	1.011	−48.10	321.3	165.6
$AgNO_3(l)^c$	572.4	61.8	0.121	0.128	7.56E−07	5.96E−09	1.011	−48.05	321.4	165.1
$AgNO_3(l)^c$	571.6	61.8	0.165	0.123	7.32E−07	5.73E−09	1.011	−48.13	321.4	165.0
$Cd(NO_3)_2(s)$	573.7	58.2	0.371	1.10	7.07E−06	5.45E−08	4.065	−71.53	649.9	178.5
$Cd(NO_3)_2(s)$	553.5	58.2	0.377	0.48	3.09E−06	2.34E−08	4.065	−74.92	651.9	176.4
$Cd(NO_3)_2(l)^c$	658.6	62.7	0.50	1.43	8.98E−06	7.04E−08	4.065	−70.30	612.6	197.1
$Cd(NO_3)_2(l)^c$	660.7	62.7	0.49	1.21	7.59E−06	5.97E−08	4.065	−70.97	612.4	198.6
$Cd(NO_3)_2(l)^c$	651.4	62.7	0.49	0.76	4.76E−06	3.72E−08	4.065	−72.86	613.4	198.5

[a] $J = (\Delta m/\Delta t)/(2.8\ s_m)$ in all cases

[b] Mixture of $AgNO_3$ with Al_2O_3 (1:5)

[c] Mixture of $AgNO_3$ or $Cd(NO_3)_2$ with Al_2O_3 (1:1)

Table 16.39 Thermochemical parameters for nitrate decompositions

Reaction	T (K)	$\Delta_r H^\circ_T/\nu$ (kJ mol^{-1})	$\Delta_v H^\circ_T/\nu$ (kJ mol^{-1})	$\Delta_c H^\circ_T$ (kJ mol^{-1})	c_2	τ Eq. 7.2	τ Eq. 7.5
AgNO$_3$(s) $\leftrightarrow$ Ag(g)$_\downarrow$ + NO$_2$ + $^1\!/_2$ O$_2$	472	146.6 ± 0.4	176.0	−284.2	4.28	0.259	0.384
AgNO$_3$(l) $\leftrightarrow$ Ag(g) + NO$_2$ + $^1\!/_2$ O$_2$	573	165.5 ± 0.8	167.7		0	0	0
Cd(NO$_3$)$_2$(s) $\leftrightarrow$ CdO(g)$_\downarrow$ + 2NO$_2$ + O	563	177.5 ± 1.0	210.5	−335.4	4.27	0.394	0.380
Cd(NO$_3$)$_2$(l) $\leftrightarrow$ CdO(g) + 2NO$_2$ + O	657	198.1 ± 0.8	204.3		0	0	0

Table 16.40 Calculated values of the vaporization coefficients for solid and melted AgNO$_3$ and Cd(NO$_3$)$_2$

Nitrate	T (K)	Primary Products	P_{eqp} (bar)	Equilibrium Products	P_{eq} (bar)	α_v
AgNO$_3$(s)	472	Ag(g) + NO$_2$ + $^1\!/_2$ O$_2$	2.3E−09	Ag(s) + NO$_2$ + $^1\!/_2$ O$_2$	5.5E−04	4.3E−06
AgNO$_3$(l)	573	Ag(g) + NO$_2$ + $^1\!/_2$ O$_2$	5.8E−09	Ag(s) + NO$_2$ + $^1\!/_2$ O$_2$	3.3E−02	1.8E−07
Cd(NO$_3$)$_2$(s)	563	CdO(g) + 2NO$_2$ + O	3.9E−08	CdO(s) + 2NO$_2$ + $^1\!/_2$ O$_2$	4.8E−02	8.2E−07
Cd(NO$_3$)$_2$(l)	657	CdO(g) + 2NO$_2$ + O	5.6E−08	CdO(s) + 2NO$_2$ + $^1\!/_2$ O$_2$	3.5E−00	1.6E−08

- The molar enthalpies of decomposition of both molten nitrates (Table 16.39) appear to be 20 kJ mol^{-1} higher compared to the solid nitrates, which is in full agreement with the CDV mechanism involving partial transfer of the condensation energy to the reactant in the zone of the reaction between the solid reactant and solid product. If there is no such zone (in particular, in the case of reactant melting), the enthalpy of the decomposition $(\Delta_r H_T^\circ / \nu)$ should correspond to the enthalpy of the straight vaporization process $(\Delta_v H_T^\circ / \nu)$, calculated from the thermochemical data. The experimental results (165.5 and 198.1 kJ mol^{-1}) can be considered as being consistent with the calculated values (167.7 and 204.3 kJ mol^{-1}), taking into account the relatively low reliability of the tabulated $\Delta_f H_T^\circ$ values for both nitrates.
- The molar enthalpies measured for molten silver nitrate (165.5 $\pm$ 0.8 kJ mol^{-1}) and molten cadmium nitrate (198.1 $\pm$ 0.8 kJ mol^{-1}) by the third-law method [91] are consistent with the results of their determination from Arrhenius plots: 167 $\pm$ 3 kJ mol^{-1} [90] and 186 $\pm$ 11 kJ mol^{-1} [92], respectively. The molar enthalpy measured by the third-law method for solid cadmium nitrate (177.5 $\pm$ 1.0 kJ mol^{-1}) [90] coincides with the value found in [90], 177 $\pm$ 3.0 kJ mol^{-1}.
- The coefficients τ (Table 16.39) calculated with the approximation Eq. 8.5 and defining Eq. 8.2 agree reasonably with each other. The calculated vaporization coefficients α_v are within 10^{-6}–10^{-8} (Table 16.40).

16.12 Sulphates

Introduction Thermal decomposition of metal sulphates is one of the techniques for commercial production of sulfur dioxide and various metal oxides. Therefore, kinetic and mechanistic studies of these reactions are of both scientific and practical interest. The majority of studies in the field of decompositions of sulphates were performed in the period up until the 1970s [45, 93–97]. The decompositions of $BaSO_4$ and $MgSO_4$ were studied in more detail. Their decompositions are still commonly interpreted as two-step processes [45]:

$$MSO_4 \leftrightarrow MO(s) + SO_3, \qquad (16.11)$$
$$SO_3 \leftrightarrow SO_2 + 1/2O_2 \qquad (16.12)$$
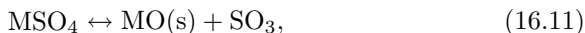
However, even in 1976, Mohazzabi and Searcy [97] examined the decomposition products by mass spectrometry and concluded that the following scheme is more adequate:

$$BaSO_4 \leftrightarrow BaO(s) + SO_2 + 1/2O_2 \qquad (16.13)$$
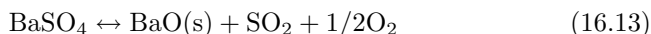
Two decades later, L'vov and Novichikhin [5] performed a thermochemical analysis of the published data for $BaSO_4$ and $MgSO_4$, and concluded that

the decomposition follows the CDV mechanism, common for solids, with the formation of gaseous oxides (followed by their condensation), SO_2 and atomic oxygen:

$$BaSO_4 \leftrightarrow BaO(g) + SO_2 + O \qquad (16.14)$$

$$MgSO_4 \leftrightarrow MgO(g)_{\downarrow} + SO_2 + O \qquad (16.15)$$
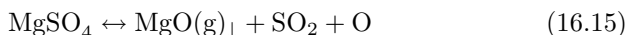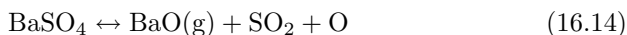
The discussion below is based on L'vov and Ugolkov's recent paper [98], dealing with further experimental and theoretical studies of the decompositions of these sulphates.

Experimental Experiments were performed with an STA 429 thermal analyser under the conditions described above (Sect. 16.10). To reveal the chemical form of oxygen released in the course of the decomposition, comparative experiments were performed on the kinetics of the $MgSO_4$ decomposition in nitrogen and in air. The thermodynamic functions of $MgSO_4$ and $BaSO_4$ and of their decomposition products are given in Tables 16.41 and 16.42, and the main measurement results, in Tables 16.43–16.45.

Results and Discussion The results of these studies are as follows.

- The rates of $MgSO_4$ decomposition in nitrogen and in air appeared to be virtually equal, whereas a decrease in the decomposition rate in air (in the presence of 0.21 bar of O_2) by a factor of 15.4 would be expected if the primary decomposition product were molecular oxygen. This fact means that, in the course of decomposition of crystalline sulphates, in accordance with Eq. 16.13, oxygen is released in the atomic form.

Table 16.41 Values of the thermodynamic functions for $MgSO_4$ and the products of its decomposition [6]

Function[a]	Species	T (K)		
		1,000	1,100	1,200
$\Delta_f H_T^\circ$	$MgSO_4(s)$	−1198.3	−1182.9	−1167.0
	$MgO(s)$	−568.6	−563.5	−558.3
	$MgO(g)$	62.7	68.3	73.8
	$SO_2(g)$	−262.5	−257.0	−251.5
	$O(g)$	264.0	266.1	268.2
$\Delta_c H_T^\circ$	$MgO(g)_{\downarrow}$	−631.3	−631.7	−632.1
$\Delta_v H_T^\circ/\nu$		420.9	420.1	419.2
S_T°	$MgSO_4(s)$	241.1	255.8	269.6
	$MgO(s)$	82.2	87.1	91.6
	$MgO(g)$	262.7	268.0	272.8
	$SO_2(g)$	305.5	310.7	315.6
	$O(g)$	186.7	188.7	190.5
$\Delta_r S_T^\circ/\nu$		171.3	170.5	169.8

[a] ΔH_T° and S_T° values are in kJ mol^{-1} and J mol^{-1}K^{-1}, respectively

Table 16.42 Values of the thermodynamic functions for BaSO$_4$ and the products of its decomposition [6]

Function[a]	Species	T (K)			
		1,400	1,423[b]	1,423[b]	1,500
$\Delta_f H_T^\circ$	BaSO$_4$(s)	-1292.9	-1288.7	-1278.7	-1265.6
	BaO(s)	-487.1			-481.1
	BaO(g)	-87.7			-83.9
	SO$_2$(g)	-240.3			-234.6
	O(g)	272.4			274.5
$\Delta_c H_T^\circ$	BaO(g)$_\downarrow$	-399.4			-397.2
$\Delta_v H_T^\circ/\nu$		412.5			407.2
S_T°	BaSO$_4$(s)	350.5	353.5	360.5	369.5
	BaO(s)	155.1			159.2
	BaO(g)	290.8			293.4
	SO$_2$(g)	324.2			328.1
	O(g)	193.7			195.1
$\Delta_r S_T^\circ/\nu$		152.7			149.0

[a] ΔH_T° and S_T° values are in kJ mol^{-1} and J mol^{-1}K^{-1}, respectively

[b] $T = 1,423$ K corresponds to the phase transition $\alpha \to \beta$ for BaSO$_4$

- The equivalent pressure P_{SO2} in the decomposition of the crystal was calculated assuming the vaporization of all the decomposition products including BaO. In the decomposition of powders, only the vaporization of SO$_2$ and O was taken into account assuming that the major fraction of BaO condensed in the colder inner layers of the powder. The averaged experimental molar enthalpy $\Delta_r H_{1400}^\circ/\nu = 420.9 \pm 3.0$ kJ mol^{-1} agrees with the calculated value $\Delta_v H_{1400}^\circ/\nu = 412.5$ kJ mol^{-1} (Table 16.42).
- A comparison of the temperatures and molar enthalpies of decomposition of MgSO$_4$ and BaSO$_4$ shows that they differ essentially (by approximately 400 K and 90 kJ mol^{-1}), which seems strange at first glance, taking into account the close thermochemical characteristics of these compounds. This fact can be accounted for by a significant difference in the extent of oversaturation of the MgO and BaO vapours at the decomposition temperatures, leading to a difference in the condensation energy transferred to the reactant. The saturated vapour pressure of BaO at 1,400 K (1.5×10^{-8} bar) is comparable with the equivalent pressure P_{eqp}. For the decomposition of MgSO$_4$, the saturated vapour pressure of MgO at 1,000 K is 3×10^{-24} bar, which is lower by 15 orders of magnitude than the equilibrium pressure of the primary products. Therefore, the transfer coefficient τ for BaSO$_4$ is close to 0, whereas for MgSO$_4$ it is as high as 0.44.
- The results obtained in different studies (Table 16.44) are fairly consistent. A relatively small discrepancy between the molar enthalpies for BaSO$_4$, calculated from the data of [97] by the second- and third-law methods (384 and 410 kJ mol^{-1}), is due to the fact that the transfer coefficient for BaSO$_4$ is close to zero and the condensation has no effect on the enthalpy. The residual discrepancy is caused exclusively by self-cooling. The results

Table 16.43 The experimental conditions and results of determination of the molar enthalpies for decomposition of $MgSO_4$ and $BaSO_4$ by the third-law method [98]

Sulphate	Sample	T (K)	s_0 (mm²)	α_m	s_m (mm²)	$\Delta m/\Delta t$ (μg s⁻¹)	J^a (kg m⁻² s⁻¹)	P_{SO2} (bar)	δ	K_P (bar³)	$\Delta_r S°_T/\nu$ (J mol⁻¹ K⁻¹)	$\Delta_r H°_T/\nu$ (kJ mol⁻¹)
$MgSO_4$	Powder	1,005.8	61.8	0.046	61.3	0.117	6.82E−07	6.18E−09	2.52	9.38E−26	171.3	332.9
$MgSO_4$	Powder	1,005.5	61.8	0.023	61.6	0.089	5.16E−07	4.68E−09	2.52	4.08E−26	171.3	335.2
$BaSO_4$	Powder	1,396.9	57.3	0.151	56.3	0.216	1.37E−06	1.46E−08	1.29	2.43E−24	152.7	423.8
$BaSO_4$	Powder	1,396.3	57.3	0.095	56.7	0.227	1.43E−06	1.53E−08	1.29	2.76E−24	152.7	423.1
$BaSO_4$ [b]	Powder	1,396.0	56.4	0.150	55.6	0.321	2.06E−06	2.20E−08	1.29	8.28E−24	152.7	418.8
$BaSO_4$ [b]	Powder	1,406.7	56.4	0.250	55.1	0.342	2.22E−06	2.37E−08	1.29	1.03E−23	152.6	421.0
$BaSO_4$ [c]	Crystal	1,426.6	18.7	0.036	18.2	0.232	1.27E−05	3.76E−08	1.29	4.11E−23	150.0	417.8

[a] $J = (\Delta m/\Delta t)/(2.8\, s_m)$ for powders and $J = (\Delta m/\Delta t)/s_m$ for $BaSO_4$ crystal

[b] Residual pressure of air was 2×10^{-4} bar, whereas in other experiments it was 4×10^{-8} bar

[c] Value of P_{SO2} for crystal was calculated at assumption of vaporization of all products, whereas in cases of powders, of only SO_2 and O

Table 16.44 Experimental conditions and the molar enthalpies for Mg and Ba sulphates according to different studies

Sulphate	Sample	Medium	T (K)	Point Number	Method of measurement	$\Delta_r H_T^\circ/\nu$ (kJ mol^{-1})	Ref.
MgSO$_4$	Powder	N$_2$ flow	1,293–1,333	3	Arrhenius plot	661.1; 369.4[a]	[94]
MgSO$_4$	Powder	Air	1,164–1,245	5	Arrhenius plot	343.1 ± 10	[95]
MgSO$_4$	Powder	Air	1,193–1,353	7	Arrhenius plot	311.7 ± 13	[96]
MgSO$_4$	Powder	Vacuum	1,006	2	Third-law	334.1 ± 1.2	[98]
BaSO$_4$	Crystal	Vacuum	1,422–1,540	42	Second-law	383.5 ± 8.4[b]	[97]
BaSO$_4$	Crystal	Vacuum	1,450	1	Third-law	409.7[c]	[97]
BaSO$_4$	Powder	Vacuum	1,400	4	Third-law	421.7 ± 2.3	[98]
BaSO$_4$	Crystal	Vacuum	1,430	2	Third-law	417.8	[98]

[a] For pure MgSO$_4$ and MgSO$_4$ + 5%Fe$_2$O$_3$, respectively
[b] Recalculated from the "apparent enthalpy of activation" for equilibrium reaction (15.15): 75.3 ± 12.6 kJ (mole of BaSO$_4$)$^{-1}$ [97]
[c] Calculated in [98] on the basis of data reported in [97]: $P = 1.15 \times 10^{-7}$ bar at $T = 1,450$ K ($\Delta_r S_{1450}^\circ/\nu = 149.7$ J mol^{-1}K^{-1})

Table 16.45 Calculated values of the vaporization coefficients for Mg and Ba sulphates

Sulphate	T (K)	Primary products	P_{eqp} (bar)	Equilibrium products	P_{eq} (bar)	α_v
MgSO$_4$	1,006	MgO(g)$_\downarrow$ + SO$_2$ + O	5.4E−09	MgO(s) + SO$_2$ + ½O$_2$	1.7E−04	3.2E−05
BaSO$_4$	1,397	BaO(g)$_\downarrow$ + SO$_2$ + O	3.9E−08	BaO(s) + SO$_2$ + ½O$_2$	2.4E−06	1.6E−02

obtained by the Arrhenius plot and second-law methods, on the one hand, and by the third-law method, on the other, differ in their precision by an order of magnitude.

• The vaporization coefficients of magnesium and barium sulphates (Table 16.45) are equal to 3.2×10^{-5} and 1.6×10^{-2}, respectively. For BaSO$_4$, this value is due exclusively to the chemical form of oxygen (O), being different from the equilibrium form (O$_2$). The value of α_v that Mohazzabi and Searcy [97] determined for BaSO$_4$ by measuring the vaporization rates under the conditions of the Knudsen and Langmuir methods is 1.4×10^{-2}.

16.13 Carbonates

Introduction Alkaline-earth metal carbonates and especially calcite are the most popular reactants in studying the decomposition kinetics of solids. This is caused, not only by the use of carbonates as mineral raw materials for some industrial processes (in particular, production of lime), but also by the fact that the decomposition of calcite is a convenient model reaction for studying the kinetics and mechanism of solid-state reactions as a whole. An enormous number of papers, summarized in part in several monographs [43, 45, 99] and reviews [100–102], deal with the decomposition of carbonates. A series

of papers concerning this subject were recently published in *Thermochimica Acta* [103–109].

In this monograph, the kinetics of carbonate decompositions have been considered in several sections concerning the formation of oversaturated vapour and nucleation (Sect. 2.4), the structure of the solid product (Sect. 2.6), the influence of the reaction mode and stoichiometry on the molar enthalpy (Sect. 5.4), the experimental estimation of the self-cooling (Sect. 6.3), the T–S effect (Sect. 7.3), the variation of the enthalpy of decomposition with temperature (Sect. 8.2), the compensation effect (Chapter 12), and the determination of the absolute rates of decomposition of single crystals and powders in a vacuum and in air (Sects. 15.1 and 15.5).

From these measurements, only those results are presented below that are useful for comparison with the results of measurements made by other researchers, or are of interest for further studies. The thermodynamic functions of $MgCO_3$, $CaCO_3$, $CaMg(CO_3)_2$, $SrCO_3$, and $BaCO_3$, used in a thermochemical analysis of the decomposition kinetics of these carbonates by the third-law method, are listed in Tables 16.46–16.50.

Experimental The majority of TG experiments were made with an STA 429 thermal analyser. The samples were separate crystals and powders prepared by milling of the natural minerals (magnesite, calcite, dolomite), and also chemically pure grade strontium and barium carbonates. The experiments were performed in a vacuum ($n \times 10^{-8}$ or $n \times 10^{-4}$ bar), in a CO_2 atmosphere (1 bar), and in air. When calculating the molar enthalpy by the third-law method, the congruence of vaporization and the variation of the sample surface area during the course of the decomposition were taken into account.

Table 16.46 Values of the thermodynamic functions for $MgCO_3$ and the products of its decomposition [6]

Function[a]	Species	T (K)				
		500	600	700	800	900
$\Delta_f H_T^\circ$	$MgCO_3(s)$	−1078.0	−1067.6	−1056.5	−1044.6	−1032.0
	$MgO(s)$	−593.0	−588.3	−583.5	−578.6	−573.6
	$MgO(g)$	39.2	43.1	47.4	52.2	57.3
	$CO_2(g)$	−385.2	−380.6	−375.8	−370.7	−365.5
$\Delta_c H_T^\circ$	$MgO(g)_\downarrow$	−632.2	−631.4	−630.9	−630.8	−630.9
$\Delta_v H_T^\circ/\nu$		366.0	365.1	364.1	363.0	361.9
S_T°	$MgCO_3(s)$	110.7	129.6	146.7	162.6	177.4
	$MgO(s)$	48.6	57.1	64.5	71.0	76.9
	$MgO(g)$	230.9	238.0	244.6	251.0	257.0
	$CO_2(g)$	234.8	243.2	250.6	257.4	263.5
$\Delta_r S_T^\circ/\nu$		177.5	175.8	174.3	172.9	171.6

[a] ΔH_T° and S_T° values are in kJ mol^{-1} and J mol^{-1} K^{-1}, respectively

Table 16.47 Values of the thermodynamic functions for $CaCO_3$ and the products of its decomposition [6]

Function[a]	Species	T (K)				
		800	900	1,000	1,100	1,200
$\Delta_f H_T^\circ$	$CaCO_3(s)$	−1153.7	−1141.7	−1129.4	−1116.8	−1103.9
	$CaO(s)$	−610.4	−605.1	−599.8	−594.4	−589.0
	$CaO(g)$	60.7	64.4	68.1	71.8	75.6
	$CO_2(g)$	−370.7	−365.5	−360.1	−354.6	−349.0
$\Delta_c H_T^\circ$	$CaO(g)_\downarrow$	−671.0	−669.5	−667.9	−666.2	−664.6
$\Delta_v H_T^\circ/\nu$		421.8	420.3	418.7	417.0	415.2
S_T°	$CaCO_3(s)$	193.2	207.3	220.2	232.2	243.5
	$CaO(s)$	86.0	92.2	97.8	102.9	107.6
	$CaO(g)$	254.0	258.4	262.3	265.8	269.1
	$CO_2(g)$	257.4	263.5	269.2	274.4	279.3
$\Delta_r S_T^\circ/\nu$		159.1	157.3	155.7	154.0	152.5

[a] ΔH_T° and S_T° values are in kJ mol^{-1} and J mol^{-1} K^{-1}, respectively

Table 16.48 Values of the thermodynamic functions for $CaMgCO_3$ and the products of its decomposition [6, 7]

Function[a]	Species	T (K)	
		800	900
$\Delta_f H_T^\circ$	$CaMg(CO_3)_2(s)$	−2211.8	−2187.3
	$CaO(s)$	−610.4	−605.1
	$CaO(g)$	60.7	64.4
	$MgO(s)$	−578.6	−573.6
	$MgO(g)$	52.2	57.3
	$CO_2(g)$	−370.7	−365.5
$\Delta_v H_T^\circ/\nu$		395.8	394.5
S_T°	$CaMg(CO_3)_2(s)$	355.8	384.6
	$CaO(s)$	86.0	92.2
	$CaO(g)$	254.0	258.4
	$MgO(s)$	71.0	76.9
	$MgO(g)$	251.0	257.0
	$CO_2(g)$	257.4	263.5
$\Delta_r S_T^\circ/\nu$		166.0	164.5

[a] ΔH_T° and S_T° values are in kJ mol^{-1} and J mol^{-1} K^{-1}, respectively

Results and Discussion The measurement conditions and the results of the measurements and calculations are given in Tables 16.51–16.61. The results given in the tables allow the following conclusions.

- Despite the many-fold differences in the molar enthalpies (parameter E) for calcite and other alkaline-earth metal carbonates, measured on the basis of different kinetic models and, above all, under different conditions (in a vacuum and in the presence of CO_2), the enthalpies measured in the equimolar and isobaric modes by the third-law method (Table 16.58) appear to be reasonably consistent (the largest difference, by a factor of 1.13, is

Table 16.49 Values of the thermodynamic functions for $SrCO_3$ and the products of its decomposition [6]

Function[a]	Species	900	1,000	1,100	1,198[b]	1,200	1,300	1,400	1,500
					T (K)				
$\Delta_f H_T^\circ$	$SrCO_3(s)$	−1213.7	−1201.4	−1188.5	−1174.9	−1157.9	−1143.2	−1128.6	−1114.0
	$SrO(s)$	−559.5	−553.9	−548.2		−542.5	−536.7	−530.8	−524.8
	$SrO(g)$	7.4	11.1	14.8		18.6	22.3	26.2	30.1
	$CO_2(g)$	−365.5	−360.1	−354.6		−349.0	−343.4	−337.6	−331.8
$\Delta_v H_T^\circ/\nu$	$SrO(g)_\downarrow$	−566.8	−565.0	−563.1		−561.1	−559.0	−557.0	−554.9
$\Delta_c H_T^\circ$		427.8	426.2	424.3	422.2	413.7	411.1	408.6	406.2
S_T°	$SrCO_3(s)$	210.5	223.4	235.7	247.6	261.7	273.4	284.2	294.3
	$SrO(s)$	111.4	117.2	122.7		127.7	132.3	136.7	140.8
	$SrO(g)$	269.1	273.1	276.6		279.9	283.0	285.8	288.5
	$CO_2(g)$	263.5	269.2	274.4		279.3	283.8	288.1	292.1
$\Delta_r S_T^\circ/\nu$		161.1	159.5	157.7	155.8	148.8	146.7	144.9	143.2

[a] $\Delta_f H_T^\circ$ and S_T° values are in kJ mol^{-1} and J mol^{-1}K^{-1}, respectively

[b] The values at 1,198 K correspond to α-SrCO$_3$ (α → β phase transition)

Table 16.50 Values of the thermodynamic functions for $BaCO_3$ and the products of its decomposition [6]

Function[a]	Species	T (K)				
		1,100	1,200	1,300	1,400	1,500
$\Delta_f H_T^\circ$	$BaCO_3(s)$	−1098.3	−1082.5	−1063.7	−1047.7	−1032.0
	$BaO(s)$	−504.8	−499.0	−493.1	−487.1	−481.1
	$BaO(g)$	−98.9	−95.1	−91.4	−87.7	−83.9
	$CO_2(g)$	−354.6	−349.0	−343.4	−337.6	−331.8
$\Delta_c H_T^\circ$	$BaO(g)_\downarrow$	−405.9	−403.8	−401.7	−399.4	−397.2
$\Delta_v H_T^\circ/\nu$		322.4	319.2	314.5	311.2	308.2
S_T°	$BaCO_3(s)$	275.3	289.1	304.2	316.0	327.1
	$BaO(s)$	140.9	145.9	150.7	155.1	159.2
	$BaO(g)$	281.8	285.0	288.0	290.8	293.4
	$CO_2(g)$	274.4	279.3	283.8	288.1	292.1
$\Delta_r S_T^\circ/\nu$		140.5	137.6	133.8	131.5	129.2

[a] $\Delta_f H_T^\circ$ and S_T° values are in $kJ\ mol^{-1}$ and $J\ mol^{-1}K^{-1}$, respectively

Table 16.51 The experimental conditions and results of determination of the molar enthalpy for decomposition of $MgCO_3$ in a vacuum by the third-law method

Sample	Vacuum (bar)	T (K)	m_0 (mg)	s_0 (mm^2)	α_m	s_m (mm^2)	$\Delta m/\Delta t$ (μg s^{-1})	J^a (kg m^{-2} s^{-1})	P_{eqp} (bar)	K_P^b (bar^2)	$\Delta_r S_T^\circ/\nu$ (J mol^{-1} K^{-1})	$\Delta_r H_T^\circ/\nu$ (kJ mol^{-1})
Powder	4E−04	711.0	20	58.2	0.147	57.1	1.283	8.02E−06	7.38E−08	5.21E−15	174.2	221.1
Powder	4E−04	690.6	20	58.2	0.037	57.9	0.567	3.50E−06	3.17E−08	9.62E−16	174.5	219.8
Powder	4E−04	670.8	20	58.2	0.064	57.7	0.283	1.75E−06	1.56E−08	2.33E−16	174.8	217.6
Powder	4E−04	670.7	20	58.2	0.072	57.7	0.237	1.47E−06	1.31E−08	1.64E−16	174.8	218.6

^{a} $J = (\Delta m/\Delta t)/(2.8\, s_0)$
^{b} At $\beta = 1.045$

Table 16.52 The experimental conditions and results of determination of the molar enthalpy for decomposition of $CaCO_3$ in a vacuum (10^{-8} bar) by the third-law method

T (K)	J^a (kg m^{-2}s^{-1})	P_{eqp} (bar)	K_P^b (bar^2)	$\Delta_r S_T^\circ/\nu$ (J mol^{-1}K^{-1})	$\Delta_r H_T^\circ/\nu$ (kJ mol^{-1})
863	3.00E−06	1.32E−08	1.97E−16	158.0	266.1
890	5.73E−06	2.56E−08	7.40E−16	157.5	269.1
892	6.08E−06	2.72E−08	8.35E−16	157.5	269.2
921	1.49E−05	6.77E−08	5.17E−15	157.0	270.5
948	2.91E−05	1.34E−07	2.03E−14	156.5	272.6

^{a} At $\beta = 0.886$

Table 16.53 The experimental conditions and results of determination of the reaction enthalpy for the decomposition of $CaCO_3$ in air

Sample	P^{ext} (bar)	T (K)	m_0 (mg)	s_0 (mm²)	α_m	s_m (mm²)	$\Delta m/\Delta t$ (µg s⁻¹)	J (kg m⁻²s⁻¹)	P_{eqp} (bar)	$K_P{}^a$ (bar²)	$\Delta_r S_T°$ (J mol⁻¹K⁻¹)	$\Delta_r H_T°$ (kJ mol⁻¹)
Crystal	4E−04	950	17.8	24.8	0.055	23.9	0.80	3.35E−05	3.52E−07	1.59E−10	313.0	475.6
Crystal	4E−04	999	20.6	26.0	0.136	23.6	2.23	9.45E−05	1.02E−06	4.60E−10	311.4	489.7
Crystal	4E−04	995	19.9	27.0	0.110	24.9	0.687	2.75E−05	2.97E−07	1.34E−10	311.6	498.1
Powder	4E−04	970	20	58.2	0.281	56.2	0.96	6.10E−06	6.55E−08	2.96E−11	312.4	498.6

^{a} At $\beta = 0.886$

Table 16.54 The results of determination of the molar enthalpy for the decomposition of $CaMg(CO_3)_2$ in a vacuum by the third-law method

Sample^a	Vacuum (bar)	T (K)	m_0 (mg)	s_0 (mm²)	α_m	s_m (mm²)	$\Delta m/\Delta t$ (µg s⁻¹)	J^a (kg m⁻²s⁻¹)	P_{eqp} (bar)	$K_P{}^b$ (bar²)	$\Delta_r S_T°/\nu$ (J mol⁻¹K⁻¹)	$\Delta_r H_T°/\nu$ (kJ mol⁻¹)
Crystal	2E−04	835.4	10.7	15.7	0.146	14.2	0.235	1.65E−05	8.23E−08	1.24E−29	165.5	253.8
Crystal	2E−04	812.0	10.4	15.3	0.117	14.1	0.108	7.66E−06	3.75E−08	5.34E−31	165.8	252.3
Powder (1)	2E−04	835.5	10.7	55.7	0.510	53.3	1.45	9.72E−06	4.83E−08	1.47E−30	165.5	257.6
Powder (1)	2E−04	811.0	10.7	55.7	0.365	54.0	0.943	6.24E−06	3.06E−08	2.37E−31	165.8	253.3
Powder (2)	2E−04	834.5	10.7	54.6	0.511	52.8	1.55	1.05E−05	5.21E−08	1.99E−30	165.5	256.7
Powder (2)	2E−04	811.8	10.7	54.6	0.353	53.3	1.06	7.10E−06	3.48E−08	3.96E−31	165.8	252.7
Powder (2)	2E−04	835.5	40.0	64.6	0.147	62.6	2.32	1.32E−05	6.58E−08	5.06E−30	165.5	255.4
Powder (2)	2E−04	811.3	40.0	64.6	0.100	63.2	1.23	6.95E−06	3.40E−08	3.61E−31	165.8	252.7
Powder (2)	8E−08	807.3	40.0	64.6	0.088	63.4	1.17	6.59E−06	3.22E−08	2.90E−31	165.9	251.9
Powder (2)	8E−08	806.9	40.0	64.6	0.087	63.4	1.04	5.86E−06	2.86E−08	1.81E−31	165.9	252.6

^{a} Powder (1): 71–100 µm; powder (2): 0–71 µm
^{b} At $\beta = 3.704$

Table 16.55 The results of determination of the molar enthalpy for the decomposition of $Sr(CO_3)_2$ in a vacuum by the third-law method

Sample	Vacuum (bar)	T (K)	m_0 (mg)	s_0 (mm^2)	α_m	s_m (mm^2)	$\Delta m/\Delta t$ (μg s^{-1})	J^a (kg m^{-2}s^{-1})	P_{eqp} (bar)	K_P^b (bar^2)	$\Delta_r S_T^\circ/\nu$ (J mol^{-1}K^{-1})	$\Delta_r H_T^\circ/\nu$ (kJ mol^{-1})
Powder	8E−08	907.8	40	61.8	0.0057	61.7	0.180	1.04E−06	1.08E−08	1.79E−16	161.0	283.0
Powder	8E−08	907.1	40	61.8	0.0064	61.7	0.173	1.00E−06	1.04E−08	1.66E−16	161.0	283.1
Powder	1E−04	908.7	40	61.8	0.0121	61.7	0.127	7.35E−07	7.65E−09	8.98E−17	161.0	285.9
Powder	1E−04	908.7	40	61.8	0.0228	61.6	0.173	1.00E−06	1.04E−08	1.66E−16	161.0	283.6

^{a} $J = (\Delta m/\Delta t)/(2.8\, s_0)$
^{b} At $\beta = 0.652$

Table 16.56 The results of determination of the molar enthalpy for the decomposition of $Ba(CO_3)_2$ in a vacuum by the third-law method

Sample	Vacuum (bar)	T (K)	m_0 (mg)	s_0 (mm^2)	α_m	s_m (mm^2)	$\Delta m/\Delta t$ (μg s^{-1})	J^a (kg m^{-2}s^{-1})	P_{eqp} (bar)	K_P^b (bar^2)	$\Delta_r S_T^\circ/\nu$ (J mol^{-1}K^{-1})	$\Delta_r H_T^\circ/\nu$ (kJ mol^{-1})
Powder	3E−08	1,232	40	63.9	0.59	56.3	4.59	2.9E−05	3.5E−07	2.29E−13	136.7	317.5
Powder	3E−08	1,154	40	63.9	0.279	60.3	2.49	1.5E−05	1.7E−07	5.39E−14	139.0	307.0
Powder	3E−08	1,115	40	63.9	0.188	61.5	1.33	7.7E−06	8.9E−08	1.48E−14	140.1	303.8
Powder	3E−08	1,076	40	63.9	0.109	62.5	0.79	4.5E−06	5.1E−08	4.85E−15	141.2	299.4
Powder	2E−04	1,077	40	63.9	0.115	62.4	0.960	5.5E−06	6.2E−08	7.17E−15	141.2	297.9
Powder	2E−04	1,077	40	63.9	0.092	62.7	0.647	3.7E−06	4.2E−08	3.29E−15	141.2	301.4
Powder	2E−04	1,078	40	63.9	0.102	62.6	0.773	4.4E−06	5.0E−08	4.66E−15	141.2	300.1

^{a} $J = (\Delta m/\Delta t)/(2.8\, s_m)$
^{b} At $\beta = 0.536$

Table 16.57 The results of determination of the molar enthalpies for the decompositions of carbonates in an atmosphere of CO_2 by the third-law method

Carbonate	Sample	P^{ext} (bar)	T (K)	m_0 (mg)	s_0 (mm²)	α_m	s_m (mm²)	$\Delta m/\Delta t$ (μg s⁻¹)	J^a (kg m⁻² s⁻¹)	P_{eqp} (bar)	K_P^b (bar²)	$\Delta_r S_T^\circ/\nu$ (J mol⁻¹ K⁻¹)	$\Delta_r H_T^\circ/\nu$ (kJ mol⁻¹)
$MgCO_3$	Powder	1.0	810	20	60.0	0.199	58.2	1.96	1.20E−05	1.18E−07	1.13E−07	345.6	387.7
$MgCO_3$	Powder	1.0	800	20	60.0	0.187	58.3	0.98	6.00E−06	5.90E−08	5.65E−08	345.7	387.6
$CaCO_3$	Powder	1.0	1,200	40	63.5	0.010	63.4	0.693	3.41E−06	4.05E−08	4.57E−08	304.9	534.5
$CaCO_3$	Crystal	1.0	1,214	10.7	17.1	0.004	17.0	0.171	1.01E−05	1.19E−07	1.34E−07	304.4	529.3
$CaCO_3$	Crystal	1.0	1,215	11.4	17.0	0.055	16.4	0.135	7.96E−06	9.48E−08	1.07E−07	304.4	532.0
$SrCO_3$[c]	Powder	1.0	1,456	20	47.2	0.054	47.2	0.219	1.66E−06	2.18E−08	3.34E−08	288.0	627.8
$SrCO_3$[c]	Powder	1.0	1,456	20	47.2	0.049	47.2	0.180	1.37E−06	1.79E−08	2.75E−08	288.0	630.1
$BaCO_3$[c]	Powder	1.0	1,496	40	42.7	0.004	42.7	0.133	1.11E−06	3.31E−09	6.18E−09	258.4	621.7
$BaCO_3$[d]	Powder	1.0	1,516	20	66.2	0.130	64.2	1.153	6.41E−06	1.91E−08	3.56E−08	257.6	606.7
$BaCO_3$[d]	Powder	1.0	1,514	20	66.2	0.126	64.3	1.053	5.85E−06	1.74E−08	3.25E−08	257.6	607.1

[a] $J = (\Delta m/\Delta t)/s_m$ for crystals and $J = (\Delta m/\Delta t)/(2.8 s_m)$ for powders

[b] Values of β equal to 1.045 for $MgCO_3$, 0.886 for $CaCO_3$, 0.652 for $SrCO_3$ and 0.536 for $BaCO_3$

[c] As a result of phase transition (1,198 K for $SrCO_3$ and 1,083, and 1,233 K for $BaCO_3$) the tablet diameter at the instant of decomposition can be lower

[d] Mixture of $BaCO_3$ and Al_2O_3 (1:1). The tablet size in the process of phase transition is kept constant

Table 16.58 The reaction enthalpies of the decomposition of carbonates in a vacuum and in CO_2 atmosphere

Carbonate	Vacuum		CO_2 atmosphere		
	T (K)	$\Delta_r H_T^\circ$ (kJ mol^{-1})	T (K)	P^{ext} (bar)	$\Delta_r H_T^\circ$ (kJ mol^{-1})
$MgCO_3$	686	438.5 ± 3.0	805	1.0	387.7 ± 0.2
$CaCO_3$	903	539.0 ± 4.8	1,210	1.0	531.9 ± 2.0
$1/2CaMg(CO_3)_2$	820	507.8 ± 4.0			
$SrCO_3$	908	567.8 ± 2.8	1,456	1.0	629.0 ± 1.2
$BaCO_3$	1,116	607.7 ± 13.4	1,509	1.0	611.8 ± 8.0

Table 16.59 The reaction enthalpies of the decomposition of carbonates (single crystals) in a vacuum calculated by the third-law method (from the data reported in [110–112])

Carbonate	T (K)	P_{eqp} (bar)	K_P[a] (bar^2)	$\Delta_r S_T^\circ$ (J mol^{-1} K^{-1})	$\Delta_r H_T^\circ$ (kJ mol^{-1})	Ref.
$CaCO_3$	909	3.7E−08	1.55E−15	314.4	543.5	[110]
$1/2CaMg(CO_3)_2$	824	3.9E−08	4.11E−16	331.2	515.6	[111]
$BaCO_3$	1,162	7.0E−08	9.14E−15	277.4	634.7	[112]

[a] Values of β equal to 0.886 for $CaCO_3$, 3.704 for $CaMg(CO_3)_2$ and 0.536 for $BaCO_3$

Table 16.60 Values of the τ parameter for decomposition of carbonates

Carbonate	T (K)	$\Delta_r H_T^\circ$ (kJ mol^{-1})	$\Delta_v H_T^\circ$ (kJ mol^{-1})	$\Delta_c H_T^\circ$ (kJ mol^{-1})	c_2[a]	τ	$\dfrac{\tau + 1.127}{0.353 c_2}$
$MgCO_3$	800	387.7	726.0	−630.8	4.55	0.536	1.04
$CaCO_3$	1,200	531.9	830.4	−664.6	4.20	0.449	1.06
$1/2CaMg(CO_3)_2$	824	507.8	791.0	−630.8	4.52	0.449	0.99
$SrCO_3$	1,456	629.0	814.7	−555.9	3.83	0.334	1.08
$BaCO_3$	1,500	611.8	616.4	−397.2	3.46	0.012	0.93

[a] $c_2 \equiv \ln[-\Delta_c H_T^\circ/(RT)]$

Table 16.61 Calculated values of vaporization coefficients for some carbonates

Carbonate	T (K)	Primary Products	P_{eqp} (bar)	Equilibrium Products	P_{eq} (bar)	α_v
$MgCO_3$	686	$MgO(g)_\downarrow + CO_2$	3E−08	$MgO(s) + CO_2$	3E+01	1E−09
$CaCO_3$	903	$CaO(g)_\downarrow + CO_2$	3E−08	$CaO(s) + CO_2$	7E−03	4E−06
$CaMg(CO_3)_2$	820	$MgO(g)_\downarrow + CaO(g)_\downarrow + 2CO_2$	4E−08	$MgO(s) + CaO(s) + 2CO_2$	6E−03	7E−06
$SrCO_3$	908	$SrO(g)_\downarrow + CO_2$	1E−08	$SrO(s) + CO_2$	6E−05[a]	1E−04
$BaCO_3$	1,116	$BaO(g)_\downarrow + CO_2$	9E−08	$BaO(s) + CO_2$	1E−04	9E−04

[a] In calculation of P_{eq}, the value of $\Delta_f H_{298}^\circ$ for $SrO(s)$ was assumed to be 641.4 kJ mol^{-1} [113] instead of 590.5 kJ mol^{-1}, which is recommended in handbook [6]. For the last magnitude of $\Delta_f H_{298}^\circ$, the calculated P_{eq} value is equal to P_{eqp} value, which seems improbable. A refinement of the $\Delta_f H_{298}^\circ$ value is necessary

observed with $MgCO_3$). This result, on the whole, fully complies with the CDV mechanism.

- The enthalpy measurements in the isobaric mode for all the carbonates were performed at 120–550 K higher temperatures than the measurements in the equimolar mode. Therefore, taking into account the temperature dependence of the condensation effect (Sect. 8.2), the quantities $\Delta_r H_T^\circ$ measured in the isobaric mode should be appreciably higher than those measured in the equimolar mode. This is true for strontium carbonate (Table 16.58), but for magnesite the quantity $\Delta_r H_T^\circ$ measured in the isobaric mode appeared to be 13% lower. This is probably due to overestimation of $\Delta_r H_T^\circ$ measured in a vacuum because of self-cooling (for $MgCO_3$, owing to the low decomposition temperature, the self-cooling is more significant than for the other carbonates). For calcium carbonate, both effects (self-cooling in a vacuum and a decrease in the contribution of the heat of condensation to the enthalpy with increasing temperature) increase the enthalpy to virtually the same extent. For the decomposition of $CaCO_3$ in air at 970 K (Table 16.53), $\Delta_r H_T^\circ = 490.5 \pm 10.7\,\text{kJ mol}^{-1}$, which is $41\,\text{kJ mol}^{-1}$ lower than $\Delta_r H_T^\circ$ at 1,210 K. For $BaCO_3$, the enthalpy remains essentially unchanged, because both the above-mentioned effects are absent: self-cooling in a vacuum, because of the high decomposition temperature, and the contribution of the heat of condensation, because BaO does not condense under the experimental conditions (at 1,500 K $P_\infty = 1.5 \times 10^{-7}$ bar). The experimental value, $\Delta_r H_{1507}^\circ = 611.8 \pm 8.6\,\text{kJ mol}^{-1}$, coincides within the measurement error with the calculated value, $\Delta_v H_{1500}^\circ = 616.4\,\text{kJ mol}^{-1}$ (Table 16.50).

- The kinetic characteristics of the examined carbonates differ essentially. The temperatures and enthalpies of decomposition in a vacuum of the most thermostable $BaCO_3$ and the least thermostable $MgCO_3$ differ by 430 K and $170\,\text{kJ mol}^{-1}$, respectively (Table 16.58), although the initial thermodynamic parameters (heats of vaporization, $\Delta_v H_T^\circ/\nu$, of the corresponding carbonates without taking the condensation of the oxides into account) give no grounds to expect so large a difference. The observed difference is due to the difference in the contributions of the energy of condensation of the oxides to the enthalpy of the reaction. For $BaCO_3$, this contribution is considerably smaller than for $MgCO_3$. As found for barium and magnesium sulphates (see Sect. 16.12), a decisive factor is the degree of oversaturation of the vapour of low-volatility oxides at the decomposition temperature. For $BaCO_3$ at 1,100 K and for $MgCO_3$ at 700 K, the saturated vapour pressures of the respective oxides are about 10^{-12} and 10^{-38} bar, i.e., the oversaturation factors are 10^4 and 10^{30}, respectively.

- Among the numerous published papers dealing with the decomposition of carbonates, those by Searcy et al. [110–112] seem to be the most reliable. In these studies, experiments on the decomposition of $CaCO_3$, $CaMg(CO_3)_2$, and $BaCO_3$ were performed in a high vacuum under free-surface vaporization conditions (after Langmuir). However, the enthalpies of decomposition of these carbonates, found by the second-law method (418, 390, and

452 kJ mol^{-1}, respectively), are 120–150 kJ mol^{-1} lower than those presented in Table 16.58. This discrepancy is caused by systematic underestimation of the data obtained by the second-law method because of the condensation and self-cooling effects. This conclusion is confirmed by the enthalpies (Table 16.59), calculated by the author with the third-law method from the same primary data as those used for the second-law calculations [110–112]. For $CaCO_3$ and $CaMg(CO_3)_2$, the results coincide within the experimental error with the data (for vacuum) given in Table 16.58. For $BaCO_3$, the results differ slightly (by 4%), which is caused in part by the higher temperature of the experiments in [112].

- The transfer coefficients τ calculated from the equality $\Delta_r H_T^\circ = \Delta_v H_T^\circ + \tau a \Delta_c H_T^\circ(A)$, where $\Delta_v H_T^\circ$ is the enthalpy of dissociative vaporization (without taking into account the oxide condensation) and $\Delta_c H_T^\circ(A)$ is the enthalpy of the oxide condensation, range from 0.012 for $BaCO_3$ to 0.536 for $MgCO_3$ (Table 16.60), which, in accordance with approximating Eq. 8.5, is consistent with the variation of c_2. The ratio $(\tau + 1.127)/(0.353c_2) = 1.02 \pm 0.06$.

- The calculated vaporization coefficients (Table 16.61) range from 10^{-3} for $SrCO_3$ and $BaCO_3$ to 10^{-9} for $MgCO_3$. According to the experimental estimates [110–112] based on comparison of the vaporization rates measured after Langmuir and Knudsen [22], α_v is about 10^{-5} for $CaCO_3$, 10^{-4} for $CaMg(CO_3)_2$, and 2×10^{-4} for $BaCO_3$. These values differ from the calculated values by no more than an order of magnitude, which is quite acceptable taking into account the errors of measurements and theoretical calculations.

Thus, the *decomposition kinetics of carbonates are in full agreement with the theoretical concepts based on the CDV mechanism.* The analysis shows that long-term discussions concerning the decomposition mechanism and the influence of the experimental conditions (in particular, the presence of CO_2) on the reaction rate, initiated 70 years ago in a well-known paper by Zawadzki and Bretsznajder [114] and continuing up to now [108], are chiefly associated with the fundamental limitations of the Arrhenius plot and second-law methods used for estimating the kinetic parameters.

16.14 Oxalates

Introduction The thermal decompositions of metal oxalates have been studied for more than 130 years. The first paper on the decomposition of PbC_2O_4 was published in 1870 [115]. The kinetics of these reactions have been considered in numerous reviews [45, 99, 116–121]. The decompositions of the oxalates of some metals (Ag, Ni, and Pb) have often been used as model reactions. Nevertheless, many features of these processes remained unclear until recently.

Among them are the relatively high thermal stability of explosive mercury and silver oxalates, the existence of a long induction period for the majority of oxalates and its absence for HgC_2O_4, and the significant $(60\text{–}70\,\text{kJ mol}^{-1})$ difference in the parameters E for the induction and acceleration periods in the decompositions of $Ag_2C_2O_4$ and NiC_2O_4.

Thermochemical Analysis An attempt to solve these problems within the framework of the CDV mechanism was made by L'vov [121]. The thermochemical analysis below is based on the results of that study. The thermodynamic functions required for the calculations are given in Table 16.62 [31, 121, 122].

In the available literature, no direct measurements of the absolute decomposition rates or equivalent pressures are reported. Therefore, when comparing the experimental and calculated enthalpies of decomposition, consideration has been restricted to determination of the parameter E (molar enthalpy) from Arrhenius plots.

The parameters E and the initial reaction temperatures T_{in} (in a vacuum) for Ag, Hg, Ni, Mn, and Pb oxalates were taken from the available literature [123–144]. The corresponding initial data and averaged parameters are given in Table 16.63. To check the reliability of the data thus obtained, the experimental and theoretical ratios T_{in}/E are compared. The theoretical ratios were calculated with Eq. 5.2, assuming that the equivalent pressure of the gaseous product (CO) at the initial decomposition temperature was 10^{-7} bar in all the cases. As seen from Table 16.63, the agreement is very good. Only for Hg and Pb oxalates does the discrepancy exceed 10%. Taking into account the approximate calculation scheme and the experimental errors, such an agreement reliably confirms the correctness of the results obtained.

The composition of the primary products was determined by choosing the decomposition scheme whose enthalpy $(\Delta_r H_T^\circ)$ would agree with the experimental value equal to νE. For mercury oxalate decomposing only to gaseous

Table 16.62 Values of the thermodynamic functions for Ni, Mn, Ag, Hg, Pb oxalates, and the products of their decompositions [31, 121, 122]

Species	$\Delta_f H_{298}^\circ$ (kJ mol^{-1})	S_{298}° (J mol^{-1} K^{-1})	Species	$\Delta_f H_{298}^\circ$ (kJ mol^{-1})	S_{298}° (J mol^{-1} K^{-1})
Ni(s)	0	29.9	Hg(l)	0	75.9
Ni(g)	428.8	182.1	Hg(g)	61.4	174.9
NiC_2O_4(s)	−863.2	132.9	HgC_2O_4(s)	−672.8	146.0[b]
MnO(s)	−385.1	61.5	PbO(s)	−218.6	67.8
MnO(g)	123.8	226.4	PbO(g)	68.1	239.9
MnC_2O_4(s)	−1020.9[a]	42.1[b]	PbC_2O_4(s)	−851.0	146.0
Ag(s)	0	42.6	CO(g)	−110.5	197.5
Ag(g)	284.9	172.9	CO_2(g)	−393.5	213.7
$Ag_2C_2O_4$(s)	−674.5	181.1	O(g)	249.2	160.9
			O_2(g)	0	205.0

[a] Average value from: −1029.7 [31] and −1012.0 kJ mol^{-1} [122]
[b] Our evaluation [121]

Table 16.63 Ratio of the initial temperature of reaction T_{in} to the E parameter for the steady-state mode of oxalate decompositions in a vacuum

Oxalate	T_{in} (K)	$\overline{T}_{in}$ (K)	E (kJ mol⁻¹)	$\overline{E}$ (kJ mol⁻¹)	$\Delta_r S°_{298}/\nu$ (J mol⁻¹ K⁻¹)	$\overline{T}_{in}/\overline{E}$ (K mol kJ⁻¹) Expt	Theory
Ag₂C₂O₄	410 [139], 399 [140], 385 [141], 383 [131], 378 [138], 373 [123, 136], 360 [137]	383	113 [138], 107 [123], 98 [142]	106	151	3.6	3.4
HgC₂O₄	453 [126], 373 [143]	413	110 [143], 107 [126]	109	150	3.8	3.3
NiC₂O₄	571 [133], 563 [132], 542 [27], 535 [130], 526 [129], 513 [128], 503 [119]	536	169 [116], 167 [128], 159 [119], 134 [127]	157	161	3.4	3.5
MnC₂O₄	610 [125], 608 [134]	609	180 [134], 171 [116], 141 [135]	176	166	3.5	3.5
PbC₂O₄	582 [124], 523 [144]	552	151 [124]	151	169	3.7	3.3

products, the quantities $\Delta_r H_T^\circ$ were compared directly. For the other oxalates decomposing with the formation of a solid metal or oxide, when comparing the calculated enthalpy for one or another composition of products with the experimental value, the partial contribution of the heat of condensation, $\Delta_c H_T^\circ$, needs to be taken into account. For this purpose, as for the decomposition of azides (Sect. 16.7), the value of $a\tau\Delta_c H_T^\circ$ was subtracted from the experimental value of νE. The difference between these quantities corresponds to the molar enthalpy $\Delta_v H_T^\circ$ of a hypothetical reaction of oxalate vaporization with formation of gaseous products without condensation. The coefficient a corresponds to the number of moles of the solid product and is equal to unity for all of the oxalates except $Ag_2C_2O_4 (a = 2)$. The parameter τ was calculated from Eq. 8.4 using the approximate dependence $\tau_1 = f(c_1)$. The quantity $a\tau_1\Delta_c H_T^\circ$ ranged from $-109\,\text{kJ mol}^{-1}$ for PbC_2O_4 to $-285\,\text{kJ mol}^{-1}$ for $Ag_2C_2O_4$.

Results and Discussion The values of the above-mentioned parameters and the compositions of the primary products, found from their comparison, are listed in Table 16.64. The discrepancies between the calculated and experimental values of $\Delta_v H_T^\circ$ do not exceed 5% for Ag, Ni, and Mn oxalates and 10% for Hg and Pb oxalates. For the latter two reactants, the discrepancies are most likely due to underestimation of the initial parameter E. This is confirmed by the overestimated experimental values of the T_{in}/E ratio for these oxalates (Table 16.63). When determining the optimal composition of the primary gaseous products, the similarity of the decomposition schemes for the reactions yielding similar solid products (metals or oxides) was taken into account. The most unexpected result was that the primary gaseous products contained, instead of equilibrium CO_2 molecules, a mixture of CO and $\frac{1}{2}O_2$ molecules for Ag, Ni, Mn, and Pb oxalates and a mixture of CO and O for Hg oxalate. The corresponding differences in the enthalpies are 283 and $532\,\text{kJ mol}^{-1}$, respectively, exceeding by an order of magnitude the possible measurement and calculation errors.

Additional evidence for the presence of oxygen in the primary decomposition products of oxalates is a decrease in the rate of their decomposition in the presence of O_2. Published data on the depressing effect exerted by O_2 and CO_2 on the decomposition of $Ag_2C_2O_4$ and by Hg vapour on the decomposition of HgC_2O_4 are given in Table 16.65. In all cases, the calculation results are fairly consistent with experiment. For the pathway of HgC_2O_4 vaporization to $Hg(g) + 2CO_2$, the calculated factor by which the vaporization rate should decrease in the presence of 17 mbar of Hg is 130, instead of 30 [121]. For the pathway of $Ag_2C_2O_4$ decomposition to $2Ag(g) + 2CO_2$, in a CO_2 atmosphere the rate should decrease by a factor of 10^4, instead of 15 [122]. Jacobs and Kureishy [128] examined the dependence of the decomposition rate of NiC_2O_4 on the CO_2 pressure. With an increase in the CO_2 pressure from 54 to 384 Torr, the rate constant decreased by a factor of 1.9. This value is consistent with the theoretically expected difference, $(384/54)^{1/2.5} \cong 2.2$, and differs essentially

Table 16.64 Experimental and calculated values of the reaction enthalpies and the corresponding composition of primary products for oxalate decompositions

Oxalate	Primary Products	ν	$\bar{T}$ (K)	$P_\infty(A)^a$ (bar)	τ_1	$-\Delta_c H_T^\circ$ (kJ mol^{-1})	$\bar{E}$ (kJ mol^{-1})	$\nu\bar{E}$ (kJ mol^{-1})	$\Delta_v H_T^\circ$ (kJ mol^{-1}) Expt	Theory	Difference %
$Ag_2C_2O_4$	$2Ag(g)_\downarrow + CO + CO_2 + \frac{1}{2}O_2$	4.5	383	3.6E−32	0.50	284.9	106	477	761	740	−3.0
HgC_2O_4	$Hg(g) + CO + CO_2 + O$	4.0	413				109	436	436	479	10.0
NiC_2O_4	$Ni(g)_\downarrow + CO + CO_2 + \frac{1}{2}O_2$	3.5	536	1.5E−34	0.51	428.8	157	550	769	788	2.4
MnC_2O_4	$MnO(g)_\downarrow + 2CO + \frac{1}{2}O_2$	3.5	609	9.2E−36	0.52	508.9	176	616	880	924	5.0
PbC_2O_4	$PbO(g)_\downarrow + 2CO + \frac{1}{2}O_2$	3.5	552	7.2E−19	0.38	286.7	151	529	638	698	9.4

[a] (A): low-volatility product

Table 16.65 Reduction of the decomposition rate of oxalate in the presence of gaseous product (B)

Oxalate	T (K)	P_B (bar)	P_{eqp} (bar)		Rate Decrease		Ref.
			e-mode	i-mode	Calculated	Measured	
$Ag_2C_2O_4$	404	0.21 (O_2)	2.2E−05	4.7E−06	5	4	[124]
$Ag_2C_2O_4$	457	1.0 (O_2)	7.3E−04	2.0E−04	4	2	[142]
$Ag_2C_2O_4$	457	1.0 (CO_2)	7.3E−04	4.7E−05	15	9	[142]
HgC_2O_4	463	0.017 (Hg)	6.4E−06	2.1E−07	30	25	[126]

Table 16.66 Calculated values of the vaporization coefficients for some oxalates

Oxalate	T (K)	Primary Products	P_{eqp} (bar)	Equilibrium Products	P_{eq} (bar)	α_v
$Ag_2C_2O_4$	383	$2Ag(g)_\downarrow + CO + CO_2 + \frac{1}{2}O_2$	1E−07	$2Ag(s) + 2CO_2$	1E+17	1E−24
HgC_2O_4	413	$Hg(g) + CO + CO_2 + O$	1E−07	$Hg(l) + 2CO_2$	5E+16	2E−24
NiC_2O_4	536	$Ni(g)_\downarrow + CO + CO_2 + \frac{1}{2}O_2$	1E−07	$Ni(s) + 2CO_2$	2E+05	5E−12
MnC_2O_4	609	$MnO(g)_\downarrow + 2CO + \frac{1}{2}O_2$	1E−07	$MnO(s) + CO + CO_2$	4E+03	3E−11
PbC_2O_4	552	$PbO(g)_\downarrow + 2CO + \frac{1}{2}O_2$	1E−07	$PbO(s) + CO + CO_2$	5E+02	2E−10

from the factor of 50 expected for the pathway of NiC_2O_4 decomposition to $Ni(g) + 2CO_2$.

The compositions of the primary products in the suggested schemes contradict the results of numerous studies of the gas-phase composition by gas chromatography and mass spectrometry. However, all these measurements were performed under conditions where the primary non-equilibrium gas mixture could come to equilibrium owing to the reactions of CO with O or $\frac{1}{2}O_2$ with the formation of CO_2. Nevertheless, even under these conditions, the CO/CO_2 ratio in some experiments (e.g., on decomposition of MnC_2O_4 [125]) exceeded the equilibrium value by 20–40%. It is notable that the excess was observed only in the initial step of the decomposition (at $\alpha < 0.2$). As α and, correspondingly, the thickness of the oxide layer on the surface of the oxalate particle increased, the ratio approached the equilibrium value. Apparently, equilibration of the $CO + \frac{1}{2}O_2$ mixture had already occurred as the gases passed through the shell of the solid product.

The calculated vaporization coefficients of the oxalates are listed in Table 16.66. The lowest values of α_v, of the order of 10^{-24}, are characteristic of silver and mercury oxalates. Both compounds are explosives. The enthalpies of the exothermic (at hypothetical equilibrium) decomposition of these compounds are −112.5 and −114.2 kJ mol^{-1}, respectively, so that the equilibrium pressure of CO_2 at 400 K should reach 10^{17} bar. However, the decomposition actually occurs considerably more slowly, because the composition of the primary vaporization products is essentially non-equilibrium.

Conclusions The mechanisms of the decompositions of Ag, Ni, Hg, Mn, and Pb oxalates can be considered as occurring by congruent dissociative vaporization of the reactants with the formation of the following primary products: for Ag, Ni, and Hg oxalates, atomic metal (Ag, Ni, and Hg) and a mixture of $CO + CO_2 + \frac{1}{2}O_2$ (or O); for Mn and Pb oxalates, gaseous oxides (MnO and PbO), and a mixture of $2CO + \frac{1}{2}O_2$. This composition of the products is confirmed by agreement between the experimental enthalpies of vaporization and the calculated enthalpies of the corresponding reactions, and also by the depressing effect of gaseous products on the decomposition rate. The difference in the chemical form of oxygen (O_2 or O) is consistent with that observed in the dissociative vaporization of the corresponding oxides: Ag_2O, NiO, and HgO (see Sect. 10.1).

This mechanism accounts for some of the above-mentioned common features and differences in the reaction course for various oxalates. The condensation of the solid products accounts for the induction period observed for Ag, Ni, Mn, and Pb oxalates. For HgC_2O_4, where no solid products are formed, the induction period is absent. The difference in the parameters E for the induction and acceleration periods in the decomposition of $Ag_2C_2O_4$ and NiC_2O_4, $59\,kJ\,mol^{-1}$ [141] and $68\,kJ\,mol^{-1}$ [119], respectively, is consistent with the calculated condensation energy per mole of products ($-\tau_1 \Delta_c H_T^\circ / \nu$), equal to $63\,kJ\,mol^{-1}$ for both reactants.

References

1. Nesmeyanov AnN (1961) Vapour pressure of chemical elements. Akad. Nauk SSSR, Moscow (in Russian)
2. Melville HW, Gray SC (1936) Trans Faraday Soc 32:1026–1030
3. Brewer L, Kane JS (1955) J Phys Chem 59:105–109
4. Somorjai GA, Lester JE (1967) Evaporation mechanism of solids. In: Reiss H (ed) Progress in solid state chemistry. Pergamon, Oxford, pp 1–52
5. L'vov BV, Novichikhin AV (1997) Thermochim Acta 290:239–251
6. Glushko VP (1978–1982) (ed) Thermodynamic properties of individual substances, Handbook in 4 volumes. Nauka, Moscow (in Russian)
7. Ryabin VA, Ostroumov MA, Svit TF (1977) Thermodynamic characteristics of substances, Handbook. Khimiya, Leningrad (in Russian)
8. Rosenblatt GM, Lee P-K, Dowell MB (1966) J Chem Phys 45:3454–3455
9. Kireev VA (1975) Methods of practical calculations in thermodynamics of chemical reactions. Khimiya, Moscow (in Russian)
10. Mitani K, Harano Y (1960) Bull Chem Soc Jpn 33:1147–1150
11. Mitani K, Asakura Y (1965) Bull Chem Soc Jpn 38:901–904
12. Malinin GV, Tolmachev YuM, Yadrintsev VB (1968) Zh Neorg Khim 13:1746–1749 (in Russian)
13. Kazenas YeK, Chizhikov DM (1976) Vapour pressure and composition under oxides of chemical elements. Nauka, Moscow (in Russian)
14. Kazenas YeK, Tsvetkov YuV (1997) Vaporization of oxides. Nauka, Moscow (in Russian)

15. L'vov BV (1997) Thermochim Acta 333:21–26

16. Derbinsky IA, Pavlyuchenko MM, Prodan EA, et al. (1970) Thermal decomposition of mercury oxide in vacuum and oxygen atmosphere. In: Pavlyuchenko MM, Prodan EA (eds) Heterogeneous chemical reactions. Nauka Tekhnika, Minsk, (in Russian) pp 190–204

17. Pavlyuchenko MM Effect of solid product and gaseous phase on the kinetics of solid decomposition. In: Pavlyuchenko MM, Prodan EA (eds) Heterogeneous chemical reactions and their reactivity. Nauka Tekhnika, Minsk, (in Russian) pp 5–35

18. L'vov BV, Ugolkov VL, Grekov FF (2004) Thermochim Acta 411:187–193

19. Firsova LP, Nesmeyanov AnN (1960) Zh Fiz Khim 34:2719–2722 (in Russian)

20. Nagai S, Niwa K, Shinmei M, Yokokawa T (1973) J Chem Soc Faraday Trans I 69:1628–1634

21. Shimazaki E, Matsumoto N, Niwa K (1957) Bull Chem Soc Japan 30:969–971

22. Hoenig CL, Searcy AW (1966) J Am Ceram Soc 49:128–134

23. Stolyarova VL, Ambrok AG, Nikolaev EN, Semenov GA (1977) Fiz Khim Stekla 3:635–637 (in Russian)

24. Munir ZA, Hirth JP (1970) J Appl Phys 41:2697–2704

25. Somorjai GA, Jepsen DW (1964) J Chem Phys 41:1389–1393

26. Wösten WJ (1961) J Phys Chem 1949–1951

27. Somorjai GA (1964) The evaporation rate of CdS and CdSe. In: Rutner E, Goldfinger P, Hirth JP (eds) Condensation and evaporation of solids. Gordon & Breach, New York, pp 417–433

28. Munir ZA, Mitchell MJ (1969) High Temp Sci 1:381–387

29. Hassan MS, Munir ZA (1973) High Temp Sci 5:34–39

30. Lee WT, Munir ZA (1967) J Electrochem Soc 114:1236–1239

31. Glushko VP (1965–1982) (ed) Thermodynamic constants of substances, Handbook in 10 volumes. Akad. Nauk SSSR, Moscow (in Russian)

32. Hoenig CL, Searcy AW (1967) J Am Ceram Soc 50:460–466

33. Blank BAH, Searcy AW (1968) J Phys Chem 72:2241–2243

34. Dreger LH, Dadape VV, Margrave JL (1962) J Phys Chem 66:1556–1559

35. Ambacher O, Brandt MS, Dimitrov R, et al. (1996) J Vac Sci Technol B 14:3532–3542

36. Munir ZA, Searcy AW (1965) J Chem Phys 42:4223–4228

37. Ryklis EA, Bolgar AS, Fesenko VV (1969) Poroshkovaya Metallurgiya 73:92–96 (in Russian)

38. Brandt O, Yang Hui, Ploog KH (1996) Phys Rev B 54:4432–4435

39. Edgar JH (1994) (ed) Properties of group III nitrides. INSPEC, London

40. Leitner J, Strejc A, Sedmidubsky D, Růžička K (2003) Thermochim Acta 401: 169–173

41. L'vov BV (2000) Thermochim Acta 360:85–91

42. L'vov BV, Ugolkov VL (2005) Thermochim Acta 438:1–8

43. Garner WE (1955) (ed) Chemistry of the solid state. Butterworths, London

44. Fox PG, Hitchinson RW (1977) Slow thermal decomposition. In: Fair HD, Walker RF (eds) Energetic materials. V 1 Physics and chemistry of the inorganic azides. Plenum Press, New York, Chapter 6, pp 251–284

45. Brown ME, Dollimore D, Galwey AK (1980) Reactions in the solid state. Elsevier, London

46. Manelis GB, Nazin GM, Rubtsov YuI, Strunin VA (1996) Thermal decomposition and combustion of explosives and powders. Nauka, Moscow (in Russian)

47. L'vov BV (1997) Thermochim Acta 291:179–185

48. Choi CS (1977) The crystal structures. In: Fair HD, Walker RF (eds) Energetic materials. V 1 Physics and chemistry of the inorganic azides. Plenum Press, New York, Chapter 3, pp 97–130

49. Walker RF (1968) J Phys Chem Solids 29:985–1000
50. Garner WE (1958) Proc Roy Soc 246:203–206
51. Fox PG, Soria-Ruiz J (1970) Proc Roy Soc A317:79–90
52. Garner WE, Reeves LE (1955) Trans Faraday Soc 51:694–704
53. Audubert R (1938) C R Acad Sci Paris 206:748
54. Kondratiev VN, Nikitin EE (1974) Kinetics and mechanism of gaseous phase reactions. Nauka, Moscow (in Russian)
55. L'vov BV, Ugolkov VL (2004) Thermochim Acta 413:7–15
56. Holt JB (1965) Chem Abstr 62:8426h
57. Gordon RS, Kingery WD (1967) J Am Ceram Soc 50:8–14
58. Galwey AK, Laverty GM (1993) Thermochim Acta 228:359–378
59. Criado JM, Morales J (1976) J Therm Anal 10:103–110
60. Pavlyuchenko MM, Prodan EA, Kramarenko FG, et al. (1979) Effect of gaseous phase on the decomposition kinetics of some carbonates and hydroxides. In: Prodan EA (ed) Heterogeneous chemical reactions. Nauka Tekhnika, Minsk, (in Russian) pp 37–57
61. Pavlyuchenko MM, Novoselova MYu, Prodan EA (1969) Izv AN BSSR Ser Khim 1:5–10 (in Russian)
62. Jacobs T (1958) Nature 182:1086–1087
63. Holt JB, Cutler IB, Wadsworth ME (1962) J Am Ceram Soc 45:133–136
64. Toussaint F, Fripiat JJ, Gastuche MC (1963) J Phys Chem 67:26–30
65. Weber JN, Roy R (1965) Am Mineral 50:1038–1045
66. Brindley GW, Sharp JH, Patterson JH, Nakahira BN (1967) Am Mineral 52:201–211
67. Johnson HB, Kessler F (1969) J Am Ceram Soc 52:199–204
68. Anthony GD, Garn PD (1974) J Am Ceram Soc 57:132–135
69. Nahdi K, Llewellyn P, Rouquerol F, Rouquerol J, et al. (2002) Thermochim Acta 390:123–132
70. L'vov BV, Ugolkov VL (2005) J Therm Anal Cal 82:15–22
71. Holt B, Cutler IB, Wadsworth ME (1964) Kinetics of the thermal dehydration of hydrous silicates. In: Bradeley WF (ed) Proceedings of 12th National Conference Clay and Clay Minerals, Atlanta, Georgia. Pergamon, Oxford, pp 55–67
72. Ward JR (1975) Thermochim Acta 13:7–14
73. Brown ME, Flynn RM, Flynn JH (1995) Thermochim Acta 256:477–483
74. L'vov BV, Novichikhin AV (1995) Spectrochim Acta Part B 50:1459–1468
75. L'vov BV (1998) Thermochim Acta 315:145–157
76. L'vov BV, Novichikhin AV, Dyakov AO (1998) Thermochim Acta 315:169–179
77. L'vov BV, Ugolkov VL (2003) J Therm Anal Cal 74:697–708
78. L'vov BV, Ugolkov VL (2005) Russ J Appl Chem 78:379–385
79. L'vov BV (2006) J Therm Anal Cal 84:581–587
80. Smith ML, Topley B (1931) Proc Roy Soc A:134 224
81. Okhotnikov VB, Yakobson BI, Lyakhov NZ (1983) React Kinet Catal Lett 23:125–130
82. Okhotnikov VB, Lyakhov NZ (1984) J Solid State Chem 53:161–167
83. Okhotnikov VB, Petrov SE, Yakobson BI, Lyakhov NZ (1987) React Solids 2:359–372
84. Kirdyashkina NA, Okhotnikov VB (1988) React Kinet Catal Lett 36:417–422
85. Modestov AN, Poplaukhin PV, Lyakhov NZ (2001) J Therm Anal Cal 65:121–130
86. Kazenas YeK (2004) Vaporization thermodynamics of double oxides. Nauka, Moscow (in Russia)
87. Addison CC, Logan N (1964) Adv Inorg Chem Radiochem 6:72–142
88. Stern KH (1972) J Phys Chem Ref Data 1:747–772
89. L'vov BV (1990) Zh Analit Khim 45:2144–2153 (in Russian)
90. L'vov BV, Novichikhin AV (1995) Spectrochim Acta Part B 50:1427–1448
91. L'vov BV, Ugolkov VL (2004) Thermochim Acta 424:7–13
92. Mu J, Perlmutter DD (1982) Thermochim Acta 56:253–260

93. Stern KH, Weise EL (1966) High temperature properties and decomposition of inorganic salts. Part 1. Sulfates. NSRDS-NBS, Washington
94. Brownell WE (1963) J Am Ceram Soc 46:125–128
95. Pechkovsky VV, Zvezdin AG, Beresneva TI (1963) Kinet Katal 4:208–213 (in Russian)
96. Hulbert SF (1967/68) Mater Sci Eng 2:262–268
97. Mohazzabi P, Searcy AW (1976) J Chem Soc Faraday Trans I 72:291–295
98. L'vov BV, Ugolkov VL (2004) Thermochim Acta 411:73–79
99. Galwey AK, Brown ME (1999) Thermal decomposition of ionic solids. Elsevier, Amsterdam
100. Stern KH, Weise EL (1969) High temperature properties and decomposition of inorganic salts. Part 2. Carbonates. NSRDS-NBS, Washington
101. Brown ME, Maciejewski M, Vyazovkin S, et al. (2000) Thermochim Acta 355:125–143
102. Maciejewski M (2000) Thermochim Acta 355:145–154
103. L'vov BV (2002) Thermochim Acta 386:1–16
104. L'vov BV, Polzik LK, Ugolkov VL (2002) Thermochim Acta 390:5–19
105. L'vov BV, Ugolkov VL (2003) Thermochim Acta 401:139–147
106. L'vov BV, Ugolkov VL (2004) Thermochim Acta 409:13–18
107. L'vov BV, Ugolkov VL (2004) Thermochim Acta 410:47–55
108. Beruto DT, Searcy AW, Kim MG (2004) Thermochim Acta 424:99–109
109. L'vov BV (2004) Thermochim Acta 424:183–199
110. Powell EK, Searcy AW (1980) Metall Trans B 11:427–432
111. Powell EK, Searcy AW (1978) J Am Ceram Soc 61:216–221
112. Basu TK, Searcy AW (1976) J Chem Soc Faraday Trans I 72:1889–1895
113. Dejardin G, Meshard G, Uzan R, Cabaud B (1962) C R Acad Sci Paris 255:1712
114. Zawadzki J, Bretsznajder S (1935) Z Elektrochem 41:215–223
115. Maumené M (1870) Bull Soc chim 13:194
116. Kornienko VP (1957) Ukr Chem J 23:159–167 (in Russian)
117. Dollimore D (1987) Thermochim Acta 117:331–363
118. Coetzee A, Eve DJ, Brown ME (1993) J Thermal Anal 39:947–973
119. Dominey DA, Morley H, Young DA (1965) Trans Faraday Soc 61:1246–1255
120. Boldyrev VV (2002) Thermochim Acta 388:63–90
121. L'vov BV (2000) Thermochim Acta 364:99–109
122. Brown ME, Dollimore D, Galwey AK (1977) Thermochim Acta 21:103–110
123. Benton AF, Cunningham GL (1935) J Am Chem Soc 57:2227–2234
124. Bircumschaw LL, Harris I (1948) J Chem Soc 1898–1902
125. Brown ME, Dollimore D, Galwey AK (1974) J Chem Soc Faraday Trans I, 70: 1316–1324
126. Prout EG, Tompkins FC (1947) Trans Faraday Soc 43:148–157
127. Danes V, Ponec V (1958) Coll Czech Chem Commun 23:848–859
128. Jacobs PWM, Kureishy ART (1962) Trans Faraday Soc 58:551–560
129. Jach J, Griffel M (1964) J Phys Chem 68:731–736
130. Tournayan L, Charcosset H, Wheeler BR, McGinn JM, Galwey AK (1971) J Chem Soc A 868–871
131. Erofeev VB, Belkevich PI, Volkova AA (1946) Zh Fiz Khim 20:1103–1112 (in Russian)
132. Erofeev VB, Mostovaya LYa, Kravchuk LK (1971) Dokl AN BSSR 15:225–227 (in Russian)
133. Coetzee A, Eve DJ, Brown ME (1993) J Thermal Anal 39:947–973
134. Yankwich PE, Zavitsanos PD (1964) Pure Appl Chem 8:287–304
135. Dollimore D, Dollimore J, Little J (1969) J Chem Soc A 2946–2951
136. Macdonald JY (1936) J Chem Soc 832–839
137. Macdonald JY, Sandison R (1938) Trans Faraday Soc 34:589–595
138. Finch A, Jacobs PWM, Tompkins FC (1954) J Chem Soc 2053–2060

139. Szabo ZG, Biro-Sugar E (1956) Z Elektrochem 60:869–874
140. Haynes RM, Young DA (1961) Discuss Faraday Soc 31:229–237
141. Deren J, Mania R (1973) Bull Acad Pol Sci 21:387–394
142. Dollimore D, Evans TA (1991) Thermochim Acta 178:263–271
143. Prout EG, Moore DJ (1966) ASTM Spec Tech Publ 400:1–16
144. Yankwich PE, Copeland JL (1957) J Am Chem Soc 79:2081–2086

Chapter 17
Final Remarks

The main results of the development and application of the described thermochemical approach to decomposition kinetics are summarized in Table 17.1.

Table 17.1 Main achievements in the interpretation of decomposition kinetics on the basis of the thermochemical approach and the CDV mechanism

Mechanism, Effect, Regularity	Interpetation	Section
Appearance of low-volatility products in the gas phase in the decomposition stage	Quantitative	2.3
Thermochemistry of the induction, acceleratory, and deceleratory periods	Quantitative	2.4
Effect of reaction localization	Qualitative	2.4
Mechanism of formation and growth of nuclei, their morphology	Qualitative	2.4; 2.5
Vapour oversaturation and structure of the product (X-ray amorphous or crystalline)	Qualitative	2.6
The equimolar and isobaric modes of decomposition	Quantitative	3.5
Relationship between the rate constant k and the absolute rate of decomposition J	Quantitative	3.7
Physical essence of the Arrhenius parameters (A and E)	Quantitative	3.7
Criteria for vaporization/desorption identification	Quantitative	5.1; 5.2
Dependence of the E^i/E^e ratio on the stoichiometry of the decomposition reaction	Quantitative	5.3
Invariance of the E^i parameter under pressure of gaseous products in the isobaric mode of decomposition	Quantitative	5.5
The retardation effect of gaseous products: $A^i \propto (P_B)^{-b/a}$	Quantitative	5.3; 5.4
Temperature distribution in powder reactants	Quantitative	6
Theoretical evaluation of self-cooling	Quantitative	6
The Topley–Smith effect	Quantitative	7
Vapour oversaturation and the contribution of the condensation energy to the enthalpy	Quantitative	8.1
Increase of the reaction enthalpy with temperature for reactants decomposed to solids	Quantitative	8.2
Reduction of the decomposition rate for melted reactants	Quantitative	8.3
Thermochemical analysis of the composition of primary products of decomposition	Quantitative	9
Effect of crystal structure on the composition of the primary gaseous products	Qualitative	10
The vaporization coefficient α_v	Quantitative	11
The kinetic compensation effect	Qualitative	12

These include the qualitative or quantitative interpretation of phenomena, effects, and regular trends observed in the course of thermal decomposition. The most significant achievements are the explanation of the mechanism of the nucleation and growth of nuclei and the interpretation of such effects as localization of the decomposition process, the T–S effect, a decrease in the decomposition rate upon melting of the reactant, differences in the structure (amorphous or crystalline) of the solid product, and the effect of gaseous products and foreign gases on the decomposition rate.

These achievements can be considered as a reliable confirmation of the CDV mechanism underlying the studies described. New trends have been revealed in the course of these studies, such as deceleration of the decomposition upon melting of the reactant, increase in the enthalpy of the reaction with temperature (for decomposition reactions yielding a solid product), correlation of the decomposition temperature with the molar enthalpy and existence of two basic decomposition modes (equimolar and isobaric).

This success would be impossible without a new methodology of thermochemical studies, based on the third-law method, and without certain additional techniques (such as measurements of the absolute rates of decomposition for powders and melts, and determinations of the molar enthalpies of decompositions in the excess of gaseous product) that have greatly improved the precision and accuracy of measurements and simplified and extended the current thermal methods used to study decomposition kinetics (Table 17.2).

Table 17.2 Development of methodology in kinetic investigations of decomposition reactions

Method, Procedure, Analysis	Section
Analysis of restrictions of the Arrhenius plot and second-law methods as applied to thermochemical determination of the composition of the primary products of decomposition	4.2; 6.3; 8.2
Substantiation of the metrological advantages of the third-law method and its application in solid-state kinetics	4.4–4.8
Estimation of the molar entropies for decomposition reactions	4.5
A consideration of the vaporization congruence in calculation of the equilibrium constants of decomposition reactions	3.5; 15.6
Estimation of the molar enthalpies on the basis of the initial temperatures of decomposition	5.1
Evaluation of self-cooling	6.3
Measurement of the absolute rates of decomposition for powders and melts	15.1
Thermal decompositions in an excess of gaseous product	15.4
Determination of the molar enthalpies of decompositions for hydrates and carbonates in the isobaric mode in air or inert gas	15.5

The correctness of new ideas and theories in scientific research is commonly evaluated by their fruitfulness in interpretation of problems accumulated in one or another field and by their capability to predict unknown trends and effects. The other general criteria that are applied to new theories are simplicity, internal consistency, experimental reliability (verifiability), and compliance with previous theories. *The thermochemical approach to the kinetics of solid-state reactions used in this study meets these criteria.*

It appears to be applicable not only to one or several particular examples of decomposition, but to virtually all of the most popular classes of reactions considered as models. *The kinetic and mechanistic analysis within the framework of a thermochemical approach is based on fundamental concepts of molecular physics (statistical mechanics) and chemical thermodynamics.*

The common CDV decomposition mechanism for different substances and some well-forgotten or unclaimed ideas (Langmuir vaporization models and third-law method), underlying this approach, appeared to be the necessary and mutually supplementing elements. Without any of them it would be impossible to develop a sufficiently rigorous and consistent theory. The essence of these three aspects of the approach is expressed in a simplified form in Table 17.3.

However, as new approaches or new theories are developed, the solution of problems insoluble within the framework of traditional concepts is accompanied by appearance of new problems and enigmas. This approach is not an exception. In particular, the mechanism of the transfer of the condensation energy of the low-volatility product to the reactant and the effect of the symmetry of the reactant crystal-lattice on the composition of the gaseous decomposition products remain unclear. To solve these problems on the basis of the new mechanistic and kinetic concepts discussed in this book, it would be appropriate to use the experience accumulated in solid-state physical chemistry and in crystal chemistry. The systematic differences between the enthalpies measured by the third-law method and those measured by the second-law and Arrhenius plot methods undoubtedly deserves a more thorough study. This problem is especially important for successful application to reactions involving the formation of solid products.

To conclude, it is necessary to note the possible use of the new concepts of thermal decomposition (in particular, CDV mechanism) for interpretation of

Table 17.3 Basics of the thermochemical approach

Aspect	Essence	Formalism
Mechanism	Congruent dissociative vaporization	$R(s/l) \leftrightarrow A(g)_{\downarrow} + B(g)$
Kinetics	Langmuir vaporization equations	$P_{\mathrm{eqp}} = f(J)$
Methodology	Third-law method	$\Delta_{\mathrm{r}} H_T^{\circ} = T(\Delta_{\mathrm{r}} S_T^{\circ} - \nu R \ln P_{\mathrm{eqp}})$

more complex types of solid-state reactions involving two reacting solids:

$$A(s) + B(s) \rightarrow C(s)$$
$$A(s) + B(s) \rightarrow C(s) + D(g)$$
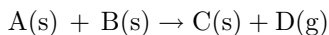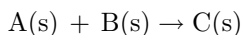
or more complex synthesis processes accompanied by decomposition of both solid reactants,

$$AB(s) + CD(s) \rightarrow AD(s) + CB(s)$$
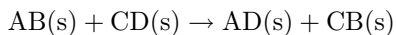
As a rule, such reactions are considered separately from decomposition reactions [1–4], although there are hardly any fundamental differences between them except an additional problem of diffusion of the reactants through a product layer.

References

1. Hauffe K (1955) Reaktionen in und an festen Stoffen. Springer, Berlin
2. Budnikov PP, Ginstling AM (1968) Principles of solid state chemistry. MacLaren, London
3. Tretyakov YuD (1978) Solid state reactions. Khimiya, Moscow (in Russian)
4. West AR (1984) Solid state chemistry and its applications. Wiley, Chichester

Appendix

Table A1 Fundamental physical constants [1]

Quantity	Symbol	Value in SI Units
Speed of light in vacuum	c	$2.997\ 925 \times 10^8\,\mathrm{m\ s^{-1}}$
Elementary charge	e	$1.602\ 177 \times 10^{-19}\,\mathrm{C}$
Electron rest mass	m_e	$9.109\ 390 \times 10^{-31}\,\mathrm{kg}$
Proton rest mass	m_p	$1.672\ 623 \times 10^{-27}\,\mathrm{kg}$
Neutron rest mass	m_n	$1.674\ 929 \times 10^{-27}\,\mathrm{kg}$
Planck constant	h	$6.626\ 076 \times 10^{-12}\,\mathrm{J\ s}$
Avogadro constant	N_A	$6.022\ 137 \times 10^{23}\,\mathrm{mol^{-1}}$
Boltzmann constant	k	$1.380\ 658 \times 10^{-23}\,\mathrm{J\ K^{-1}}$
Gas constant	R	$8.134\ 510\,\mathrm{J\ K^{-1}\ mol^{-1}}$
Faraday constant	F	$9.648\ 530 \times 10^4\,\mathrm{C\ mol^{-1}}$
Zero of the Celsius scale	$0\,^\circ\mathrm{C}$	$273.15\,\mathrm{K}$
Standard atmosphere	atm	$101\ \ 325\,\mathrm{Pa}$
Molar volume, ideal gas, $P = 1\,\mathrm{bar}$ and $T = 0\,^\circ\mathrm{C}$		$22.711\ 082 \times 10^{-3}\,\mathrm{m^3\ mol^{-1}}$
Stefan–Boltzmann constant	σ	$5.670\ 512\,\mathrm{W\ m^{-2}\ K^{-4}}$
Pythagorean number	π	$3.141\ \ 593$
Base of natural logarithms	e	$2.718\ \ 282$
Natural logarithm of 10	ln 10	$2.302\ \ 585$

Table A2 Standard atomic masses of elements (except radioactive elements) [1]

Symbol	Atomic Number	Name	Relative Atomic Mass	M (kg mol^{-1})
Ag	47	Silver	107.868	0.10787
Al	13	Aluminum	26.981	0.02698
Ar	18	Argon	39.948	0.03995
As	33	Arsenic	74.921	0.07492
Au	79	Gold	196.966	0.19697
B	5	Boron	10.811	0.01081
Ba	56	Barium	137.327	0.13733
Be	4	Beryllium	9.012	0.00901
Bi	83	Bismuth	208.980	0.20898
Br	35	Bromine	79.904	0.07990
C	6	Carbon	12.011	0.01201
Ca	20	Calcium	40.078	0.04008
Cd	48	Cadmium	112.411	0.11241
Ce	58	Cerium	140.115	0.14012
Cl	17	Chlorine	35.452	0.03545
Co	27	Cobalt	58.933	0.05893
Cr	24	Chromium	51.996	0.05200
Cs	55	Cesium	132.905	0.13291
Cu	29	Copper	63.546	0.06355
Dy	66	Dysprosium	162.503	0.16250
Er	68	Erbium	167.263	0.16726
Eu	63	Europium	151.966	0.15197
F	9	Fluorine	18.998	0.01900
Fe	26	Iron	55.847	0.05585
Ga	31	Gallium	69.723	0.06972
Gd	64	Gadolinium	157.253	0.15725
Ge	32	Germanium	72.612	0.07261
H	1	Hydrogen	1.008	0.00101
He	2	Helium	4.003	0.00400
Hf	72	Hafnium	178.492	0.17849
Hg	80	Mercury	200.593	0.20059
Ho	67	Holmium	164.930	0.16493
I	53	Iodine	126.904	0.12690
In	49	Indium	114.821	0.11482
Ir	77	Iridium	192.223	0.19222
K	19	Potassium	39.098	0.03910
Kr	36	Krypton	83.801	0.08380
La	57	Lanthanum	138.906	0.13891
Li	3	Lithium	6.941	0.00694
Lu	71	Lutetium	174.967	0.17497
Mg	12	Magnesium	24.305	0.02431
Mn	25	Manganese	54.938	0.05494

(continued)

Table A2 (continued)

Symbol	Atomic Number	Name	Relative Atomic Mass	M (kg mol^{-1})
Mo	42	Molybdenum	95.941	0.09594
N	7	Nitrogen	14.007	0.01401
Na	11	Sodium	22.990	0.02299
Nb	41	Niobium	92.906	0.09291
Nd	60	Neodymium	144.243	0.14424
Ne	10	Neon	20.180	0.02018
Ni	28	Nickel	58.691	0.05869
O	8	Oxygen	15.999	0.01600
Os	76	Osmium	190.21	0.19021
P	15	Phosphorus	30.974	0.03097
Pa	91	Protactinium	231.036	0.23104
Pb	82	Lead	207.21	0.20721
Pd	46	Palladium	106.421	0.10642
Pr	59	Praseodymium	140.908	0.14091
Pt	78	Platinum	195.083	0.19508
Rb	37	Rubidium	85.468	0.08547
Re	75	Rhenium	186.207	0.18621
Rh	45	Rhodium	102.906	0.10291
Ru	44	Ruthenium	101.072	0.10107
S	16	Sulfur	32.067	0.03207
Sb	51	Antimony	121.753	0.12175
Sc	21	Scandium	44.956	0.04496
Se	34	Selenium	78.963	0.07896
Si	14	Silicon	28.086	0.02809
Sm	62	Samarium	150.363	0.15036
Sn	50	Tin	118.710	0.11871
Sr	38	Strontium	87.621	0.08762
Ta	73	Tantalum	180.948	0.18095
Tb	65	Terbium	158.925	0.15893
Te	52	Tellurium	127.603	0.12760
Th	90	Thorium	232.038	0.23204
Ti	22	Titanium	47.883	0.04788
Tl	81	Thallium	204.383	0.20438
Tm	69	Thulium	168.934	0.16893
U	92	Uranium	238.029	0.23803
V	23	Vanadium	50.942	0.05094
W	74	Tungsten	183.853	0.18385
Xe	54	Xenon	131.292	0.13129
Y	39	Yttrium	88.906	0.08891
Yb	70	Ytterbium	173.043	0.17304
Zn	30	Zinc	65.392	0.06539
Zr	40	Zirconium	91.224	0.09122

Table A3   Coefficients of mutual diffusion of gases[a] [2]

System	$D_0 \times 10^4$ $(m^2\,s^{-1})$	n	Ω (K)	Temperature Interval (K)
He–CH$_4$	0.57	1.750		$298 - 10^4$
He–O$_2$	0.45	1.710		$244 - 10^4$
He–air	0.62	1.729		$244 - 10^4$
He–CO$_2$	0.52	1.720		$200 - 530$
He–SF$_6$	0.35	1.627		$290 - 10^4$
Ne–H$_2$	0.99	1.731		$90 - 10^4$
Ne–N$_2$	0.28	1.743		$293 - 10^4$
Ne–CO	0.22	1.776		$195 - 10^4$
Ar–CH$_4$	0.172	1.785		$307 - 10^4$
Ar–N$_2$	0.17	1.752		$244 - 10^4$
Ar–CO	0.17	1.752		$244 - 10^4$
Ar–O$_2$	0.167	1.736		$243 - 10^4$
Ar–air	0.165	1.749		$244 - 10^4$
Ar–CO$_2$	0.177	1.646	89.1	$276 - 1800$
Ar–SF$_6$	0.114	1.596	145.4	$328 - 10^4$
H$_2$–CH$_4$	0.62	1.765		$293 - 10^4$
H$_2$–O$_2$	0.69	1.732		$252 - 10^4$
Kr–N$_2$	0.13	1.766		$248 - 10^4$
Kr–CO	0.13	1.766		$242 - 10^4$
Xe–H$_2$	0.54	1.712	16.9	$242 - 10^4$
Xe–N$_2$	0.106	1.789		$248 - 10^4$
H$_2$–air	0.66	1.750		$252 - 10^4$
H$_2$–CO$_2$	0.56	1.750	11.7	$200 - 550$
H$_2$–SF$_6$	0.52	1.570	102.5	$298 - 10^4$
CH$_4$–N$_2$	0.20	1.750		$298 - 10^4$
CH$_4$–O$_2$	0.22	1.695	44.2	$294 - 10^4$
CH$_4$–air	0.186	1.747		$298 - 10^4$
CH$_4$–SF$_6$	0.119	1.657	69.2	$298 - 10^4$
N$_2$–O$_2$	0.182	1.724		$285 - 10^4$
N$_2$–H$_2$O	0.204	2.072		$282 - 373$

(continued)

Table A3 (continued)

System	$D_0 \times 10^4$ (m^2s^{-1})	n	Ω (K)	Temperature Interval (K)
N_2–CO_2	0.208	1.570	113.6	$288 - 1800$
N_2–SF_6	0.122	1.590	119.4	$328 - 10^4$
CO–O_2	0.175	1.724		$285 - 10^4$
CO–air	0.182	1.730		$285 - 10^4$
CO–CO_2	0.142	1.803		$282 - 473$
CO–SF_6	0.129	1.84	139.4	$297 - 10^4$
O_2–H_2O	0.207	2.072		$282 - 450$
O_2–CO_2	0.174	1.661	61.3	$287 - 1083$
O_2–SF_6	0.138	1.522	129.0	$297 - 10^4$
Air–H_2O	0.205	2.072		$282 - 450$
O_2–CO_2	0.174	1.661	61.3	$287 - 1083$
O_2–SF_6	0.138	1.522	129.0	$297 - 10^4$
Air–H_2O	0.26	1.632		$450 - 1070$
Air–CO_2	0.207	1.590	102.1	$280 - 1800$
Air–SF_6	0.126	1.576	121.1	$328 - 10^4$
Air–H_2O	0.205	2.072		$282 - 450$
Air–CO_2	0.207	1.590	102.1	$280 - 1800$
Air–SF_6	0.126	1.576	121.1	$328 - 10^4$
H_2O–CO_2	0.41	1.500	307.9	$296 - 1640$
CO_2–N_2O	0.095	1.866		$195 - 550$
CO_2–C_3H_4	0.074	1.896		$298 - 550$
CO_2–SF_6	0.069	1.886		$328 - 472$
H–He	2.35	1.732		$275 - 10^4$
H–Ar	0.112	1.597		$275 - 10^4$
H–H_2	0.184	1.728		$190 - 10^4$
N–N_2	0.29	1.774		$280 - 10^4$
O–He	0.84	1.749		$280 - 10^4$
O–Ar	0.23	1.841		$280 - 10^4$
O–N_2	0.28	1.774		$280 - 10^4$
O–O_2	0.28	1.774		$280 - 10^4$

[a] For systems presented in this table, the empirical temperature dependence has the form:
$D = D_0(T/273)^n \exp(-\Omega/T)$

Table A4   Spectral and integrated radiant emittance for some metals and oxides[a] [2, 3]

Substance	λ (µm)	T_1 (K)	$\varepsilon(\lambda, T_1)$	T_2, (K)	ε (T_2)
Ag	0.66	1300	0.07	900	0.032
Al	0.66	1300	0.13	900	0.060
C (graphite)	0.5–0.7	2000	0.89	2000	0.84
Cu	0.66	1000	0.11	1400	0.15
Fe	0.66	1300	0.39		
Mo	0.66	1600	0.37	1775	0.19
Pt	0.66	1000	0.29	900	0.098
Pt	0.66	2000	0.31	1300	0.138
W	0.66	2000	0.45	2000	0.26
Al_2O_3	0.66	1600	0.17	1500	0.23
Al_2O_3	0.66	2000	0.21	2000	0.34
BeO	0.66	1300	0.54	1300	0.71P
CaO				1300	0.27
CoO			0.75		
Cr_2O_3	1–5	1273	0.68	1123	0.86
CuO			0.70	475	0.60
Fe_2O_3			0.70	1800	0.80
MgO	0.66	1300	0.18	1300	0.33
MgO	0.66	1400	0.23	1400	0.30
MgO	0.66	1700	0.35	1700	0.28
MgO	0.66	2000	0.47	2000	0.36
NbO			0.70		
NiO	1.0	1273	0.78	475	0.37
PbO				295	0.28
SiO_2	1–3	293	0.25	573	0.72
SiO_2	1–3	1273	0.60	1173	0.48
ThO_2	0.65	1600	0.35		
TiO_2			0.50		
UO_2	0.65	2200	0.51P		
V_2O_5			0.70		
Yb_2O_3			0.60		
ZrO_2	0.66	1400	0.46P	1600	0.37

[a] P: for a powder, in all other cases, for a flat surface

Table A5 Composition of dry ambient air [4]

Species	Volume Percents	Mass Percents
N_2	78.03	75.47
O_2	20.99	23.20
Ar	0.933	1.28
CO_2	0.030[a]	0.046
H_2	0.01	0.001
Ne	0.0018	0.0012
He	0.0005	0.00007
Kr	0.0001	0.0003
Xe	0.000009	0.00007

[a] At latest measurements [5], the average concentration of CO_2 in air is attained 0.038%

Table A6 Saturated vapour pressure of water (in bars) [4]

Tens	Temperature (°C) Units									
	0	1	2	3	4	5	6	7	8	9
0	0.0063	0.0067	0.0072	0.0078	0.0084	0.0090	0.0096	0.0103	0.0110	0.0118
10	0.0126	0.0135	0.0144	0.0154	0.0154	0.0176	0.0187	0.0200	0.0213	0.0226
20	0.0241	0.0256	0.0273	0.0290	0.0308	0.0327	0.0347	0.0368	0.0390	0.0413
30	0.0438	0.0464	0.0491	0.0519	0.0549	0.0580	0.0613	0.0648	0.0684	0.0722
40	0.0762	0.0803	0.0847	0.0892	0.0940	0.0990	0.1042	0.1096	0.1153	0.1212
50	0.1274	0.1339	0.1406	0.1477	0.1550	0.1626	0.1706	0.1789	0.1875	0.1965
60	0.2058	0.2155	0.2257	0.2361	0.2470	0.2584	0.2701	0.2824	0.2951	0.3082
70	0.3219	0.3361	0.3509	0.3661	0.3819	0.3983	0.4152	0.4329	0.4510	0.4698
80	0.4893	0.5095	0.5303	0.5519	0.5742	0.5972	0.6210	0.6456	0.6711	0.6973
90	0.7244	0.7523	0.7812	0.8110	0.8417	0.8733	0.9060	0.9397	0.9743	1.0101

References

1. Mills I (1988) (ed) Quantities, units and symbols in physical chemistry. Blackwell Scientific, Oxford
2. Kikoin IK (1976) (ed) Tables of physical constants. Atomizdat, Moscow (in Russian)
3. Samsonov GV (1978) (ed) Physical and chemical properties of oxides. Handbook. Metallurgiya, Moscow (in Russian)
4. Nikolsky BP (1971) (ed) Handbook of chemist, vol. I. Khimiya, Leningrad (in Russian)
5. Brook EJ (2005) Science 310:1285–1287

Subject Index

HOT TOPICS IN THERMAL ANALYSIS AND CALORIMETRY

1. M. E. Brown: *Introduction to Thermal Analysis.* Techniques and Applications. 2nd rev. ed. 2001   ISBN 1-4020-0211-4; Pb 1-4020-0472-9
2. W. Zielenkiewicz and E. Margas: *Theory of Calorimetry.* 2002   ISBN 1-4020-0797-3
3. O. Toft Sørensen and J. Rouquerol (eds.): *Sample Controlled Thermal Analysis.* Origin, Goals, Multiple Forms, Applications and Future. 2003   ISBN 1-4020-1563-1
4. T. Hatakayama and H. Hatakayama: *Thermal Properties of Green Polymers and Biocomposites.* 2004   ISBN 1-4020-1907-6
5. D. Lörinczy (ed.): *The Nature of Biological Systems as Revealed by Thermal Methods.* 2004   ISBN 1-4020-2218-2
6. M. Reading and D. J. Hourston (eds.): *Modulated-Temperature Differential Scanning Calorimetry.* Theoretical and Practical Applications in Polymer Characterisation. 2006   ISBN 1-4020-3749-X
7. B. V. Ľvov: *Thermal Decomposition of Solids and Melts.* New Thermochemical Approach to the Mechanism, Kinetics and Methodology. 2007   ISBN 978-1-4020-5671-0